Aus der Abteilung für Mikrogravitation und Translationale Regenerative Medizin der
Klinik für Plastische, Ästhetische und Handchirurgie
der Medizinischen Fakultät
der Otto-von-Guericke-Universität Magdeburg

Der Einfluss von realer und simulierter Mikrogravitation auf die biologischen Prozesse humaner Prostatakarzinomzellen

Dissertation

zur Erlangung des Doktorgrades

Dr. med.
(doctor medicinae)

an der Medizinischen Fakultät
der Otto-von-Guericke-Universität Magdeburg

vorgelegt von **Dorothea Dietrichs**
aus **Berlin, Deutschland**
Magdeburg 2022

Bibliographische Angaben:

Dietrichs, Dorothea:

Der Einfluss von realer und simulierter Mikrogravitation auf die biologischen Prozesse humaner Prostatakarzinomzellen. - 2022. - 51 Bl., 8 Abb., 0 Tab., 3 Anl.

Kurzreferat

Das Prostatakarzinom ist eine der Hauptursachen für die Krebssterblichkeit bei Männern weltweit. Eine ungewöhnliche, aber einzigartige Umgebung zur Untersuchung von Tumorzellprozessen bietet die Mikrogravitation. Diese findet sich entweder real im Weltraum oder kann auf der Erde durch international anerkannte Bodenanlagen wie mit einer ‚*Random Positioning Machine*' (RPM) simuliert werden. Es ist bekannt, dass Faktoren, die an der Tumorprogression und an der Metastasierung beteiligt sind, eine Schlüsselrolle bei der durch Mikrogravitation ausgelösten Bildung von dreidimensionalen Tumorsphäroiden spielen. Insbesondere die hohe Mortalitätsrate bei Männern mit metastasiertem Prostatakarzinom macht eine Optimierung der Diagnose durch neue Biomarker erforderlich.

Die vorliegende Dissertation fasst hierzu drei Publikationen zusammen: Zum einen wurden niedrig differenzierte PC-3-Prostatakarzinomzellen in Kurz- und Langzeitexperimenten sowohl simulierter als auch realer Mikrogravitation ausgesetzt. Zur Simulation der Mikrogravitation wurden die Zellen auf der RPM kultiviert. Die Ergebnisse sind in den ersten beiden Publikationen veröffentlicht worden. Darüber hinaus nahmen wir 2019 an der 34. Parabelflugkampagne des Deutschen Zentrums für Luft- und Raumfahrt teil. Parabelflüge mit 31 Parabelflugmanövern bieten die Möglichkeit humane Zellen unter realer Mikrogravitation und Hypergravitation zu untersuchen. Diese Ergebnisse sind in der dritten Publikation veröffentlicht worden.

Schlüsselwörter

Prostatakarzinom; Parabelflug; reale Mikrogravitation; ‚*Random Positioning Machine'*; simulierte Mikrogravitation; multizelluläre Sphäroide; ‚*Next-Generation-Sequencing*'; Zytoskelett; extrazelluläre Matrix; fokale Adhäsionsmoleküle; Zytokine; microRNA

Die vorliegende Doktorarbeit basiert auf den folgenden chronologisch aufgeführten Publikationen:

1. Hybel TE, **Dietrichs D**, Sahana J, Corydon TJ, Nassef MZ, Wehland M, Krüger M, Magnusson NE, Bauer J, Utpatel K, Infanger M, Grimm D, Kopp S: Simulated Microgravity Influences VEGF, MAPK, and PAM Signaling in Prostate Cancer Cells. Int J Mol Sci. 21. 1263 (2020)
2. **Dietrichs D**, Grimm D, Sahana J, Melnik D, Corydon TJ, Wehland M, Krüger M, Vermeesen R, Baselet B, Baatout S, Hybel TE, Kahlert S, Schulz H, Infanger M, Kopp S: Three-Dimensional Growth of Prostate Cancer Cells Exposed to Simulated Microgravity. Front Cell Dev Biol. 10. 841017 (2022)
3. Schulz H[†], **Dietrichs D**[†], Wehland M, Corydon TJ, Hemmersbach R, Liemersdorf C, Melnik D, Hübner N, Saar K, Infanger M, Grimm D. In Prostate Cancer Cells Cytokines Are Early Responders to Gravitational Changes Occurring in Parabolic Flights. Int J Mol Sci. 23. 7876 (2022)

[†]These authors contributed equally to this work.

Die zugrundeliegenden Publikationen sind dem Anhang dieser Dissertation beigefügt.

Inhalt

1. Vorwort

Die in dieser Dissertation vorgestellten Experimente wurden zwischen Januar 2019 und August 2020 in den Laboratorien der Universitätsklinik der Otto-von-Guericke-Universität Magdeburg (Klinik für Plastische, Ästhetische und Handchirurgie) durchgeführt und die erzielten Ergebnisse im Jahr 2021 ausgewertet. Die Langzeitsimulationsexperimente mit der ‚*Random Positioning Machine'* erfolgten in der Arbeitsgruppe von Frau Professor Dr. med. Daniela Grimm, Institut für Biomedizin, Universität Aarhus, Dänemark. Das ‚*Next-Generation-Sequencing'* wurde am Max-Delbrück-Centrum für Molekulare Medizin in Berlin-Buch durchgeführt. Die Experimente in realer Mikrogravitation fanden im Rahmen der 34. Parabelflugkampagne des Deutschen Zentrums für Luft- und Raumfahrt (finanziert durch die Projekte 50WB1924 und 50WB2219) in Kooperation mit der französischen Firma Novespace, Bordeaux-Mérignac, Frankreich statt.

Betreuer der Doktorarbeit:

Professor Dr. med. Daniela-Gabriele Grimm
Seit 6/2020 Leiterin der Abteilung für Mikrogravitation und Translationale Regenerative Medizin (MTRM)
Klinik für Plastische, Ästhetische und Handchirurgie
Otto-von-Guericke-Universität
Universitätsklinikum Magdeburg A.ö.R.
Medizinische Fakultät und Fakultät für Maschinenbau
Universitätsplatz 2
39106 Magdeburg

Professor Dr. med. Manfred Infanger
Leiter der Klinik für Plastische, Ästhetische und Handchirurgie (KCHP)
Otto-von-Guericke-Universität
Medizinische Fakultät
Universitätsklinikum Magdeburg A.ö.R.
Leipziger Str. 44
39120 Magdeburg

Mentoren:

Dr. rer. medic. Sascha Kopp
Institut für Chemie
Otto-von-Guericke-Universität,
Fakultät für Verfahrens- und Systemtechnik
Universitätsplatz 2
39106 Magdeburg

Dr. rer. medic. Herbert Schulz
Arbeitsgruppe Bioinformatik in der Weltraummedizin
Abteilung Mikrogravitation und Translationale Regenerative Medizin (MTRM)
Klinik für Plastische, Ästhetische und Handchirurgie
Otto-von-Guericke-Universität
Universitätsklinikum Magdeburg A.ö.R.
Medizinische Fakultät und Fakultät für Maschinenbau
Universitätsplatz 2
39106 Magdeburg

2. Preface

The experiments presented in this doctoral thesis were performed between January 2019 and August 2020 in the laboratories at the University Hospital of Otto-von-Guericke-University Magdeburg (Clinic for Plastic, Aesthetic and Hand Surgery) and evaluated in 2021. The long-term simulation experiments with the '*random positioning machine*' were done by the research group of Professor Daniela Grimm, Institute of Biomedicine, Aarhus University, Denmark. The '*next generation sequencing*' was performed at the Max Delbrück Center for Molecular Medicine in Berlin-Buch. The experiments in real microgravity took place in the framework of the 34th Parabolic Flight Campaign of the German Aerospace Center (funded by the DLR projects 50WB1924 and 50WB2219) in cooperation with the company Novespace, Bordeaux-Mérignac, France.

Supervisors of the doctoral thesis:

Professor Daniela-Gabriele Grimm, MD
Since 6/2020 Head of the Department of Microgravity and Translational Regenerative Medicine (MTRM)
Clinic for Plastic, Esthetic and Hand Surgery
Otto-von-Guericke-University
University Hospital Magdeburg
Medical Faculty and Faculty for Mechanical Engineering
Universitätsplatz 2
39106 Magdeburg

Professor Manfred Infanger, MD
Director of the Clinic for Plastic, Esthetic and Hand Surgery
Otto-von-Guericke-University
Medical Faculty
University Hospital Magdeburg
Leipziger Str. 44
39120 Magdeburg

Mentoren:

Dr. Sascha Kopp
Institute for Chemistry
Otto-von-Guericke-University,
Faculty for Process and Systems Engineering
Universitätsplatz 2
39106 Magdeburg

Dr. Herbert Schulz
Working Group Bioinformatics in Space Medicine
Department of Microgravity and Translational Regenerative Medicine (MTRM)
Clinic for Plastic, Esthetic and Hand Surgery
Otto-von-Guericke-University
University Hospital Magdeburg
Medical Faculty and Faculty for Mechanical Engineering
Universitätsplatz 2
39106 Magdeburg

3. Abkürzungsverzeichnis

2D	Two-dimensional (Zweidimensional)
3D	Three-dimensional (Dreidimensional)
ACTB	Beta-Actin
AD	Adhärente Zellen
AKT	RAC-alpha serine/threonine-protein kinase
AR	Androgen receptor (Androgen-Rezeptor)
BRAF	B-RAF Protoonkogene
CASP3	Caspase-3
CASP8	Caspase-8
CASP9	Caspase-9
CCL2/MCP-1	CC-chemokine ligand 2/monocyte chemotactic protein 1
CCL20	Chemokine (C-C motif) ligand 20
CCL7	Chemokine (C-C motif) ligand 7
CDH1	Cadherin 1
CDKN1B	Cyclin-dependent kinase inhibitor 1B
CDKN1B/p27	Cyclin-dependent kinase inhibitor 1B/p27
CDKN1C/p57	Cyclin-dependent kinase inhibitor 1C/p57
COL1A1	Collagen-1A1
COL4A5	Collagen-4A5
c-REL/REL	REL proto-oncogene NF-kappa-B subunit
CRISPR	Clustered regularly interspaced short palindromic repeats
CRPC	Castrate-resistant prostate cancer
C-Src	Proto-oncogene tyrosine-protein kinase
CTGF	Connective tissue growth factor
CX3CL1	Chemokine (C-X3-C motif) ligand 1
CXCL1	Chemokine (C-X-C motif) ligand 1
CXCL10	Chemokine (C-X-C motif) ligand 10
CXCL12	Chemokine (C-X-C motif) ligand 12
CXCL16	Chemokine (C-X-C motif) ligand 16
CXCL3	Chemokine (C-X-C motif) ligand 3
CXCL8	Interleukin-8
CXCR1	Chemokine (C-X-C Motif) receptor 1
CXCR2	Chemokine (C-X-C Motif) receptor 2
DAVID	Database for annotation, visualization and integrated discovery
DLR	Deutsches Zentrum für Luft- und Raumfahrt
EAP	Experimental autoimmune prostatitis
ECM	Extracelullar matrix (Extrazelluläre Matrix)
EGF	Epidermal growth factor
EGFR	Epidermal growth factor receptor
EMBL	European molecular biology laboratory
EMT	Epithelial-mesenchymal transition
ERK1	Extracellular signal regulated kinase 1
ERK2	Extracellular signal regulated kinase 2
ESA	European Space Agency
FA	Focal adhesion (Fokale Adhäsion)
FLK1	Fms-related tyrosine kinase 1
FLT1	Fetal liver kinase 1
FN1	Fibronectin
GBF	Ground-based facility (Bodenanlagen)
GTP	Guanosine triphosphate
HARV	High aspect rotating wall vessel
HCC	Hepatocellular carcinoma
hsa-miR-107	Homo-sapiens-microRNA-107

Hyper-G	Hypergravitation
ICAM1	Intercellular adhesion molecule 1
IFN-β	Interferon beta
IL-1	Interleukin-1
IL-17/17-A	Interleukin-17/interleukin-17-alpha
IL-1α/1F1	Interleukin-1-alpha/interleukin-1-F-1
IL-1β/1F2	Interleukin-1-beta/interleukin-1-F-2
IL-2	Interleukin-2
IL-6	Interleukin-6
IL-7	Interleukin-7
ISS	International space station (Internationale Weltraumstation)
KDR	Kinase insert domain receptor
Ki-67	Marker of proliferation Ki-67
LAMA1	Laminin subunit alpha-1 (Laminin-Untereinheit alpha-1)
LAMA3	Laminin subunit alpha-3 (Laminin-Untereinheit alpha-3)
LAMB2	Laminin subunit beta-2 (Laminin-Untereinheit beta-2)
LIF	Leukemia inhibitory factor
LNCaP	Lymph node carcinoma of the prostate
lncRNA	Long non-coding RNA
MAP2K1	Mitogen-activated protein kinase-kinase 1
MAPK	Mitogen-activated protein kinase
MCS	Multicellular spheroids (Multizelluläre Sphäroide)
MEK1	Mitogen-activated protein kinase kinase 1
MEK2	Mitogen-activated protein kinase kinase 2
miR-221	MicroRNA-221
miR-221del	MicroRNA-221 deletion
miR-222	MicroRNA-222
miRNA	MicroRNA
MMP-2	Matrix metallopeptidase-2
MMP9	Matrix metallopeptidase-9
mRNA	Messenger ribonucleic acid (Messenger-Ribonukleinsäure)
mTOR	Mechanistic target of rapamycin kinase
NASA	National Aeronautics and Space Administration
NF-κB	Nuclear factor kappa-light-chain-enhancer of activated B cells
NF-κB	p65 nuclear factor NF-kappa-B p65 subunit
NGAL	Neutrophil gelatinase-associated lipocalin
NGS	RNA Next-generation sequencing
OPN	Osteopontin
P1	First parabola (Parabel eins)
P31	31st parabola (Parabel 31)
PAI-1	Plasminogen activator inhibitor-1
PAM	PI3K/AKT/mTOR
PDK1	Phosphoinositide-dependent kinase-1
PDK2	Phosphoinositide-dependent kinase-2
PFA	Paraformaldehyde
PI3K	Phosphoinositide 3-kinase
PIP2	Phosphatidylinositol4,5-bisphosphat
PIP3	Phosphatidylinositol (3-5) -Trisphosphat
PKB	Protein kinase B
PSA	Prostate-specific antigen
PTEN	Phosphatase and tensin homolog
PTK2	Protein tyrosine kinase 2
qPCR	quantitative polymerase chain reaction (quantitative Polymerase-Kettenreaktion)
r-μg	Real microgravity (reale Mikrogravitation)

RAF	Rapidly accelerated fibrosarcoma
RANKL	Receptor activator of NF-κB ligand
RAS	Rat sarcoma
RELB	RELB proto-oncogene NF-kappa-B subunit
RGD-Motive	Arginylglycylaspartic acid
RPM	Random positioning machine
RTK	Rezeptor tyrosine kinase
RWV	Rotating wall vessel
SCNC	Small-cell neuroendocrine carcinoma
SRC1	Steroid receptor coactivator 1
STRING	Search tool for the retrieval of interacting genes/proteins
s-µg	Simulated microgravity (simulierte Mikrogravitation)
TGFβ	Transforming growth factor beta
TIMP-1	Tissue inhibitor of metalloproteinases/Metallopeptidase inhibitor 1
TLN1	Talin-1
TNFAIP3	Tumor necrosis factor, alpha-induced protein 3
TNF-α	Tumor necrosis factor alpha
TRIFMA	Time-resolved immunofluorometric assay
TUBB	Tubulin beta
TUNEL	TdT-mediated dUTP-biotin nick end labeling
VCAM1	Vascular cell adhesion molecule 1
VCL	Vinculin
VEGF	Vascular endothelial growth factor
VEGFA	Vascular endothelial growth factor A
VEGFR	Vascular endothelial growth factor receptor
ZFP36	Zinc finger protein 36 homolog

4. Ziel und Hypothesen

Wenn humane Prostatakarzinomzellen simulierter Mikrogravitation (s-µ*g*) ausgesetzt werden, die durch eine RPM erzeugt wird, zeigen sie unter anderem eine Vielzahl von Veränderungen im Zytoskelett, in der Zusammensetzung der extrazellulären Matrix (ECM) und dem fokalen Adhäsionskomplex. Zudem bilden sich bei länger einwirkender s-µ*g* 3D-Aggregate. Diese 3D-Gewebe werden auch als multizelluläre Sphäroide (MCS) bezeichnet.
Ziel dieser Arbeit war es, die molekularen und morphologischen Veränderungen zu untersuchen, die in humanen Prostatatumorzellen während simulierter und realer Mikrogravitation (r-µ*g*) auftreten.
Dazu analysierte ich Proben von Prostatakarzinomzellen, die Bedingungen der s- und r-µ*g*, Hypergravitation (hyper-*g)* und Vibration ausgesetzt waren. Die Auswertung erfolgte mit Hilfe von ‚*Next Generation Sequencing*', quantitativer real-time PCR (qPCR), mikroskopischen Techniken, Vitalitätstests sowie Analysen der Signaltransduktionswege.

Vorrangiges Ziel dieser Dissertation war es, den Einfluss von s- und r-µ*g* auf Prostatakarzinomzellen zu untersuchen und zu bewerten. Besonderes Augenmerk lag dabei auf den durch µ*g* hervorgerufenen Veränderungen auf Ebene des gesamten Transkriptoms der PC-3-Prostatakarzinomzelllinie.
Dazu wurden in dieser Dissertation die folgenden drei Hypothesen überprüft:

1. Das Zytoskelett nimmt eine Schlüsselrolle in der frühzeitigen Schwerkraftwahrnehmung von Prostatatumorzellen ein.
2. Die VEGF-, MAPK- und PAM-Signalwege sind an der Bildung von Sphäroiden beteiligt.
3. Die Genexpression und Sekretionsrate von Zytokinen und Chemokinen werden durch kurzeitige r-µ*g* verändert und haben ebenfalls einen Einfluss auf das 3D Tumorzellwachstum.

5. Einleitung und Zusammenfassung der drei Publikationen

In den folgenden Kapiteln werde ich eine Einleitung in die wichtigsten Themenschwerpunkte dieser Dissertation und eine Zusammenfassung der drei dieser Dissertation zugrundeliegenden Publikationen geben.

5.1. Die Auswirkungen der Mikrogravitation auf den menschlichen Körper

Die veränderte Schwerkraft, die Astronauten während ihrer Einsätze im Weltall erfahren, hat erhebliche Auswirkungen auf den menschlichen Körper (1, 2). Wenn man auf der Erde aufrecht steht, sammelt sich Flüssigkeit in den unteren Extremitäten an. Unter µ*g* wird diese dagegen in den Brustkorb und den Kopf verlagert (sogenanntes ‚*Puffy Face*' (aufgedunsenes Gesicht) und die ‚*Bird Legs*' (sehr schlanke Beine) der Astronauten) (3). Infolgedessen kommt es zu einem Anstieg der Herzfüllung und der Diurese, was insgesamt zu einem geringeren Blutvolumen und zur Erhöhung des Hämatokrits führt. Astronauten

scheiden in den ersten Stunden im Weltall ca. 1.5 l Urin aus. Darüber hinaus klagen viele Raumfahrer über die Weltraumreisekrankheit, das sogenannte Space Adaption Syndrom (SAS), das mit Übelkeit und Erbrechen einhergeht (4). Das SAS kann beispielsweise mit Skopolamin (National Aeronautics and Space Administration (NASA)-Spray) oder transdermalen Dimenhydrinat Pflastern behandelt werden.
Ein weiteres gesundheitliches Problem der Astronauten stellt das Weltraumflug-assoziierte neurookulare Syndrom (SANS; *spaceflight associated neuro-ocular syndrome*) dar (5). Es handelt sich hierbei um Veränderungen des Sehvermögens, die bei einer Untergruppe der Astronauten und der Weltraumbesatzung festgestellt wurden, die an langfristigen (d. h. Dauer mehr als zwei Wochen) Weltraummissionen beteiligt sind. Es kommt durch die Mikrogravitation zu spezifischen Augenveränderungen: Schwellung des Punkts, wo der Sehnerv in das Auge eintritt, Abflachung des Bulbus, Aderhautfalten, und Flecken (kleine, gelb-weiße Läsionen im Augenhintergrund) (6). Zur Behandlung des SANS empfiehlt die NASA Acetazolamid zur Reduktion des intrakranialen Drucks (Carboanhydrasehemmer) und eine vitaminreiche Ernährung. Zusätzlich werden den Astronauten verschiedene Brillen mit unterschiedlicher Stärke (‚*Space Anticipation Glasses')* mit ins All gegeben.
Ein weiteres Problem stellen die Rückenschmerzen im All dar, da sich die Wirbelsäule durch die fehlende Schwerkraft streckt und nahezu gerade wird. Die Körpergröße der Astronauten erhöht sich bis 7,5 cm auf der ISS. Nach dem Flug haben viele Weltraumfahrer weiterhin Schmerzen im Rückenbereich und mit den Bandscheiben (7).
Darüber hinaus verringert die Schwerelosigkeit die Belastung der Skelettmuskeln. Längerfristig führt das zu einer Abnahme der Muskelmasse, der Muskelkraft und der Ausdauer (2). Ferner erhöht die niedrige Schwerkraft den Kalziumverlust aus den Knochen und wirkt hemmend auf die Knochenbildung und führt zur Reduktion der Knochenmasse und Osteoporose (8). Es resultiert eine erhöhte Nierensteinbildung. Weiterhin kommt es zu einer Beeinträchtigung des Immunsystems der Weltraumfahrer mit erhöhter Infektanfälligkeit, Reaktivierung schlafender Viren und Wundheilungsstörungen bei Langzeitmissionen (2). Ferner sind die kardiovaskulären Veränderungen zu nennen wie z. B. kardiale Atrophie, Hypotonie, Herzrhythmusstörungen und orthostatische Intoleranz (9).

5.2. Die reale Mikrogravitation

Unter r-µ*g* versteht man den Zustand von einem konstanten und kräftelosen freien Fall. Um diesen Zustand zu erreichen, stehen verschiedene Plattformen zur Verfügung. Beispielsweise herrschen bei Experimenten auf der Internationalen Weltraumstation (‚*International Space Station*', ISS), bei einem Weltraumflug im Orbit, bei Parabelflügen und in Höhenforschungsraketen Bedingungen der r-µ*g*.
Parabelflüge sind sehr wichtige Hilfsmittel für die Forschung im Bereich r-µ*g*, für die Vorbereitung von Weltraumflügen und für das Astronautentraining. Das Deutsche Zentrum für Luft- und Raumfahrt (DLR) organisiert dazu regelmäßig Parabelflugkampagnen. Während eines Parabelflugmanövers wird

der Zustand von r-µ*g* erreicht, indem sich das Parabelflugzeug und dementsprechend auch die Gegenstände und Personen an Bord kurzzeitig in freiem Fall befinden. Während des Parabelflugs werden 31 Parabeln in Folge geflogen, sodass kumulativ circa 12 Minuten r-µ*g* herrschen (10). Eine Parabel, wie in Abbildung 1 dargestellt, wird aus dem horizontalen Flug mit einem Anstieg von 15° für 20 s gestartet. Währenddessen wirkt eine Kraft von circa 1,8 *g* auf die Passagiere und die Experimente an Bord des Flugzeugs ein. Dann wird die Schubkraft der Turbinen gedrosselt und das Flugzeug folgt einer parabelförmigen Flugbahn. Das stellt dann die eigentliche Phase der r-µ*g* dar und dauert 22 s. Danach startet der Pilot die Triebwerke wieder vollständig durch, und eine weitere Phase von 1,8 *g* für 20 s schließt sich an, bis das Flugzeug wieder in den horizontalen Flug gebracht wird und die Parabel beendet ist (11).

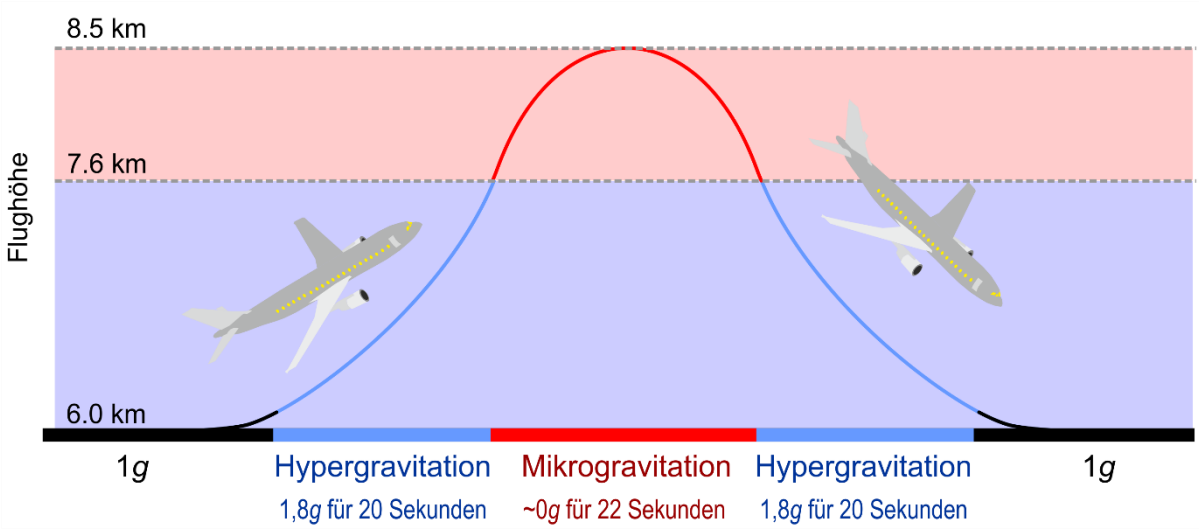

Abbildung 1 angelehnt an Quelle (12): Schematische Darstellung einer Parabel mit Flughöhe, Fluggeschwindigkeit und Abfolge der einzelnen Phasen (1 *g*, Hyper-*g* (1,8 *g*), r-µ*g* (0 *g*)).

Wie beschrieben, gibt es bei jeder Parabel neben der r-µ*g*-Phasen zwei Perioden von Hyper-*g* (1,8 *g*). Diese Wechsel der Beschleunigungsprofile und die damit einhergehenden Veränderungen müssen bei der Interpretation der Ergebnisse berücksichtigt werden. Zudem treten während eines Parabelflugs auch Störgrößen wie Vibrationen auf und diese wirken somit auf die Zellen an Bord ein. Deshalb bestand die Notwendigkeit, Kontrollexperimente zu den Auswirkungen von Vibrationen und Hyper-*g* durchzuführen (13).

Unterhalb des Erdorbits sind neben Parabelflügen ansonsten nur Falltürme in der Lage, echte Bedingungen des freien Falls über einen Zeitraum von wenigen Sekunden zu schaffen (14).

5.3. Die simulierte Mikrogravitation

Da Experimente in r-µ*g* ein kostspieliges Unterfangen darstellen, wurden Anlagen entwickelt, mit deren Hilfe einige Aspekte der r-µ*g* simuliert werden können.

Diese von der ‚*European Space Age*ncy' (Europäische Weltraumagentur: ESA) und der NASA anerkannten Bodenanlagen (engl. *ground-based facilitie*s, GBFs) bieten neben der Kostenersparnis den

Vorteil, dass sie es erlauben, schneller und effizienter neue Hypothesen zu testen oder Ergebnisse zu validieren. Zudem sind sie jederzeit zugänglich und erfordern weniger Vorbereitungszeit für die Durchführung eines Experiments als jene in r-µ*g*. Dennoch erzeugt jede GBF (deutsch Bodenanlage) auch unerwünschte „Nebenwirkungen", die in der Interpretation der Ergebnisse berücksichtigt werden müssen, wie zum Beispiel Zentrifugalbeschleunigungen, Vibrationen oder Scherkräfte (14).

Die geläufigsten Bodenanlagen zur Erzeugung von s-µ*g* sind die 2D-Klinostaten, die ‚*Rotating Wall Vessel*' (RWV), die ‚*Random Positioning Machine*' (RPM) oder der 3D-Klinostat. Geräte wie die RPM heben die Schwerkraft nicht auf, sondern verändern konstant nach dem Zufallsprinzip die Richtung des Schwerkraftvektors, der auf die Probe im Laufe der Zeit einwirkt, indem sie um eine oder alle drei Achsen im Raum rotieren. Über die Zeit gemittelt befindet sich die Probe dann in s-µ*g* (14).

In einem 2D-Klinostaten werden die Proben mit konstanter Geschwindigkeit und Richtung um eine Achse rotiert, die senkrecht zum einwirkenden Gravitationsvektor steht. Dabei muss die Rotationsgeschwindigkeit so gewählt werden, dass sowohl Sedimentation bei zu langsamer als auch Zentrifugation bei zu schneller Drehung vermieden werden (15).
Dasselbe Prinzip macht sich die ‚*Rotating Wall Vessel'* (RWV), auch ‚*Rotating Cell Culture System'* (RCCS) genannt, zunutze. Hierbei wird ein mit suspendierten Zellen und Kulturmedium gefüllter und bis zu 20 cm im Durchmesser großer Plexiglaszylinder ebenso wie beim 2D-Klinostaten senkrecht zum Gravitationsvektor rotiert, um der Sedimentation entgegenzuwirken (14).
Erfolgt die Drehung der Probe um zwei Achsen, kann es sich bei dem Gerät um einen 3D-Klinostaten oder eine ‚*Random Positioning Machine'* (RPM) handeln. Prinzipiell sind beide Maschinen identisch aufgebaut und bestehen aus zwei kardanisch aufgehängten Rahmen, bei denen jede Achse durch einen eigenen elektrischen Antrieb motorisiert ist. Erfolgt die Rotation um beide Achsen mit konstanter Richtung und Geschwindigkeit handelt es sich um einen 3D-Klinostaten, werden diese beiden Parameter dagegen randomisiert spricht man von einer RPM (Abbildung 2). Hierbei werden durch einen speziellen Algorithmus die Proben ständig in Bezug auf den Gravitationsvektor neu ausgerichtet. Über die Zeit wird dadurch für hinreichend kleine Proben die Wirkung der Schwerkraft zu nahezu null gemittelt (17). Die RPM als Bodenanlage bietet den Vorteil, dass über einen längeren Zeitraum eine gerüstfreie 3D-Sphäroidzüchtung möglich ist und zusätzlich weniger Nekrosen der Aggregate auftreten. Daher können mittels Langzeitexperimenten auch größere Sphäroide hergestellt werden (18).

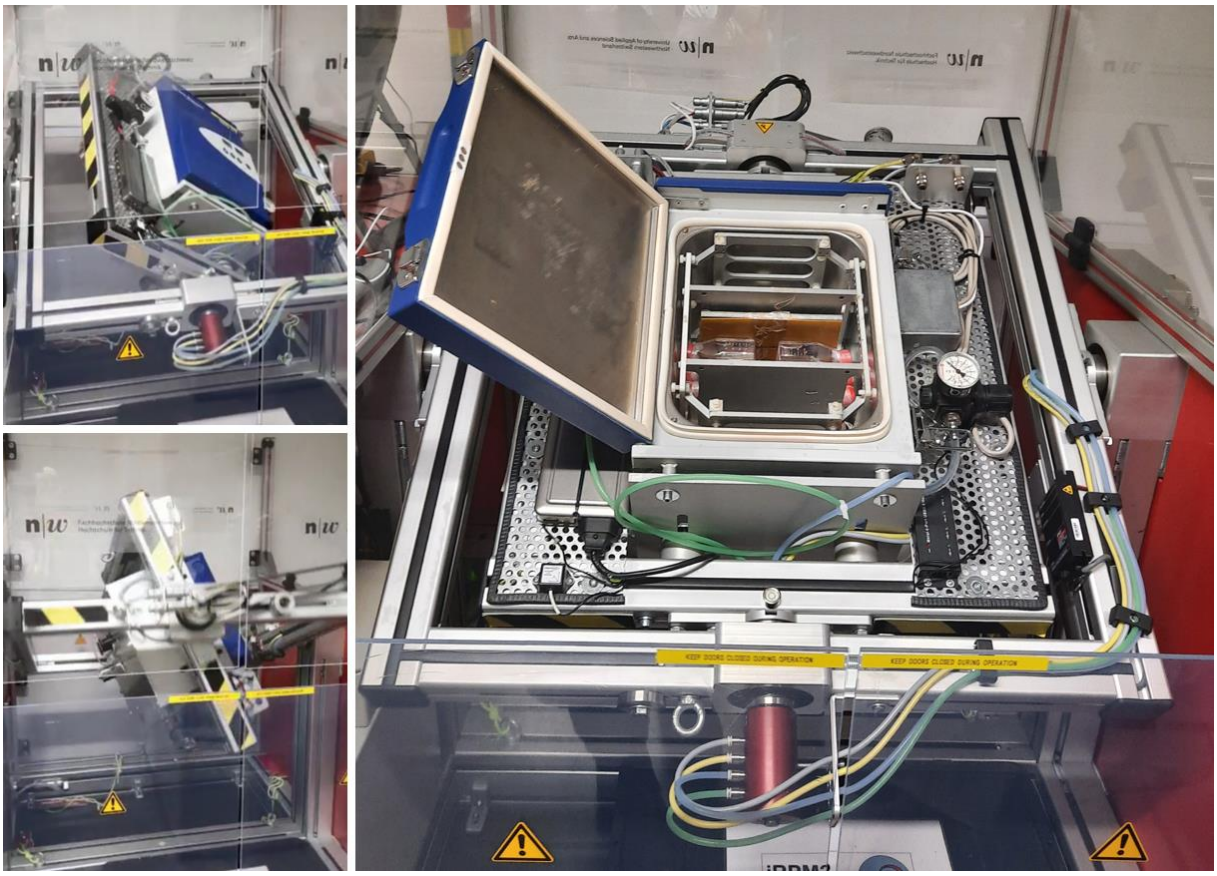

Abbildung 2 Fotografie einer speziellen RPM. Der ‚*Random-Positioning-Inkubator'* (RPI) wurde von der Fachhochschule Nordwestschweiz in Zusammenarbeit mit der ETH Zürich entwickelt. Der RPI besteht aus zwei kardanisch aufgehängten Rahmen, die von Elektromotoren angetrieben werden, und einem CO_2-Inkubator, der im Rotationsmittelpunkt der beiden Rahmen befestigt ist (17).

Insgesamt haben diese Bodenanlagen zu einer Vielzahl von Forschungsarbeiten beigetragen und stellen ein valides und kostengünstiges Modell dar, um Hypothesen zu testen und Vorversuche durchzuführen. Um Aussagen über den Einfluss von Mikrogravitation treffen zu können, müssen Experimente in r-µ*g* durchgeführt werden.

5.4. Hypergravitation und Vibration

Da bei Experimenten während eines Parabelflugs neben Phasen von µ*g* auch weitere komplexe mechanische Faktoren auf die Zellen einwirken, unter anderem Vibrationen und kurzzeitige Phasen von Hyper-*g*, bestand die Notwendigkeit, deren Einfluss auf zellulärer Ebene zu analysieren. Dazu wurden separate Bodenexperimente mit einem sogenannten Vibraplex-Gerät und einer speziellen Zentrifuge durchgeführt.

Das Vibraplex-Gerät wurde entwickelt, um Vibrationen zu erzeugen. Es wurde vom DLR gebaut, um Vibrationsexperimente an Zellen *in vitro* durchführen zu können. Dabei werden Vibrationen mit Frequenzen zwischen 0,2 Hz und 14 kHz erzeugt, die in vergleichbarer Form während eines Parabelflugs entstehen (11).

Mittels einer Zentrifuge konnte der Einfluss von Hyper-*g*-Kräften auf Zellkulturen untersucht werden. Dazu entwickelte das DLR eine Multi-Proben-Inkubator-Zentrifuge (MuSIC). Die MuSIC Zentrifuge ist in der Lage, die Hyper-*g*-Phasen nachzubilden, die bei einem Parabelflug auftreten (19).

Insgesamt riefen Hyper-*g* und Vibration nur geringe transkriptionelle Veränderungen in Zellen hervor, während µ*g* einen weitaus stärkeren Stimulus darstellte (19).

5.5. Multizelluläre Tumorsphäroide

Die herkömmliche 2D-Zellkulturtechnik wird immer noch in der experimentellen *in vitro* Forschung eingesetzt. Allerdings besitzt dieses Modell seine Limitationen bezüglich der Übertragbarkeit auf die *in vivo* Zellphysiologie und ist daher als valides Modell zunehmend umstritten. In einer 2D-Zellkultur wachsen die Zellen als einlagiger Zellrasen (Monolayer), der fest am Kunststoffboden der Zellkulturflasche haftet. In diesem Fall interagieren die Zellen überwiegend mit dem Kunststoff und weniger mit der Extrazellularmatrix oder anderen Zellen.
Zellen hingegen, die in einer 3D Umgebung gezüchtet werden, weisen komplexe Zell-Zell- und Zell-Matrix-Interaktionen auf. 3D-Zellkulturen spiegeln die *In vivo*-Architektur von natürlichen Organen und Geweben wider und stellen somit die normale Zellfunktion besser dar.
Daher wird nun zunehmend anerkannt, dass ein Bedarf an 3D-Zellkultursystemen besteht, die das mechanische und biochemische Umfeld nachempfinden können (20).
Zur Induktion von 3D-Wachstum und MCS-Bildung bedarf es spezieller Techniken.
Zum einen gibt es matrix-gestützte Techniken, die auf Hydrogel- oder Polymergerüsten basieren. Zum anderen gibt es matrix-freie Methoden, wie z. B. die „Liquid-Overlay"-Technik, die „Hanging-Drop"-Technik oder die Suspensionskultur unter Zuhilfenahme nicht adhäsiver Oberflächen (21).
Darüber hinaus induziert sowohl r- als auch s-µ*g* die spontane Aggregation von Zellen aus Zellmonolayern, indem die Zellsedimentation verhindert wird. Mikrogravitation, die während eines Parabelflugs auftritt, ist dafür allerdings zu kurzanhaltend. Um diesen Effekt zu erzielen, bedarf es langanhaltender Mikrogravitation, wie es z. B. während Weltraumflügen im Orbit oder bei Experimenten auf der ISS der Fall ist.
Die Bildung von MCS kann auf Zelladhäsion und/oder Zelldifferenzierung zurückzuführen sein und umfasst drei entscheidende Schritte (21).
Zunächst nähern sich die dispergierten Zellen an und bilden lose Aggregate. Dazu binden die langkettigen ECM-Fasern über ihre RGD-Sequenzen an das Integrin auf der Zellmembranoberfläche. Während des Vorgangs der Aggregation führt der direkte Zell-Zell-Kontakt zu einer erhöhten Cadherin-Expression (Abbildung 3). Cadherin wird an der Membranoberfläche akkumuliert. Die Zellen werden aufgrund der homophilen Cadherin-Cadherin-Bindung zu festen Aggregaten verdichtet und bilden

MCS. Die ECM-Fasern und der Cadherin-Typ sowie die Konzentration können bei verschiedenen Zelltypen variieren.

Es bilden sich MCS als kugelförmige Zellaggregate mit komplexer Zell-Zell-Adhäsion und Zell-Matrix-Interaktion aus. Das führt zu einer Gradientenbildung und Abnahme der Konzentration von Nährstoffen, Gasen, Wachstumsfaktoren und Signalfaktoren im Inneren des Sphäroids. Außerdem weisen MCS unter physiologischen *In vivo* Bedingungen ähnliche Eigenschaften auf wie ihr Ursprungsgewebe, z. B. schlagen Kardiomyozyten-Sphäroide mit herzähnlichen Rhythmen, Hepatozyten-Sphäroide führen leberähnliche Funktionen aus, und menschliche Endothelzellen vaskularisieren in Fibroblasten-Mikrogewebe (21).

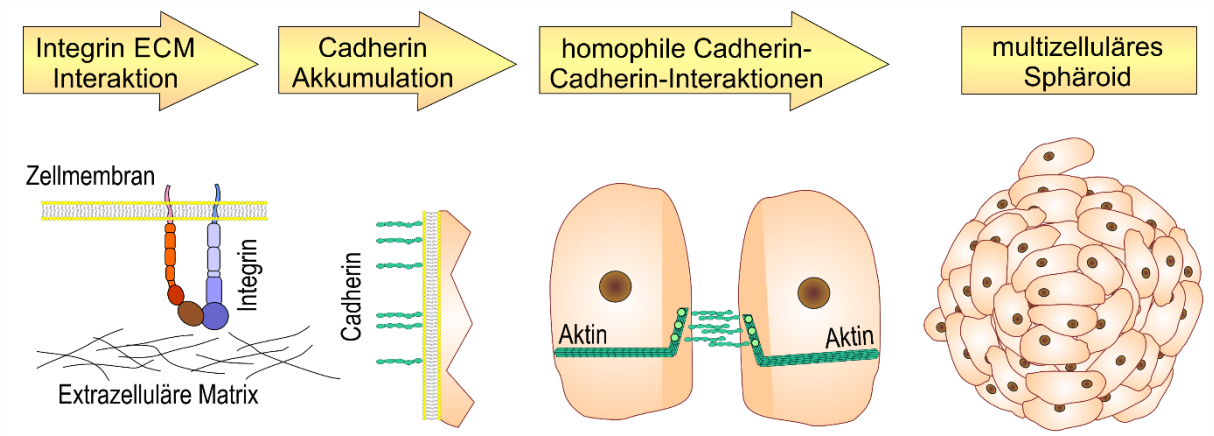

Abbildung 3 angelehnt an Quelle (21) MCS-Bildungsprozess: Die Zellen bilden lose Bindungen durch Integrin-ECM-Interaktion. Es folgt eine Phase der Cadherin-Expression und Akkumulation auf der extrazellulären Oberfläche. Ein kompaktes MCS bildet sich durch homophile Cadherin-Cadherin-Interaktionen.

Aufgrund dieser Charakteristika können MCS und Organoide auch als *in vitro* 3D-Tumormodelle dienen (Abbildung 4). Sie bieten ein hohes Potenzial für die präklinische Entwicklung von Krebsmedikamenten und für die Untersuchung der Prozesse der Tumorprogression und Metastasierung auf molekularer Ebene.

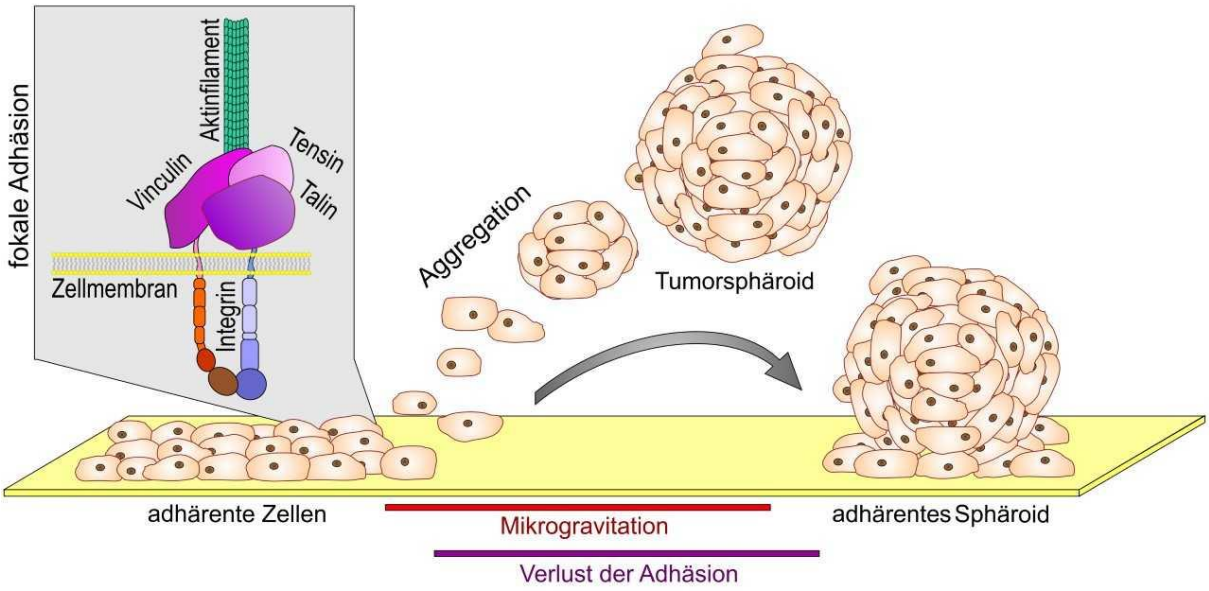

Abbildung 4 angelehnt an Quelle (13) Schematische Darstellung des µ*g*-induzierten *in vitro* Metastasierungsmodells: Wenn adhärente Tumorzellen µg ausgesetzt werden, regulieren sie die fokalen Adhäsionsmoleküle (FA) herunter. Die Zellen lösen sich ab und es bilden sich den Mikrometastasen ähnliche Tumorsphäroide. Wenn die Schwerkraft wiederhergestellt ist, heften sich die Sphäroide wieder an ihr Substrat.

5.6. Tensegrity-Modell und das Zytoskelett als Gravitations-Sensor

Da sich das Leben auf der Erde unter dem ständigen Einfluss der Schwerkraft entwickelt hat, ist es wichtig, die Auswirkungen dieser Kraft auf die Zellphysiologie zu verstehen.

Mechanische Kräfte wie die Schwerkraft sind grundlegende Regulatoren der Gewebeentwicklung. Allerdings ist der genaue Mechanismus der sogenannten Mechanotransduktion noch nicht abschließend erforscht. Unter Mechanotransduktion versteht man den Vorgang, der in einer Zelle abläuft, wenn mechanische Signale wahrgenommen und diese dann in eine biochemische Reaktion umgewandelt werden (22).

Aktin-Mikrofilamente, Mikrotubuli und Intermediärfilamente bilden die drei wichtigsten Filament-Komponenten des Zytoskeletts. Sie sind durch verschiedene Vernetzungsproteine sowohl zur Bildung größerer Fibrillen miteinander als auch zur Bildung strukturell gekoppelter Netzwerke untereinander verbunden. Die verschiedenen Filamentsysteme des Zytoskeletts sind außerdem mit Zell-Zell-Adhäsionskomplexen verknüpft. Durch diese Koppelungen wird im Zytoskelett eine Art Zugvorspannung erzeugt, da ein Gleichgewicht zwischen entgegengesetzten Kräften herrscht, die in diesem Netzwerk verteilt sind. Das sind einerseits die kontraktilen Aktomyosin-Filamente, die aktiv Zugkräfte aufbauen, und andererseits sowohl die intrazellulären Mikrotubuli als auch die extrazellulären Anbindungsstellen an die ECM und an andere Zellen, die der erzeugten Kompression entgegenwirken, wie in Abbildung 5 dargestellt ist.

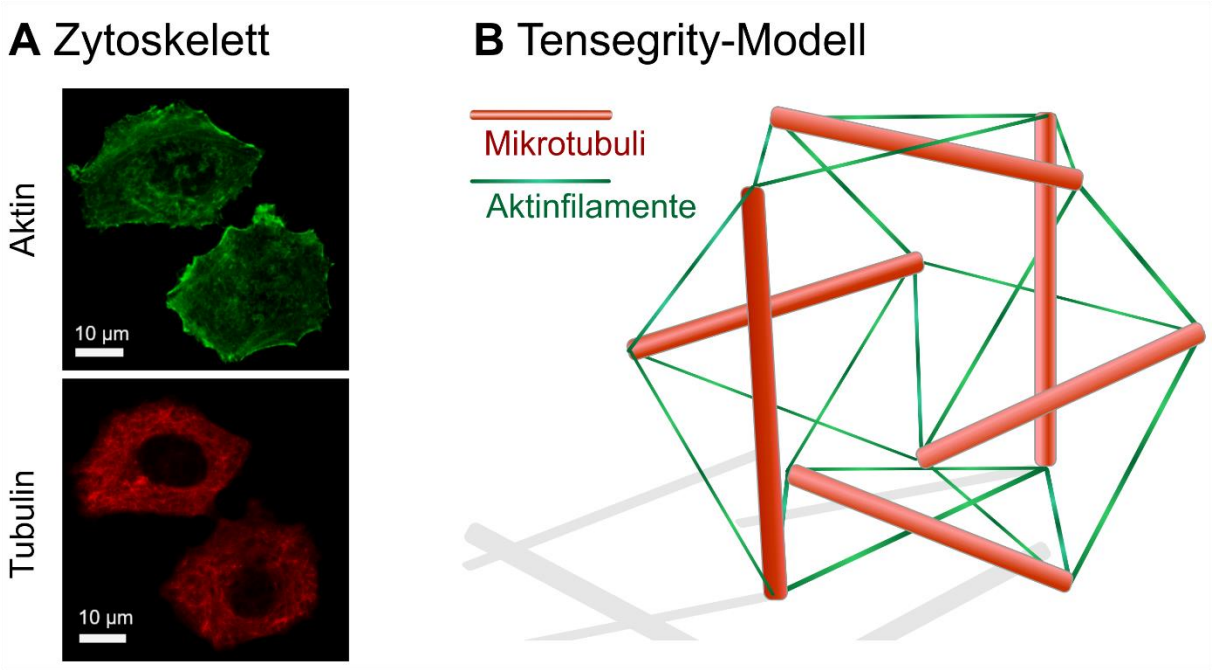

Abbildung 5 angelehnt an Quelle (23) Vergleich des zellulären Zytoskeletts mit einer Tensegrity-Struktur: **A** Bild zweier Zellen, aufgenommen mit Fluoreszenzmikroskopie. In Grün sind die Aktinfilamente und in Rot die Mikrotubuli dargestellt. **B** Beispiel eines Tensegrity-Modells, das aus sechs Streben = Mikrotubuli (24) als Druckelemente und 19 Kabeln = Aktinfilamente (grün) als Vorspannungselemente besteht.

Die Zelle wird auch als eine hierarchische und multimodulare Tensegrity-Struktur betrachtet. Sie ist hierarchisch, weil kleinere Elemente der Zelle ihrerseits ein eigenes unabhängiges und selbststabilisierendes Netzwerk besitzen. Beispielsweise wird der Zellkern durch sein eigenes molekulares Skelett oder Kerngerüst gestützt. Unter der Oberflächenmembran der Zelle befindet sich das submembranöse Zytoskelett als eigene Struktur. Die Aktomyosin-Filamentbündel, die die Spannung innerhalb der Zelle erzeugen, stellen ein weiteres Netzwerk dar.

Der Nukleus, das submembranöse Zytoskelett und die Aktomyosin-Filamentbündel setzen sich wiederum aus Molekülen und Molekülgruppen zusammen, die ihre Formstabilität auf ähnliche Weise durch die Herstellung von Spannungsintegrität aufrechterhalten (25). Dieses flexible Netzwerk verleiht der Zelle sowohl Form als auch mechanische Stabilität, die für eine normale Zellfunktion unabdingbar sind.

Vorselen *et al.* vermuten, dass das Zytoskelett der Zelle als möglicher Sensor der Gravitation fungiert (26). Das Zytoskelett ist in der Lage, die durch die Schwerkraft verursachten Veränderungen wahrzunehmen. Um dies zu tun und Veränderungen auf zellulärer Ebene zu bewirken, muss diese Kraft jedoch zunächst auf Rezeptoren an der Zellmembran übertragen werden, die für mechanische Signale empfänglich sind, und dann auf nachgeschaltete Signalwege, die schließlich die Zellfunktion beeinflussen (1). Die Membranrezeptoren, auf die das mechanische Signal übertragen wird, sind spannungsempfindliche Proteine in FA und mechanosensitive Ionenkanäle.

FAs sind eine Klasse von Transmembrankomplexen, die mit der extrazellulären Matrix und dem Aktinzytoskelett in der Zelle verbunden sind. Interne oder externe Kräfte können auf verschiedene

Weise auf FAs einwirken, indem entsprechende Proteine innerhalb der FA reguliert werden und z.B. neue Proteinbindungsstellen erzeugt werden.
Mechanosensitive Ionenkanäle sind eine Klasse von Kanälen, die von einem geschlossenen in einen offenen Zustand übergehen können, wenn die Spannung auf der Zellmembran zunimmt. Die Öffnung der meisten Kanäle erfordert eine Bindung des Kanals an krafttragende Elemente, d. h. an die extrazelluläre Matrix außerhalb der Zelle und das Zytoskelett innerhalb der Zelle.
Neuere Studien, zusammengefasst in Quelle (27), deuten auch darauf hin, dass Aktin selbst als mechanosensitive Struktur fungieren kann.
Neben der Rolle des Zytoskeletts als lasttragende Struktur und als Regulator für die Mechanotransduktion spielt es auch eine wesentliche Rolle bei der Kraftübertragung (26).

5.7. Das Prostatakarzinom

Das Prostatakarzinom ist die häufigste Tumorerkrankung des Mannes. Dabei stellt es nach dem Lungenkarzinom die zweithäufigste Todesursache durch Karzinome dar. Die Lebenszeitprävalenz eines Mannes, an einem Prostatakarzinom zu erkranken, beträgt circa 15%. Das mittlere Erkrankungsalter liegt bei 70 Jahren. Das Lebensalter stellt somit den Hauptrisikofaktor für eine Erkrankung dar (28).
Die maligne Transformation der Prostatazellen erfolgt in einem mehrstufigen Prozess, der mit einer intraepithelialen Neoplasie im Prostatagewebe beginnt, gefolgt von einem lokal begrenzten Prostatakarzinom und einem fortgeschrittenen Adenokarzinom der Prostata mit lokaler Invasion, das schlussendlich zu einem metastasierten Prostatakarzinom führt. Ein zentrales Merkmal des Prostatakarzinoms ist seine Hormonempfindlichkeit. Daher ist die Androgendeprivationstherapie mit Wirkstoffen, die den Androgen-Signalweg blockieren heute der Behandlungsstandard bei Prostatatumoren. Im Therapieverlauf kann sich allerdings eine Resistenz gegen die Androgendeprivationstherapie entwickeln, die zu primärem kastrationsresistenten oder metastasiertem kastrationsresistenten Prostatakrebs führt. In den letzten Jahren hat die Zahl der Prostatakarzinome mit niedrigem Androgenrezeptor (AR) oder aggressiver AR-Variante mit neuroendokrinen Merkmalen oder kleinzelligen Merkmalen in der Klinik zugenommen, was mit dem Einsatz potenter AR-Antagonisten zusammenhängen könnte (29).
Im Vergleich zu anderen Tumorarten metastasiert das Prostatakarzinom vor allem in das Skelett (84 %) und in die Lymphknoten (10,6 %). Darüber hinaus ist eine Ausbreitung in die Leber (10,2 %) und den Thorax (9,1 %) ebenfalls häufig (24).
Im Allgemeinen schreitet das Prostatakarzinom sehr langsam voran. Die 5-Jahres-Überlebensrate für die meisten Männer mit regional begrenztem Prostatakarzinom liegt bei fast 100 %. Wird allerdings bereits eine Metastasierung (ab M1-Stadium nach TNM) diagnostiziert, sinkt die 5-Jahres-Überlebensrate drastisch auf 31 % (24).

Daraus lässt sich ableiten, dass der Prozess der Metastasierung einen großen Einfluss auf die Sterblichkeit und die allgemeine Lebensqualität der Patienten mit Prostatakarzinom hat (24). Im metastasierten Stadium endet das Prostatakarzinom selbst nach intensiver multimodaler Behandlung meist tödlich. Daher ist es dringend erforderlich, das Wissen über die Biologie, die Genomik und die Proteomik des Prostatakarzinoms zu erweitern, um neue Angriffspunkte für die Arzneimittelentwicklung zu finden.

In meiner durchgeführten Versuchsreihe wurde die Prostatakarzinomzelllinie PC-3 verwendet. Die PC-3-Zelllinie (ECACC 90112714) wurde von der '*European Collection of Authenticated Cell Cultures*' (ECACC) erworben. Die Zellen stammen aus dem Tumorgewebe eines 62-jährigen kaukasischen Mannes, der an einem Prostata-Adenokarzinom Grad 4 litt.
Diese Zellen reagieren nicht auf Androgene, Glukokortikoide oder Fibroblasten-Wachstumsfaktoren (30), aber es gibt Hinweise darauf, dass die Zellen von epidermalen Wachstumsfaktoren beeinflusst werden können (31).
PC-3-Zellen haben ein hohes Metastasierungspotenzial, während die Prostatakarzinomzelllinien DU145 und LNCaP ein mäßiges bis geringes Metastasierungspotenzial besitzen (32). Vergleiche der Proteinexpression von PC-3, LNCaP und anderen Zelllinien haben gezeigt, dass die PC-3-Zelllinie für das kleinzellige neoendokrine Karzinom charakteristisch ist. Bei der Mehrzahl der Prostatakarzinome handelt es sich um Adenokarzinome, die durch Drüsenbildung und die Expression der luminalen Differenzierungsmarker, wie dem AR und dem prostataspezifischen Antigen (PSA), gekennzeichnet sind. Die meisten Adenokarzinome sind indolent und androgenabhängig. Das kleinzellige neuroendokrine Karzinom der Prostata (SCNC) ist eine Variante des Prostatakrebses. Im Gegensatz zum Adenokarzinom bilden die Tumorzellen des SCNC keine Drüsen und sind negativ für AR und PSA. SCNC ist äußerst aggressiv und spricht nicht auf eine Hormontherapie an. Die PC-3- Zelllinie exprimiert weder PSA noch AR und ist eher durch aggressives Wachstum gekennzeichnet, sodass sie eher die Charakteristika des kleinzelligen Prostatakarzinoms besitzt (30).

5.8. Ergebnisse und Diskussion der zugrundeliegenden Publikationen

In diesem Abschnitt werde ich die drei dieser Dissertation zugrundeliegenden Publikationen erläutern und zusammenfassen.

5.8.1 Der Einfluss von simulierter Mikrogravitation auf den VEGF-, MAPK- und PIK3-Signalweg

Verschiedene Experimente mit Schilddrüsentumorzellen und Mammakarzinomzellen (33, 34) ergaben, dass diese Tumorzellen durch s-µ*g*-Exposition (RPM) Sphäroide bilden. Auch PC-3 Zellen in Fibroblasten-Co-Kultur bilden MCS aus, wenn sie auf der High-Aspect-Ratio-Vessel (HARV) gezüchtet werden (35).
Aufgrund dieser Kenntnisse war im Rahmen der ersten Publikation ***Hybel TE, Dietrichs D, Sahana J, Corydon TJ, Nassef MZ, Wehland M, Krüger M, Magnusson NE, Bauer J, Utpatel K, Infanger M, Grimm D, Kopp S: Simulated Microgravity Influences VEGF, MAPK, and PAM Signaling in Prostate Cancer Cells. Int J Mol Sci. 21. 1263 (2020)*** das Ziel zu erarbeiten, ob die Exposition von PC-3-Zellen auf der RPM die Bildung von MCS induziert und die Expression von Genen verändert, die mit der Angiogenese, der Metastasierung, dem Zytoskelett, der ECM und den FAs assoziiert sind.
Insbesondere wurde dabei die Genexpression von Signalfaktoren des vaskulären endothelialen Wachstumsfaktors (VEGF), der mitogen-aktivierten Proteinkinase (MAPK) und des PI3K/AKT/mTOR (PAM)-Signalwegs untersucht. In dieser Publikation konnte eine detaillierte transkriptionelle und immunhistochemische Analyse der PC-3 Sphäroidbildung erhoben werden.
Dazu wurden PC-3-Zellen über einen Zeitraum von 3 und 5 Tagen auf der RPM kultiviert. Nach RPM-Exposition konnten zwei unterschiedliche Zellverbände unterschieden werden: Am Boden der Zellkulturflasche wuchsen weiterhin adhärente Zellen (AD) in Monolayern (einlagige Zellschicht). Einige Zellen gingen allerdings in Suspension und bildeten kleinere MCS. Je länger die Zellen der s-µ*g* ausgesetzt waren, desto mehr formten sich 3D Sphäroide.

Das Genexpressionsmuster der entstandenen MCS und AD Zellen wurde nach drei und fünf Tagen s-µ*g*-Exposition miteinander und mit den statischen 1*g*-Kontrollen verglichen. Als weitere Analyseverfahren wurden Immunfluoreszenzfärbungen zur Untersuchung des Zytoskeletts, histologische Färbungen zur Bestimmung der Morphologie und ein ‚*Time-Resolved Immunofluorometric Assay*' (TRIFMA) zur Analyse der Zellkulturüberstände durchgeführt.

1. Untersuchung des Zytoskeletts und der Extrazellulären Matrix

Der Einfluss der RPM-Exposition auf das Zytoskelett wurde durch Rhodamin Phalloidin zur Detektierung von F-Aktin und durch β-Aktin Immunfluoreszenzfärbung visualisiert. Es fand eine Umverteilung von F-Aktin sowohl nach drei als auch nach fünf Tagen auf der RPM statt. In den AD-

Zellen akkumulierte das F-Aktin vor allem kortikal, während in den Zellen der MCS eine Anhäufung von F-Aktin an der Zellmembran ersichtlich war. Nach drei Tagen begann die Bildung von Filopodien und Lamellipodien, nach fünf Tagen waren zusätzlich auch Stressfasern nachweisbar. Die Bildung von Lamellipodien und Filopodien sowie die verstärkte Transkription des *VCL*-Gens, welches die FA-Komponente Vinculin kodiert, könnten ein Ausdruck dessen sein, dass die zelluläre Anhaftung an die ECM durch s-µ*g* erschwert wird und die Hochregulation von *VCL* als gegenregulatorisches Ereignis auftritt. Die entstandenen Stressfasern sprechen für eine Kompensation der reduzierten Zelladhäsion und der veränderten Zellmorphologie (36).
Die beschriebenen morphologischen Veränderungen sind vereinbar mit der erhöhten *ACTB*- und *TUBB*-Genexpression nach 5 Tagen RPM-Exposition. Ähnliche Effekte zeigten sich bei s-µ*g* Experimenten mit follikulären Schilddrüsentumorzellen und Endothelzellen (37, 38).
Im Allgemeinen bestand die Tendenz zu erhöhten mRNA-Leveln der ECM-Komponenten als Reaktion auf die RPM-Exposition. Die mRNA-Level der *COL1A1*-, *COL4A5*-, *LAMA3*-, *LAMB2*- und *FN1*-Gene waren bis auf wenige Ausnahmen hochreguliert oder unverändert. Darüber hinaus wurde in den Sphäroiden eine Kollagenablagerung festgestellt. Eine mögliche Erklärung für diesen Befund könnte sein, dass die Zellen versuchen, die ECM zu expandieren, um den Belastungen durch s-µ*g* zu widerstehen. Die ECM bietet den Zellen strukturelle Unterstützung (39), die ihnen nach der Ablösung durch die RPM-Exposition fehlt. Die Ergebnisse in Bezug auf die ECM passen zu den Ergebnissen einer Studie mit humanen fötalen Osteoblasten, die s-µ*g* ausgesetzt waren, in der die Zellen ebenfalls Kollagenablagerungen in Sphäroiden und eine erhöhte *FN1*- und *LAMA1*-Genexpression zeigten (40).

2. Untersuchung der Signaltransduktion

Die verstärkte Angiogenese ist einer der biologischen Prozesse, die an der Metastasierung von Tumoren beteiligt sind, da eine verstärkte Neovaskularisierung und Sauerstoffversorgung das Tumorwachstum, die Invasion und die Metastasierung erleichtern.
Der VEGF-Signalweg ist dabei von besonderem Interesse, da metastasierende Prostatakarzinomzelllinien allgemein eine erhöhte Genexpression der proangiogenen Zytokine IL-8, TGFβ und von Proteinen aus der VEGF-Familie zeigen (41). Sowohl die physiologische als auch die pathologische Angiogenese wird in erster Linie durch die VEGF-Familie reguliert. Diese Familie setzt sich aus verschiedenen Protein-Isoformen zusammen, die jeweils an ihren spezifischen Tyrosinkinase-Rezeptor an der Zelloberfläche binden. Vor allem VEGF-A ist in die Angiogeneseprozesse des Prostatakarzinoms involviert und wird bei Prostatatumoren sowohl in Endothel- als auch in Tumorzellen überexprimiert. Eine hohe VEGF-A-Konzentration korreliert außerdem mit dem Auftreten von Fernmetastasen und einer schlechteren Prognose (42).
Dass der VEGF-Signalweg nach s-µ*g* Exposition herunterreguliert wurde, spricht für die Entwicklung eines weniger aggressiven Phänotyps unter s-µ*g*-Bedingungen. Vergleichbare Resultate konnten auch bei niedrig differenzierten FTC-133 Schilddrüsenkarzinomzellen festgestellt werden, die ebenfalls in s-

µ*g*-Bedingungen auf der RPM kultiviert worden waren. Dabei war die Genexpression von *VEGFA* ebenfalls sowohl in RPM-AD-Zellen als auch in MCS-Kulturen herunterreguliert (17, 43).
Im Gegensatz dazu war die Expression der Gene für die VEGF-Rezeptoren *FLT1* und *FLK1* nach fünf Tagen in MCS hochreguliert. Dies könnte auf eine Gegenregulation der Rezeptoren hinweisen, die durch die abnehmende VEGF-Konzentration induziert wurde.

Die Tendenz zu einem weniger aggressiven Phänotyp lässt sich auch aus der hochregulierten *CDH1*-Genexpression ableiten. *CDH1* ist ein Tumorsuppressor-Gen und kodiert das Protein E-Cadherin. E-Cadherin gehört zu einer Familie hochkonservierter Transmembranglykoproteine, die die kalziumabhängige Zelladhäsion unterstützen. Das wird erreicht, indem die E-Cadherine einen Komplex mit den Cateninen bilden, die eine andere Gruppe zytosolischer Proteine darstellt (44). Die Inaktivierung von E-Cadherin ist nachweislich an der Entstehung von Prostatakarzinomen beteiligt (45, 46).

Der PI3K/AKT/mTOR-Signalweg spielt eine Schlüsselrolle bei der Metastasierung von Tumoren und könnte gleichzeitig an der Bildung von 3D-Sphäroiden in s-µ*g* beteiligt sein. Die Dysregulation der mTOR- und PI3K/ERK1/2-Signalwege, die eine gegenseitige Rückkoppelung aufweisen, ist bei der Tumorentstehung von *Glioblastoma multiforme* involviert. Die Zellproliferation wurde durch die kombinierte MEK1/2- und mTOR-Inhibition im Vergleich zur alleinigen mTOR-Inhibition signifikant unterdrückt. Daraus könnte als Grundlage für die Therapie des Glioblastoma multiforme eine Behandlung mit kombinierten Inhibitoren abgeleitet werden (47).
Die Genexpression von AKT/PKB war sowohl in AD- als auch in MCS-Proben nach einer fünftägigen RPM-Exposition erhöht. Außerdem konnte eine Hochregulierung der *MTOR*-Genexpression in allen RPM-exponierten Zellproben nach fünf Tagen beobachtet werden. Dies stimmt mit den Ergebnissen von Clejan *et al.* (48) überein. In dieser Studie wurden DU-145-Zellen des menschlichen Prostatakarzinoms für 14 Tage s-µ*g* ausgesetzt, indem sie auf dem HARV kultiviert wurden. Nach sechs Tagen konnte ebenfalls eine Aktivierung des PI3K/AKT-Signalwegs beobachtet werden. Dabei konnte eine Interaktion zwischen den Ceramid- und PI3K-Signalwegen festgestellt werden. Einhergehend mit der Aktivierung von PI3K tritt die Herabregulierung von Ceramid auf (48). Ceramid moduliert die Aktivität von Enzymen des Sphingolipid-Stoffwechsels, dadurch kommt es unter anderem zur Hemmung des Zellwachstums, zur Induktion von Apoptose, zur Förderung der Zelldifferenzierung und der Zellalterung (49). Zusammen mit weiteren Aktivierungen und Überschneidungen von mehreren Signalwegen könnten diese Ergebnisse das 3D-Wachstum erklären (48).

Der RAS/MAPK-Signalweg ist bei menschlichen Tumoren einschließlich dem Prostatakarzinom häufig dysreguliert. Mutationen oder Amplifikationen im *RAS*-Gen oder *BRAF*-Gen wurden bei primärem und metastasiertem Prostatakarzinom mit einer Inzidenz von 1–8 % festgestellt. Zudem wird berichtet, dass

eine verstärkte MAPK-Signalübertragung mit Kastrationsresistenz und metastatischem Wachstum korreliert (50).

Es ist zu beachten, dass aktives Ras auch andere Signalwege wie den PI3K/AKT/mTOR (PAM) Signaltransduktionsweg aktivieren kann (51). Zur Analyse des MAPK-Signalwegs wurden die Genexpression von *RAF1*, *MEK1* und *ERK1/2* bestimmt. Es wurde festgestellt, dass *RAF1* in AD-Zellen, nicht aber in MCS-Zellen hochreguliert ist. Dies deutet auf seine Aktivierung durch s-µ*g* und seine mögliche Beteiligung an der Sphäroidbildung hin. Die *MEK1*-Genexpression war mit dem mRNA-Level von *RAF1* vergleichbar und war in den AD-Zellen nach 5 Tagen RPM-Exposition signifikant erhöht. Auch die *ERK1/2*-Genexpression war nach 5 Tagen s-µ*g* in AD und MCS im Vergleich zu 1*g*-Proben signifikant hochreguliert. Sowohl *ERK1* als auch *ERK2* scheinen ebenfalls an der 3D-Aggregation in µ*g* beteiligt zu sein.

Darüber hinaus ergaben sich interessante Ergebnisse durch die Analyse der Signaltransduktionswege (Pathway-Analyse). Die Abbildung 6 zeigt die Ergebnisse der Pathway-Analyse von 23 relevanten differenziell exprimierten Genen. Diese ist im molekularen Aktionsmodus dargestellt. Es ist zu erkennen, dass die untersuchten Gene Mitglieder eines komplizierten Netzwerks sind, das die zentralen Faktoren *CDH1, VCL, TLN1, FN1, VEGFA, KDR, RAF1, ERK1/2, MAP2K1, MTOR, AKT1, PTK2* und *SRC1* umfasst. Von diesen Komponenten ist *CDH1* als der wichtigste zentrale Knotenpunkt zu ermitteln.

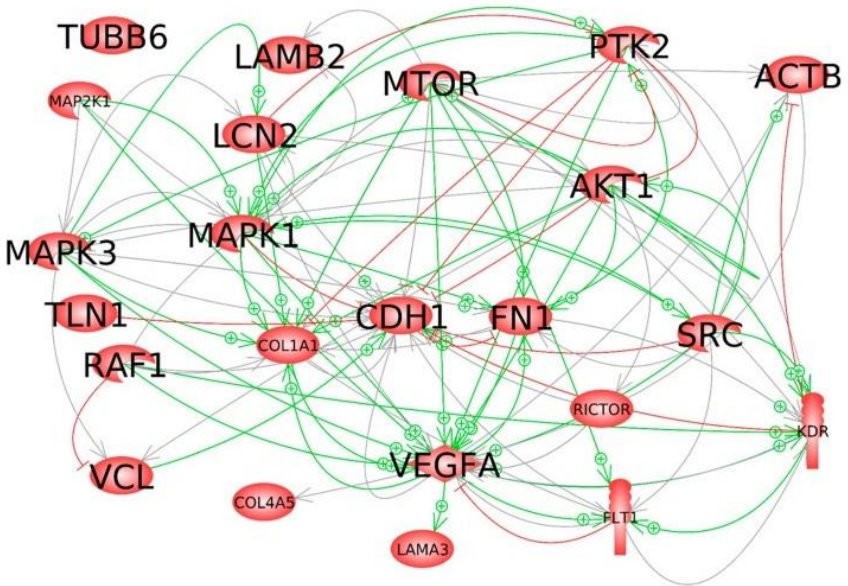

Abbildung 6 (aus Publikation 1, Abb. 6) Interaktionsnetz ausgewählter Elemente auf Genexpressionsebene: 22 von 23 ausgewählten Genen, die mittels qPCR analysiert wurden, tragen zu dem umfassenden Netzwerk von 114 Interaktionen bei. Grüne Pfeile zeigen die Aktivierung und rote Pfeile die Hemmung an. Graue Linien zeigen an, dass Wechselwirkungen stattfinden, deren Auswirkungen noch nicht geklärt sind. Das Interaktionsnetzwerk wurde mit der Elsevier Pathway Studio plus Software erstellt.

Durch diese Analyse wurden verschiedene Interaktionen gefunden, von denen *VCL, FN1, mTOR, SRC1* und *VEGFA* als dominante Zielgene angegeben werden.
Es gibt Wechselwirkungen unter anderem zwischen Vinculin und Fibronektin. *FN1* und *VCL1* wurden beide in MCS nach drei- und fünftägiger RPM-Exposition hochreguliert. Kliewe et al. (52) zeigten in *FN1*-Knock-Out-Podozyten eine signifikante Herabregulierung der FA-Proteine Talin, Vinculin und Paxillin. Zudem konnte eine verminderte Zellausbreitung festgestellt werden. Diese Ergebnisse legen nahe, dass FN1 eine wichtige Rolle bei der Adhäsion spielt (52).
Diese Daten unterstützen die Hypothese, dass die Interaktion mit Vinculin ein adaptiver Mechanismus zum Schutz von µ*g*-exponierten Prostatatumorzellen und anderen Zelltypen ist.

3. Zusammenfassung der Publikation 1

Zusammenfassend konnte diese Studie zeigen, dass die Exposition von PC-3 Tumorzellen über einen längeren Zeitraum in simulierter Mikrogravitation die Expression von Genen reguliert, die am VEGF-, MAPK-, und PAM-Signalweg, an der Signaltransduktion im Zytoskelett, der ECM und den FAs beteiligt sind.
Darüber hinaus wurde eine Umverteilung von F-Aktin in den Zellen, eine Ablagerung von Kollagen im MCS und eine verringerte Sekretion von VEGF und NGAL festgestellt. Dadurch konnte nachgewiesen werden, dass s-µ*g* Einfluss auf die Prozesse der Angiogenese, Zellmorphologie, Migration, Adhäsion, ECM und 3D-Wachstum hat.
Ein weiterer Fokus lag auf der Bildung von Sphäroiden unter s-µ*g* Bedingungen. MCS könnten als wertvolle Werkzeuge für künftige Medikamentenstudien in der Onkologie dienen, da sie die zelluläre Umgebung in Tumormetastasen besser widerspiegeln als Monolayer-Zellkulturen. Ein künftiges Projekt könnte darin bestehen, die Auswirkungen von Medikamenten unter s-µ*g* Bedingungen zu untersuchen, die auf die in dieser Studie regulierten Schlüsselproteine oder Signalwege in PC-3-Zellen abzielen. Langfristig könnten auf diese Weise Experimente mit Prostatakarzinomzellen unter den Bedingungen von s- und/oder r-µ*g* zu Erkenntnissen über mögliche neue Behandlungsmöglichkeiten von Prostatatumoren beitragen und daher auch die Notwendigkeit von Tierversuchen in der Forschung reduzieren.

5.8.2 Kurzzeit-RPM-Versuche beeinflussen die Sekretionsrate und Genexpression von Zytokinen

Im Rahmen der zweiten Publikation ***Dietrichs D, Grimm D, Sahana J, Melnik D, Corydon TJ, Wehland M, Krüger M, Vermeesen R, Baselet B, Baatout S, Hybel TE, Kahlert S, Schulz H, Infanger M, Kopp S: Three-Dimensional Growth of Prostate Cancer Cells Exposed to Simulated Microgravity. Front Cell Dev Biol. 10. 841017 (2022)*** wurden die Auswirkungen einer kurzzeitigen (30 min, 2, 4 und 24 Stunden) s-µ*g*-Exposition mittels einer RPM auf PC-3-Prostatakarzinomzellen untersucht.

Von Vorteil ist, dass so bereits frühe Effekte der RPM-Exposition detektiert werden können. Das Hauptziel dieser Studie war es, mögliche Veränderungen der Genexpression und der Sekretionsleistung der PC-3-Prostatatumorzellen, die auf der RPM gezüchtet wurden, zu untersuchen. Zudem lag weiterhin ein Schwerpunkt dieser Untersuchung auf möglichen Veränderungen im Zytoskelett, der ECM, dem PAM-Signalweg und der Sekretion von Zytokinen durch die PC-3-Zellen.
In einem weiteren Versuchsansatz wurden 3D-Sphäroide unter 1*g*-Bedingungen mit der Liquid-Overlay-Technik hergestellt, um sie als Kontrolle für die 3D-Sphäroide, die unter s-µ*g* entstanden sind, zu verwenden. Die Liquid-Overlay-Technik ist eine seit langer Zeit etablierte Methode zur Erzeugung von Sphäroiden in statischen Zellkulturen. Dabei werden Zellen in Suspension an der Adhäsion am Substrat durch einen dünn aufgebrachten Agarosefilm gehindert und auf diese Weise die Sphäroidbildung induziert (53). Die Genexpression ausgewählter Faktoren wurde in den 1*g*-MCS anschließend untersucht.
Im Anschluss erfolgten qPCR Untersuchungen, eine Immunofluoreszenz-Färbung zur Visualisierung des zellulären Fibronektins, ein ‚*Terminal deoxynucleotidyl transferase dUTP nick end labeling*' (TUNEL)-Assay zum Nachweis von entstandenen DNA-Brüchen in der Endphase der Apoptose, ein ‚*Multiplex Bead Array*' zur Konzentrationsbestimmung ausgewählter Proteine im Zellkulturüberstand und eine STRING/EMBL-Analyse zur Detektion von möglichen Wechselwirkungen und gegenseitigen Expressionsabhängigkeiten der untersuchten Proteine.

1. Morphologische Veränderungen unter simulierter Mikrogravitation

Morphologische Veränderungen nach Kurzzeit-RPM-Exposition, die mit denen nach drei- und fünftägiger RPM-Exposition vergleichbar sind, traten erst nach 24 Stunden auf.
Mit der Liquid-Overlay-Technik wurden MCS unter 1*g*-Bedingungen innerhalb von 24 h erzeugt. Die MCS-Bildung und die Vitalität der PC-3 Sphäroide wurden mikroskopisch untersucht. In den 1*g*-MCS sind die Zellen nur lose miteinander verbunden, während sich die RPM-MCS runder und kompakter präsentierten. Der TUNEL-Assay ergab eine geringere Lebensfähigkeit der 1*g*-MCS mit entsprechend erhöhter Genexpression von *CASP3*, *CASP8* und *CASP9* im Vergleich zur Kontrolle, was möglicherweise die Expression der Zytokine, der Zytoskelettkomponenten und anderer Faktoren beeinflussen könnte.
Bei den RPM-MCS war keine Erhöhung der Caspasen mRNAs oder andere Anzeichen für Apoptose nachweisbar.
Es lässt sich daher folgern, dass die 1*g*-MCS, die mit der Liquid-Overlay-Technik hergestellt wurden, kein geeignetes Modell darstellen, um die frühen Phasen der Tumorprogression und Metastasierung beim Prostatakarzinom zu untersuchen.

2. Simulierte Mikrogravitation beeinflusst die Expression und Freisetzung von inflammatorischen Zytokinen

Zytokine und Chemokine stellen zusammen mit ihren Rezeptoren und Signalwegen wichtige Faktoren dar, die die Metastasierung von Prostatakarzinomen fördern. Diese Proteine sind am Umbau der extrazellulären Matrix, an der epithelial-mesenchymalen Transition (EMT) und an der Angiogenese beteiligt. Zudem fördern sie Prozesse, die zum Metastasierungsgeschehen beitragen. Zum Beispiel spielen sie eine Rolle bei der Tumorinvasion, der Bildung prämetastatischer Nischen und bei der Umwandlung der Mikroumgebung des metastatischen Tumors. Die wichtigsten Vertreter sind unter anderem IL-6, CXCL12, TGFβ, CXCL8 (IL-8), VEGF, RANKL, CCL2, CX3CL1, IL-1, IL-7, CXCL1 und CXCL16 (41).

Es wird angenommen, dass einige Zytokine zudem eine wichtige Rolle bei der Bildung von Sphäroiden spielen. Beispielsweise ist IL-6 in PC-3-Zellen sowie in anderen Prostatakarzinomzelllinien (LNCaP, DU145) im Vergleich zu normalen Prostataepithelzellen hoch exprimiert und wirkt als proliferativer autokriner und parakriner Faktor beim Prostatakarzinom. Zudem geht ein erhöhter Serum- und Plasmaspiegel von IL-6 und des löslichen IL-6-Rezeptors mit einer Progression der Erkrankung und einer schlechten Prognose bei Patienten mit Prostatakarzinom einher (54). Darüber hinaus kann IL-6 direkt die Entwicklung neuer Blutgefäße, die Proliferation und Migration von Endothelzellen induzieren und damit tumorfördernd wirken. Das geschieht mit einer ähnlichen Effektivität wie durch VEGF. Allerdings weisen die Blutgefäße, deren Bildung durch IL-6 induziert wurde, im Gegensatz zu physiologischen Blutgefäßen einen Mangel an Pericyten auf. Interessanterweise können derartige Blutgefäße die Metastasierung in größerem Umfang fördern (55).

Nach zweistündiger RPM-Exposition stieg die *IL6*-Genexpression kurzzeitig stark an. Dabei erreichte sie im Vergleich zu statischen 1*g*-Kontrollen einen 10-fach erhöhten Anstieg. Dieses Resultat steht im Einklang mit Daten von Grosse *et al.* (56), die vergleichbare Experimente mit FTC-133-Schilddrüsentumorzellen durchführten und zeigten, dass FTC-133-Zellen nach Inkubation auf der RPM vermehrt IL-6 sezernieren, und daraus die Schlussfolgerung zogen, dass IL-6 zusammen mit IL-8, OPN, TLN1, CTGF und NF-κB p65 an der Sphäroidbildung beteiligt ist (56).

In einer anderen Studie mit den Schilddrüsenkarzinomzelllinien ML-1 und RO-82-W-1 in Liquid-Overlay-Technik wurde nachgewiesen, dass sowohl die Zytokine IL-6 als auch IL-8 die 3D-Aggregation verbessern und dass diese Zytokine die Proteinexpression von β-Actin, β1-Integrin, Talin-1 und Ki-67 induzieren (15).

Die Genexpression und entsprechende Proteinsekrektion von CXCL8/IL-8 zeigten eine vergleichbare Veränderung wie *IL6*, was auf eine ähnliche Reaktion der entzündungshemmenden Zytokine auf die Mikrogravitation hinweist. IL-8 ist ein proinflammatorisches CXC-Chemokin, dass die Chemotaxis und Degranulation von Neutrophilen fördert. Es aktiviert mehrere intrazelluläre Signalwege, denen zwei G-Protein-gekoppelten Rezeptoren an der Zelloberfläche (CXCR1 und CXCR2) nachgeschaltet sind. Eine

erhöhte Expression von IL-8 und/oder seinen Rezeptoren wurde in Tumorzellen, Endothelzellen, infiltrierenden Neutrophilen sowie tumorassoziierten Makrophagen nachgewiesen. IL-8 wirkt somit regulatorisch auf die Mikroumgebung des Tumors ein (57).
Beim androgen-unabhängigen Prostatakarzinom fördert IL-8 im Kontext der malignen Progression außerdem das Überleben der Tumorzellen. In diesem Zusammenhang interagiert IL-8 auch mit AKT und NF-κB, sodass dadurch der Apoptose-Signalweg kontrolliert werden kann. Ferner spielt IL-8 auch eine Rolle für die Invasion und die Resistenz von PC-3-Zellen gegenüber Chemotherapeutika (58).
Daneben reguliert der CXCL8-Signalweg die Transkriptionsaktivität des Androgenrezeptors und unterstützt so den Übergang zu einer androgen-unabhängigen Proliferation von Prostatatumorzellen. Daher könnte die Hemmung der Auswirkungen der CXCL8-Signalübertragung eine wichtige therapeutische Maßnahme sein, um die Mikroumgebung des Tumors zu beeinflussen (57).
Interessanterweise kann IL-8 auch die Expression verschiedener Proteine des Zytoskeletts und des fokalen Adhäsionskomplexes regulieren. Diese Proteine nehmen Einfluss auf die Tumorprogression und Metastasierung. Vor allem die Talin-vermittelte Integrin-Aktivierung spielt dabei eine entscheidende Rolle, sodass Talin zunehmend als prognostischer Marker für das Fortschreiten von Karzinomen bis hin zur Metastasierung und als therapeutisches Angriffsziel bei fortgeschrittenen Prostatakarzinomen in den Fokus rückt (59).

Darüber hinaus können Proteine des Zytoskeletts und des fokalen Adhäsionskomplexes auch Schwerkraftänderungen wahrnehmen und haben daher einen großen Einfluss auf die Sphäroidbildung.
Die Tatsache, dass IL-1B, IL-6 und IL-8 eng an die ersten Phasen der Sphäroidbildung geknüft sind, könnte einen neuen Ansatz in der Prävention der Metastasierung von Prostatakarzinomen bieten. Die Hemmung von IL-6 oder IL-8 könnte somit vor allem bei den frühen Tumorstadien von Nutzen sein, um eine Progression der Erkrankung zu verhindern. Um noch detailliertere Ergebnisse zu erheben, sollten diese beiden Faktoren in künftigen Kurz- und Langzeitversuchen gezielt untersucht werden.

3. Epidermaler Wachstumsfaktor im Zusammenhang mit Sphäroid-Bildung und Tumorprogression

Die *EGFR*-mRNA ist in den MCS im Vergleich zu den 1*g*-Kontrollzellen hochreguliert, was auf die Beteiligung von EGFR an der 3D-Sphäroidbildung hinweist. Ähnliche Ergebnisse wurden bei Experimenten mit FTC-133 follikulären Schilddrüsentumorzellen in r-µ*g* im Weltraum während der Deutsch-Chinesischen Shenzhou-8-Weltraummission erzielt. Dabei war die *EGF*-Genexpression in AD- und MCS-Zellen deutlich hochreguliert (60).
Daneben spielt EGF eine wichtige Rolle bei der Metastasierung und Entstehung von Prostatatumoren. EGF induziert die Invasion und Migration von PC-3-Zellen und fördert so die EMT während der Tumorprogression. Die EMT ist ein Prozess, bei dem Tumorzellen dramatische Veränderungen durchlaufen und stark invasive Eigenschaften annehmen (61).

4. Interaktion ausgewählter Gene und ihrer entsprechenden Produkte, ausgewertet mit der ‚Search Tool for the Retrieval of Interacting Genes/Proteins' (STRING)-Analyse und Cytoscape 3.8.2 Plattform

Die STRING-Analyse deutet auf mehrere Interaktionen für VEGFA, EGF, EGFR, IL-1B, IL-8, IL-6, MTOR, AKT1, MMP9 und FN1 hin. Von diesen Proteinen ist bekannt, dass sie an der Bildung von Sphäroiden von PC-3-Prostatatumorzellen beteiligt sind, die in s-µ*g* kultiviert wurden (13).

Die Abbildung 7 zeigt, dass diese ausgewählten Faktoren sich gegenseitig regulieren. Die Interaktion zwischen dem VEGF- und dem EGFR-Signalweg ist bereits häufig beschrieben worden. Beide Signalwege spielen eine Schlüsselrolle beim Wachstum, der Progression, der Metastasierung und der Angiogenese von Tumorzellen. Eine Therapie mit Multikinase-Inhibitoren, die unter anderem auf VEGF-A abzielt, wird heute bei verschiedenen Arten von fortgeschrittenen metastasierenden Karzinomerkrankungen eingesetzt (62-65).

Es konnte auch eine Interaktion zwischen dem EGFR und IL-6 festgestellt werden. Dieser Befund stimmt mit den Ergebnissen einer vorherigen Studie überein, in der gezeigt wurde, dass EGFR über die Aktivierung von mTOR die Induktion des IL-6-Rezeptors fördert (66).

Die erhobenen Interaktionen weisen darauf hin, dass bei der Therapie des Prostatakarzinoms berücksichtigt werden sollte, dass die medikamentöse Hemmung mehrerer in Verbindung stehender Signalwege eine effizientere Wirkung im Vergleich zu Monotherapien aufweisen könnte.

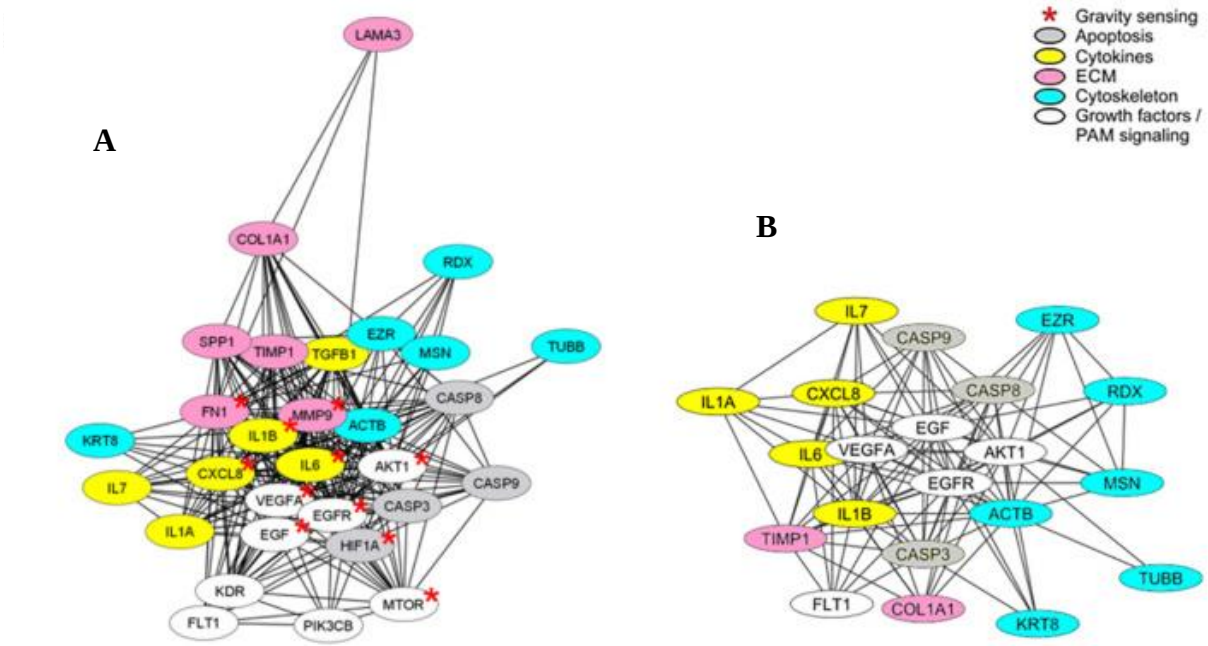

Abbildung 7 (Publikation 2, Abb. 8) Netzwerk der funktionellen Interaktion von Genen und ihren Produkten, die **A** in dieser Studie analysiert wurden und **B** die in 1*g*-MCS unterschiedlich reguliert werden. Die Analyse erfolgte mit STRING 11.0 (https://string-db.org/) und die kombinierten Ergebnisse wurden mit Cytoscape 3.8.2 visualisiert. Die Zugehörigkeit zu funktionellen Gengruppen ist farbcodiert.

Rote Sternchen kennzeichnen Gene, von denen bekannt ist, dass sie an der Schwerkraftwahrnehmung von Prostatatumoren beteiligt sind.

5. Vergleich der Kurz- und Langzeiteffekte von simulierter Mikrogravitation

Die Effekte der vorliegenden Kurz- und Langzeitexperimente in s-µ*g* sind größtenteils vergleichbar. Vor allem die Gene der ECM und des Zytoskeletts, wie z.B. *COL1A1*, *LAMA3*, *FN1* und *ACTB*, *TUBB* wurden in ähnlicher Weise durch s-µ*g* reguliert und ihre Expression erhöht, unabhängig davon, ob die PC-3-Zellen 24 Stunden, drei oder fünf Tage auf der RPM kultiviert wurden.

6. Zusammenfassung der Publikation 2

Zusammenfassend kann man aus diesen Ergebnissen ableiten, dass im Vergleich zu einem Kurzzeitsimulationsexperiment auch nach drei bzw. fünf Tagen RPM-Exposition erhebliche und größtenteils übertragbare Veränderungen der Expression von Genen des Zytoskeletts, der ECM und von Genen der PAM-Signalwege in AD-Zellen und MCS-Zellen auftraten. Das deutet darauf hin, dass zukünftig auch längere Experimente im Zeitverlauf geeignet sein könnten, um den Einfluss von Mikrogravitation auf zellulärer Ebene zu untersuchen.
Darüber hinaus konnte für mehrere zelluläre Signalwege (IL-6, IL-8, Talin und EGF) gezeigt werden, dass diese sowohl am Tumorwachstum und auf vergleichbare Weise an der Sphäroidbildung beteiligt sind. Daraus lässt sich ableiten, dass Tumorsphäroide ein geeignetes *in vitro* Modell des Metastasierungsprozesses darstellen.

5.8.3 Die 34. DLR-Parabelflugkampagne vom September 2019 (Die Effekte von kurzzeitiger Mikrogravitation auf humane Prostatakarzinomzellen)

Im Rahmen meiner Dissertation hatte ich die Gelegenheit ein Experiment auf der 34. Parabelflugkampagne des DLR durchführen zu können.
Es wurden die Effekte von kurzzeitiger Mikrogravitation auf humane Prostatakarzinomzellen untersucht (https://www.dlr.de/rd/desktopdefault.aspx/tabid-2285/3423_read-58266/). PC-3-Prostatatumorzellen wurden in einem Inkubator während eines Parabelflugs kultiviert und den Effekten von 31 Parabelflugmanövern ausgesetzt.
Die Ergebnisse wurden in der Publikation ***Schulz H, Dietrichs D, Wehland M, Corydon TJ, Hemmersbach R, Liemersdorf C, Melnik D, Hübner N, Saar K, Infanger M, Grimm D. In Prostate Cancer Cells Cytokines Are Early Responders to Gravitational Changes Occurring in Parabolic Flights. Int J Mol Sci. 23. 7876 (2022)*** zusammengefasst.

Die isolierte RNA aus den PC-3-Proben wurde mittels NGS (RNAseq) und qPCR-Techniken analysiert. Zur Visualisierung von F-Aktin wurde eine Rhodamin-Phalloidin-Färbung und anschließende mikroskopische Untersuchungen durchgeführt.
Wie bereits beschrieben (Abbildung 1) treten während eines Parabelflugs auch Phasen von Hyper-*g* (1,8 *g*) und Vibrationen auf. Um die Mikrogravitation von diesen Einflüssen zu unterscheiden, wurde die Expression von Schlüsselgenen der ECM, der FA, der PAM-Signaltransduktion, des Zellwachstums und der Apoptose zusätzlich unter 1,8 *g*-Bedingungen und unter dem Einfluss von Vibrationen untersucht.

Die Analyse und die Interaktionen differenziell exprimierter Gene und ihrer korrespondierenden Proteine wurden mittels der STRING-Datenbank, Bioconductor R-Paket DESeq2 und der ‚*Database for Annotation, Visualization and Integrated Discovery'* (DAVID) untersucht.

Durch die NGS-Analyse konnten Daten von über 298 gravitationssensitiven Genen bei den PC-3-Zellen erhoben werden und durch anschließende Anreicherungs- und Interaktionsnetzwerkanalysen kategorisiert und annotiert werden. Entscheidend für die Nutzbarkeit und Aussagekraft der erhobenen Daten ist deren Interpretation im Bezug zur Kanzerogenese.
Es konnte vor allem eine Anreicherung von Zytokinen und besonders eindrücklich von Chemokinen festgestellt werden. Im Vergleich zur Auswertung mittels qPCR, die eine niedrigere Empfindlichkeit besitzt als die NGS, konnten zusätzliche Gene identifiziert werden, die während des Parabelflugs reguliert werden. Mit Ausnahme von *TUBB* konnten alle anderen qPCR-Befunde auch in der NGS bestätigt werden. Von den 30 qPCR-getesteten Genen zeigten dabei nur die Zytokine *IL6* und *CXCL8* eine signifikante differenzielle Expression in der NGS der P1- und P31-Proben im Vergleich zur 1*g* Kontrolle.
Die 34. DLR-Parabelflugkampagne fand vom 2. bis 13. September 2019 in Bordeaux am Flughafen Bordeaux-Mérignac in Frankreich statt. Die Flüge wurden mit dem Airbus A310 ZERO-G der französischen Firma Novespace durchgeführt (67).
Normalerweise besteht eine Kampagne aus drei Flugtagen mit jeweils gleichem Versuchsaufbau. Bedauerlicherweise musste der Parabelflug des dritten Flugtags aufgrund technischer Probleme am Flugzeug abgebrochen werden. Die vorliegenden Ergebnisse leiten sich daher lediglich aus den ersten beiden Flugtagen ab.
Die PC-3-Zellen wurden nach der ersten und nach der 31. Parabel mit RNA*later* (Invitrogen, Thermo Fischer Scientific, Waltham, MA, United States) stabilisiert, wodurch die zelluläre RNase deaktiviert wird und die RNA bis zur Isolierung fixiert ist. Die Zellkulturflaschen befanden sich in einem vorgeheizten Inkubator an Bord des Flugzeugs (Abbildung 8), der im sogenannten Flight-Rack (Abbildung 8) befestigt wurde. RNA*later* wurde zu den beschriebenen Zeitpunkten manuell über Spritzen in die Zellkulturflasche eingeleitet.

Für die F-Aktin-Färbung wurden PC-3 Zellen zudem in Slideflasks (Thermo Scientific, Waltham, MA, USA) gezüchtet und ebenfalls an Bord des Flugzeugs im Flight-Rack inkubiert. Die Zellen wurden dann zu den festgelegten Zeitpunkten mit 4 % PFA (Sigma-Aldrich, St. Louis, MO, USA) fixiert. Die Slideflasks verblieben bis zur Färbung in 4 % PFA.

Abbildung 8 A Quelle (67) Die 14 Teams der 34. PFC. **B** Interview mit ESA-Astronaut Matthias Maurer an Bord des Parabelflugzeugs kurz vor Take-Off. **C** Letzte Arbeiten am Inkubator im Flight-Rack an Bord des Air-Zero-G. **D** Inkubator mit PC-3-Zellkulturflaschen und PC-3-Slideflasks innerhalb des Flight-Racks. **E** Blick in den Experimentalbereich mit den verschiedenen Flight-Racks an Bord des Parabelflugzeugs, **F** Fixierung der Zellen nach P1 mit RNA*later* **G** R-µg-Phase innerhalb einer Parabel.

Es konnten bereits nach der ersten Parabel morphologische Veränderungen mittels der F-Aktin-Färbung detektiert werden (Abbildung 9B). Dazu zählen vor allem Stressfasern und einige sporadische Ansammlungen von Pseudopodien. Nach der 31. Parabel waren diese Veränderungen deutlich stärker ausgeprägt (Abbildung 9B). Zusätzlich waren auch Lamellipodien sehr eindrücklich zu erkennen.

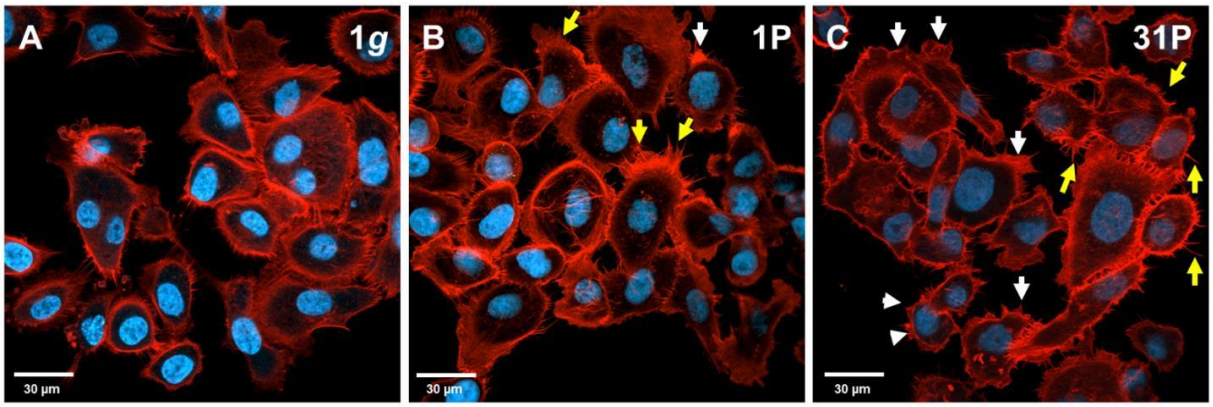

Abbildung 9 (Publikation 3, Anhang) Auswirkungen der veränderten Schwerkraft auf die intrazelluläre Organisation von F-Aktin: Konfokale Laser-Scanning-Mikroskopie von TRITC-konjugierten Phalloidin-gefärbten F-Aktin Proben. **A-C** PC-3-Zellen, die unter veränderten Schwerkraftbedingungen kultiviert wurden. **A** Statische 1 *g* Bodenkontrolle. **B** Nach der P1. **C** Nach der P31. Die weißen Pfeile

zeigen Pseudopodien und Lamellipodien und gelbe Pfeile zeigen Stressfasern an. Der dargestellte Maßstab entspricht 30 µm.

Die qPCR-Analysen der Hyper-*g*- und Vibrationsproben ergaben nur eine geringe durch die Vibration hervorgerufene Hochregulation von *IL6* und eine ebenfalls leichte Herunterregulation von *PIK3CB* durch Hyper-*g*. Die restlichen der 32 untersuchten Gene zeigten keine signifikante Veränderung für die in dieser Studie untersuchten Gene bei den Hyper-*g*- und Vibrationsexperimenten.

Die Gene der Zytokine *IL6* und *CXCL8* waren nach der P1 und der P31 bei der NGS- und qPCR-Analyse deutlich hochreguliert. Allerdings wurde *IL6* auch im Vibrationsversuch in geringerem Ausmaß hochreguliert, sodass man annehmen muss, dass die *IL6*-Regulierung zumindest teilweise auf die Flugzeugvibration zurückzuführen ist.

Darüber hinaus wurde mit Hilfe der Hauptkomponentenanalyse der Read-Counts das Expressionsprofil der 1*g*, P1 und P31 Proben bestimmt (Abbildung 10). Es konnte ein hoher Anteil der Varianz in den ersten beiden Hauptkomponenten (PC, 65 % der Varianz in PC #1 und 18 % der Varianz in PC #2) festgestellt werden. Dies ist auf die geringe Probenzahl von 15 und auf einen starken Effekt der Mikrogravitation auf die PC-3-Zellen entsprechend der eindrücklichen Veränderungen des F-Aktin-Zytoskeletts während des Parabelflugs zurückzuführen.

Die drei Bedingungen sind in der Hauptkomponente 1 (PC #1) unvollständig voneinander getrennt, mit einer tendenziellen Zwischenstellung der Messungen nach P31. Dies deutet auf einen Gewöhnungseffekt der PC-3-Zellen an die wechselnden Schwerkraftbedingungen während des Fluges hin.

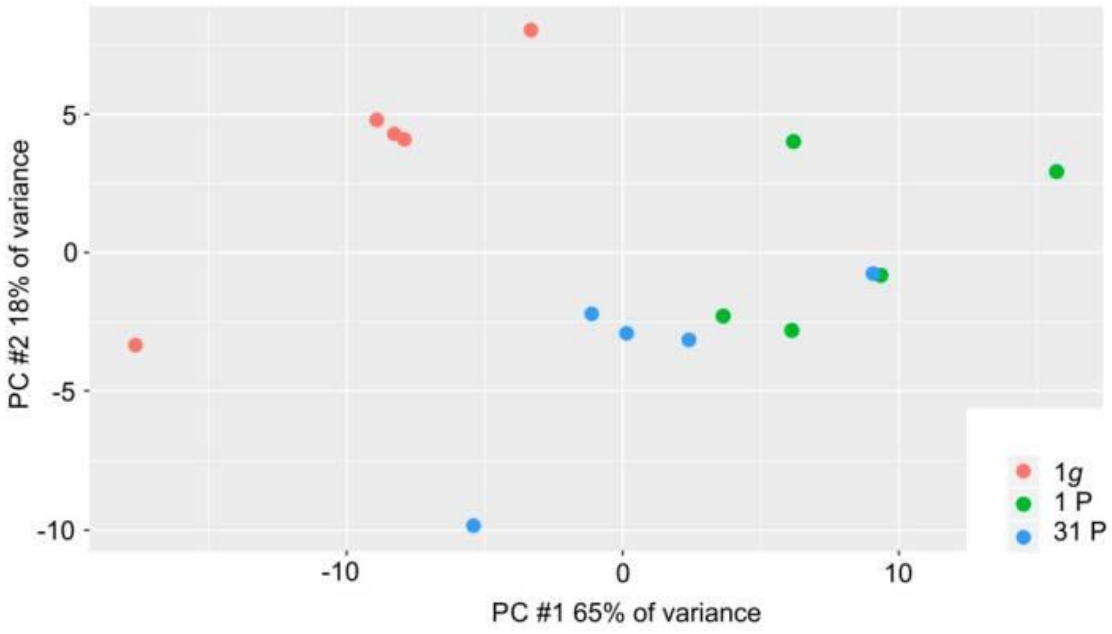

Abbildung 10 (Publikation 3, Abb. 2) Verteilung der 15 PC-3-Proben in den ersten beiden Hauptkomponenten; 1*g*-Kontrollproben, P1- und P31-Inflight-Proben sind rot, grün bzw. blau kodiert.

1. Regulation von Caspasen und NF-κB-Signalweg

Sowohl bei der qPCR-Auswertung als auch bei der NGS-Analyse fand sich bei einigen untersuchten Caspasen eine moderat erhöhte Genexpression. Weitere Schlüsselgene der Apoptosekaskade werden nicht durch den Parabelflug reguliert. Obwohl die gemessenen Auswirkungen an der Nachweisgrenze liegen, wird der Befund bei der NGS und qPCR validiert. Daher sollte in zukünftigen Langzeitexperimenten in r-µ*g* der Apoptose-Signalweg im Auge behalten werden.

Nach der 31. Parabel konnte durch NGS eine signifikante Hochregulierung des *RELB*-Proto-Onkogens der NF-κB-Untereinheit gezeigt werden, die mit der Regulierung von NF-κB-verwandten Entzündungsgenen einhergeht.
Beispielsweise ist das Gen *REL*, das für c-REL kodiert, nach der ersten Parabel signifikant hochreguliert. Es fanden sich weiterhin ebenfalls signifikant hochregulierte Zytokine und Wachstumsfaktoren nach der P1, wie unter anderem *CCL2, CXCL1, TNFAIP3, IL6, CXCL2, CCL20* und *ICAM1*. Dies entspricht den Ergebnissen der Studie von de Jesús und Ramakrishnan (68) mit embryonalen c-REL-Knockout Fibroblasten der Maus. Es konnte die Funktion der NF-κB-Untereinheit c-REL als transkriptioneller Repressor von Entzündungsgenen identifiziert werden. Die genetische Deletion von c-REL verstärkt dabei die Expression mehrerer TNF-α-induzierter REL-A-abhängiger Entzündungsmediatoren erheblich. Konkret führte die c-REL-Deletion zu einer Hochregulierung von *CCL2, CCL7, CXCL10, CXCL1, TNFAIP3, IL6, CXCL2, CCL20, ZFP36, ICAM1* und *VCAM1*.
Die NF-κB/REL-Familie von Transkriptionsfaktoren spielt eine zentrale Rolle bei der Auslösung und Beendigung von Entzündungsreaktionen (68). Eine Schlüsselstellung nimmt dabei auch *ICAM1* ein, dass nach der P1 hochreguliert gemessen wurde. Die Unterdrückung von *ICAM1* stellt einen entscheidenden Mechanismus dar, durch den sich Karzinomzellen während der Tumorentstehung dem Angriff von natürlichen Killerzellen entziehen und so die Detektion durch das Immunsystem teilweise umgehen (69).

2. Untersuchung von Zytokinen und Chemokinen

TNF-α, LIF, IL-1β, IL-6 und IFN-β verstärken die Expression von *CXCL8* mRNA in Pankreaskarzinomzellen, wodurch die Zellproliferation beeinflusst wird (70). *TNF*, *LIF* und *CXCL8* wurden in unserem Experiment bereits nach der ersten Parabel hochreguliert.
Die Genexpression und das korrespondierende Genprodukt von CXCL3 sowie seinem Rezeptor CXCR2 sind in Prostatakarzinomzellen, Prostataepithelzellen und Prostatatumorgeweben überexprimiert, was bei der Progression und Metastasierung von Prostatakarzinomen eine vielfältige Wirkung haben kann.

Generell lässt sich bei der PC-3 Zelllinie eine stark erhöhte Sekretion des Chemokins CXCL3 nachweisen, während bei den Prostatakarzinomzelllinien DU145 und LNCaP eine erhöhte

Genexpression von *CXCR2* beobachtet wird. Exogenes CXCL3 trägt nicht zur Proliferation bei, hat aber eine signifikante Wirkung auf die Migration von Prostatatumorzellen (71).
Darüber hinaus fördert IL-17 die Produktion von CXCL1 und CXCL2. Das konnte mit Experimenten mit EAP-Prostatagewebe der Maus nachgewiesen werden, in dem das proinflammatorische Zytokin IL-17 und die Chemokin-Liganden CXCL1 und CXCL2 hochreguliert waren (72). Dieser Befund ist mit den Ergebnissen der vorliegenden Studie vergleichbar. Hier waren *CXCL1* und *CXCL2* nach der P1 hochreguliert.

3. Regulation von Non-Coding RNA

Interessanterweise wurden durch das NGS auch signifikante Regulierungen der Genexpression nicht kodierender Gene festgestellt, obwohl die angewandte Methode durch die Poly-A-Tail-Filterung eigentlich auf kodierende Gene abzielt. Im speziellen handelt es sich dabei um lncRNAs und miRNA anteilig zu 23,9 % bzw. 25 %. MiRNAs und lncRNAs sind wichtige Regulatoren der Translation bzw. Transkription. Daher gilt es zu untersuchen, ob die Expression der nichtkodierenden Gene durch die Mikrogravitation frühzeitig verändert wurde.
In Zellen, die nach der P1 fixiert wurden, konnte eine signifikant erhöhte Expression von miR-221 und gleichzeitig eine verringerte Expression von CDKN1B festgestellt werden.
MiR-221 und miR-222 sind bekannte Onkogene, die beim Mamma-, Leber-, Bauchspeicheldrüsen- und Lungenkarzinomen überexprimiert werden, doch ihr Stellenwert und ihre biologischen Funktionen beim Prostatakarzinom sind nach wie vor umstritten. Es wird vermutet, dass miR-221/-222 als Onkogene fungieren und die Proliferation von Prostatatumorzellen sowie die Entwicklung von kastrationsresistenten Prostatakarzinomen (‚*castrate-resistant prostate cancer*', CRPC) fördern.
Eine Hochregulierung von miR-221/222 bei CRPC wird mit einer Modulation des AR während der Karzinogenese in Verbindung gebracht (73).
Dart *et al.* (74) zeigten, dass die Ausschaltung von miR-221 durch CRISPR in PC-3-Zellen zu einer verringerten Wachstumsrate und zur Expression von Zellzyklusgenen führt. Darüber hinaus weisen PC-3-miR-221del-Zellen eine reduzierte Adhäsions-, Invasions- und Motilitätsfähigkeit, eine Veränderung der F-Aktin-Lokalisierung und eine Verminderung der EMT-Marker auf (74).
Eine weitere Studie mit HCC-Zellen ergab, dass miR-221 eine onkogene Funktion bei der Hepatokarzinogenese hat, indem es auf CDKN1B/p27 und CDKN1C/p57 abzielt und somit die Proliferation durch die Kontrolle von Zellzyklusinhibitoren fördert. Dabei bestand eine signifikante inverse Korrelation zwischen miR-221 und sowohl CDKN1B/p27 als auch CDKN1C/p57 (75).

Die lncRNA LINC02605 ist in PC-3-Zellen nach der ersten Parabel und noch stärker nach der 31. Parabel hochreguliert. LINC02605 ist an der angeborenen antiviralen Immunantwort beteiligt. Die Deaktivierung von LINC02605 führt zu einer verminderten antiviralen Immunantwort und zu einer verstärkten viralen Replikation. LINC02605 fördert über die Hemmung von hsa-miR-107 die

Expression von PTEN (‚*Phosphatase and tensin homolog*') (76). Sowohl miR-107 als auch PTEN sind wichtige Akteure in der Karzinogenese.

Beispielsweise deaktiviert die Überexpression von miR-107 bei der Tumorgenese des Plattenepithelkarzinoms des Hypopharynx den PI3K/Akt-Signalweg und hemmt dadurch signifikant das Tumorwachstum (77).

Der Funktionsverlust des Tumorsuppressors PTEN, der zu einer dysregulierten Aktivierung des PI3K-Signalnetzwerks führt, gilt ebenfalls als eine der häufigsten Ursachen für die Entstehung des Prostatakarzinoms (78). PTEN ist eine duale Lipid- und Proteinphosphatase, die unter anderem das Lipidsubstrat PIP3 dephosphoryliert. Darüber interagiert PTEN negativ regulatorisch mit dem PI3K-Signalweg (79).

4. Zusammenfassung der Publikation 3

Zusammenfassend wurde bereits in früheren Studien festgestellt, dass entscheidende Schlüsselpositionen der Karzinogenese durch die Mikrogravitation beeinflusst werden und verschiedene Schlüsselfaktoren, die sensitiv gegenüber Veränderungen der Gravitation sind, eher einen milderen Verlauf fördern.

Da der Einfluss von s-µ*g* auf bereits bekannte Hauptakteure der Tumorgenese des Prostatakarzinoms untersucht wurde, war das Ziel dieser Publikation sehr frühe Reaktionen auf Schwerkraftänderungen im gesamten Transkriptom der PC-3-Zelllinie zu identifizieren. Durch den Fokus auf frühe Responder in diesem Versuchsaufbau werden weniger sekundäre Expressionsänderungen detektiert. Für die Forschung sind sowohl transkriptionelle Primäreffekte als auch Sekundäreffekte relevant. Eine getrennte Analyse beider Effekte ist für das detaillierte Verständnis der hervorgerufenen Veränderungen sinnvoll.

Aus der frühen Reaktion der PC-3-Zellen auf den Gravitationsreiz kann eher auf die Ursache der aufgetretenen Veränderungen, die sich vor allem auf genetischer und epigenetischer Ebene widerspiegelt, geschlossen werden. Spätere sekundäre Effekte entsprechen eher den physiologischen und morphologischen Veränderungen, wie z. B. der Tumorprogression. Insbesondere die Untersuchung der ersten Parabel eröffnet die Möglichkeit, die primäre transkriptionelle Reaktion auf Veränderungen der Gravitation zu beobachten. Danach lassen sich die primären transkriptionellen Veränderungen nicht mehr scharf von späteren sekundären regulatorischen Reaktionen abgrenzen.

Besonders die Regulation der miR-221/222 und LINC02605 durch r-µ*g* stellt einen neuen Ansatzpunkt für potentielle Biomarker des Prostatakarzinoms dar.

Zusammenfassend lässt sich sagen, dass die Kenntnis der primären Reaktion des Transkriptoms auf Schwerkraftänderungen für die Bewertung der späteren Auswirkungen der Tumorgenese des Prostatakarzinoms unter µ*g* von wesentlicher Bedeutung ist.

5.9. Schlussfolgerungen

PC-3 Prostatakarzinomzellen, die s-µ*g* für mehr als 24 h auf der RPM ausgesetzt waren, wuchsen in Form von zwei Phänotypen: Als adhärente Monolayer und als dreidimensionale multizelluläre Sphäroide. Die PC-3-Zellen begannen nach 24 Stunden auf der RPM multizelluläre Sphäroide zu bilden. Sowohl Kurz- und Langzeitsimulation von µ*g* als auch kurzzeitige r-µ*g* während eines Parabelflugs führen zu morphologischen Veränderungen im Zytoskelett sowie Veränderungen der Genexpression von Zytoskelett-, FA-Faktoren und ECM-Komponenten der PC-3-Zellen. Die VEGF-, MAPK- und PAM-Signalwege sind an der Sphäroidbildung von PC-3 Prostatatumorzellen beteiligt. Die meisten dieser Faktoren sind hochreguliert, was auf ihren Einfluss auf das Wachstum und die Progression dieser Zellen hinweist.

Kurzzeit s-µ*g* und r-µ*g* induzieren einen signifikanten Anstieg der Genexpression von Zytokinen und Chemokinen. Besonders deutlich zeigte sich dieser Anstieg bei den proinflammatorischen Zytokinen IL-6 und CXCL8. Daraus lässt sich ableiten, dass diese Zytokine frühzeitig auf Schwerkraftänderungen ansprechen und dass die Hemmung von IL-6 oder CXCL8 bereits in frühen Krebsstadien von Vorteil sein könnte, indem sie die Metastasierung verhindert oder verlangsamt. Beide Faktoren werden in künftigen Kurz- und Langzeit-Experimenten gezielt untersucht werden.

Bei der NGS-Analyse der r-µ*g* Parabelflugproben wurde zusätzlich festgestellt, dass die Zytokine (CCL2, CXCL1, CXCL2, CCL20), ein Zinkfingerprotein (TNFAIP3), ein Glykoprotein (ICAM1) und die miR-221 bei Parabelflügen unterschiedlich reguliert werden. Da diese Faktoren sowohl bei Tumoren als auch bei Entzündungen eine Rolle spielen, könnten die vorgestellten Ergebnisse zur Entwicklung verbesserter Diagnoseinstrumente für das Prostatakarzinom beitragen.

6. Zusammenfassung

Die Kultivierung von Zellen unter den Bedingungen der Mikrogravitation fördert die Entwicklung und die Produktion von großen, gut differenzierten dreidimensionalen Aggregaten, den multizellulären Sphäroiden. Sowohl r- als auch s-µ*g*-Plattformen wie ein Aufenthalt im Weltraum oder die RPM bieten eine neue Technologie für die Herstellung von Sphäroiden für die Tumorforschung und die Arzneimittelprüfung.

Die vorliegende kumulative Promotion basiert auf den Ergebnissen aus drei thematisch in einem Zusammenhang stehenden Publikationen.

In der ersten Publikation wurden PC-3-Zellen über einen Zeitraum von drei und fünf Tagen auf der RPM kultiviert. Die Genexpression von 30 ausgewählten Genen wurde mittels qPCR untersucht. Wir führten Immunfluoreszenzfärbungen zur Untersuchung des Zytoskeletts, F-Aktinfärbungen, histologische Färbungen zur Untersuchung der Morphologie und einen TRIFMA-Test zur Analyse der Zellkulturüberstände durch. Die RPM-Exposition der PC-3-Zellen induzierte Veränderungen der

Morphologie, des Zytoskeletts, der ECM, des fokalen Adhäsionskomplexes und des Wachstumsverhaltens. Die signifikante Hochregulierung von Genen, die zum PAM-Signalweg gehören, deutet darauf hin, dass sie an den in der Schwerelosigkeit auftretenden zellulären Veränderungen beteiligt sind.

Im Rahmen der zweiten Publikation wurden die PC-3-Zellen für 30 Minuten, zwei, vier und 24 Stunden auf der RPM kultiviert. Insgesamt induzierte s-µ*g* das 3D-Wachstum der PC-3-Karzinomzellen in Verbindung mit der veränderten Expression der Zytokine IL-1α, IL-1β, IL-6 und CXCL8, was ihre Beteiligung am Wachstum und der Progression von Prostatatumorzellen unterstützt.

Um auch die frühen Auswirkungen von r-µ*g* auf die PC3-Zellen zu analysieren, nahmen wir im September 2019 an einem Parabelflug teil. Diese Ergebnisse sind in der 3. Publikation zusammengefasst.

Die resultierende RNA wurde mit der Next-Generation-Sequenzierung und der qPCR-Technologie untersucht. Nach der ersten Parabel sind Veränderungen des F-Aktin-Zytoskeletts sichtbar. Darüber hinaus sind zahlreiche signifikante transkriptionelle Veränderungen zu erkennen, sodass ein Netzwerk relevanter Zytokine und Chemokine identifiziert werden konnte, die aufgrund von Schwerkraftveränderungen insbesondere während der frühen Flugphasen eine unterschiedliche Expression aufweisen. Zusammen mit differentiell exprimierten regulatorischen lncRNAs und Mikro-RNAs ergibt sich eine Gruppe von 298 potenziellen Biomarkern. Mittels qPCR konnten IL-6 und PIK3CB identifiziert werden, die empfindlich auf Vibrationseinflüsse bzw. Hyper-*g* reagierten.

7. Summary

Culturing cells under microgravity conditions promotes the development and production of large, well-differentiated three-dimensional aggregates, so called multicellular spheroids. Both r- and s-µg platforms, such as a stay in orbit or culturing cells on the RPM, provide a new technology for producing spheroids for cancer research and drug testing.

This doctoral thesis is based on the results from three thematically related publications.

In the first publication, PC-3 prostate cancer cells were cultured on the RPM for periods of 3 and 5 days. The gene expression pattern of 30 selected genes was examined by qPCR. We performed immunofluorescence to examine the cytoskeleton, F-actin staining, histological staining to study the morphology, and a time-resolved immunofluorometric assay to analyze the cell culture supernatants. RPM-exposure of PC-3 cells elicited changes in their morphology, the cytoskeleton, the extracellular matrix, as well as in the focal adhesion complex and growth behavior. The significant upregulation of genes belonging to the PAM pathway suggests that they are involved in the cellular changes that occur in microgravity.

In the second publication, PC-3 cells were cultured on the RPM for 30 minutes, 2, 4, and 24 hours. Overall, s-µg induced 3D growth of PC-3 cancer cells in conjunction with the differential expression of

the cytokines IL-1α, IL-1β, IL-6, and CXCL8, supporting their involvement in prostate cancer cell growth and progression.

In order to analyze the early effects of short-term r-µ*g* on PC-3 prostate cancer cells, we attended the 34th DLR parabolic flight campaign in September 2019. The results are summarized in the 3rd publication.

The resulting RNA was subjected to next-generation sequencing and also to qPCR technology. After the first parabola, changes in the F-actin cytoskeleton are visible. In addition, numerous significant transcriptional changes are evident, allowing identification of a network of relevant cytokines and chemokines that exhibit differential expression due to gravity changes, particularly during the early phases of the flight. Together with differentially expressed regulatory lncRNAs and microRNAs, this results in a list of 298 potential biomarkers. Using qPCR, IL-6 and PIK3CB were identified to be sensitive to vibration effects as well as to the influence of hypergravity, respectively.

8. Literaturverzeichnis

1. Najrana, T. and J. Sanchez-Esteban, Mechanotransduction as an Adaptation to Gravity. Front Pediatr, 2016. 4: 140.
2. White, R.J. and M. Averner, Humans in space. Nature, 2001. 409(6823): 1115-8.
3. Blaber, E., H. Marcal, and B.P. Burns, Bioastronautics: the influence of microgravity on astronaut health. Astrobiology, 2010. 10(5): 463-73.
4. Russomano, T., M. da Rosa, and M.A. Dos Santos, Space motion sickness: A common neurovestibular dysfunction in microgravity. Neurol India, 2019. 67(Supplement): S214-S218.
5. Marshall-Goebel, K., R. Damani, and E.M. Bershad, Brain Physiological Response and Adaptation During Spaceflight. Neurosurgery, 2019. 85(5): E815-E821.
6. Nelson, E.S., L. Mulugeta, and J.G. Myers, Microgravity-induced fluid shift and ophthalmic changes. Life (Basel), 2014. 4(4): 621-65.
7. Penchev, R., et al., Back Pain in Outer Space. Anesthesiology, 2021. 135(3): 384-395.
8. Baran, R., et al., Microgravity-Related Changes in Bone Density and Treatment Options: A Systematic Review. Int J Mol Sci, 2022. 23(15).
9. Baran, R., et al., The Cardiovascular System in Space: Focus on In Vivo and In Vitro Studies. Biomedicines, 2021. 10(1).
10. Nassef, M.Z., et al., Real Microgravity Influences the Cytoskeleton and Focal Adhesions in Human Breast Cancer Cells. Int J Mol Sci, 2019. 20(13).
11. Aleshcheva, G., et al., Moderate alterations of the cytoskeleton in human chondrocytes after short-term microgravity produced by parabolic flight maneuvers could be prevented by up-regulation of BMP-2 and SOX-9. FASEB J, 2015. 29(6): 2303-14.
12. AIRBUS A310 ZERO G. Available from: https://www.airzerog.com/de/airbus-a310-zero-g-de/.
13. Grimm, D., et al., The Fight against Cancer by Microgravity: The Multicellular Spheroid as a Metastasis Model. Int J Mol Sci, 2022. 23(6).
14. Herranz, R., et al., Ground-based facilities for simulation of microgravity: organism-specific recommendations for their use, and recommended terminology. Astrobiology, 2013. 13(1): 1-17.
15. Svejgaard, B., et al., Common Effects on Cancer Cells Exerted by a Random Positioning Machine and a 2D Clinostat. PLoS One, 2015. 10(8): e0135157.
16. Calvaruso, M., et al., Biological and Mechanical Characterization of the Random Positioning Machine (RPM) for Microgravity Simulations. Life (Basel), 2021. 11(11).
17. Benavides Damm, T., et al., Cell cultivation under different gravitational loads using a novel random positioning incubator. Biotechnol Bioeng, 2014. 111(6): 1180-90.
18. Kruger, M., et al., Fighting Thyroid Cancer with Microgravity Research. Int J Mol Sci, 2019. 20(10).
19. Ma, X., et al., Interleukin-6 expression under gravitational stress due to vibration and hypergravity in follicular thyroid cancer cells. PLoS One, 2013. 8(7): e68140.
20. Achilli, T.M., J. Meyer, and J.R. Morgan, Advances in the formation, use and understanding of multi-cellular spheroids. Expert Opin Biol Ther, 2012. 12(10): 1347-60.
21. Cui, X., Y. Hartanto, and H. Zhang, Advances in multicellular spheroids formation. J R Soc Interface, 2017. 14(127).
22. Ingber, D., How cells (might) sense microgravity. FASEB J, 1999. 13 Suppl: S3-15.

23. Zappetti, D., et al. Bio-inspired tensegrity soft modular robots. in Conference on Biomimetic and Biohybrid Systems. 2017. Springer.

24. Gandaglia, G., et al., Distribution of metastatic sites in patients with prostate cancer: A population-based analysis. Prostate, 2014. 74(2): 210-6.

25. Ingber, D.E., N. Wang, and D. Stamenovic, Tensegrity, cellular biophysics, and the mechanics of living systems. Rep Prog Phys, 2014. 77(4): 046603.

26. Vorselen, D., et al., The role of the cytoskeleton in sensing changes in gravity by nonspecialized cells. FASEB J, 2014. 28(2): 536-47.

27. Galkin, V.E., A. Orlova, and E.H. Egelman, Actin filaments as tension sensors. Curr Biol, 2012. 22(3): R96-101.

28. Leitlinienprogramm Onkologie (Deutsche Krebsgesellschaft, Deutsche Krebshilfe, AWMF): S3-Leitlinie Prostatakarzinom, Langversion 6.2, 2021, AWMF Registernummer: 043/022OL. 02.09.2022]; Available from: http://www.leitlinienprogramm-onkologie.de/leitlinien/prostatakarzinom/.

29. Wang, G., et al., Genetics and biology of prostate cancer. Genes Dev, 2018. 32(17-18): 1105-1140.

30. Tai, S., et al., PC3 is a cell line characteristic of prostatic small cell carcinoma. Prostate, 2011. 71(15): 1668-79.

31. Johnston, S.T., et al., Estimating cell diffusivity and cell proliferation rate by interpreting IncuCyte ZOOM assay data using the Fisher-Kolmogorov model. BMC Syst Biol, 2015. 9: 38.

32. Pulukuri, S.M., et al., RNA interference-directed knockdown of urokinase plasminogen activator and urokinase plasminogen activator receptor inhibits prostate cancer cell invasion, survival, and tumorigenicity in vivo. J Biol Chem, 2005. 280(43): 36529-40.

33. Kopp, S., et al., Mechanisms of three-dimensional growth of thyroid cells during long-term simulated microgravity. Sci Rep, 2015. 5: 16691.

34. Kopp, S., et al., Identifications of novel mechanisms in breast cancer cells involving duct-like multicellular spheroid formation after exposure to the Random Positioning Machine. Sci Rep, 2016. 6: 26887.

35. Ingram, M., et al., Three-dimensional growth patterns of various human tumor cell lines in simulated microgravity of a NASA bioreactor. In Vitro Cell Dev Biol Anim, 1997. 33(6): 459-66.

36. Tojkander, S., G. Gateva, and P. Lappalainen, Actin stress fibers - assembly, dynamics and biological roles. J Cell Sci, 2012. 125(Pt 8): 1855-64.

37. Ulbrich, C., et al., Differential gene regulation under altered gravity conditions in follicular thyroid cancer cells: relationship between the extracellular matrix and the cytoskeleton. Cell Physiol Biochem, 2011. 28(2): 185-98.

38. Grosse, J., et al., Short-term weightlessness produced by parabolic flight maneuvers altered gene expression patterns in human endothelial cells. FASEB J, 2012. 26(2): 639-55.

39. Bonnans, C., J. Chou, and Z. Werb, Remodelling the extracellular matrix in development and disease. Nat Rev Mol Cell Biol, 2014. 15(12): 786-801.

40. Mann, V., et al., Changes in Human Foetal Osteoblasts Exposed to the Random Positioning Machine and Bone Construct Tissue Engineering. Int J Mol Sci, 2019. 20(6).

41. Adekoya, T.O. and R.M. Richardson, Cytokines and Chemokines as Mediators of Prostate Cancer Metastasis. Int J Mol Sci, 2020. 21(12).

42. Melegh, Z. and S. Oltean, Targeting Angiogenesis in Prostate Cancer. Int J Mol Sci, 2019. 20(11).

43. Ma, X., et al., Differential gene expression profile and altered cytokine secretion of thyroid cancer cells in space. FASEB J, 2014. 28(2): 813-35.

44. Shenoy, S., CDH1 (E-Cadherin) Mutation and Gastric Cancer: Genetics, Molecular Mechanisms and Guidelines for Management. Cancer Manag Res, 2019. 11: 10477-10486.

45. Birchmeier, W. and J. Behrens, Cadherin expression in carcinomas: role in the formation of cell junctions and the prevention of invasiveness. Biochim Biophys Acta, 1994. 1198(1): 11-26.

46. Semb, H. and G. Christofori, The tumor-suppressor function of E-cadherin. Am J Hum Genet, 1998. 63(6): 1588-93.

47. Albert, L., et al., Inhibition of mTOR Activates the MAPK Pathway in Glioblastoma Multiforme. Cancer Genomics Proteomics, 2009. 6(5): 255-61.

48. Clejan, S., K. O'Connor, and N. Rosensweig, Tri-dimensional prostate cell cultures in simulated microgravity and induced changes in lipid second messengers and signal transduction. J Cell Mol Med, 2001. 5(1): 60-73.

49. Venable, M.E., et al., Role of ceramide in cellular senescence. J Biol Chem, 1995. 270(51): 30701-8.

50. Shorning, B.Y., et al., The PI3K-AKT-mTOR Pathway and Prostate Cancer: At the Crossroads of AR, MAPK, and WNT Signaling. Int J Mol Sci, 2020. 21(12).

51. Yuan, J., et al., The MAPK and AMPK signalings: interplay and implication in targeted cancer therapy. J Hematol Oncol, 2020. 13(1): 113.

52. Kliewe, F., et al., Fibronectin is up-regulated in podocytes by mechanical stress. FASEB J, 2019. 33(12): 14450-14460.

53. Carlsson, J. and J.M. Yuhas, Liquid-overlay culture of cellular spheroids. Recent Results Cancer Res, 1984. 95: 1-23.

54. Azevedo, A., et al., IL-6/IL-6R as a potential key signaling pathway in prostate cancer development. World J Clin Oncol, 2011. 2(12): 384-96.

55. Gopinathan, G., et al., Interleukin-6 Stimulates Defective Angiogenesis. Cancer Res, 2015. 75(15): 3098-107.

56. Grosse, J., et al., Gravity-sensitive signaling drives 3-dimensional formation of multicellular thyroid cancer spheroids. FASEB J, 2012. 26(12): 5124-40.

57. Waugh, D.J. and C. Wilson, The interleukin-8 pathway in cancer. Clin Cancer Res, 2008. 14(21): 6735-41.

58. Singh, R.K. and B.L. Lokeshwar, Depletion of intrinsic expression of Interleukin-8 in prostate cancer cells causes cell cycle arrest, spontaneous apoptosis and increases the efficacy of chemotherapeutic drugs. Mol Cancer, 2009. 8: 57.

59. Desiniotis, A. and N. Kyprianou, Significance of talin in cancer progression and metastasis. Int Rev Cell Mol Biol, 2011. 289: 117-47.

60. Pietsch, J., et al., Spheroid formation of human thyroid cancer cells in an automated culturing system during the Shenzhou-8 Space mission. Biomaterials, 2013. 34(31): 7694-705.

61. Bhat, F.A., et al., Quercetin reverses EGF-induced epithelial to mesenchymal transition and invasiveness in prostate cancer (PC-3) cell line via EGFR/PI3K/Akt pathway. J Nutr Biochem, 2014. 25(11): 1132-1139.

62. Wehland, M., et al., Target-based anti-angiogenic therapy in breast cancer. Curr Pharm Des, 2012. 18(27): 4244-57.

63. Ancker, O.V., et al., The Adverse Effect of Hypertension in the Treatment of Thyroid Cancer with Multi-Kinase Inhibitors. Int J Mol Sci, 2017. 18(3).

64. Randrup Hansen, C., et al., Effects and Side Effects of Using Sorafenib and Sunitinib in the Treatment of Metastatic Renal Cell Carcinoma. Int J Mol Sci, 2017. 18(2).

65. Sarkar, C., et al., Angiogenesis Inhibition in Prostate Cancer: An Update. Cancers (Basel), 2020. 12(9).

66. Garbers, C., et al., Cellular senescence or EGFR signaling induces Interleukin 6 (IL-6) receptor expression controlled by mammalian target of rapamycin (mTOR). Cell Cycle, 2013. 12(21): 3421-32.

67. 20 Jahre DLR-Parabelflug - Grundlagenforschung mit Alltagsbezug. 22.09.2022]; Available from: https://www.dlr.de/content/de/artikel/news/2019/03/20190916_20-jahre-parabelflug.html.

68. de Jesus, T.J. and P. Ramakrishnan, NF-kappaB c-Rel Dictates the Inflammatory Threshold by Acting as a Transcriptional Repressor. iScience, 2020. 23(3): 100876.

69. Saga, K., et al., NANOG helps cancer cells escape NK cell attack by downregulating ICAM1 during tumorigenesis. J Exp Clin Cancer Res, 2019. 38(1): 416.

70. Kamohara, H., et al., Induction of interleukin-8 (CXCL-8) by tumor necrosis factor-alpha and leukemia inhibitory factor in pancreatic carcinoma cells: Impact of CXCL-8 as an autocrine growth factor. Int J Oncol, 2007. 31(3): 627-32.

71. Gui, S.L., et al., Overexpression of CXCL3 can enhance the oncogenic potential of prostate cancer. Int Urol Nephrol, 2016. 48(5): 701-9.

72. Zhang, C., et al., IL-17 exacerbates experimental autoimmune prostatitis via CXCL1/CXCL2-mediated neutrophil infiltration. Andrologia, 2022. 54(8): e14455.

73. Gui, B., et al., Androgen receptor-mediated downregulation of microRNA-221 and -222 in castration-resistant prostate cancer. PLoS One, 2017. 12(9): e0184166.

74. Dart, D.A., et al., MiR-221 Is Specifically Elevated in PC3 Cells and its Deletion Reduces Adhesion, Motility and Growth. Anticancer Res, 2019. 39(10): 5311-5327.

75. Fornari, F., et al., MiR-221 controls CDKN1C/p57 and CDKN1B/p27 expression in human hepatocellular carcinoma. Oncogene, 2008. 27(43): 5651-61.

76. Xu, R., et al., Interferon-Inducible LINC02605 Promotes Antiviral Innate Responses by Strengthening IRF3 Nuclear Translocation. Front Immunol, 2021. 12: 755512.

77. Gao, X., et al., Overexpression of microRNA-107 suppressed proliferation, migration, invasion, and the PI3K/Akt signaling pathway and induced apoptosis by targeting Nin one binding (NOB1) protein in a hypopharyngeal squamous cell carcinoma cell line (FaDu). Bioengineered, 2022. 13(3): 7881-7893.

78. Wise, H.M., M.A. Hermida, and N.R. Leslie, Prostate cancer, PI3K, PTEN and prognosis. Clin Sci (Lond), 2017. 131(3): 197-210.

79. Chen, C.Y., et al., PTEN: Tumor Suppressor and Metabolic Regulator. Front Endocrinol (Lausanne), 2018. 9: 338.

9. Abbildungsverzeichnis

10. Danksagung

Mein besonderer Dank gilt Frau Professor Dr. med. Daniela Grimm, die durch Ihre Begeisterung für die Wissenschaft, den außergewöhnlich herzlichen Umgang mit den Mitarbeitern und auch uns Studenten und den inhaltlichen Hilfestellungen einen großen Anteil zum Gelingen meiner Doktorarbeit beigetragen hat. Zudem war es für mich eine wirklich einmalige Erfahrung in einem wissenschaftlichen Kontext an einem Parabelflug teilnehmen zu dürfen. Vielen Dank für diese Möglichkeit.

Des Weiteren danke ich sehr herzlich Herrn Professor Dr. med. Manfred Infanger für die angenehme Betreuung und Nutzung der Laborräume der Klinik für Plastische, Ästhetische und Handchirurgie.

Ich möchte mich auch bei Herrn Dr. Sascha Kopp bedanken. Sowohl bei inhaltlichen als auch bei praktischen Fragen wurde ich stets geduldig begleitet und immer wieder ermutigt, mich in Eigeninitiative der einen oder anderen Herausforderung zu stellen.

Außerdem danke ich auch Herrn Dr. Herbert Schulz, der vor allem bei bioinformatischen Fragestellungen auf angenehme Art und Weise Licht ins Dunkle gebracht hat.

Schließlich möchte ich mich auch bei Frau Daniela Melnik, Herrn Dr. Markus Wehland, Herrn Dr. Marcus Krüger und natürlich auch der gesamten Arbeitsgruppe für die kontinuierliche Unterstützung im Entstehungsprozess bedanken. Es herrschte stets sowohl inhaltlich als auch persönlich eine angenehme und produktive Atmosphäre.

11. Ehrenerklärung

Ich erkläre, dass ich die der Medizinischen Fakultät der Otto-von-Guericke-Universität zur Promotion eingereichte Dissertation mit dem Titel

„Der Einfluss von realer und simulierter Mikrogravitation auf die biologischen Prozesse humaner Prostatakarzinomzellen“

in der Abteilung für Mikrogravitation und Translationale Regenerative Medizin, Klinik für Plastische, Ästhetische und Handchirurgie

ohne sonstige Hilfe durchgeführt und bei der Abfassung der Dissertation keine anderen als die dort aufgeführten Hilfsmittel benutzt habe.

Bei der Abfassung der Dissertation sind Rechte Dritter nicht verletzt worden.

Ich habe diese Dissertation bisher an keiner in- oder ausländischen Hochschule zur Promotion eingereicht. Ich übertrage der Medizinischen Fakultät das Recht, weitere Kopien meiner Dissertation herzustellen und zu vertreiben.

Magdeburg, den 09.11.2022

12. Darstellung des Bildungsweges

Persönliche Daten

Name:	Dorothea Dietrichs
Geburtsdatum:	10.02.1996
Adresse:	[redacted]
	[redacted]
Handynummer:	[redacted]

Ausbildung

2006-2014	Canisius Kolleg Berlin
	• Abitur (2014)
Seit 2014	Otto-von-Guericke-Universität Magdeburg
	• Studium der Humanmedizin • Physikum (Herbst 2016) • 2. Medizinisches Staatsexamen (Frühjahr 2020) • Medizinisches Staatsexamen (Dezember 2021)
Seit 2019	Otto-von-Guericke-Universität Magdeburg
	• Promotion in der Forschungsabteilung Mikrogravitation und Translationale Regenerative Medizin (MTRM) unter Leitung von Frau Prof. Dr. med. Daniela-Gabriele Grimm • Teilnahme an der 34. DLR-Parabelflugkampagne in Bordeaux-Mérignac, Frankreich (September 2019)

Praktische Erfahrung

2015	Krankenhaus Waldfriede (Berlin-Zehlendorf)
	• Pflegepraktikum (Februar-März & August-September 2015)
2017	Helios Klinikum Emil von Behring Berlin- Zehlendorf
	• Famulatur (März 2017)
	Immanuel-Krankenhaus (Berlin-Wannsee)
	• Famulatur (August 2017)
2018	Hausärztliche Gemeinschaftspraxis Grube und Dr. Krieger (Berlin-Wilmersdorf)
	• Famulatur (März 2018)
	Neurologische Gemeinschaftspraxis Dr. Brockmeier & Dr. Schrey (Berlin-Zehlendorf)
	• Famulatur (September 2018)
2020 – 2021	Uniklinikum Magdeburg & Gemeinschaftskrankenhaus Havelhöhe Berlin
	• Praktisches Jahr (November 2020 – Oktober 2021) **1.** Kinderchirurgie & Thoraxchirurgie **2.** Institut für Humangenetik **3.** Palliativmedizin/Integrative Onkologie & Kardiologie
2022	Helios Klinikum Emil von Behring Berlin-Zehlendorf
	• Weiterbildung zum Facharzt für Innere Medizin (seit 1. Oktober 2022)

13. Anlagen

13.1. Publikation 1

Hybel TE, **Dietrichs D**, Sahana J, Corydon TJ, Nassef MZ, Wehland M, Krüger M, Magnusson NE, Bauer J, Utpatel K, Infanger M, Grimm D, Kopp S: Simulated Microgravity Influences VEGF, MAPK, and PAM Signaling in Prostate Cancer Cells. Int J Mol Sci. 21. 1263 (2020)

International Journal of
Molecular Sciences

MDPI

Article

Simulated Microgravity Influences VEGF, MAPK, and PAM Signaling in Prostate Cancer Cells

Trine Engelbrecht Hybel [1], Dorothea Dietrichs [2], Jayashree Sahana [1], Thomas J. Corydon [1,3], Mohamed Z. Nassef [2,4], Markus Wehland [2,4], Marcus Krüger [2,4], Nils E. Magnusson [5], Johann Bauer [6], Kirsten Utpatel [7], Manfred Infanger [2,4], Daniela Grimm [1,2,4,8,*] and Sascha Kopp [2,4,*]

1 Department of Biomedicine, Aarhus University, 8000 Aarhus C, Denmark; trihyb@rm.dk (T.E.H.); jaysaha@biomed.au.dk (J.S.); corydon@biomed.au.dk (T.J.C.)
2 Clinic for Plastic, Aesthetic and Hand Surgery, Otto von Guericke University Magdeburg, 39120 Magdeburg, Germany; dorothea.dietrichs@st.ovgu.de (D.D.); mohamed.nassef@med.ovgu.de (M.Z.N.); markus.wehland@med.ovgu.de (M.W.); marcus.krueger@med.ovgu.de (M.K.); manfred.infanger@med.ovgu.de (M.I.)
3 Department of Ophthalmology, Aarhus University Hospital, 8200 Aarhus N, Denmark
4 Research Group "Magdeburger Arbeitsgemeinschaft für Forschung unter Raumfahrt-und Schwerelosigkeitsbedingungen" (MARS), Otto von Guericke University, Universitätsplatz 2, 39106 Magdeburg, Germany
5 Diabetes and Hormone Diseases—Medical Research Laboratory, Department of Clinical Medicine, Faculty of Health, Aarhus University, 8200 Aarhus N, Denmark; nm@clin.au.dk
6 Max Planck Institute of Biochemistry, 82152 Martinsried, Germany; jbauer@biochem.mpg.de
7 Institute for Pathology, University of Regensburg, 95053 Regensburg, Germany; kirsten.utpatel@ukr.de
8 Department of Microgravity and Translational Regenerative Medicine, Otto von Guericke University, Pfälzer Platz, 39106 Magdeburg, Germany
* Correspondence: dgg@biomed.au.dk (D.G.); sascha.kopp@med.ovgu.de (S.K.); Tel.: +45-871-67693 (D.G.); +49-391-6721267 (S.K.)

Received: 23 November 2019; Accepted: 11 February 2020; Published: 13 February 2020

Abstract: Prostate cancer is one of the leading causes of cancer mortality in men worldwide. An unusual but unique environment for studying tumor cell processes is provided by microgravity, either in space or simulated by ground-based devices like a random positioning machine (RPM). In this study, prostate adenocarcinoma-derived PC-3 cells were cultivated on an RPM for time periods of 3 and 5 days. We investigated the genes associated with the cytoskeleton, focal adhesions, extracellular matrix, growth, survival, angiogenesis, and metastasis. The gene expression of signaling factors of the vascular endothelial growth factor (VEGF), mitogen-activated protein kinase (MAPK), and PI3K/AKT/mTOR (PAM) pathways was investigated using qPCR. We performed immunofluorescence to study the cytoskeleton, histological staining to examine the morphology, and a time-resolved immunofluorometric assay to analyze the cell culture supernatants. When PC-3 cells were exposed to simulated microgravity (s-µg), some cells remained growing as adherent cells (AD), while most cells detached from the cell culture flask bottom and formed multicellular spheroids (MCS). After 3-day RPM exposure, PC-3 cells revealed significant downregulation of the *VEGF*, *SRC1*, *AKT*, *MTOR*, and *COL1A1* gene expression in MCS, whereas *FLT1*, *RAF1*, *MEK1*, *ERK1*, *FAK1*, *RICTOR*, *ACTB*, *TUBB*, and *TLN1* mRNAs were not significantly changed. *ERK2* and *TLN1* were elevated in AD, and *FLK1*, *LAMA3*, *COL4A5*, *FN1*, *VCL*, *CDH1*, and *NGAL* mRNAs were significantly upregulated in AD and MCS after 3 days. After a 5-day culture in s-µg, the PC-3 cells showed significant downregulations of *VEGF* mRNA in AD and MCS, and *FN1*, *CDH1*, and *LAMA3* in AD and *SCR1* in MCS. In addition, we measured significant upregulations in *FLT1*, *AKT*, *ERK1*, *ERK2*, *LCN2*, *COL1A1*, *TUBB*, and *VCL* mRNAs in AD and MCS, and increases in *FLK1*, *FN1*, and *COL4A5* in MCS as well as *LAMB2*, *CDH1*, *RAF1*, *MEK1*, *SRC1*, and *MTOR* mRNAs in AD. *FAK1* and *RICTOR* were not altered by s-µg.

In parallel, the secretion rate of VEGFA and NGAL proteins decreased. Cytoskeletal alterations (F-actin) were visible, as well as a deposition of collagen in the MCS. In conclusion, RPM-exposure of PC-3 cells induced changes in their morphology, cytoskeleton, and extracellular matrix protein synthesis, as well as in their focal adhesion complex and growth behavior. The significant upregulation of genes belonging to the PAM pathway indicated their involvement in the cellular changes occurring in microgravity.

Keywords: microgravity; prostate cancer; VEGF signaling; cytoskeleton; focal adhesion; extracellular matrix

1. Introduction

Space research and investigations on cell signaling processes in the growth and development of cells exposed to microgravity (μg) is currently a hot topic in cancer research and regenerative medicine [1–5]. Prostate cancer is the fifth leading cause of cancer mortality in men, with the second highest cancer incidence worldwide. It is the most frequently diagnosed cancer in more than half of the countries in the world. In 2018, 1,276,106 cases of prostate cancer and 358,989 deaths were recorded worldwide [6]. Therefore, it is important to increase the current knowledge and develop novel treatment strategies for prostate cancer.

According to the 2016 World Health Organization (WHO) classification of tumors of the prostate, one of the main groups of prostate carcinomas are epithelial tumors, including the subtype acinar adenocarcinoma [7], which is by far the most common type of prostate carcinoma [8,9]. Initially, this carcinoma is local and confined to the prostate. If not detected early, it can progress to advanced stages, characterized by local invasion of the vesicular glands. The cancer can eventually progress to metastatic disease, usually resulting in death [9]. Moreover, the disease can change to a state of androgen independence, increasing the difficulty of treatment [9].

Many studies have shown that changes in gravity have extensive effects on cell functions [10–12]. Microgravity can induce alterations in morphology, growth, and protein biosynthesis and secretion [10], depending on the responding cell type [12]. In addition, cell cultures in μg can be performed scaffold-free to engineer three-dimensional (3D) aggregates, including multicellular spheroids (MCS), tissues, and tubular structures [13–15]. These organoids can be used for research in space medicine [13,16] and for testing the delivery and efficacy of drugs [17].

However, real μg can only be experienced during spaceflights, unmanned Bion flights, suborbital flights, rocket flights, parabolic flights, or with the help of a drop tower [18]. As these opportunities are rare and costly, devices have been developed to simulate μg on Earth, including the random positioning machine (RPM), rotating wall vessel (RWV), and the two-dimensional (2D) or 3D clinostat [16,18].

An RPM consists of two independently rotating frames, each moving at a randomized speed and direction [16]. By placing a sample of sufficiently small objects or cells in the middle of the RPM, the gravity vector perceived by the sample is averaged to zero over time; thus, the objects are exposed to simulated μg (s-μg) [16,19]. It has been shown for various cell types, including thyroid [20] and breast cancer cells [21], that cultivation on an RPM results in MCS formation [16].

This method facilitates long-term scaffold-free 3D-aggregate formation with the advantage of a lack of necrosis. This makes it possible to conduct long-term experiments where huge spheroids can be produced [22]. Experiments with follicular thyroid cancer cells cultured in a scaffold-free manner on an RPM for 14 days [23] and endothelial cells exposed to s-μg for 28 and 35 days revealed no necrosis. The endothelial cells grew in a large number of 3D organoids and tubular structures [15,24]. The liquid overlay and spinner flask techniques and other 1 g methods provide specific environments for 3D formation [25]. Unfortunately, after two weeks the spheroids revealed a necrotic center [26].

MCS are spherical cell clusters containing networks of cell–cell and cell–matrix interactions [17]. They are similar to in vivo tissue regarding the complexity of cell types, cell–cell interactions, extracellular matrix (ECM) deposition, and chemical gradients [17]. The concentration of oxygen and nutrients is highest in the outer layers, while metabolic wastes accumulate in the center [17,27], which resembles the conditions in avascular tumors but is "inside-out" compared to tumors containing capillaries in the center [28]. It has been shown that when MCS are formed from cancer cells, they mimic tumors formed in vivo [29] better than monolayers of cells [28]. Therefore, they can be used as in vitro model systems and for high-throughput screening assays [30] to measure the responses of tumors to potential anticancer drugs [28–30]. This increases the opportunity for cell-based research in drug development [30] and can be used as an addition to in vivo models and/or to reduce animal experiments [28].

Various studies have shown that μg can affect the secretion of vascular endothelial growth factors (VEGFs) in different cell types [15,23,31]. VEGFs are signaling molecules important for the process of angiogenesis [32]. Abnormal angiogenesis is one of the hallmarks of cancer [33], and overexpression of VEGF-A has been implicated in pathological angiogenesis in tumors and other diseases, causing the development of dysfunctional and disorganized types of blood vessels [32]. In tumors, neoangiogenesis changes blood flow, oxygenation, and interstitial fluid pressure, creating an abnormal microenvironment, increasing cancer progression, and decreasing the efficacy of treatment [33]. Anti-VEGF treatment has been developed and successfully utilized as cancer treatment [33,34].

The actions of VEGF-A are mediated through the molecule binding to its two receptors, VEGFR-1/fetal liver kinase 1 (FLT1) and VEGFR-2 Fms-related tyrosine kinase 1 (FLK1). Upon VEGF-A binding to VEGFR-2, phosphorylation of specific tyrosine residues leads to recruitment of downstream effector proteins and initiation of specific signaling pathways [35]. The extracellular signal regulated kinase 1/2 (ERK1/2)/rapidly accelerated fibrosarcoma (raf)-mitogen-activated protein kinase kinase 1 (MEK1)-mitogen-activated protein kinase (MAPK) pathway is activated, leading to increased proliferation [35,36]. Apoptosis is inhibited through the steroid receptor coactivator (SRC) proto-oncogene, non-receptor tyrosine kinase (Src)/phosphoinositide 3-kinase (PI3K)/protein kinase B (PKB, also known as Akt) signaling pathway, leading to increased cell survival [35,37]. Mammalian target of rapamycin (mTOR) signaling, which includes mTOR complex 2 (mTORC2), containing the subunits mTOR and rapamycin-insensitive companion of mTOR (RICTOR), is activated through the PI3K/Akt signaling pathway, regulating processes such as cell growth and differentiation [38]. VEGF signaling through VEGFR-2 also leads to activation of focal adhesion kinase (FAK), which stimulates increased vascular permeability [39] as well as migration and anti-apoptosis via Src [40]. Moreover, p38MAPK is activated, affecting cell motility through actin cytoskeleton reorganization [35].

In comparison to other VEGFRs, the signaling functions of VEGFR-1 are less well characterized [41]. It has been associated with the ERK/MAPK, PI3K/AKT, and p38MAPK signaling pathways [42]. Furthermore, VEGFR-1 has been shown to bind VEGF with a higher affinity than VEGFR-2 and thereby have a negative impact on angiogenesis caused by VEGFR-2 [41].

Previous findings showed 3D growth patterns of PC-3 cells when cultured in an RWV culture system [14]. Spheroid formation followed within a few hours after reducing gravitational conditions, and expression of cell adhesion molecules (CD44 and E-cadherin) was increased in the MCS. In parallel, Zhau and co-workers established a 3D human prostatic cancer model by co-culturing prostate fibroblasts with prostate cancer cells under s-μg conditions using an RWV system [43]. Using a similar setup, Clejan and colleagues studied the effects of RWV cultivation on DU-145 human prostate carcinoma cells [44]. Notably, after 6 days of RWV growth, the activation of the PI3K pathway was observed. From this study the authors concluded that RWV cultivation provides a 3D growth model of prostate cancer that imitates in vivo tissue growth. In addition, Margolis et al. reported long-term maintenance (minimum of 28 days) of benign explanted human prostate tissue grown in culture medium in an RWV [45]. This study investigated the impact of s-μg on PC-3 prostate cancer cells in vitro.

The principal aims of this study are to (i) investigate the changes and behavior of PC-3 prostate cancer cells exposed to s-μg created by an RPM; (ii) test, based on previous findings, the hypothesis that exposure of PC-3 cells to s-μg induces the formation of MCS and alters the expression of genes related to angiogenesis, metastasis, the cytoskeleton, the ECM, and focal adhesions (FAs); and (iii) focus on the VEGF, MAPK, and PI3K/AKT/mTOR (PAM) signaling pathways.

2. Results

2.1. Morphology and Cell Growth

In order to examine whether PC-3 cells will form MCS when cultured under s-μg conditions, cell culture flasks containing PC-3 cells were placed on the RPM for 3 and 5 days; 1 g controls were cultured in parallel.

The 1 g control cells (Figure 1A,D) kept dividing throughout the experiment, reaching 100% confluence. The cells on the RPM (Figure 1B,C,E,F) were exposed to s-μg conditions. Only a few cells remained adherent, growing as a 2D monolayer (AD), while the majority detached and aggregated to MCS. After 3 days (Figure 1B,C), there were numerous MCS floating in the medium. In addition, a smaller number of loose aggregates could be found among the spheroids. After 5 days (Figure 1E,F), the spheroids had grown significantly. The size, shape, and density varied among the spheroids, as well as among the cell culture flasks used in the same experiment.

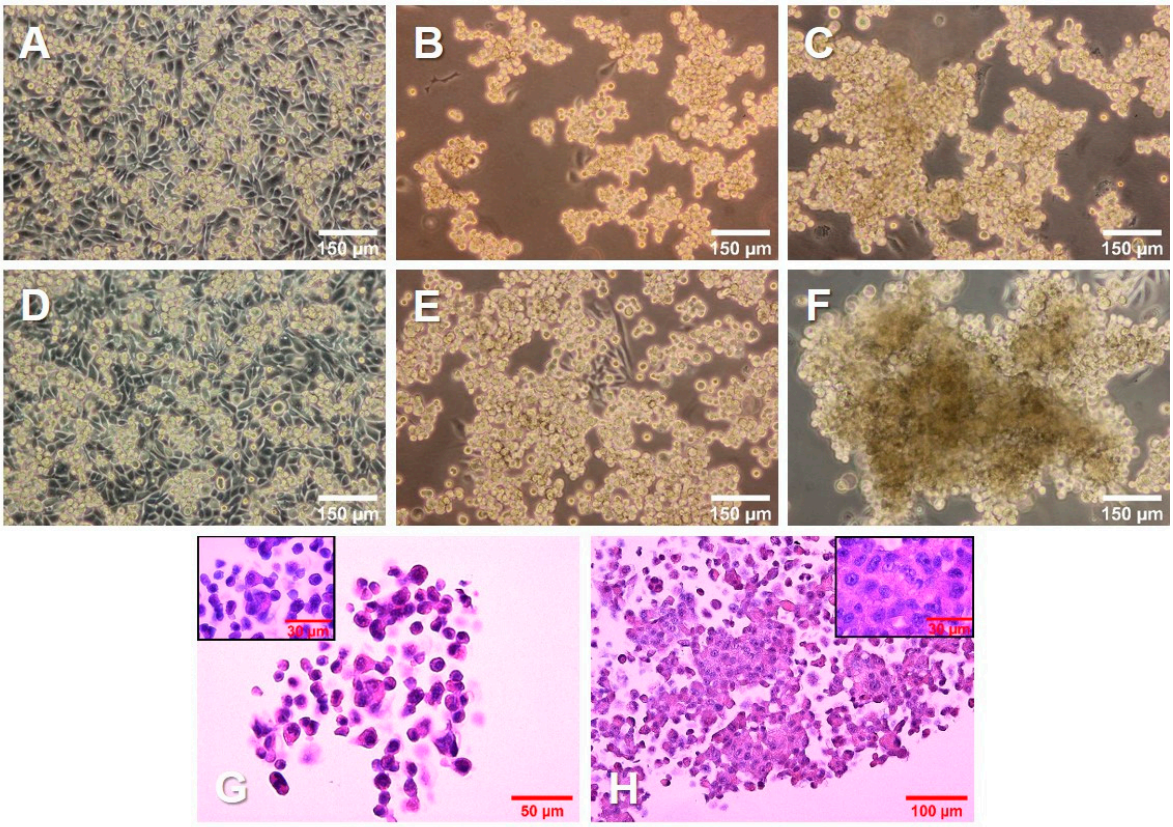

Figure 1. Growth of PC-3 prostate cancer cells in simulated microgravity. PC-3 cells were cultured (**A**,**D**) under 1 g conditions or (**B**,**C**,**E**,**F**) on an RPM for 3 days (**A**–**C**) and 5 days (**D**–**F**). (**G**,**H**) PC-3 cells growing in MCS, stained with hematoxylin and eosin (HE) after a 3-day (**G**) and 5-day (**H**) RPM exposure, respectively.

Hematoxylin–eosin (HE) staining of spheroids grown after 3 days (Figure 1G) and 5 days (Figure 1H) on the RPM presented a condensation of cells together with an increased amount of ECM.

In addition, the cells in all groups were viable and did not undergo apoptosis or necrosis, as seen from the normal cell shape, cytoplasm staining, and intact nuclei.

2.2. VEGF, MAPK, and PAM Signaling Pathways

Quantitative real-time polymerase chain reaction (qPCR) analysis was performed to examine the gene expression of relevant genes of the VEGF, MAPK, and PAM signaling pathways. The qPCR data revealed a significant decrease in the amount of *VEGFA* mRNA in MCS compared to 1 g controls after 3 days and 5 days (Figure 2A).

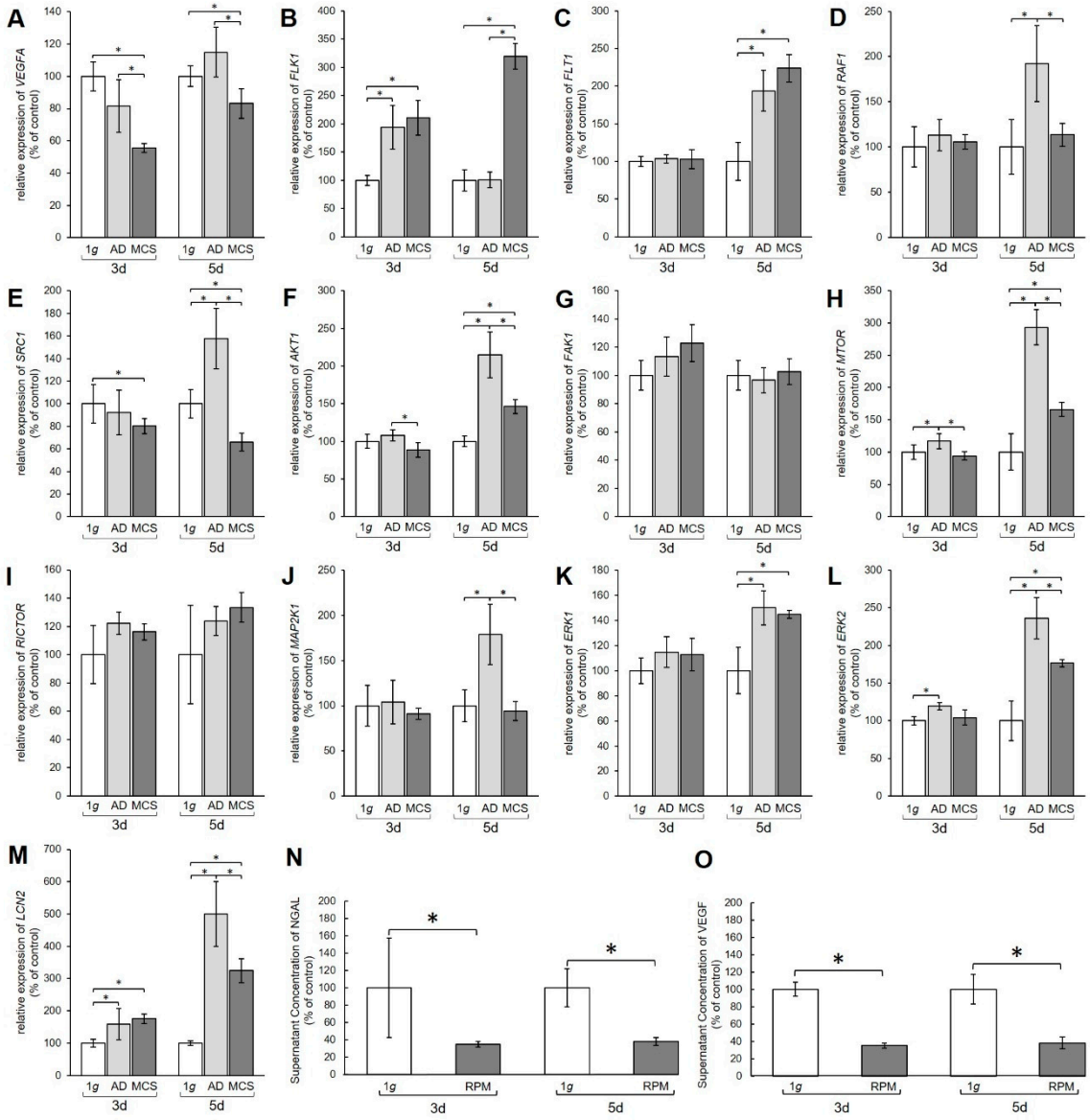

Figure 2. Gene expression of various proteins from the vascular endothelial growth factor (VEGF) signaling pathway. Results show relative mRNA transcription levels from (**A**) *VEGFA*, (**B**) *FLK1*, (**C**) *FLT1*, (**D**) *RAF1*, (**E**) *SRC1*, (**F**) *AKT1*, (**G**) *FAK1*, (**H**) *MTOR*, (**I**) *RICTOR*, (**J**) *MAP2K1*, (**K**) *ERK1*, (**L**) *ERK2*, and (**M**) *LCN2* genes. Results are shown as percentages of 3-day and 5-day 1 g controls. Time-resolved immunofluorometric assay (TRIFMA) results show amounts of (**N**) NGAL and (**O**) VEGF proteins in the supernatant taken from 3-day and 5-day flasks containing PC-3 cells, shown as percentages of 3-day and 5-day 1 g controls. * $p < 0.05$.

The mRNA levels of the VEGFA receptors *FLK1* and *FLT* also showed changes (Figure 2B,C). After 3 days the *FLK1* gene expression was significantly upregulated in both AD and MCS compared to 1 g. After 5 days the *FLK1* mRNA level in AD was unchanged, while MCS showed an increase compared to 1 g and AD (Figure 2B). The *FLT1* mRNA was unchanged after 3 days, but clearly upregulated in both 5-day AD and MCS groups compared with 1 g controls (Figure 2C).

Furthermore, the MAPK pathway was affected by the s-μg conditions. The *RAF1* mRNA was not changed after 3 days, but significantly increased in AD cells after 5 days (Figure 2D). The *SRC1* mRNA expression was significantly downregulated in 3-day MCS compared to corresponding 1 g samples, whereas a 5-day exposure induced upregulation of *SRC1* mRNA in AD and downregulation in MCS compared with 1 g controls and AD samples (Figure 2E). *AKT1* was downregulated in MCS compared to AD, but not significantly changed compared with 1 g after a 3-day RPM exposure. After 5 days, we measured an upregulation of the *AKT1* gene in AD and MCS compared with 1 g (Figure 2F). Interestingly, the *FAK1* gene expression was not significantly changed in all samples (Figure 2G). *MTOR* mRNA was significantly elevated in AD after 3 days and further enhanced after 5 days in both AD and MCS samples (Figure 2H). *RICTOR* gene expression was not differentially displayed in all groups (Figure 2I). Similarly, there was also no change in *MAP2K1* mRNA after 3 days, whereas after 5 days *MAP2K1* mRNA was significantly upregulated in AD cells (Figure 2J). *ERK1* was not changed in 3-day samples, but significantly enhanced in AD and MCS after 5 days (Figure 2K). *ERK2* was upregulated in AD samples after 3 days and, like *ERK1*, clearly upregulated in AD and MCS after 5 days (Figure 2L).

The transcription level of the lipocalin 2/NGAL protein neutrophil gelatinase-associated lipocalin (*LCN2*) gene, however, was increased in both AD and MCS compared to 1 g after 3 and 5 days, but decreased from AD to MCS after 5 days (Figure 2M). Furthermore, the amount of VEGF and NGAL protein secreted from the PC-3 cells into the medium was examined using time-resolved immunofluorometric assay (TRIFMA) (Figure 2N,O). Secreted amounts of VEGF and NGAL were significantly decreased after both 3 and 5 days of RPM-exposure.

2.3. Cytoskeleton

The effect of RPM exposure on the cytoskeleton was examined by qPCR analysis for the genes encoding β-actin and β-tubulin. In addition, F-actin and β-actin were visualized by immunofluorescence (IF). A redistribution of F-actin was observed in PC-3 cells when exposed to s-μg for 3 and 5 days (Figure 3A–C and Figure 3D–F, respectively). AD cells showed an accumulation of cortical actin compared to 1 g control cells. After 3 days, the formation of filopodia and lamellipodia could be observed (Figure 3B). After 5 days, filopodia, lamellipodia, and cortical stress fibers were prominent (Figure 3E). F-actin was accumulated at the cell membrane in MCS after both 3 and 5 days (Figure 3C,F). IF staining for β-actin (Figure 3G–L) did not show a clear difference in the distribution of the protein, although the AD at 3 days (Figure 3H) showed some membrane blebbing. *ACTB* gene expression revealed a significant upregulation in MCS compared to AD after 3 days (Figure 3M), while *TUBB* presented no expression changes (Figure 3N). After 5 days, *ACTB* and *TUBB* mRNAs were increased in both AD and MCS compared to 1 g control cells, and were lower in MCS than AD (Figure 3M,N).

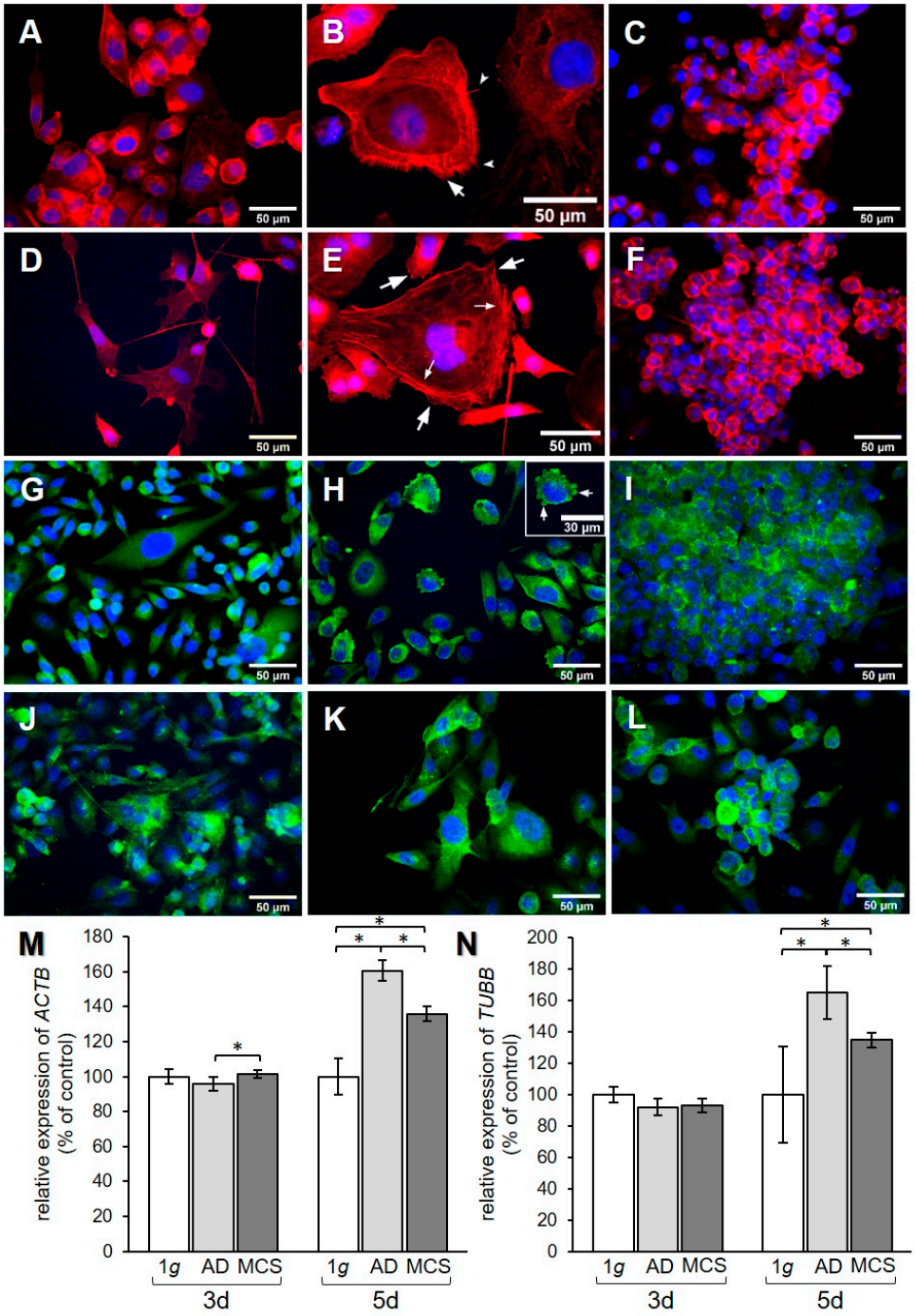

Figure 3. Investigation of the cytoskeleton. F-actin visualized by means of phalloidin and immunofluorescence (IF) staining for β-actin. F-actin pictures show (**A**) 3-day 1 g control, (**B**) 3-day AD, (**C**) 3-day MCS, (**D**) 5-day 1 g, (**E**) 5-day AD, and (**F**) 5-day MCS. Big arrows in (**B**) and (**E**) point to lamellipodia, notched arrows in (**B**) point to filopodia, and small arrows in (**E**) point to stress fibers. β-actin pictures show (**G**) 3-day 1 g control, (**H**) 3-day AD, (**I**) 3-day MCS, (**J**) 5-day 1 g, (**K**) 5-day AD, and (**L**) 5-day MCS. Arrows in (**H**) point to membrane blebbing. Relative mRNA transcription levels of (**M**) *ACTB* and (**N**) *TUBB* genes in 3-day and 5-day samples were analyzed by qPCR. * $p < 0.05$.

2.4. Extracellular Matrix

To examine the effect of s-µg on the ECM, the regulation of collagen, laminin, and fibronectin at the mRNA level and collagen deposition were investigated (Figure 4).

Sirius red staining of PC-3 cells revealed that 1 g cell samples (Figure 4A,D) and AD (Figure 4B,E) were negative for extracellular collagen after 3 and 5 days. However, collagen was found in RPM-exposed samples and was detectable in MCS. After 3-day exposure, a rim of collagen was formed around the cells in the MCS (Figure 4C). After 5 days, larger amounts of collagen were detectable in the center of the MCS, as demonstrated by the prominent red structures (Figure 4F).

qPCR data of the *COL1A1* gene expression revealed a decrease of this gene in MCS compared to both 1 g and AD after 3 days. After 5 days, an upregulation of *COL1A1* mRNA was measured in both AD and MCS compared to 1 g controls (Figure 4G). The gene expression of *COL4A5* was increased after 3 days in AD and MCS compared to 1 g, but decreased in MCS compared to AD. After 5 days, the *COL4A5* mRNA level was strongly elevated in MCS, while no difference was found between AD and 1 g (Figure 4H). The mRNA expression of the genes for the laminin α3 and β2 subunits was investigated. The mRNA level of the *LAMA3* gene was upregulated in AD and MCS compared to 1 g after 3 days, while the *LAMA3* mRNA level in MCS was lower than in AD. After 5 days, the *LAMA3* mRNA in AD was decreased compared to both 1 g and MCS, while MCS did not show a difference compared to 1 g (Figure 4I).

The *LAMB2* mRNA level in AD and MCS was unchanged after 3 days compared to 1 g. *LAMB2* was downregulated in MCS compared to AD. After 5 days, the *LAMB2* mRNA transcription was very high in AD compared to both 1 g and MCS (Figure 4J). The qPCR data for *FN1* showed an increase in AD and MCS cells compared to 1 g after 3 days (Figure 4K). After 5 days, the *FN1* mRNA level was decreased in AD samples compared to both 1 g and MCS (Figure 4K).

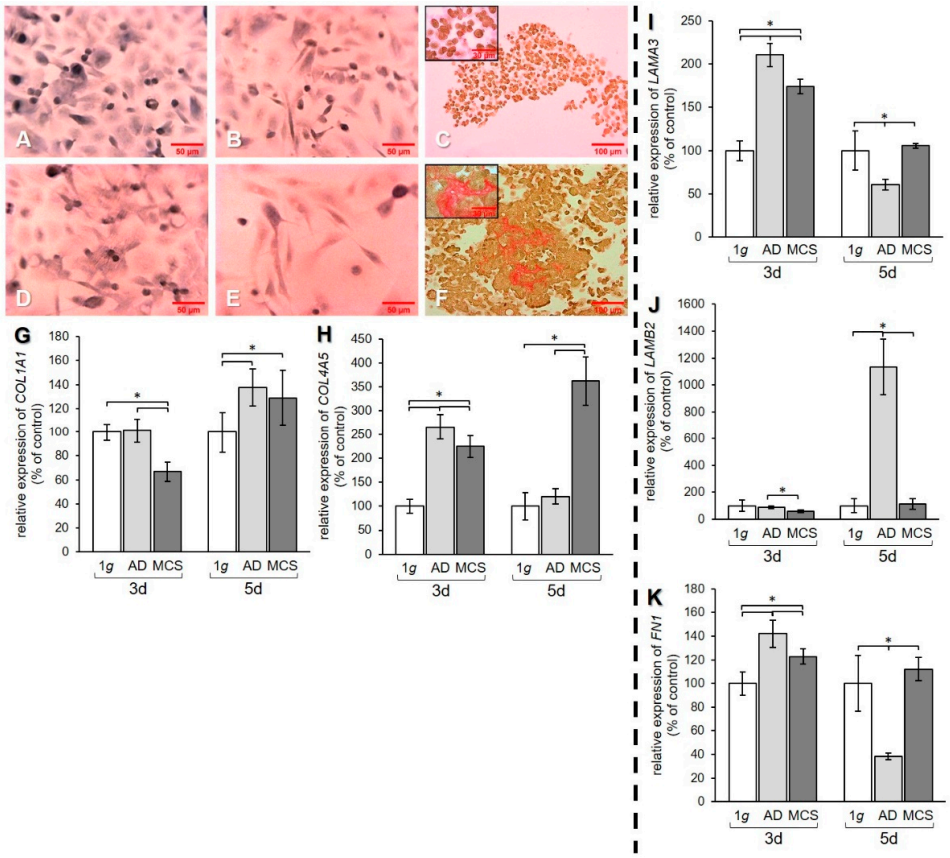

Figure 4. Investigation of ECM components. Collagen deposition in PC-3 cells stained with Sirius red (SR) after (**A**–**C**) 3 days and (**D**–**F**) 5 days. 1 g control cells (**A**,**D**) AD (**B**,**E**) and MCS (**C**,**F**). Depositions of collagen I and III are stained in red. qPCR results show relative mRNA transcription levels of (**G**) *COL1A1*, (**H**) *COL4A5*, (**I**) *LAMA3*, (**J**) *LAMB2*, and (**K**) *FN1* genes in 3-day and 5-day AD and MCS. * $p < 0.05$.

2.5. Altered Expression of Genes of the Focal Adhesion Complex

Finally, we examined the effect of s-μg-exposure of PC-3 cells on the transcription of genes involved in FA.

TLN1 gene expression was upregulated mRNA level after 3 days in AD, but not in MCS compared to 1 g, whereas after 5 days no significant changes were measured (Figure 5A). The mRNA expression of *VCL* was significantly elevated in AD and MCS samples compared to 1 g controls. This elevation of *VCL* was further enhanced after 5 days in both AD and MCS (Figure 5B). Moreover, the *CDH1* gene expression was clearly upregulated after an RPM-exposure in 3-day AD and MCS samples. In contrast, the *CDH1* mRNA expression was downregulated in AD after 5 days, while the *CDH1* level was still upregulated in MCS compared to both 1 g and AD (Figure 5C).

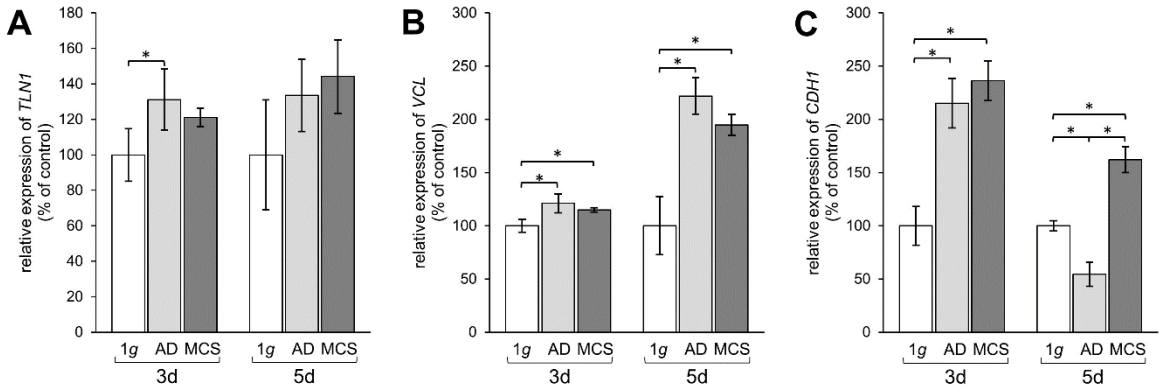

Figure 5. Investigation of gene expression of focal adhesion molecules talin-1, vinculin, and E-cadherin. qPCR results show relative mRNA transcription levels of (**A**) *TLN1*, (**B**) *VCL*, and (**C**) *CDH1* genes in 3-day and 5-day samples. * $p < 0.05$.

2.6. Interaction of Genes Investigated by Pathway Analysis

The various genes analyzed by qPCR (Figure 6A) were differentially regulated in μg samples (AD and RPM). Figure 6A presents a summary of the qPCR data, already described in Figures 2–5, and gives a comparable overview on the results. A closer look at the 3-day samples reveals that most genes involved in VEGF signaling (blue bars) are upregulated in AD samples compared to 1 g, while the gene expression in MCS presents a more heterogeneous pattern. Notably, *VEGFA*, *FLK1*, and *LCN2* are equally regulated in AD and MCS samples after 3 days. After a 5-day RPM-exposure, most of the investigated VEGF signaling molecules are significantly upregulated in AD samples. In comparison, 5-day MCS samples presented a significant regulation, which is in contrast to 3-day samples. Remarkably, *VEGFA* is not regulated in 5-day AD samples compared to 1 g. In addition, *LCN2* is strongly upregulated in all conditions. The cytoskeletal molecules of interest (green bars) are not regulated after 3 days. However, after 5 days, both conditions are upregulated. The investigated ECM molecules (violet bars) after a 3-day RPM-exposure present a comparable image in AD and MCS samples. After 5 days, AD cells show a heterogeneous expression image, while *LAMB2* is strikingly upregulated. In MCS, however, collagens are clearly enhanced, while *LAMB2* is not changed compared to the controls. Genes of the focal adhesion molecule complex (orange bars), especially *CDH1* mRNA, are highly upregulated in both 3-day conditions. Even though *CDH1* is still significantly upregulated, it seems to be reduced in 5-day conditions.

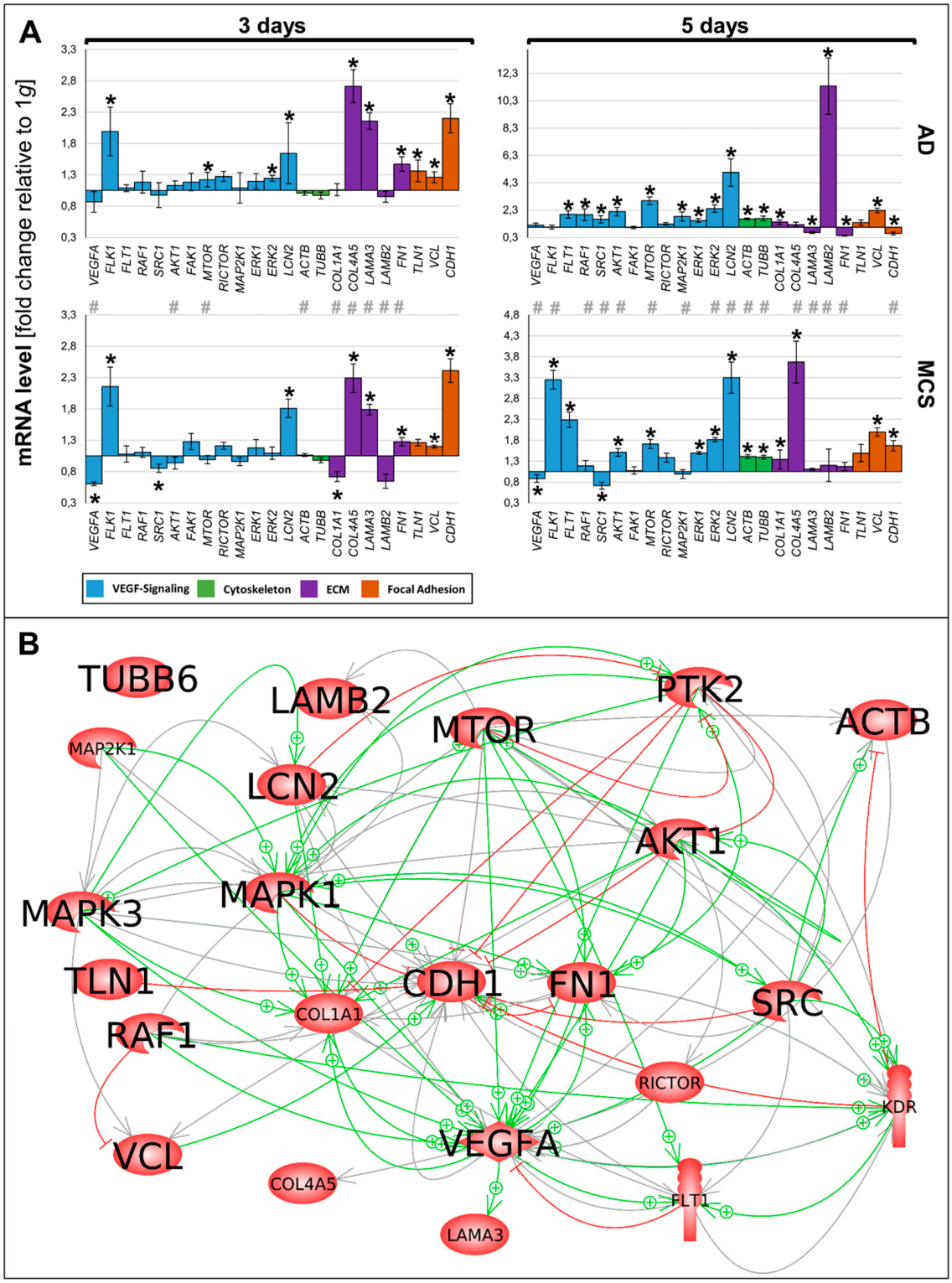

Figure 6. (**A**) Summary of gene expression fold change measured by qPCR of 3- and 5-day RPM-exposed PC-3 samples. Results determined in AD and MCS in relation to 1 g are shown. Color-coded bars represent genes of related biological processes. * $p < 0.01$ 1 g vs. AD/MCS, # $p < 0.01$ AD vs. MCS. (**B**) Interaction network of selected items at gene expression level; 22 of 23 selected genes analyzed by qPCR contribute to the network comprising 114 relations. Green arrows indicate activation and red arrows indicate inhibition. Gray lines signify that interactions take place whose effects have not been clarified. The interaction network was built using Elsevier Pathway Studio plus.

The 23 genes of interest were investigated in regard to their 114 possible interaction and mutual expression dependence. A pathway analysis of these items, represented in molecular action mode, is shown in Figure 6B. It can be seen that the components investigated are members of a complicated network, which includes the central factors *CDH1*, *VCL*, *TLN1*, *FN1*, *VEGFA*, *KDR*, *RAF1*, *ERK1/2*, *MAP2K1*, *MTOR*, *AKT1*, *PTK2*, and *SRC1*. Of these components, *CDH1* seemed to be the main node point.

3. Discussion

In this study, we focused on the changes induced in PC-3 cells when they were cultured under s-μg conditions. Possible simulation devices included RPM, RVW, and 2D clinostat. The RPM was chosen as this device rotates samples around two axes, thus enabling the cells to float freely and randomly in the medium, which increases the chances of interactions and MCS formation [16]. In addition, the RPM provides efficient diffusion of nutrients, gases, and waste through a small fluid flow [16]. The optimal method would be to cultivate the cells on a spaceflight, as this would provide real μg. In contrast, simulation devices average the gravity level to near zero without neutralizing it [18] and expose the cells to small fluid shear forces [46], which might slightly decrease the reproducibility in real μg. However, previous studies have noted that in many cases s-μg produces results similar to real μg [47]. Genes and proteins involved in the regulation of cancer cell proliferation and metastasis, such as IL6, IL8, and VEGFA, were similarly regulated under RPM and spaceflight conditions [47]. Therefore, in the future, it would be interesting to expose PC-3 cells to real μg to compare its effects to our results, as only space experiments can validate results obtained on devices on Earth [18].

When PC-3 cells were placed on the RPM, some of the cells remained adherent, while others detached and formed multicellular tumor-like spheroids. After 5 days, only a few cells remained growing adherently, while the majority were growing in MCS. Notably, variations in the shape, size, and density of the spheroids were observed. This could be due to variations in placement on the RPM. Nevertheless, various cell types exposed to s-μg have grown as multicellular spheroids and also as an adherent monolayer. Examples are thyroid cancer cells [20], breast cancer cells [21], and nonmalignant cells, such as endothelial cells [15].

3.1. Signaling Pathways Involved in Three-Dimensional Growth

3.1.1. VEGF Signaling

We examined the expression of genes belonging to the VEGF signaling pathway and found that the gene expression of *VEGFA* was downregulated after 3 and 5 days of exposure, except in 5-day AD. Accordingly, significant decreases in the amount of secreted VEGF and NGAL were found. This points toward development of a less-aggressive phenotype as a result of cultivation on the RPM, as VEGFA has been implicated in pathological angiogenesis and tumor development [32,48], while NGAL induces *VEGFA* expression [49], among other cancer-promoting functions [50–52]. The *LCN2* gene expression, on the other hand, was increased in all groups, potentially due to a counterregulatory mechanism. Possibly, mRNA levels increase in order to compensate the elevated protein secretion of NGAL protein in the supernatant. The development of a less-aggressive phenotype is supported by the findings in thyroid cancer cells [22,47] and human adult retinal pigment epithelium cells [31]. In contrast, the VEGF and NGAL secretion was elevated in endothelial cells exposed to μg [15]. Future studies should explore this μg-induced shift in greater detail. This can be elucidated by investigating the regulation of other genes and proteins linked to metastasis and proliferation of cancer cells, such as interleukin 6 (IL6), IL8, osteopontin, and fibroblast growth factor 17 [22,47].

In contrast to these findings, we found the expression of genes for the VEGF receptors *FLT1* and *FLK1* to be upregulated after 5 days in MCS, which might indicate a counterregulatory effect of the two VEGF receptors. Furthermore, we found a significant regulation of downstream signaling molecules,

with a general trend to upregulate the gene expression. This was especially evident after 5 days on the RPM.

3.1.2. MAPK Signaling

Factors of the MAPK signaling pathway are known to be involved in 3D growth and metastasis [1]. The biological process of the epithelial–mesenchymal transition (EMT) is known to increase migration and spreading of cancer cells, progression of the cell cycle, and resistance to apoptosis and chemotherapy [53]. Thus, we focused on *RAF1* mRNA expression. RAF1 acts as a regulatory link between the membrane-associated Ras GTPases and the MAPK/ERK cascade and functions as a switch determining, among others, proliferation, differentiation, and oncogenic transformation of human cells. Its main cellular role is in phosphorylation and activation of the MAP kinase kinases MEK1 and MEK2 [54].

In this study we found *RAF1* to be upregulated in AD cells but not in MCS. This indicates its activation by s-µg and its possible involvement in spheroid formation (Figure 2D). As RAF1 activation initiates a mitogen-activated protein kinase cascade, we also determined *MAP2K1* (also known as *MEK1*) gene expression. *MAP2K1* gene expression was comparable to the *RAF1* mRNA level and was significantly elevated in 5-day AD cells (Figure 2J). In a next step, we determined the expression of *ERK1* and *ERK2.* The ERK subfamily consists of typical (ERK 1/2/5) and atypical (ERK 3/4/7/8) members. ERKs are known to regulate EMT and promote tumor progression [54]. *ERK1/2* gene expression was significantly upregulated after 5 days in AD and MCS compared to 1 g samples (Figure 2K,L). Both ERK1 and ERK2 seem to be involved in 3D aggregation in µg.

3.1.3. PI3K/AKT/mTOR (PAM) Signaling

Tee et al. showed that the PAM signaling pathway is frequently mutated in prostate cancer [55]. The PAM pathway is involved in the regulation of growth, metabolism, and migration [55]. In our experiment, the *AKT* gene expression was enhanced in AD and MCS samples after a 5-day RPM-exposure of prostate cancer cells. Activated AKT phosphorylates a host of proteins involved in cell growth, including mTOR [56]. Interestingly, we observed an upregulation of the *MTOR* gene expression in AD after 3 days and in all RPM-exposed cell samples after 5 days. According to the clinicaltrials.gov database, various inhibitors of this pathway are currently being tested in 36 phase I/II clinical trials for prostate cancer, either as monotherapy or in combination with conventional chemotherapies [57].

Finally, we focused on the *SRC1* gene, which belongs to the p160 family of SRCs. SRCs promote cancer cell proliferation, survival, metabolism, migration, invasion, and metastasis. In prostate cancer, *SRC1* is highly expressed [58]. We found an upregulated *SRC1* gene in AD cells after 5 days, indicating its involvement in migration and 3D formation.

Together with MAP1K2, SRC-1 regulates the transcriptional activity of STAT3 [59]. In addition, it blocks upregulation of the VEGF-A receptors [60] and inhibits expression of E-cadherin [61]. On the other side, SRC-1 activates FAK1 [62], which strengthens vinculin, containing focal adhesion complexes [63] that link cells to fibronectin or other components of the ECM [64] and include talin-1 as a hinge between the cytoskeleton and the extracellular space [65]. Downregulation of talin favors activation of the MAPK1/MAPK3 pathway [66].

3.2. Changes in the Cytoskeleton and the Extracellular Matrix

In this study we observed s-µg-induced changes in the F-actin network of the cells. The formation of lamellipodia and filopodia in our cells under s-µg might indicate that the cells are trying to adhere better to the ECM to resist the s-µg conditions, because these structures are involved in migration and adherence of cells to the substrate [67]. In addition, the stress fibers also present might have formed in order to compensate for changes in adhesion and cell morphology [68].

The cortical F-actin accumulation is consistent with earlier findings in endothelial cells, although the latter also showed perinuclear accumulation [12]. An increase in the density of F-actin was also found in A431 cells, although the actin filaments became less organized [69]. Just like PC-3 cells, human fetal osteoblasts showed formation of filopodia and lamellipodia [70]. In contrast, osteoblasts had reduced cortical actin and fewer stress fibers [71]. It is clear from these examples that the changes in F-actin induced by µg depend on the cell type.

Moreover, we found that the mRNA level of *ACTB* was increased after 5 days. This is in accordance with similar findings in follicular thyroid cancer cells [72]. In addition, our qPCR analysis showed an increased *TUBB* mRNA level in PC-3 cells exposed to s-µg, which is similar to earlier results in endothelial cells [73].

In general, we found a tendency of elevated ECM components at the mRNA level when PC-3 cells were exposed to s-µg on the RPM. The mRNA levels of the *COL1A1*, *COL4A5*, *LAMA3*, *LAMB2*, and *FN1* genes were upregulated or unchanged, with only a few exceptions. In addition, collagen deposition was found in spheroids. A possible explanation for this finding could be that the cells try to increase the ECM to resist the s-µg conditions, because the ECM provides structural support for the cells [74], which they lack after detaching because of the RPM-exposure. Our results concerning the ECM fit the findings of a study of human fetal osteoblasts exposed to s-µg, where the cells showed collagen deposition in spheroids and increased *FN1* and *LAMA1* gene expression [70]. However, the gene expression of *COL4A5*, *FN1*, and *LAMB2* was reduced in s-µg-exposed adult retinal pigment epithelial cells [31]. Thus, regulation of ECM compounds because of µg-exposure must depend on the cell type.

We found an increase in the focal adhesion component *VCL* mRNA. It is plausible that this change occurs because the cells are trying to resist the s-µg conditions and hold onto the ECM, although this does not match the generally unchanged amounts of *TLN1* gene expression in our experiment. In contrast to the results of this study, FTC-133 cells exposed to µg showed no change in *VCL* expression and decreased *TLN* mRNA [75]. Thus, PC-3 cells and FTC-133 cells show a different regulation of FA gene expression and, possibly, synthesis or secretion of proteins.

Finally, we detected a general upregulation of the *CDH1* gene expression. In conjunction with our observations on the secretion of VEGF and NGAL described above, this could also indicate a tendency toward a less-aggressive phenotype, as *CDH1* is a tumor suppressor gene, and inactivation of E-cadherin is involved in the development of prostate cancer [76,77]. E-cadherin was enhanced in papillary thyroid carcinoma cells [78], but decreased in human breast cancer cells [79] exposed to s-µg conditions. Thus, E-cadherin acts depending on the cell type.

3.3. Interaction Network of Selected Genes Evaluated by Pathway Analysis

In the pathway analysis various interactions were found, but *VCL*, *FN1*, *mTOR*, *SRC1*, and *VEGFA* are indicated as dominant target genes, as many arrows point to their icons (Figure 6B).

There are interactions between vinculin and fibronectin. *FN1* and *VCL1* were both upregulated in MCS after 3- and 5-day RPM-exposure (Figures 4K and 5B). Similar findings were reported after 24- and 48-h clinostat-exposures of poorly differentiated follicular thyroid cancer cells exhibiting increased expression of vinculin and among other ECM proteins as well as fibronectin in MCS compared with 1 g controls [11]. A recent paper reported that FN1 KO podocytes showed significant downregulated FA molecules (talin, vinculin, and paxillin) and reduced cell spreading, indicating an important role of FN1 in adhesion [80]. FN1 plays a key role in the adaptation of podocytes to mechanical stress. Moreover, this supports the hypothesis that its interaction with vinculin is an adaptive mechanism to protect µg-exposed prostate cancer cells and other cell types.

In addition, there is an interaction between vinculin and MAPK1 (ERK2). Both factors are involved in transmitting and transducing environmental signals to biochemical cascades. The protein kinases are known to regulate the activity of FA proteins [81]. Vinculin also interacts with MAPK3 (ERK1). Macrophages grown on polished surfaces changed from spherical to well-spread cells. These

morphological changes were associated with an altered distribution of vinculin [82]. The pFAK, pSrc, pERK1/2 levels were associated with cell shape and a more spread morphology [82].

There is an interesting interaction between FN1 and MAPK3 (ERK2). Treatment of PC-3 cells with 1 µM FN1 resulted in a decrease of activated ERK1/2 [83]. In clear-cell renal cancer, eight differentially expressed genes were identified as biomarkers, including *VEGFA*, *FLT1*, *FN1*, and others [84]. Both fibronectin and VEGF are known to stimulate blood vessel formation. Patient data showed that circulating fibronectin modulates blood vessel formation and tumor growth by modifying the amount of and response to VEGF [85]. In addition, measuring the fibronectin level can serve as a prognostic biomarker for prostate cancer and possibly others.

The *SRC1* mRNA was significantly downregulated in MCS after 3- and 5-day RPM-exposure of prostate cancer cells (Figure 2E), whereas *VCL* was elevated in MCS in our experimental setting (Figure 5B). Moreover, *CDH1* mRNA expression was enhanced in PC-3 MCS after 3 and 5 days on the RPM (Figure 5C). The product of the human SRC gene, *c-Src*, is overexpressed and often activated in many human cancers. The relationship between Src activation and cancer progression appears to be significant [86].

Interestingly, the exposure of PC-3 cells induced a decrease in *SRC1*, which supports the hypothesis that the PC-3 cells showed a more moderate expansion behavior as compared to MCF-7 breast cancer cells. In contrast, in MCF-7 breast cancer spheroids, c-Src was elevated and E-cadherin was reduced [79]. MCS formation could be prevented by inhibition of c-Src and enhanced by blocking of E-cadherin. These results suggest that the balance of proteins that up- or downregulate E-cadherin mediates the tendency of breast cancer cells to form MCS during s-µg-exposure [79].

In addition, there was another detectable interaction between SRC and laminin subunit alpha-3 (LAMA3). *LAMA3* gene expression was upregulated in AD and MCS after a 3-day RPM-exposure of the cells. It also was shown earlier that the recently identified Lm3B11, consisting of laminin α3B (encoded by *LAMA3*), β1, and γ1 chains, stimulated the phosphorylation of Src and Akt more strongly than other laminins in vascular basement membranes [87]. This unique activity of Lm3B11 appears to be favorable to the process of angiogenesis.

SRC has been found to play a crucial role in VEGF-dependent vascular permeability involved in angiogenesis. Chou et al. showed that the two main VEGFRs, kinase insert domain-containing receptor/fetal liver kinase-1 (KDR/Flk-1) and Fms-like tyrosine kinase-1 (Flt-1), interact with SRC. VEGF stimulation elevated SRC activity associated with activated KDR/Flk-1 in endothelial cells [88]. The gene expression of *VEGFA* was downregulated, whereas both VEGFA-receptor genes, *KDR* and *FLT1*, were upregulated in all 5-day RPM samples, which might indicate a counterregulatory effect (Figure 2A–C). In colon cancer cells, SRC induced VEGF, thus enhancing angiogenesis [89,90]. The relationship between Src and VEGF appears to be somewhat reciprocal [86]. VEGF-induced activity is negated with the inhibition of Src activity. Src also appears to provide a link in VEGF signaling of MAPK pathways, contributing to spreading and metastasis [90].

In PC-3 prostate cancer cells, we found a significant downregulation of *VEGFA* mRNA and protein secretion, indicating a lower metastatic potential of the cells when exposed to microgravity. These results are similar to those obtained from low-differentiated follicular thyroid cancer cells in space [47], where we also found a downregulation of both VEGFA gene and protein secretion.

The PI3K/AKT/mTOR signaling pathway plays a key role in cancer metastasis. The activation of a mitogenic pathway involving a feedback mechanism between mTOR and PI3K/ERK1/2 is important for the tumorigenesis of glioblastoma multiforme [91] and may be involved in 3D spheroid formation in s-µg. The MAPK and PI3K/AKT/mTOR pathways regulate cell survival, proliferation, and motility. In addition to their independent signaling programs, the pathways engage in an extensive crosstalk to both positively and negatively regulate each other. Encouragingly, co-inhibition of both pathways has been successful in reducing tumor growth in xenograft cancer models and, importantly, also in genetically engineered mouse models [92,93]. mTOR catalyzes the phosphorylation of multiple targets such as AKT, protein kinase C (PKC), and others, thereby regulating various biological processes such

as tumor growth and metastasis. Many mTOR inhibitors have been developed to treat cancer. While some of them have been approved to treat human cancer, more mTOR inhibitors are being evaluated in clinical trials. In addition, current research is designed to optimize the use of VEGF/VEGF receptor inhibitors and mTOR inhibitors for combination or sequential treatment of patients with advanced cancer [94,95].

In short, the s-µg conditions created by the RPM caused differential regulations of the expression of the VEGF, MAPK, and PAM pathway-involved genes *VEGFA*, *FLK1*, *FLT1*, *RAF1*, *SRC1*, *AKT1*, *MTOR*, *MAP2K1*, *ERK1*, and *ERK2*, as well as the genes *ACTB*, *TUBB*, *COL1A1*, *COL4A5*, *LAMA3*, *LAMB2*, *FN1*, *TLN1*, *VCL*, and *CDH1*, involved in signal transduction in the cytoskeleton, ECM, and FAs. Furthermore, a redistribution of F-actin was found in the cells, as well as a deposition of collagen in MCS and decreased secretion of VEGF and NGAL. Thus, s-µg resulted in the regulation of proteins and genes involved in angiogenesis, cell morphology, migration, attachment, ECM, and 3D growth. Possibly, some changes are due to attempts to resist the alterations in µg. Moreover, the PC-3 cells formed spheroids when cultured in s-µg conditions. These 3D constructs might be useful in future studies on the effects of anticancer drugs, as they more closely mimic the cellular environment in actual metastasis, including, for example, the need for diffusion of the drug into the core of the spheroid as opposed to monolayer cell cultures. A future project could be to examine the effects of drugs targeting the proteins regulated in the PC-3 cells when exposed to µg. This was done, for example, with dexamethasone targeting NFκB in breast cancer cells [21], and possible drug investigations are planned for thyroid cancer cells in µg [22]. In addition, it is also important to apply different signaling pathway inhibitors as well as an agonist to investigate the role of µg in prostate cells. Further examination of prostate cancer cells in weightlessness may thus contribute to investigations concerning treatment options and possibly reduce animal experiments in the field of prostate cancer.

4. Materials and Methods

4.1. Cell Culturing and Microgravity Simulation on the RPM

The human prostatic carcinoma cell line PC-3 was established from a human prostatic adenocarcinoma metastatic to bone, enabling investigations concerning the changes involved in advanced prostate cancer as well as response to treatment [96]. PC-3 cells (ECACC 90112714) were thawed from a frozen aliquot preserved in liquid nitrogen. They were seeded in T75 flasks (Sarstedt, Nümbrecht, Germany) with RPMI 1640 medium (Gibco, Fisher Scientific, Schwerte, Germany) containing 14% fetal bovine serum (FBS) (Sigma-Aldrich) and 1% penicillin/streptomycin (Gibco, Fisher Scientific, Schwerte, Germany). Afterwards, the medium was changed when necessary, using RPMI 1640 medium with 7% FBS and 1% penicillin/streptomycin. When the cells had grown appropriately, they were subcultured in T25 flasks (Sarstedt) and slideflasks (Thermo Scientific, Waltham, MA, USA) and left in 1 g conditions until reaching approximately 60% confluence.

After reaching 60% confluence, all flasks were filled completely with RPMI medium containing 10% FBS and 1% penicillin/streptomycin. Filling the flasks completely and without air bubbles was important to reduce shear stress and disturbance of the cells. Half of the flasks were mounted on the middle frame of the RPM. The other half were placed beside the RPM in 1 g conditions as controls. The RPM used in this experiment (a desktop model from Airbus, Defense and Space, Leiden, the Netherlands) was, along with all flasks, placed in an incubator at 37 °C and 5% CO_2. Then, the RPM was started, exposing the cells to s-µg conditions for the chosen time periods (3 or 5 days). The RPM simulates µg with a calculated residual acceleration of approximately ~10^{-3} g [97]. The maximal distance to the rotation center was chosen to be 7 cm, and the rotational acceleration was 20°/s^2. The device was described in detail by Grimm et al. [98].

4.2. Sample Collection

Three groups were collected from the RPM experiments: 1 g, AD, and MCS. In addition, aliquots of medium (cell supernatants) were collected for the TRIFMA experiment.

The control cells were collected from the T25 flasks exposed to 1 g conditions. First, several aliquots of medium from the flasks were collected. The rest of the medium was discarded, the cells were washed with 5 mL of phosphate-buffered saline (PBS) and then scraped off the bottom of each flask with a cell scraper, and another 5 mL PBS (Gibco, Fisher Scientific, Schwerte, Germany). The cell suspensions were transferred to tubes and subsequently centrifuged. After discarding the supernatant, the cell pellets were resuspended in PBS and transferred to reaction tubes.

MCS were collected from the T25 flasks from the RPM. First, the flasks were left until the spheroids had all fallen to the bottom. Then, several aliquots of medium were collected, after which the flasks were shaken to allow the MCS to redistribute themselves in the liquid. The medium was transferred to new tubes and centrifuged. The supernatant was discarded and the pellets containing the MCS were resuspended in PBS and transferred to Eppendorf tubes.

AD were collected from the RPM flasks by scraping the cells in PBS, then transferred to Eppendorf tubes.

Following the collection, all Eppendorf tubes were centrifuged, the supernatant was discarded, and pellets were snap-frozen in liquid nitrogen and stored at −80 °C. The supernatant aliquots were frozen and stored at −20 °C. All centrifugation steps were performed at 3000 rpm and 4 °C for 10 min.

4.3. RNA Isolation

RNA isolation was done using the RNeasy Mini Kit (Qiagen, Hilden, Germany). The samples were thawed and kept on ice. First, 10 µL of β-mercaptoethanol (BME) was added to 1 mL of lysis buffer (RTL), followed by the addition of 600 µL of this mixture to each sample. The samples were incubated for 2 min and the cells were lysed by applying shear force while passing them through a 20 G needle. Finally, 600 µL of 70% ethanol was added to each sample.

Then 700 µL of each sample was transferred to RNeasy Mini spin columns and 700 µL of Buffer RW1 and 500 µL of Buffer RPE were added. Between these steps the samples were centrifuged for 15 s at 8000× *g*, and flow-through was discarded. Then 500 µL of Buffer RPE was added again, this time followed by centrifugation for 2 min at 8000× *g*, and flow-through was discarded. Finally, the samples were centrifuged for 1 min to dry the membrane and remove any remaining ethanol.

The RNeasy spin columns were placed in new collection tubes, followed by the addition of 35 µL of RNase-free water directly to the membrane. The RNA was eluted from the membrane by centrifugation for 1 min at 8000× *g*.

4.4. Quantitative Real-Time Polymerase Chain Reaction

Before performing qPCR, primers were designed using NCBI Primer Blast, which were selective for cDNA by spanning exon–exon junctions and had a melting temperature of around 60 °C. The primers were synthesized by TIB Molbiol (Berlin, Germany). The primers used are listed in Table 1.

Table 1. List of primer sequences used in quantitative PCR. All sequences are listed in the 5′–3′ direction.

Factor	Primer Name	Sequence 5′–3′
18S-rRNA	18s-F	GGAGCCTGCGGCTTAATTT
	18s-R	CAACTAAGAACGGCCATGCA
Actin-beta (***ACTB***)	ACTB-F	TGCCGACAGGATGCAGAAG
	ACTB-R	GCCGATCCACACGGAGTACT
RAC-alpha Serine/threonine-protein kinase (***AKT1***)	Akt1-F	CTTCTATGGCGCTGAGATTGTG
	Akt1-R	CAGCATGAGGTTCTCCAGCT
Collagen 1 alpha 1 (***COL1A1***)	COL1A1-F	ACGAAGACATCCCACCAATCAC
	COL1A1-R	CGTTGTCGCAGACGCAGAT
Collagen 4 alpha 5 (***COL4A5***)	COL4A5-F	GGTACCTGTAACTACTATGCCAACTCCTA
	COL4A5-R	CGGCTAATTCGTGTCCTCAAG
E-cadherin (***CDH1***)	CDH1-F	GCTGGACCGAGAGAGTTTCC
	CDH1-R	CAGCTGTTGCTGTTGTGCTT
Extracellular signal-regulated kinase 1 (***ERK1***)	ERK1-F	ACCTGCGACCTTAAGATTTGTGA
	ERK1-R	AGCCACATACTCCGTCAGGAA
Extracellular signal-regulated kinase 2 (***ERK2***)	ERK2-F	TTCCAACCTGCTGCTCAACA
	ERK2-R	TCTGTCAGGAACCCTGTGTGAT
Focal adhesion kinase 1 (Protein-tyrosin kinase 2) (FAK1 (***PTK2***))	FAK1-F	TGTGGGTAAACCAGATCCTGC
	FAK1-R	CTGAAGCTTGACACCCTCGT
Fibronectin (***FN1***)	FN1-F	TGAGGAGCATGGTTTTAGGAGAA
	FN1-R	TCCTCATTTACATTCGGCGTATAC
Laminin alpha 3 (***LAMA3***)	LAMA3-F	AAAGCAAGAAGTCAGTCCAGC
	LAMA3-R	TCCCATGAAGACCATCTCGG
Laminin β2 (***LAMB2***)	LAMB2-F	TGCTCATGGTCAATGCTAATCTG
	LAMB2-R	TCTATCAATCCTCTTCCTTGGACAA
Mitogen-activated protein kinase kinase 1 (***MAP2K1***)	MAP2K1-F	CGTTACCCGGGTCCAAAATG
	MAP2K1-R	TCCAAGTTGGTCTCCGCA
Mechanistic target of rapamycin kinase (***MTOR***)	MTOR-F	ATCTTGGCCATAGCTAGCCTC
	MTOR-R	ACAACTGGGTCATTGGAGGG
Neutrophil gelatinase-associated lipocalin (NGAL, ***LCN2***)	LCN2-F	AGGGAGTACTTCAAGATCACCCTCTA
	LCN2-R	AGAGATTTGGAGAAGCGGATGA
Raf-1 proto-oncogene, serine/threonine kinase (***RAF1***)	RAF1-F	GGGAGCTTGGAAGACGATCAG
	RAF1-R	ACACGGATAGTGTTGCTTGTC
Rapamycin-insensitive companion of MTOR (***RICTOR***)	RICTOR-F	GGAAGCCTGTTGATGGTGAT
	RICTOR-R	GGCAGCCTGTTTTATGGTGT
Steroid receptor coactivator-1 (***SRC1***)	SRC1-F	CCACCTTTGTGGCCCTCTAT
	SRC1-R	CCTCTGTGTTGTTGACAATCTGG
Talin-1 (***TLN1***)	TLN1-F	GATGGCTATTACTCAGTACAGACAACTGA
	TLN1-R	CATAGTAGACTCCTCATCTCCTTCCA
Tubulin-beta (***TUBB***)	TUBB-F	CTGGACCGCATCTCTGTGTACTAC
	TUBB-R	GACCTGAGCGAACAGAGTCCAT
Vascular endothelial growth factor A (***VEGFA***)	VEGFA-F	GCGCTGATAGACATCCATGAAC
	VEGFA-R	CTACCTCCACCATGCCAAGTG
Vascular endothelial growth factor receptor 1 (***FLT1***)	FLT1-F	CCCTCGCCGGAAGTTGTAT
	FLT1-R	GATAATTAACGAGTAGCCACGAGTCAA
Vascular endothelial growth factor receptor 2 (***FLK1***)	FLK1-F	TCTTCTGGCTACTTCTTGTCATCATC
	FLK1-R	GATGGACAAGTAGCCTGTCTTCAGT
Vinculin (***VCL***)	VCL-F	GTCTCGGCTGCTCGTATCTT
	VCL-R	GTCCACCAGCCCTGTCATTT

The first step was to generate cDNA from the RNA using the high capacity cDNA reverse transcription kit (Applied Biosystems, Foster City, CA, USA). The RNA concentrations of all samples were measured using a NanoDrop. The results were used to calculate the amount of RNA and

nuclease-free water needed to obtain 1 μg of RNA in a final volume of 10 μL. The nuclease-free water was pipetted into wells on a 96-well plate, followed by addition of RNA, then 10 μL of master mix was added to each well. This contained RT buffer, dNTP mix, RT random primers, reverse transcriptase, and nuclease-free water. The plate was sealed and centrifuged briefly to eliminate any air bubbles and spin down liquid. The thermal cycler was run using the following program: primer annealing for 10 min at 25 °C reverse transcription for 120 min at 37 °C and enzyme deactivation for 5 min at 85 °C. After this, 50 μL of nuclease-free water was added to each well to obtain a working volume of 70 μL for the next steps.

The qPCR was carried out using FAST SYBR™ Green Master Mix (Applied Biosystems) and the 7500 Fast Real-Time PCR System (Applied Biosystems). First, a master mix was prepared for measurement of all samples in triplicate as well as 3 no-template controls (NTCs). The master mix contained MM Buffer, reverse primer, forward primer, and water. Then, a sub-master mix was prepared for each sample by mixing 42 μL of master mix and 3 μL of cDNA. For each sample, 13 μL of the sub-master mix was pipetted into a 96-well plate in triplicate. NTCs were added to the last 3 wells. The plate was sealed, centrifuged briefly, and stored at 4 °C. When ready to use, the plate was placed in the instrument, and the thermal cycling conditions were set: 95 °C for 20 s, 95 °C for 3 s, and 60 °C for 30 s. The reaction volume was set to 15 μL and the program was run.

In the following analysis the samples were normalized to 18S rRNA. The comparative threshold cycle ($\Delta\Delta C_T$) method was utilized to obtain the relative transcription levels; 1 g controls were defined as 100%.

4.5. Immunofluorescence

Staining experiments were performed on cells grown in slideflasks that had been cultured on the RPM for 3 or 5 days and their corresponding 1 g controls in order to investigate the change in distribution of F-actin and β-actin.

When the flasks were taken off the RPM, the medium was discarded and the cells were washed three times with PBS and afterwards fixed with 4% paraformaldehyde (PFA; Sigma-Aldrich, St. Louis, MO, USA) in PBS. All slides were stored at 4 °C until ready to use. When ready, the PFA was removed and the slides were washed with PBS, followed by the addition of 0.1% Triton X-100 (Sigma-Aldrich, St. Louis, MO, USA), which was left for 15 min. Then, the slides were removed from the flasks and placed in a dark and moist chamber. Rhodamine–phalloidin (for F-actin; Sigma, P1951, diluted 1:250) or primary antibody (for β-actin; Sigma, A5316, diluted 1:1000) diluted in 0.5% bovine serum albumin (BSA) (Merck, Darmstadt, Germany) in PBS was pipetted onto each slide. For β-actin, the incubation was left overnight, and the next day secondary antibody (anti-mouse IgG Fab2 Alexa Fluor® 488 Molecular Probes 2 mg/mL #4408S, diluted 1:500) diluted in PBS was added. The secondary antibody was left on the slides for a minimum of 4 h.

Finally, the slides were prepared with Fluoroshield™ mounting medium containing 4′,6′-diamidino-2-phenylindole (DAPI) (Sigma-Aldrich, St. Louis, MO, USA). The slides were sealed by putting a coverslip on top and stored in a dark box at 4 °C. Between steps, the slides were washed with cold PBS.

4.6. Histochemical Staining

Histological staining was performed on 3- and 5-day 1 g controls and RPM slides using hematoxylin-eosin (HE) and Sirius red (SR) stains as described earlier [99,100].

The histological staining was done on cells on slides and on MCS on separate slides. After culturing the cells on the RPM for 3 or 5 days, the MCS were collected from the slides with a pipette, washed three times in PBS, and then fixed in 4% PFA. Then they were embedded in paraffin, followed by sectioning into 3 μm sections with a microtome. For 1 g and RPM AD samples, the medium was discarded and the slides were washed three times with PBS, and afterwards 4% PFA was applied. The

slides and sectioned spheroids were stained with HE or SR. HE staining was used to evaluate the cell morphology, while SR staining was used to investigate the collagen content.

4.7. Microscopy

All flasks containing viable cells were examined throughout growth as well as before and after RPM-exposure with a Leica phase contract microscope. Pictures were taken using a Canon EOS 550D camera. All cells stained by immunofluorescence were examined with a Leica DFC310 FX fluorescence microscope. Pictures were taken at 20×, 40×, and 100× magnification using the LAS V3.7 software. The pictures were not taken using the same settings, as the signal intensities were not quantified. The pictures were instead used to examine the locations of the proteins. Immersion oil (Sigma-Aldrich, St. Louis, MO, USA) was applied to the slides when using the higher resolution.

4.8. Time-Resolved Immunofluorometric Assay

TRIFMA was performed as described earlier [101,102]. In brief, microtiter 96-well plates were coated overnight at 4 °C with primary antibodies dissolved in PBS. They were specific for either NGAL (1 µg/mL) or VEGF (2 µg/mL). All wells were then incubated with blocking buffer (1% Tween-20 in PBS) for 2 h.

The samples were diluted 1:2 in assay buffer to a total of 100 µL and added to the plates. The assay buffer used was PBS supplemented with 0.05% Tween-20. In addition, recombinant standards (VEGF and NGAL) were added to the plate (100 µL per well). Negative control samples, containing 100 µL of assay buffer without added supernatant, were also added to the plates. All samples were added to the plates in duplicate to increase the precision of the results.

The Fluorescence was measured using a time-resolved fluorometer (PerkinElmer, Waltham, MA, USA). The concentrations of VEGF and NGAL were determined using a 4-parameter standard curve fit implemented in WorkOut 2.5 data analysis software (PerkinElmer, Waltham, MA, USA).

4.9. Pathway Analysis

To investigate the mutual regulation of genes and visualize localization and interactions between proteins, we entered relevant UniProtKB entry numbers in the Pathway Studio plus software (Elsevier Research Solutions, Amsterdam, The Netherlands). Graphs were generated for gene expression and protein regulation and binding. The method was described previously [103].

4.10. Statistical Analysis

All statistical evaluations were performed using IBM SPSS Statistics 23 (IBM Deutschland GmbH, Ehningen, Germany). The Mann–Whitney U-test was utilized to evaluate the statistical significance of the changes in expression levels following RPM exposure, thus comparing 1 g control to AD and MCS. A significance level of 0.05 was used. The standard deviation was calculated and presented together with the mean values as percentages in bar plots.

5. Conclusions

Prostate cancer cells (PC-3 cell line) exposed to s-µg conditions generated by an RPM grew as adherent cells and in the form of 3D MCS. The RPM-exposed cells revealed alterations in the cytoskeleton, as well as gene expression changes of cytoskeletal and FA factors and ECM components. The VEGF, MAPK, and PAM signaling pathways are involved in 3D formation of prostate cancer cells. The majority of the factors are upregulated, indicating their impact on growth and progression of these cells.

Overall, our study suggests that these pathways drive the regulation of metastasis, survival, and angiogenesis of prostate cancer cells.

Author Contributions: RPM experiments: T.E.H. and J.S.; conceptualization, D.G., T.J.C., and S.K.; methodology, S.K., M.Z.N., D.D., and J.S.; software, J.B., M.W., and S.K.; validation, D.G., T.J.C., S.K., and M.K.; formal analysis, M.Z.N., S.K., J.S., D.D., and M.W.; investigation, T.E.H., N.E.M., M.Z.N., J.S., M.E., and S.K.; resources, M.I. and K.U.; writing—original draft preparation, T.E.H., S.K., T.J.C., D.G., and J.B.; project administration, D.G.; funding acquisition, D.G. and M.I. All authors have read and agree to the published version of the manuscript.

Funding: This research was funded by the German Space Agency (DLR; BMWi project 50WB1924) and Aarhus University (DG).

Acknowledgments: We would like to thank Christa Baumann, Institute of Pathology, University of Regensburg, University Hospital, Regensburg, Germany for performing the paraffin sections, and HE and Sirius red staining.

Conflicts of Interest: The authors declare no conflict of interest.

Abbreviations

AD	Adherent cell(s)
BME	β-mercaptoethanol
BSA	Bovine serum albumin
DAPI	4′,6-diamidino-2-phenylindole
ECM	Extracellular matrix
EMT	Epithelial–mesenchymal transition
ERK	Extracellular signal regulated kinase
FA	Focal adhesion
FAK	Focal adhesion kinase
FLK1	Fms-related tyrosine kinase 1
FLT1	Fetal liver kinase 1
FBS	Fetal bovine albumin
HE	Hematoxylin–eosin
HRP	Horseradish peroxidase
IF	Immunofluorescence
MAPK	Mitogen-activated protein kinase
MCS	Multicellular spheroid(s)
MEK1	Mitogen-activated protein kinase kinase 1
mTOR	Mammalian target of rapamycin
mTORC2	mTOR complex 2
μg	Microgravity
NGAL (LCN2)	Neutrophil gelatinase-associated lipocalin (lipocalin 2)
NTC	No-template control
1 g	Normal gravity
PAM	PI3K/AKT/mTOR
PBS	Phosphate-buffered saline
PBST	Phosphate-buffered saline with Tween
PFA	Paraformaldehyde
PI3K	Phosphoinositide 3-kinase
PKB	Protein kinase B
qPCR	Quantitative real-time polymerase chain reaction
RAF	Rapidly accelerated fibrosarcoma
RICTOR	Rapamycin-insensitive companion of mTOR
RIPA	Radioimmunoprecipitation assay
RPM	Random positioning machine
rpm	Rounds per minute
RWV	Rotating wall vessel
SR	Sirius red
SRC (Src)	Steroid receptor coactivator (proto-oncogene, non-receptor tyrosine kinase)
S-μg	Simulated microgravity
TBST	Tris-buffered saline with Tween

VEGF	Vascular endothelial growth factor
VEGFR	Vascular endothelial growth factor receptor
WHO	World Health Organization
TRIFMA	Time-resolved immunofluorometric assay
2D	Two-dimensional
3D	Three-dimensional

References

1. Nassef, M.Z.; Kopp, S.; Melnik, D.; Corydon, T.J.; Sahana, J.; Krüger, M.; Wehland, M.; Bauer, T.J.; Liemersdorf, C.; Hemmersbach, R.; et al. Short-Term Microgravity Influences Cell Adhesion in Human Breast Cancer Cells. *Int. J. Mol. Sci.* **2019**, *20*, 5730. [CrossRef] [PubMed]
2. Fukazawa, T.; Tanimoto, K.; Shrestha, L.; Imura, T.; Takahashi, S.; Sueda, T.; Hirohashi, N.; Hiyama, E.; Yuge, L. Simulated microgravity enhances CDDP-induced apoptosis signal via p53-independent mechanisms in cancer cells. *PLoS ONE* **2019**, *14*, e0219363. [CrossRef] [PubMed]
3. Camberos, V.; Baio, J.; Bailey, L.; Hasaniya, N.; Lopez, L.V.; Kearns-Jonker, M. Effects of Spaceflight and Simulated Microgravity on YAP1 Expression in Cardiovascular Progenitors: Implications for Cell-Based Repair. *Int. J. Mol. Sci.* **2019**, *20*, 2742. [CrossRef] [PubMed]
4. Qin, W.; Liu, L.; Wang, Y.; Wang, Z.; Yang, A.; Wang, T. Mir-494 inhibits osteoblast differentiation by regulating BMP signaling in simulated microgravity. *Endocrine* **2019**, *65*, 426–439. [CrossRef] [PubMed]
5. Deng, B.; Liu, R.; Tian, X.; Han, Z.; Chen, J. Simulated microgravity inhibits the viability and migration of glioma via FAK/RhoA/Rock and FAK/Nek2 signaling. *In Vitro Cell. Dev. Biol. Anim.* **2019**, *55*, 260–271. [CrossRef] [PubMed]
6. Bray, F.; Ferlay, J.; Soerjomataram, I.; Siegel, R.L.; Torre, L.A.; Jemal, A. Global cancer statistics 2018: GLOBOCAN estimates of incidence and mortality worldwide for 36 cancers in 185 countries. *CA Cancer J. Clin.* **2018**, *68*, 394–424. [CrossRef]
7. Humphrey, P.A.; Moch, H.; Cubilla, A.L.; Ulbright, T.M.; Reuter, V.E. The 2016 WHO Classification of Tumours of the Urinary System and Male Genital Organs-Part B: Prostate and Bladder Tumours. *Eur. Urol.* **2016**, *70*, 106–119. [CrossRef]
8. Humphrey, P.A. Histological variants of prostatic carcinoma and their significance. *Histopathology* **2012**, *60*, 59–74. [CrossRef]
9. Abate-Shen, C.; Shen, M.M. Molecular genetics of prostate cancer. *Genes. Dev.* **2000**, *14*, 2410–2434. [CrossRef]
10. Feng, M.; Peng, J.; Song, C.; Wang, Y. Mammalian cell cultivation in space. *Microgravity Sci. Technol.* **1994**, *7*, 207–210.
11. Grimm, D.; Bauer, J.; Kossmehl, P.; Shakibaei, M.; Schoberger, J.; Pickenhahn, H.; Schulze-Tanzil, G.; Vetter, R.; Eilles, C.; Paul, M.; et al. Simulated microgravity alters differentiation and increases apoptosis in human follicular thyroid carcinoma cells. *FASEB J.* **2002**, *16*, 604–606. [CrossRef]
12. Grimm, D.; Wise, P.; Lebert, M.; Richter, P.; Baatout, S. How and why does the proteome respond to microgravity? *Expert Rev. Proteom.* **2011**, *8*, 13–27. [CrossRef] [PubMed]
13. Aleshcheva, G.; Bauer, J.; Hemmersbach, R.; Slumstrup, L.; Wehland, M.; Infanger, M.; Grimm, D. Scaffold-free Tissue Formation Under Real and Simulated Microgravity Conditions. *Basic Clin. Pharmacol. Toxicol.* **2016**, *119* (Suppl. 3), 26–33. [CrossRef] [PubMed]
14. Ingram, M.; Techy, G.B.; Saroufeem, R.; Yazan, O.; Narayan, K.S.; Goodwin, T.J.; Spaulding, G.F. Three-dimensional growth patterns of various human tumor cell lines in simulated microgravity of a NASA bioreactor. *In Vitro Cell. Dev. Biol. Anim.* **1997**, *33*, 459–466. [CrossRef] [PubMed]
15. Dittrich, A.; Grimm, D.; Sahana, J.; Bauer, J.; Kruger, M.; Infanger, M.; Magnusson, N.E. Key Proteins Involved in Spheroid Formation and Angiogenesis in Endothelial Cells After Long-Term Exposure to Simulated Microgravity. *Cell. Physiol. Biochem.* **2018**, *45*, 429–445. [CrossRef]
16. Grimm, D.; Wehland, M.; Pietsch, J.; Aleshcheva, G.; Wise, P.; van Loon, J.; Ulbrich, C.; Magnusson, N.E.; Infanger, M.; Bauer, J. Growing tissues in real and simulated microgravity: New methods for tissue engineering. *Tissue Eng. Part B Rev.* **2014**, *20*, 555–566. [CrossRef]
17. Mehta, G.; Hsiao, A.Y.; Ingram, M.; Luker, G.D.; Takayama, S. Opportunities and challenges for use of tumor spheroids as models to test drug delivery and efficacy. *J. Control. Release* **2012**, *164*, 192–204. [CrossRef]

18. Herranz, R.; Anken, R.; Boonstra, J.; Braun, M.; Christianen, P.C.; de Geest, M.; Hauslage, J.; Hilbig, R.; Hill, R.J.; Lebert, M.; et al. Ground-based facilities for simulation of microgravity: Organism-specific recommendations for their use, and recommended terminology. *Astrobiology* **2013**, *13*, 1–17. [CrossRef]
19. Hoson, T.; Kamisaka, S.; Masuda, Y.; Yamashita, M.; Buchen, B. Evaluation of the three-dimensional clinostat as a simulator of weightlessness. *Planta* **1997**, *203*, S187–S197. [CrossRef]
20. Warnke, E.; Pietsch, J.; Wehland, M.; Bauer, J.; Infanger, M.; Gorog, M.; Hemmersbach, R.; Braun, M.; Ma, X.; Sahana, J.; et al. Spheroid formation of human thyroid cancer cells under simulated microgravity: A possible role of CTGF and CAV1. *Cell. Commun. Signal.* **2014**, *12*, 32. [CrossRef]
21. Kopp, S.; Sahana, J.; Islam, T.; Petersen, A.G.; Bauer, J.; Corydon, T.J.; Schulz, H.; Saar, K.; Huebner, N.; Slumstrup, L.; et al. The role of NFkappaB in spheroid formation of human breast cancer cells cultured on the Random Positioning Machine. *Sci. Rep.* **2018**, *8*, 921. [CrossRef] [PubMed]
22. Kruger, M.; Melnik, D.; Kopp, S.; Buken, C.; Sahana, J.; Bauer, J.; Wehland, M.; Hemmersbach, R.; Corydon, T.J.; Infanger, M.; et al. Fighting Thyroid Cancer with Microgravity Research. *Int. J. Mol. Sci.* **2019**, *20*, 2553. [CrossRef] [PubMed]
23. Kopp, S.; Warnke, E.; Wehland, M.; Aleshcheva, G.; Magnusson, N.E.; Hemmersbach, R.; Corydon, T.J.; Bauer, J.; Infanger, M.; Grimm, D. Mechanisms of three-dimensional growth of thyroid cells during long-term simulated microgravity. *Sci. Rep.* **2015**, *5*, 16691. [CrossRef] [PubMed]
24. Grimm, D.; Infanger, M.; Westphal, K.; Ulbrich, C.; Pietsch, J.; Kossmehl, P.; Vadrucci, S.; Baatout, S.; Flick, B.; Paul, M.; et al. A delayed type of three-dimensional growth of human endothelial cells under simulated weightlessness. *Tissue Eng. Part A* **2009**, *15*, 2267–2275. [CrossRef]
25. Svejgaard, B.; Wehland, M.; Ma, X.; Kopp, S.; Sahana, J.; Warnke, E.; Aleshcheva, G.; Hemmersbach, R.; Hauslage, J.; Grosse, J.; et al. Common Effects on Cancer Cells Exerted by a Random Positioning Machine and a 2D Clinostat. *PLoS ONE* **2015**, *10*, e0135157. [CrossRef]
26. Soranzo, C.; Della Torre, G.; Ingrosso, A. Formation, growth and morphology of multicellular tumor spheroids from a human colon carcinoma cell line (LoVo). *Tumori* **1986**, *72*, 459–467. [CrossRef]
27. Cui, X.; Hartanto, Y.; Zhang, H. Advances in multicellular spheroids formation. *J. R. Soc. Interface* **2017**, *14*. [CrossRef]
28. Kunz-Schughart, L.A. Multicellular tumor spheroids: Intermediates between monolayer culture and in vivo tumor. *Cell. Biol. Int.* **1999**, *23*, 157–161. [CrossRef]
29. Mueller-Klieser, W. Method for the determination of oxygen consumption rates and diffusion coefficients in multicellular spheroids. *Biophys. J.* **1984**, *46*, 343–348. [CrossRef]
30. Kunz-Schughart, L.A.; Freyer, J.P.; Hofstaedter, F.; Ebner, R. The use of 3-D cultures for high-throughput screening: The multicellular spheroid model. *J. Biomol. Screen.* **2004**, *9*, 273–285. [CrossRef]
31. Corydon, T.J.; Mann, V.; Slumstrup, L.; Kopp, S.; Sahana, J.; Askou, A.L.; Magnusson, N.E.; Echegoyen, D.; Bek, T.; Sundaresan, A.; et al. Reduced Expression of Cytoskeletal and Extracellular Matrix Genes in Human Adult Retinal Pigment Epithelium Cells Exposed to Simulated Microgravity. *Cell. Physiol. Biochem.* **2016**, *40*, 1–17. [CrossRef]
32. Nagy, J.A.; Dvorak, A.M.; Dvorak, H.F. VEGF-A and the induction of pathological angiogenesis. *Annu. Rev. Pathol.* **2007**, *2*, 251–275. [CrossRef]
33. Goel, S.; Duda, D.G.; Xu, L.; Munn, L.L.; Boucher, Y.; Fukumura, D.; Jain, R.K. Normalization of the vasculature for treatment of cancer and other diseases. *Physiol. Rev.* **2011**, *91*, 1071–1121. [CrossRef]
34. Carmeliet, P.; Jain, R.K. Molecular mechanisms and clinical applications of angiogenesis. *Nature* **2011**, *473*, 298–307. [CrossRef]
35. Peach, C.J.; Mignone, V.W.; Arruda, M.A.; Alcobia, D.C.; Hill, S.J.; Kilpatrick, L.E.; Woolard, J. Molecular Pharmacology of VEGF-A Isoforms: Binding and Signalling at VEGFR2. *Int. J. Mol. Sci.* **2018**, *19*, 1264. [CrossRef]
36. Takahashi, T.; Ueno, H.; Shibuya, M. VEGF activates protein kinase C-dependent, but Ras-independent Raf-MEK-MAP kinase pathway for DNA synthesis in primary endothelial cells. *Oncogene* **1999**, *18*, 2221–2230. [CrossRef] [PubMed]
37. Gerber, H.P.; McMurtrey, A.; Kowalski, J.; Yan, M.; Keyt, B.A.; Dixit, V.; Ferrara, N. Vascular endothelial growth factor regulates endothelial cell survival through the phosphatidylinositol 3′-kinase/Akt signal transduction pathway. Requirement for Flk-1/KDR activation. *J. Biol. Chem.* **1998**, *273*, 30336–30343. [CrossRef]

38. Conciatori, F.; Bazzichetto, C.; Falcone, I.; Pilotto, S.; Bria, E.; Cognetti, F.; Milella, M.; Ciuffreda, L. Role of mTOR Signaling in Tumor Microenvironment: An Overview. *Int. J. Mol. Sci.* **2018**, *19*, 2453. [CrossRef]
39. Chen, X.L.; Nam, J.O.; Jean, C.; Lawson, C.; Walsh, C.T.; Goka, E.; Lim, S.T.; Tomar, A.; Tancioni, I.; Uryu, S.; et al. VEGF-induced vascular permeability is mediated by FAK. *Dev. Cell.* **2012**, *22*, 146–157. [CrossRef]
40. Abu-Ghazaleh, R.; Kabir, J.; Jia, H.; Lobo, M.; Zachary, I. Src mediates stimulation by vascular endothelial growth factor of the phosphorylation of focal adhesion kinase at tyrosine 861, and migration and anti-apoptosis in endothelial cells. *Biochem. J.* **2001**, *360*, 255–264. [CrossRef]
41. Koch, S.; Claesson-Welsh, L. Signal transduction by vascular endothelial growth factor receptors. *Cold Spring Harb. Perspect. Med.* **2012**, *2*, a006502. [CrossRef]
42. Tchaikovski, V.; Fellbrich, G.; Waltenberger, J. The molecular basis of VEGFR-1 signal transduction pathways in primary human monocytes. *Arterioscler. Thromb. Vasc. Biol.* **2008**, *28*, 322–328. [CrossRef] [PubMed]
43. Zhau, H.E.; Goodwin, T.J.; Chang, S.M.; Baker, T.L.; Chung, L.W. Establishment of a three-dimensional human prostate organoid coculture under microgravity-simulated conditions: Evaluation of androgen-induced growth and PSA expression. *In Vitro Cell. Dev. Biol. Anim.* **1997**, *33*, 375–380. [CrossRef] [PubMed]
44. Clejan, S.; O'Connor, K.; Rosensweig, N. Tri-dimensional prostate cell cultures in simulated microgravity and induced changes in lipid second messengers and signal transduction. *J. Cell. Mol. Med.* **2001**, *5*, 60–73. [CrossRef]
45. Margolis, L.; Hatfill, S.; Chuaqui, R.; Vocke, C.; Emmert-Buck, M.; Linehan, W.M.; Duray, P.H. Long term organ culture of human prostate tissue in a NASA-designed rotating wall bioreactor. *J. Urol.* **1999**, *161*, 290–297. [CrossRef]
46. Leguy, C.A.D.; Delfos, R.; Pourquié, M.; Poelma, C.; Krooneman, J.; Westerweel, J.; van Loon, J.J.W.A. Fluid motion for microgravity simulations in a random positioning machine. *Gravit. Space Biol.* **2011**, *25*, 36–39.
47. Ma, X.; Pietsch, J.; Wehland, M.; Schulz, H.; Saar, K.; Hubner, N.; Bauer, J.; Braun, M.; Schwarzwalder, A.; Segerer, J.; et al. Differential gene expression profile and altered cytokine secretion of thyroid cancer cells in space. *FASEB J.* **2014**, *28*, 813–835. [CrossRef] [PubMed]
48. Viallard, C.; Larrivee, B. Tumor angiogenesis and vascular normalization: Alternative therapeutic targets. *Angiogenesis* **2017**, *20*, 409–426. [CrossRef]
49. Yang, J.; Moses, M.A. Abstract 1293: Neutrophil gelatinase-associated lipocalin regulates the expression of angiogenic cytokines and VEGF in human breast and ovarian cancer cells. *Cancer Res.* **2010**, *70*, 1293. [CrossRef]
50. Iannetti, A.; Pacifico, F.; Acquaviva, R.; Lavorgna, A.; Crescenzi, E.; Vascotto, C.; Tell, G.; Salzano, A.M.; Scaloni, A.; Vuttariello, E.; et al. The neutrophil gelatinase-associated lipocalin (NGAL), a NF-kappaB-regulated gene, is a survival factor for thyroid neoplastic cells. *Proc. Natl. Acad. Sci. USA* **2008**, *105*, 14058–14063. [CrossRef]
51. Sun, Y.; Yokoi, K.; Li, H.; Gao, J.; Hu, L.; Liu, B.; Chen, K.; Hamilton, S.R.; Fan, D.; Sun, B.; et al. NGAL expression is elevated in both colorectal adenoma-carcinoma sequence and cancer progression and enhances tumorigenesis in xenograft mouse models. *Clin. Cancer Res.* **2011**, *17*, 4331–4340. [CrossRef] [PubMed]
52. Zhang, X.F.; Zhang, Y.; Zhang, X.H.; Zhou, S.M.; Yang, G.G.; Wang, O.C.; Guo, G.L.; Yang, G.Y.; Hu, X.Q. Clinical significance of Neutrophil gelatinase-associated lipocalin(NGAL) expression in primary rectal cancer. *BMC Cancer* **2009**, *9*, 134. [CrossRef] [PubMed]
53. Olea-Flores, M.; Zuniga-Eulogio, M.D.; Mendoza-Catalan, M.A.; Rodriguez-Ruiz, H.A.; Castaneda-Saucedo, E.; Ortuno-Pineda, C.; Padilla-Benavides, T.; Navarro-Tito, N. Extracellular-Signal Regulated Kinase: A Central Molecule Driving Epithelial-Mesenchymal Transition in Cancer. *Int. J. Mol. Sci.* **2019**, *20*, 2885. [CrossRef] [PubMed]
54. Eblen, S.T. Extracellular-Regulated Kinases: Signaling From Ras to ERK Substrates to Control Biological Outcomes. *Adv. Cancer Res.* **2018**, *138*, 99–142. [CrossRef] [PubMed]
55. Tee, S.S.; Suster, I.; Truong, S.; Jeong, S.; Eskandari, R.; DiGialleonardo, V.; Alvarez, J.A.; Aldeborgh, H.N.; Keshari, K.R. Targeted AKT Inhibition in Prostate Cancer Cells and Spheroids Reduces Aerobic Glycolysis and Generation of Hyperpolarized [1-(13)C] Lactate. *Mol. Cancer Res.* **2018**, *16*, 453–460. [CrossRef]
56. Cully, M.; You, H.; Levine, A.J.; Mak, T.W. Beyond PTEN mutations: The PI3K pathway as an integrator of multiple inputs during tumorigenesis. *Nat. Rev. Cancer* **2006**, *6*, 184–192. [CrossRef]
57. Available online: https://clinicaltrials.gov/ (accessed on 13 February 2020).

58. Magani, F.; Peacock, S.O.; Rice, M.A.; Martinez, M.J.; Greene, A.M.; Magani, P.S.; Lyles, R.; Weitz, J.R.; Burnstein, K.L. Targeting AR Variant-Coactivator Interactions to Exploit Prostate Cancer Vulnerabilities. *Mol. Cancer Res.* **2017**, *15*, 1469–1480. [CrossRef]
59. Jain, N.; Zhang, T.; Fong, S.L.; Lim, C.P.; Cao, X. Repression of Stat3 activity by activation of mitogen-activated protein kinase (MAPK). *Oncogene* **1998**, *17*, 3157–3167. [CrossRef]
60. Shen, B.Q.; Lee, D.Y.; Gerber, H.P.; Keyt, B.A.; Ferrara, N.; Zioncheck, T.F. Homologous up-regulation of KDR/Flk-1 receptor expression by vascular endothelial growth factor in vitro. *J. Biol. Chem.* **1998**, *273*, 29979–29985. [CrossRef]
61. Fan, P.; Agboke, F.A.; McDaniel, R.E.; Sweeney, E.E.; Zou, X.; Creswell, K.; Jordan, V.C. Inhibition of c-Src blocks oestrogen-induced apoptosis and restores oestrogen-stimulated growth in long-term oestrogen-deprived breast cancer cells. *Eur. J. Cancer* **2014**, *50*, 457–468. [CrossRef]
62. Calalb, M.B.; Polte, T.R.; Hanks, S.K. Tyrosine phosphorylation of focal adhesion kinase at sites in the catalytic domain regulates kinase activity: A role for Src family kinases. *Mol. Cell. Biol.* **1995**, *15*, 954–963. [CrossRef] [PubMed]
63. Dumbauld, D.W.; Shin, H.; Gallant, N.D.; Michael, K.E.; Radhakrishna, H.; Garcia, A.J. Contractility modulates cell adhesion strengthening through focal adhesion kinase and assembly of vinculin-containing focal adhesions. *J. Cell. Physiol.* **2010**, *223*, 746–756. [CrossRef] [PubMed]
64. Bauer, T.J.; Gombocz, E.; Kruger, M.; Sahana, J.; Corydon, T.J.; Bauer, J.; Infanger, M.; Grimm, D. Augmenting cancer cell proteomics with cellular images—A semantic approach to understand focal adhesion. *J. Biomed. Inform.* **2019**, *100*, 103320. [CrossRef] [PubMed]
65. Humphries, J.D.; Wang, P.; Streuli, C.; Geiger, B.; Humphries, M.J.; Ballestrem, C. Vinculin controls focal adhesion formation by direct interactions with talin and actin. *J. Cell. Biol.* **2007**, *179*, 1043–1057. [CrossRef]
66. Chen, P.; Lei, L.; Wang, J.; Zou, X.; Zhang, D.; Deng, L.; Wu, D. Downregulation of Talin1 promotes hepatocellular carcinoma progression through activation of the ERK1/2 pathway. *Cancer Sci.* **2017**, *108*, 1157–1168. [CrossRef]
67. Small, J.V.; Stradal, T.; Vignal, E.; Rottner, K. The lamellipodium: Where motility begins. *Trends Cell. Biol.* **2002**, *12*, 112–120. [CrossRef]
68. Tojkander, S.; Gateva, G.; Lappalainen, P. Actin stress fibers–assembly, dynamics and biological roles. *J. Cell. Sci.* **2012**, *125*, 1855–1864. [CrossRef]
69. Rijken, P.J.; de Groot, R.P.; Kruijer, W.; de Laat, S.W.; Verkleij, A.J.; Boonstra, J. Identification of specific gravity sensitive signal transduction pathways in human A431 carcinoma cells. *Adv. Space Res.* **1992**, *12*, 145–152. [CrossRef]
70. Mann, V.; Grimm, D.; Corydon, T.J.; Kruger, M.; Wehland, M.; Riwaldt, S.; Sahana, J.; Kopp, S.; Bauer, J.; Reseland, J.E.; et al. Changes in Human Foetal Osteoblasts Exposed to the Random Positioning Machine and Bone Construct Tissue Engineering. *Int. J. Mol. Sci.* **2019**, *20*, 1357. [CrossRef]
71. Nabavi, N.; Khandani, A.; Camirand, A.; Harrison, R.E. Effects of microgravity on osteoclast bone resorption and osteoblast cytoskeletal organization and adhesion. *Bone* **2011**, *49*, 965–974. [CrossRef]
72. Ulbrich, C.; Pietsch, J.; Grosse, J.; Wehland, M.; Schulz, H.; Saar, K.; Hubner, N.; Hauslage, J.; Hemmersbach, R.; Braun, M.; et al. Differential gene regulation under altered gravity conditions in follicular thyroid cancer cells: Relationship between the extracellular matrix and the cytoskeleton. *Cell. Physiol. Biochem.* **2011**, *28*, 185–198. [CrossRef] [PubMed]
73. Grosse, J.; Wehland, M.; Pietsch, J.; Ma, X.; Ulbrich, C.; Schulz, H.; Saar, K.; Hubner, N.; Hauslage, J.; Hemmersbach, R.; et al. Short-term weightlessness produced by parabolic flight maneuvers altered gene expression patterns in human endothelial cells. *FASEB J.* **2012**, *26*, 639–655. [CrossRef]
74. Bonnans, C.; Chou, J.; Werb, Z. Remodelling the extracellular matrix in development and disease. *Nat. Rev. Mol. Cell. Biol.* **2014**, *15*, 786–801. [CrossRef] [PubMed]
75. Kopp, S.; Kruger, M.; Bauer, J.; Wehland, M.; Corydon, T.J.; Sahana, J.; Nassef, M.Z.; Melnik, D.; Bauer, T.J.; Schulz, H.; et al. Microgravity Affects Thyroid Cancer Cells during the TEXUS-53 Mission Stronger than Hypergravity. *Int. J. Mol. Sci.* **2018**, *19*, 4001. [CrossRef] [PubMed]
76. Birchmeier, W.; Behrens, J. Cadherin expression in carcinomas: Role in the formation of cell junctions and the prevention of invasiveness. *Biochim. Biophys. Acta* **1994**, *1198*, 11–26. [CrossRef]
77. Semb, H.; Christofori, G. The tumor-suppressor function of E-cadherin. *Am. J. Hum. Genet.* **1998**, *63*, 1588–1593. [CrossRef]

78. Infanger, M.; Kossmehl, P.; Shakibaei, M.; Bauer, J.; Kossmehl-Zorn, S.; Cogoli, A.; Curcio, F.; Oksche, A.; Wehland, M.; Kreutz, R.; et al. Simulated weightlessness changes the cytoskeleton and extracellular matrix proteins in papillary thyroid carcinoma cells. *Cell. Tissue Res.* **2006**, *324*, 267–277. [CrossRef]
79. Sahana, J.; Nassef, M.Z.; Wehland, M.; Kopp, S.; Kruger, M.; Corydon, T.J.; Infanger, M.; Bauer, J.; Grimm, D. Decreased E-Cadherin in MCF7 Human Breast Cancer Cells Forming Multicellular Spheroids Exposed to Simulated Microgravity. *Proteomics* **2018**, *18*, e1800015. [CrossRef]
80. Kliewe, F.; Kaling, S.; Lotzsch, H.; Artelt, N.; Schindler, M.; Rogge, H.; Schroder, S.; Scharf, C.; Amann, K.; Daniel, C.; et al. Fibronectin is up-regulated in podocytes by mechanical stress. *FASEB J.* **2019**. [CrossRef]
81. Garakani, K.; Shams, H.; Mofrad, M.R.K. Mechanosensitive Conformation of Vinculin Regulates Its Binding to MAPK1. *Biophys. J.* **2017**, *112*, 1885–1893. [CrossRef]
82. Ghrebi, S.; Hamilton, D.W.; Douglas Waterfield, J.; Brunette, D.M. The effect of surface topography on cell shape and early ERK1/2 signaling in macrophages; linkage with FAK and Src. *J. Biomed. Mater. Res. A* **2013**, *101*, 2118–2128. [CrossRef]
83. Wei, X.; Zhou, D.; Wang, H.; Ding, N.; Cui, X.X.; Wang, H.; Verano, M.; Zhang, K.; Conney, A.H.; Zheng, X.; et al. Effects of pyridine analogs of curcumin on growth, apoptosis and NF-kappaB activity in prostate cancer PC-3 cells. *Anticancer Res.* **2013**, *33*, 1343–1350. [PubMed]
84. Wu, F.; Wu, S.; Gou, X. Identification of biomarkers and potential molecular mechanisms of clear cell renal cell carcinoma. *Neoplasma* **2018**, *65*, 242–252. [CrossRef] [PubMed]
85. von Au, A.; Vasel, M.; Kraft, S.; Sens, C.; Hackl, N.; Marx, A.; Stroebel, P.; Hennenlotter, J.; Todenhofer, T.; Stenzl, A.; et al. Circulating fibronectin controls tumor growth. *Neoplasia* **2013**, *15*, 925–938. [CrossRef] [PubMed]
86. Irby, R.B.; Yeatman, T.J. Role of Src expression and activation in human cancer. *Oncogene* **2000**, *19*, 5636–5642. [CrossRef]
87. Mori, T.; Ono, K.; Kariya, Y.; Ogawa, T.; Higashi, S.; Miyazaki, K. Laminin-3B11, a novel vascular-type laminin capable of inducing prominent lamellipodial protrusions in microvascular endothelial cells. *J. Biol. Chem.* **2010**, *285*, 35068–35078. [CrossRef]
88. Chou, M.T.; Wang, J.; Fujita, D.J. Src kinase becomes preferentially associated with the VEGFR, KDR/Flk-1, following VEGF stimulation of vascular endothelial cells. *BMC Biochem.* **2002**, *3*, 32. [CrossRef]
89. Fleming, R.Y.; Ellis, L.M.; Parikh, N.U.; Liu, W.; Staley, C.A.; Gallick, G.E. Regulation of vascular endothelial growth factor expression in human colon carcinoma cells by activity of src kinase. *Surgery* **1997**, *122*, 501–507. [CrossRef]
90. Munshi, N.; Groopman, J.E.; Gill, P.S.; Ganju, R.K. c-Src mediates mitogenic signals and associates with cytoskeletal proteins upon vascular endothelial growth factor stimulation in Kaposi's sarcoma cells. *J. Immunol.* **2000**, *164*, 1169–1174. [CrossRef]
91. Albert, L.; Karsy, M.; Murali, R.; Jhanwar-Uniyal, M. Inhibition of mTOR Activates the MAPK Pathway in Glioblastoma Multiforme. *Cancer Genom. Proteom.* **2009**, *6*, 255–261.
92. Kinkade, C.W.; Castillo-Martin, M.; Puzio-Kuter, A.; Yan, J.; Foster, T.H.; Gao, H.; Sun, Y.; Ouyang, X.; Gerald, W.L.; Cordon-Cardo, C.; et al. Targeting AKT/mTOR and ERK MAPK signaling inhibits hormone-refractory prostate cancer in a preclinical mouse model. *J. Clin. Investig.* **2008**, *118*, 3051–3064. [CrossRef]
93. Engelman, J.A.; Chen, L.; Tan, X.; Crosby, K.; Guimaraes, A.R.; Upadhyay, R.; Maira, M.; McNamara, K.; Perera, S.A.; Song, Y.; et al. Effective use of PI3K and MEK inhibitors to treat mutant Kras G12D and PIK3CA H1047R murine lung cancers. *Nat. Med.* **2008**, *14*, 1351–1356. [CrossRef] [PubMed]
94. Bendtsen, M.A.F.; Grimm, D.; Bauer, J.; Wehland, M.; Wise, P.; Magnusson, N.E.; Infanger, M.; Kruger, M. Hypertension Caused by Lenvatinib and Everolimus in the Treatment of Metastatic Renal Cell Carcinoma. *Int. J. Mol. Sci.* **2017**, *18*, 1736. [CrossRef] [PubMed]
95. Nielsen, O.H.; Grimm, D.; Wehland, M.; Bauer, J.; Magnusson, N.E. Anti-Angiogenic Drugs in the Treatment of Metastatic Renal Cell Carcinoma: Advances in Clinical Application. *Curr. Vasc. Pharm.* **2015**, *13*, 381–391. [CrossRef] [PubMed]
96. Kaighn, M.E.; Narayan, K.S.; Ohnuki, Y.; Lechner, J.F.; Jones, L.W. Establishment and characterization of a human prostatic carcinoma cell line (PC-3). *Investig. Urol.* **1979**, *17*, 16–23.
97. Wuest, S.L.; Richard, S.; Kopp, S.; Grimm, D.; Egli, M. Simulated microgravity: Critical review on the use of random positioning machines for mammalian cell culture. *Biomed. Res. Int.* **2015**, *2015*, 971474. [CrossRef]

98. Grimm, D.; Egli, M.; Kruger, M.; Riwaldt, S.; Corydon, T.J.; Kopp, S.; Wehland, M.; Wise, P.; Infanger, M.; Mann, V.; et al. Tissue Engineering Under Microgravity Conditions-Use of Stem Cells and Specialized Cells. *Stem Cells Dev.* **2018**, *27*, 787–804. [CrossRef]
99. Kopp, S.; Slumstrup, L.; Corydon, T.J.; Sahana, J.; Aleshcheva, G.; Islam, T.; Magnusson, N.E.; Wehland, M.; Bauer, J.; Infanger, M.; et al. Identifications of novel mechanisms in breast cancer cells involving duct-like multicellular spheroid formation after exposure to the Random Positioning Machine. *Sci. Rep.* **2016**, *6*, 26887. [CrossRef]
100. Grimm, D.; Jabusch, H.C.; Kossmehl, P.; Huber, M.; Fredersdorf, S.; Griese, D.P.; Kramer, B.K.; Kromer, E.P. Experimental diabetes and left ventricular hypertrophy: Effects of beta-receptor blockade. *Cardiovasc. Pathol.* **2002**, *11*, 229–237. [CrossRef]
101. Grosse, J.; Warnke, E.; Pohl, F.; Magnusson, N.E.; Wehland, M.; Infanger, M.; Eilles, C.; Grimm, D. Impact of sunitinib on human thyroid cancer cells. *Cell. Physiol. Biochem.* **2013**, *32*, 154–170. [CrossRef]
102. Magnusson, N.E.; Hornum, M.; Jorgensen, K.A.; Hansen, J.M.; Bistrup, C.; Feldt-Rasmussen, B.; Flyvbjerg, A. Plasma neutrophil gelatinase associated lipocalin (NGAL) is associated with kidney function in uraemic patients before and after kidney transplantation. *BMC Nephrol.* **2012**, *13*, 8. [CrossRef] [PubMed]
103. Lützenberg, R.; Solano, K.; Buken, C.; Sahana, J.; Riwaldt, S.; Kopp, S.; Kruger, M.; Schulz, H.; Saar, K.; Huebner, N.; et al. Pathway Analysis Hints Towards Beneficial Effects of Long-Term Vibration on Human Chondrocytes. *Cell. Physiol. Biochem.* **2018**, *47*, 1729–1741. [CrossRef] [PubMed]

13.2. Publikation 2

Dietrichs D, Grimm D, Sahana J, Melnik D, Corydon TJ, Wehland M, Krüger M, Vermeesen R, Baselet B, Baatout S, Hybel TE, Kahlert S, Schulz H, Infanger M, Kopp S: Three-Dimensional Growth of Prostate Cancer Cells Exposed to Simulated Microgravity. Front Cell Dev Biol. 10. 841017 (2022)

frontiers in Cell and Developmental Biology

ORIGINAL RESEARCH
published: 17 February 2022
doi: 10.3389/fcell.2022.841017

Three-Dimensional Growth of Prostate Cancer Cells Exposed to Simulated Microgravity

Dorothea Dietrichs[1], Daniela Grimm[1,2,3], Jayashree Sahana[3], Daniela Melnik[1], Thomas J. Corydon[3,4], Markus Wehland[1,2], Marcus Krüger[1,2], Randy Vermeesen[5], Bjorn Baselet[5], Sarah Baatout[5,6], Trine Engelbrecht Hybel[3], Stefan Kahlert[7], Herbert Schulz[1,2], Manfred Infanger[1,2] and Sascha Kopp[1,2†]*

[1]*Department of Microgravity and Translational Regenerative Medicine, Otto von Guericke University Magdeburg, Magdeburg, Germany,* [2]*Research Group "Magdeburger Arbeitsgemeinschaft für Forschung unter Raumfahrt- und Schwerelosigkeitsbedingungen" (MARS), Otto von Guericke University Magdeburg, Magdeburg, Germany,* [3]*Department of Biomedicine, Aarhus University, Aarhus, Denmark,* [4]*Department of Ophthalmology, Aarhus University Hospital, Aarhus, Denmark,* [5]*Radiobiology Unit, SCK CEN, Belgian Nuclear Research Centre, Mol, Belgium,* [6]*Department of Molecular Biotechnology, Ghent University, Ghent, Belgium,* [7]*Institute of Anatomy, Otto von Guericke University Magdeburg, Magdeburg, Germany*

OPEN ACCESS

Edited by:
Xiaohua Lei, Shenzhen Institutes of Advanced Technology (CAS), China

Reviewed by:
Lucia Morbidelli, University of Siena, Italy
Giulia Ricci, University of Campania Luigi Vanvitelli, Italy

***Correspondence:**
Daniela Grimm
dgg@biomed.au.dk

†Present Address:
Sascha Kopp, Core Facility Tissue Engineering, Otto von Guericke University Magdeburg, Magdeburg, Germany

Specialty section:
This article was submitted to Cell Growth and Division, a section of the journal Frontiers in Cell and Developmental Biology

Received: *21 December 2021*
Accepted: *25 January 2022*
Published: *17 February 2022*

Citation:
Dietrichs D, Grimm D, Sahana J, Melnik D, Corydon TJ, Wehland M, Krüger M, Vermeesen R, Baselet B, Baatout S, Hybel TE, Kahlert S, Schulz H, Infanger M and Kopp S (2022) Three-Dimensional Growth of Prostate Cancer Cells Exposed to Simulated Microgravity. Front. Cell Dev. Biol. 10:841017. doi: 10.3389/fcell.2022.841017

Prostate cancer metastasis has an enormous impact on the mortality of cancer patients. Factors involved in cancer progression and metastasis are known to be key players in microgravity (μ*g*)-driven three-dimensional (3D) cancer spheroid formation. We investigated PC-3 prostate cancer cells for 30 min, 2, 4 and 24 h on the random positioning machine (RPM), a device simulating μ*g* on Earth. After a 24 h RPM-exposure, the cells could be divided into two groups: one grew as 3D multicellular spheroids (MCS), the other one as adherent monolayer (AD). No signs of apoptosis were visible. Among others, we focused on cytokines involved in the events of metastasis and MCS formation. After 24 h of exposure, in the MCS group we measured an increase in *ACTB, MSN, COL1A1, LAMA3, FN1, TIMP1, FLT1, EGFR1, IL1A, IL6, CXCL8*, and *HIF1A* mRNA expression, and in the AD group an elevation of *LAMA3, COL1A1, FN1*, *MMP9*, *VEGFA, IL6,* and *CXCL8* mRNAs compared to samples subjected to 1 *g* conditions. Significant downregulations in AD cells were detected in the mRNA levels of *TUBB, KRT8*, *IL1B, IL7, PIK3CB, AKT1 and MTOR* after 24 h. The release of collagen-1α1 and fibronectin protein in the supernatant was decreased, whereas the secretion of IL-6 was elevated in 24 h RPM samples. The secretion of IL-1α, IL-1β, IL-7, IL-2, IL-8, IL-17, TNF-α, laminin, MMP-2, TIMP-1, osteopontin and EGF was not significantly altered after 24 h compared to 1 *g* conditions. The release of soluble factors was significantly reduced after 2 h (IL-1α, IL-2, IL-7, IL-8, IL-17, TNF-α, collagen-1α1, MMP-2, osteopontin) and elevated after 4 h (IL-1β, IL-2, IL-6, IL-7, IL-8, TNF-α, laminin) in RPM samples. Taken together, simulated μ*g* induced 3D growth of PC-3 cancer cells combined with a differential expression of the cytokines IL-1α, IL-1β, IL-6 and IL-8, supporting their involvement in growth and progression of prostate cancer cells.

Keywords: prostate cancer, cytokines, interleukins, cytoskeleton, extracellular matrix, PAM signaling, prostate cancer cells and microgravity

INTRODUCTION

As estimated by GLOBOCAN (Global Cancer Observatory) in 2020, prostate cancer (PC) comprises an incidence of almost 1.4 million new cases and 375,000 deaths worldwide (Sung et al., 2021). PC was the second most frequent cancer and the fifth leading cause of cancer death among men in 2020 (Sung et al., 2021). Adenocarcinomas are the most common types of PC, and in general PC progresses very slowly. The 5-years survival rate for most men with local or regional PC is nearly 100%, but if diagnosed with PC metastasis, the 5-years survival rate is reduced to 31% (Gandaglia et al., 2014).

This shows that metastasis of PC has a vast impact on the mortality and the overall quality of life of patients. Compared to other cancer types, PC metastasizes predominantly to the skeleton (84%) and the lymph nodes (10.6%) (Gandaglia et al., 2014). Additionally, spreading to the liver (10.2%) and thorax (9.1%) is also common (Gandaglia et al., 2014). Metastatic PC is mostly terminal even after intensive multimodal treatment. Therefore, there is an urgent need to increase the knowledge of PC biology, genomics, proteomics and advanced profiling technologies in order to find new drug development targets.

In context of PC expansion, proteins released by the PC cells (PCC) into the interstitial space are of high interest. Secreted factors such as cytokines and chemokines are released into the tumor microenvironment and play a key role in cancer progression. Cytokines are released in response to immune reactions like infection, inflammation and immunity in order to inhibit tumor development and progression. The tumor cells can respond just as well to cytokines that induce cancer growth, reduce programmed cell death and facilitate invasion and metastasis (Dranoff, 2004). Thus, cytokines, their receptors and specific signaling pathways are key factors in driving the specific events leading to metastasis of PC (Dranoff, 2004; Adekoya and Richardson, 2020).

Moreover, cytokines are key players in all events of the metastatic process and hence, they remodel the extracellular matrix, influence the epithelial-mesenchymal-transition, invasion, angiogenesis, and the processes involved in the establishment of tumor cells in the secondary organs (Adekoya and Richardson, 2020).

An extraordinary and novel approach to investigate tumor cell processes is using microgravity (μ*g*), either with real (r-) μ*g* in space or simulated (s-) μ*g* by ground-based devices like the random positioning machine (RPM) (Becker and Souza, 2013). Space provides special physical conditions which cannot be reproduced on Earth, as well as μ*g* conditions which are used to investigate molecular mechanisms and signaling processes controlling cell growth and function (Becker and Souza, 2013). Cancer research in space and molecular biological studies on cells exposed to r- and/or s-μ*g* are therefore a hot topic in space medicine (Krüger et al., 2019; Grimm et al., 2020; Nassef et al., 2020).

Previous research revealed that r- and s-μ*g* have a large impact on the biochemistry and physiology of human cells. This comprises various changes, such as alterations of the extracellular matrix (ECM), the focal adhesion complex, the cytoskeleton, growth behavior, as well as changes in differentiation and proliferation (Nassef et al., 2019). Moreover, Häder *et al.* (Häder et al., 2017) suggested a direct correlation of the μ*g*-induced cytoskeletal changes and transcriptional alterations. They concluded that the interaction of the ECM, cell adhesion and the cytoskeleton is of great importance for gravisensing in human cells. Cytoskeletal alterations detected in human cells exposed to μ*g* were described as follows: microtubules are regularly localized more around the nucleus and might lose their radial organization, are shortened, as well as more curved and bent. The F-actin network is altered and the number of stress fibers reduced. F-actin is redistributed and is situated more perinuclear or is localized more cortical. Intermediate filaments (vimentin, cytokeratin) form clusters, reveal larger meshes and are localized more perinuclear (Vorselen et al., 2014). These findings obtained from fixed cells were recently confirmed by live-cell imaging in r-μ*g* (Corydon et al., 2016a; Nassef et al., 2019).

Moreover, s- and r-μ*g* influenced ECM proteins in a time-dependent manner (Infanger et al., 2006) and cell-type dependent, resulting in increases or decreases of ECM components (Infanger et al., 2006; Marrero et al., 2009; Zhivodernikov et al., 2020). In addition, PC MCS engineered on the RPM revealed a decrease in *COL1A1* after 3 days and an increase after 5 days, whereas basement components like *COL4A5* and *LAMA3* as well as the cell adhesion molecule *FN1* were elevated in MCS at both time points (Hybel et al., 2020). These findings indicate that the cells try to expand the ECM in MCS to stabilize themselves and to resist the s-μ*g* conditions, as the ECM provides structural support for the cells (Bonnans et al., 2014).

In addition, lack of gravity and/or RPM exposure of various cell types was shown to promote cell growth in a scaffold-free three-dimensional (3D) way, forming MCS (Riwaldt et al., 2016; Grimm et al., 2020). MCS are 3D aggregates exhibiting complex cell-to-cell and cell-to-matrix interactions. These interactions have been reported to induce gradients for nutrients, gases, growth factors and signal factors. This 3D structure reflects the natural microenvironment of cells more accurately than 2D monocultures and also resembles the microenvironment of real tissues (Mehta et al., 2012; Cui et al., 2017). Several cancer cell-types like thyroid and breast cancer cells exposed to an RPM formed MCS within 24 h (Kopp et al., 2016; Riwaldt et al., 2016).

3D PC aggregates (PC-3, LNCaP and DU-145 cell lines) engineered on microgravity simulators and the subsequent formation of 3D spheroids was demonstrated on both, the NASA rotary cell culture system and the RPM (Ingram et al., 1997; Hybel et al., 2020).

Understanding the biology of spheroids is very important for a more complete appreciation of *in vivo* tissue formation and function. MCS are frequently used to study molecular mechanisms involved in angiogenesis, cancer development, and biology and for pharmacological testing. Unveiling the mechanisms of microgravity-dependent molecular and cellular changes is an up-to-date requirement for improving space medicine and cancer research (Becker and Souza, 2013; Krüger et al., 2019; Nassef et al., 2020). A clear advantage of microgravity is that it enables the engineering of MCS without any scaffolds. Moreover, long-term experiments using thyroid cancer cells show

that FTC-133 spheroids and EA.hy926 spheroids or intima constructs did not develop a central necrosis, when exposed to an RPM (Kopp et al., 2015; Dittrich et al., 2018).

Therefore, spheroids formation in μ*g* is an innovative approach to study the early phases of tumor progression and metastasis. The PI3K/AKT/mTOR (PAM) signaling pathway is frequently mutated in prostate cancer and thus a good candidate for the involvement in tumor progression (Tee et al., 2018). It is regulating growth, metabolism, and migration of PCC.

In this study we investigated the impact of short-term (30 min, 2, 4 and 24 h) s-μ*g*-exposure via RPM on PC-3 prostate cancer cells, which were established from an adenocarcinoma. The principal aim of this study was to measure the gene expression and secretion rate of cytokines in PCC. Secondly, we focused on the altered gene expression of cytoskeletal factors and the extracellular matrix (ECM). Third, a special focus was placed on the PAM signaling pathway, which is proposed to be the underlying mechanism of spheroid formation in PC. Fourth, we engineered 3D spheroids under 1*g*-conditions by the liquid-overlay technique to use them as a control for the 3D spheroids in simulated microgravity and studied the gene expression of selected factors in 1*g*-MCS.

MATERIALS AND METHODS

Cell Cultures

The PC-3 cell line (ECACC 90112714) was purchased from the European Collection of Authenticated Cell Cultures (ECACC). The cells originated from a 62-year-old male Caucasian suffering from grade 4 prostatic adenocarcinoma.

$3{\cdot}10^6$ cells were seeded into T75 cm^2 flasks (Sarstedt, Nümbrecht, Germany) and cultured using RPMI 1640 medium (Gibco, Fisher Scientific, Schwerte, Germany), supplemented with 10% FCS (Sigma Aldrich, Steinheim, Germany) and 1% penicillin/streptomycin (Life Technologies, New York, United States). Every 3 days the medium was changed, and upon reaching 70–80% confluence, the cells were split at a 1:10 ratio.

Simulated Microgravity on the iRPM and Sample Collection

In preparation for the experiments in s-μ*g* on the incubator RPM (iRPM), 10 T25 cm^2 flasks (Sarstedt, Nümbrecht, Germany; order nr. 83.3910.002 vented caps) per group were filled each with $2{\cdot}10^6$ cells in 13 ml RPMI 1640 medium (Life Technologies, Paisley, United Kingdom), complemented with 10% FCS (Sigma Aldrich, Steinheim, Germany) and 1% penicillin/streptomycin (Life Technologies, New York, United States), and kept in 1 *g* conditions (37°C, 5% CO_2) for 1 day to let the cells adhere. Afterwards, the flasks were filled entirely with growth medium, avoiding the formation of air bubbles. Furthermore, the bottle caps were secured at the edges with parafilm, sparing the ventilated area. Five flasks of each group were placed and fixed inside the incubator on the iRPM, while the other five remained under 1*g* standard conditions (both 37°C, 5% CO_2). After the duration of 30 min, 2 h, and 4 h, respectively, the cell culture supernatants were collected in 50 ml tubes and stored at −150°C. Then 2 ml RNA*later* Stabilization Solution (Invitrogen by Thermo Fischer Scientific, Waltham, MA, United States) was added to the flasks and the cells mechanically detached with cell scrapers. The resulting cell suspensions were collected in 15-ml tubes and stored at 4°C until further processing.

For the immunofluorescence staining, $0.2{\cdot}10^5$ cells were seeded into 4 slideflasks (Thermo Scientific) and incubated for 36 h. At this timepoint the culture medium was discarded, the slideflasks completely filled with fresh RPMI 1640 medium (Life Technologies, Paisley, United Kingdom) containing 10% FCS (Sigma Aldrich, Steinheim, Germany) and 1% penicillin/streptomycin (Life Technologies, New York, United States), and sealed with parafilm air bubble-free. Following, two flasks were cultured on the iRPM for 24 h, while two were left in the incubator under standard conditions as controls. After the experiment, the medium was discarded and the slides were fixed with 4% Paraformaldehyde (PFA, Sigma-Aldrich, St. Louis, Missouri, United States) in phosphate-buffered saline (PBS; Gibco, Life Technologies, Paisley, United Kingdom).

The iRPM was constructed by the group of Professor Jörg Sekler at the Fachhochschule Nordwestschweiz (Windisch AG, Switzerland). Details on the iRPM are described in (Benavides Damm et al., 2014).

Liquid Overlay

The liquid-overlay technique is an established method to generate 3D cell aggregates in static culture (Svejgaard et al., 2015). In short, 96-well plates are coated with 40 μl of 1% agarose in RPMI 1640 medium. After hardening of the gel, 4,000 cells/200 μl in RPMI 1640 supplemented with 10% FCS and 1% Pen/Strep were incubated as described in 4.1 for 24 h. This step was followed by microscopic evaluation of cell viability using Ready Probes for live cell imaging (Thermo Scientific, Waltham, Massachusetts, United States) and cell aggregate collection for quantitative real-time PCR. Five 96-well plates were seeded and spheroids of one plate were collected to make up one PCR sample. As a control, adherently growing cells were cultured for 24 h in five standard T25 cm^2 cell culture flasks.

Quantitative Real-Time Polymerase Chain Reaction (qPCR)

The expression levels of the genes of interest were determined via qPCR. Primer Express software (Applied Biosystems) was used to design appropriate primers with a T_m of ~60°C (**Table 1**). The primers were synthesized by TIB Molbiol (Berlin, Germany) and all assays were run on a 7,500 Fast Real-Time PCR System using the FAST SYBR™ Green Master Mix (both Applied Biosystems, Darmstadt, Germany). The reaction volume was 15 μL including 1 μL of template cDNA and a final primer concentration of 500 nM. PCR conditions were as follows: 20 s at 95°C, 40 cycles of 30 s at 95°C and 30 s at 60°C, followed by a melting curve analysis step (temperature gradient from 60 to 95°C with +0.3°C/cycle).

If all amplicons showed one single T_m similar to the one predicted by the Primer Express software, the PCR reactions were considered specific. Every sample was measured in triplicates, and relative quantification was performed by means of the comparative C_T ($\Delta\Delta C_T$) method. *18S rRNA* was used as a housekeeping gene to normalize the expression data.

TABLE 1 | Primers used for qPCR analyses.

Gene	Primer name	Sequence 5′–3′
18S rRNA	18s-F	GGAGCCTGCGGCTTAATTT
	18s-R	CAACTAAGAACGGCCATGCA
ACTB	ACTB-F	TGCCGACAGGATGCAGAAG
	ACTB-R	GCCGATCCACACGGAGTACT
AKT1	AKT1-F	CTTCTATGGCGCTGAGATTGTG
	AKT1	CAGCATGAGGTTCTCCAGCTT
CASP3	CASP3-F	CTCCAACATCGACTGTGAGAAGTT
	CASP3-R	GCGCCAGCTCCAGCAA
CASP8	CASP8-F	TGCAAAAGCACGGGAGAAAG
	CASP8-R	CTCTTCAAAGGTCGTGGTCAAAG
CASP9	CASP9-F	CTCCAACATCGACTGTGAGAAGTT
	CASP9-R	GCGCCAGCTCCAGCAA
COL1A1	COL1A1-F	ACGAAGACATCCCACCAATCAC
	COL1A1-R	CGTTGTCGCAGACGCAGAT
CXCL8	CXCL8-F	TGGCAGCCTTCCTGATTTCT
	CXCL8-R	GGGTGGAAAGGTTTGGAGTATG
EGF	EGF-F	TGCCAGCTGCACAAATACAGA
	EGF-R	TCTTACGGAATAGTGGTGGTCATC
EGFR	EGFR-F	TTGCCGCAAAGTGTGTAACG
	EGFR-R	GAGATCGCCACTGATGGAGG
EZR	EZR-F	GCAATCCAGCCAAATACAACTG
	EZR-R	CCACATAGTGGAGGCCAAAGTAC
FLT1	FLT1-F	CCCTCGCCGGAAGTTGTAT
	FLT1-R	GATAATTAACGAGTAGCCACGAGTCAA
FN1	FN1-F	AGATCTACCTGTACACCTTGAATGACA
	FN1-R	CATGATACCAGCAAGGAATTGG
HIF1A	HIF1A-F	TGCTTTAACTTTGCTGGCCC
	HIF1A-R	AGTTTCTGTGTCGTTGCTGC
IL1A	IL1A-F	AGTAGCAACCAACGGGAAGG
	IL1A-R	AGGCTTGATGATTTCTTCCTCTGA
IL1B	IL1B-F	TTCGAGGCACAAGGCACAA
	IL1B-R	TGGCTGCTTCAGACACTTGAG
IL6	IL6-F	CGGGAACGAAAGAGAAGCTCTA
	IL6-R	GAGCAGCCCCAGGGAGAA
IL7	IL7-F	CCAGTTGCGGTCATCATGACTA
	IL7-R	TGATGCTACTGGCAACAGAACA
KDR	KDR-F	TCTTCTGGCTACTTCTTGTCATCATC
	KDR-R	GATGGACAAGTAGCCTGTCTTCAGT
KRT8	KRT8-F	GATCTCTGAGTGAACCGGAACA
	KRT8-R	GCTCGGCATCTGCAATGG
LAMA3	LAMA3-F	AAAGCAAGAAGTCAGTCCAGC
	LAMA3-R	TCCCATGAAGACCATCTCGG
MMP9	MMP9-F	CCTGGAGACCTGAGAACCAATC
	MMP9-R	TTCGACTCTCCACGCATCTCT
MSN	MSN-F	GAAATTTGTCATCAAGCCCATTG
	MSN-R	CCATGCACAAGGCCAAGAT
MTOR	MTOR-F	ATCTTGGCCATAGCTAGCCTC
	MTOR-R	ACAACTGGGTCATTGGAGGG
PIK3CB	PIK3CB-F	AGAAAAGTTTGGCCGGTTCC
	PIK3CB-R	GCAGTCAACATCAGCGCAAA
RDX	RDX-F	GAAAATGCCGAAACCAATCAA
	RDX-R	GTATTGGGCTGAATGGCAAATT
SPP1	SPP1-F	CGAGGTGATAGTGTGGTTTATGGA
	SPP1-R	CGTCTGTAGCATCAGGGTACTG
TGFB1	TGFB1-F	CACCCGCGTGCTAATGGT
	TGFB1-R	AGAGCAACACGGGTTCAGGTA
TIMP1	TIMP1-F	GCCATCGCCGCAGATC
	TIMP1-R	GCTATCAGCCACAGCAACAACA
TUBB	TUBB-F	CTGGACCGCATCTCTGTGTACTAC
	TUBB-R	GACCTGAGCGAACAGAGTCCAT
VEGFA	VEGFA-F	CTACCTCCACCATGCCAAGTG
	VEGFA-R	GCGCTGATAGACATCCATGAAC

TABLE 2 | Materials used for immunofluorescence.

Antibody/Probe	Species	Order number	Manufacturer	Dilution in PBS
Fibronectin	mouse monoclonal	sc-18827	Santa Cruz Biotechnology	(1:100)
anti-mouse IgG (H + L)	goat secondary antibody	A11001	Invitrogen by Thermo Fischer Scientific	(1:500)

Immunofluorescence

Following the removal of PFA, the cells were washed twice with PBS and permeabilized with 0.2% Triton. After blocking with 3% bovine serum albumin (BSA) in PBS for 1 h, the primary antibody was added and incubated at 4°C overnight. The next day, the cells were washed twice with PBS, the secondary antibody was added and incubated for 1 h. Afterwards, the cells were rinsed three times with PBS and mounted with DAPI fluoroshield and a cover slip. A list of antibodies and probes used for immunofluorescence staining is given in **Table 2**.

Multiplex Bead Array

Collagen I alpha I, fibronectin, interleukin (IL)-1α/1F1, IL-1β/1F2, IL-2, IL-6, IL-7, IL-8/CXCL8, IL-17/17-A, tumor necrosis factor alpha (TNF-α), matrix metalloproteinase-2 (MMP-2), epidermal growth factor (EGF), serpin E1/plasminogen activator inhibitor-1 (PAI-1), osteopontin (OPN), chemokine (C-C motif) ligand 2 (CCL2)/ monocyte chemoattractant protein 1 (MCP-1), tissue inhibitor metalloproteinases metallopeptidase inhibitor 1 (TIMP-1) and laminin levels in cell culture supernatant were analyzed using a multiplex magnetic bead array (R&D systems, Minneapolis, United States). Assays were performed according to manufacturer's instructions. Samples were run on a MAGPIX instrument (Luminex, s-Hertogenbosch, Netherlands) and analyzed with MILLIPEX analyst standard version 5.1 (Merck, Darmstadt, Germany).

Microscopy

After immunofluorescence staining, the slides were investigated using confocal laser scanning microscopy. The observations were made with a Leica DM 2000 microscope equipped with a 40x objective and an external light source Leica EL 6000 (Leica Microsystems GmbH, Wetzlar, Germany).

Statistical Analysis

The statistics were performed using the GraphPad Prism 7.01 software (GraphPad Software, Inc., California, United States). Differences between s-μ*g* samples and related controls were assessed with the Mann-Whitney U-test, p-values < 0.05 were considered significant.

RESULTS

Cell Growth, Morphology and Cell Viability

Culture flasks containing 70% sub-confluent PC-3 cells were mounted on the RPM for 30 min, 2, 4 and 24 h. The 1*g* control samples were placed next to the RPM and cultured in parallel. PC-3 cells cultured under 1*g*-conditions grew as 2D monolayer cultures (**Figure 1A**). PC-3 cells exposed to the RPM for 30 min, 2 and 4 h showed no three-dimensional (3D) growth and grew adherently on the cell culture flask bottom (not shown). Phase contrast microscopy showed normal epithelial PC-3 cells exhibiting numerous microvilli, abnormal nuclei and nucleoli. The cells subjected to short-term exposure (30 min, 2 h, and 4 h) to the RPM compared to 1*g* samples revealed no visible morphological changes. No dead cells were detectable. 3D multicellular spheroids could be detected in the supernatant after a 24 h RPM exposure. Thus, there are two different phenotypes of PC-3 cells visible: adherently growing cells (AD) and detached 3D MCS (**Figures 1B,C**) We used a "terminal deoxynucleotidyl transferase dUTP nick end labeling" (TUNEL) assay to detect DNA breaks formed during the final phase of apoptosis, when DNA fragmentation takes place. No apoptotic cells were visible in all AD cell samples irrespective of RPM exposure or not. Sporadic apoptotic cells were detected in MCS (**Figure 1D**). In addition, we focused on apoptosis signaling. Genes associated with apoptosis such as *CASP3*, *CASP8,* and *CASP9* mRNAs were not significantly changed after short-term incubation (30 min, 2 h, and 4 h) as well as after 24 h on the RPM compared to 1*g* (**Figures 1E–G**). We studied the gene expression of *HIF1A* (hypoxia inducible factor 1) in PC-3 cells exposed for 24 h to s-μ*g* conditions. The *HIF1A* mRNA in AD cells was not altered, but significantly elevated in MCS (**Figure 1H**).

Spheroids Engineered Under 1*g*-Conditions

The liquid-overlay technique was used to obtain MCS under 1*g*-conditions within 24 h. We microscopically investigated the MCS formation and their viability. **Figure 2A** presents a representative cell aggregate formed within 24 h. In comparison to the MCS built on the RPM, the cells are loosely united. **Figure 2B** presents the cell viability staining. While all nuclei are stained blue, compromised nuclei, representing non-viable cells, are stained green. Compared to the MCS engineered on the RPM, the cell viability of MCS formed under 1*g*-conditions (**Figure 2B**) seems to be lower. The gene expression of *CASP3*, *CASP8* and *CASP9* (**Figures 2C–E**) was significantly upregulated in 1*g*-MCS compared to control samples.

The Cytoskeleton

The cytoskeletal protein β-actin (ACTB) is widely distributed in all eukaryotic cells and is involved in cell migration, cell division, cell structure, cell integrity and immune response. After 24 h RPM exposure an increase in the *ACTB* gene expression was measured in MCS, but not in the adherent cells compared to 1*g* (**Figure 3A**). MCS built under 1*g*-conditions showed a significant upregulation of *ACTB* in comparison to control samples. A short-term (30 min, 2 h, and 4 h) RPM exposure of PC-3 cells did not change the gene expression level of *ACTB*.

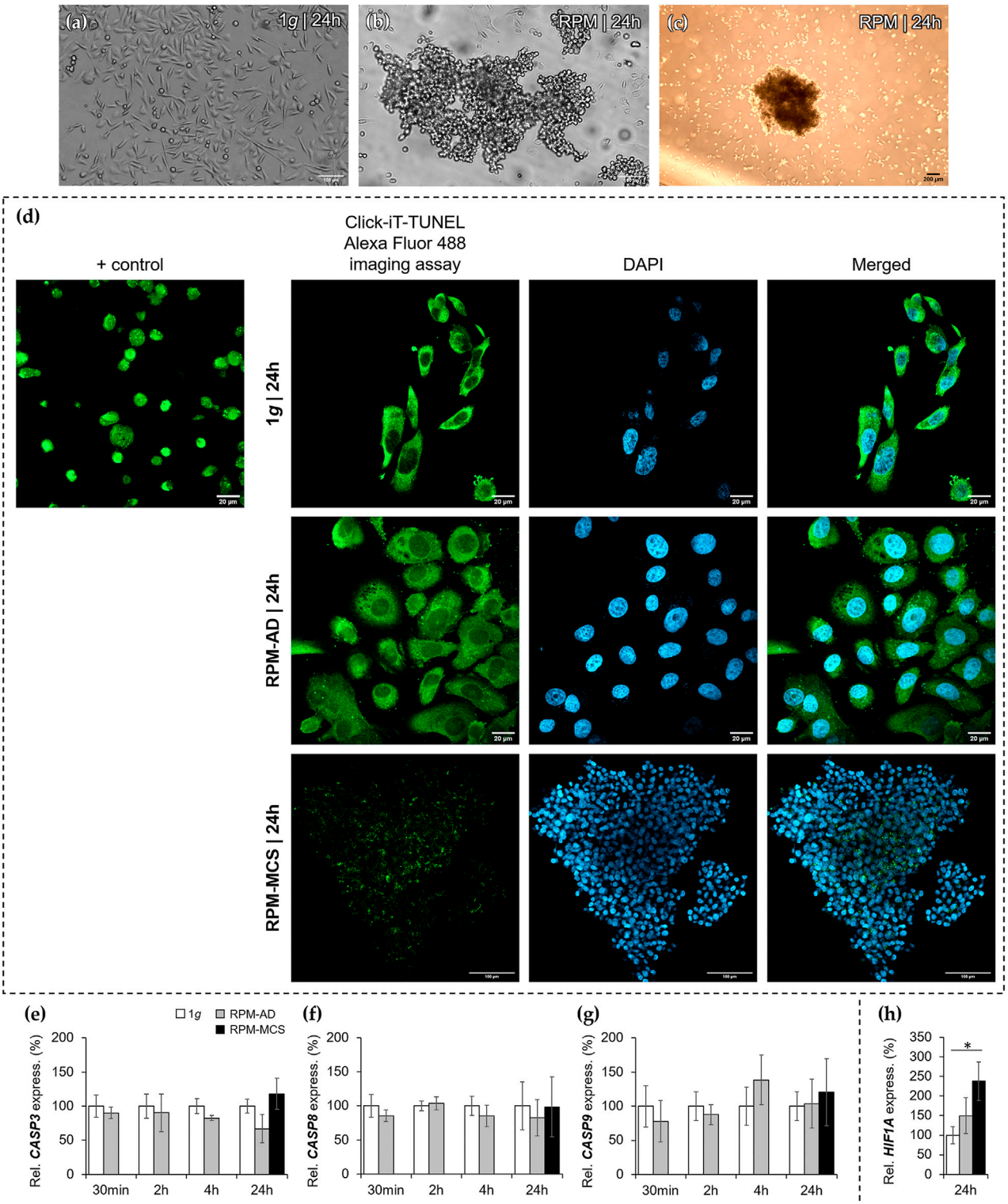

FIGURE 1 | Phase contrast microscopy of PC-3 cells: **(A)** static 1*g* control cells (Scale bar 100 µm) and **(B,C)** 24 h RPM-exposed samples showing detached spheroids swimming above adherently growing cells (scale bar **(B)** 100 µm and **(C)** 200 µm). **(D)** Terminal deoxynucleotidyl transferase dUTP nick end labeling (TUNEL) assay and 4′,6-diamidino-2-phenylindole (DAPI) staining revealed no apoptotic cells in 1*g* controls (scale bar 20 µm) and also no apoptosis in RPM-exposed AD (scale bar 20 µm and MCS cells (scale bar 100 µm). The positive control, induced by DNase, is given in the first row (Scale bar 20 µm). **(E,F,G)** The *CASP3, CASP8* and *CASP9* (30 min, 2, 4 and 24 h) gene expression was not significantly altered at all time points. **(H)** The gene expression of *HIF1A* after 24 h was not changed in AD cells, but significantly elevated in MCS compared to 1*g* (n = 5).

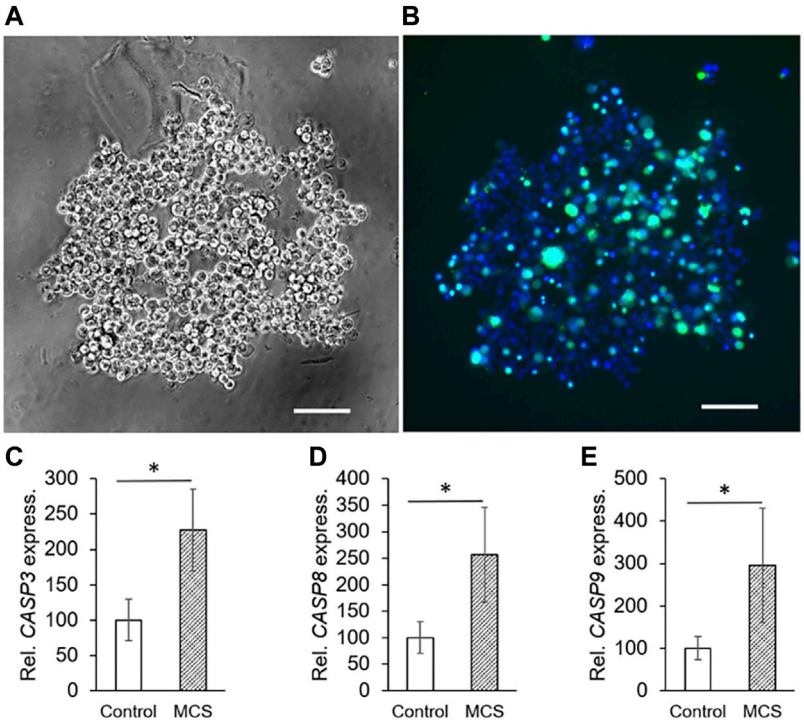

FIGURE 2 | Phase contrast microscopy of PC-3 cells: **(A)** static 1*g*-MCS after 24 h using the liquid overlay technique (scale bar 100 µm) and **(B)** same sample using the live cell viability assay, where the blue color indicates the nuclei of all cells while the green color demonstrates compromised cells. **(C,D,E)** The *CASP3, CASP8* and *CASP9* (24 h) gene expression was significantly altered in 1*g*-MCS after 24 h (n = 5).

The *TUBB* gene expression did not change when PC-3 cells were exposed to short-term s-µ*g* (**Figure 3B**). In contrast, AD cells exhibited a downregulated *TUBB* expression after 24 h compared to 1*g* cells. PC-3 cells growing in MCS did not show a change in *TUBB* expression. No significant differential *EZR* and *RDX* gene expression could be observed over the experiment duration (**Figure 3C**, **Figure 3D** respectively). Interestingly, the MSN mRNA was downregulated after a 30-min RPM exposure, whereas the gene was upregulated in MCS after 24 h compared to corresponding static 1*g* samples (**Figure 3E**). In addition, the *KRT8* mRNA was significantly downregulated in AD after 24 h compared to 1*g* (**Figure 3F**). While in RPM samples were only marginal expression changes visible, the investigations of these genes in 1*g*-MCS showed a significant upregulation of the cytoskeletal genes (**Figures 3A–F**).

The Extracellular Matrix

The mRNA expression of *FN1* was significantly upregulated in PC-3 cells growing in the AD monolayer and in MCS when cultured under conditions of s-µ*g* for 24 h. Short-term s-µ*g* did not induce changes in the *FN1* gene expression of PC-3 cells. In addition, MCS grown under 1*g*-conditions revealed no expression changes of *FN1* (**Figure 4A**). The immunofluorescence staining revealed a similar amount of fibronectin in the cytoplasm of the PC-3 cells exposed for 24 h to the RPM compared to static control cells (**Figure 4A**, right image). MCS cells revealed a loose connection between neighboring cells and an uneven distribution of fibronectin within the cells which is in contrast to the 1*g* AD and RPM AD cells. In parallel, the PC-3 cells exposed to the RPM secreted a significantly reduced amount of fibronectin into the supernatant within 24 h (**Table 3**). The amount of secreted fibronectin was similar in all groups after 2 and 4 h of RPM exposure (**Table 3**).

Moreover, the *COL1A1* gene expression was not significantly changed when exposed to short-term (30 min, 2 h, 4 h) s-µ*g*. In contrast, after a 24 h RPM exposure there was a significant upregulation of *COL1A1* detectable in both AD and MCS samples while 1*g*-MCS revealed a significantly reduced expression of *COL1A1* (**Figure 4B**). In addition, collagen-1α1 was released by the PC-3 cells in a significant lower amount after a 2 and 24 h RPM exposure compared to control samples (**Table 3**).

A similar result in respect to the gene expression was found for *LAMA3* in 24 h RPM-exposed cells. *LAMA3* was significantly upregulated in AD and MCS after 24 h. No expression change was detected in 1*g*-MCS (**Figure 4C**). The secretion of laminin by the cells was significantly elevated after 2 and 4 h in RPM samples, but the release was not significantly altered in 24 h cultures (**Table 3**).

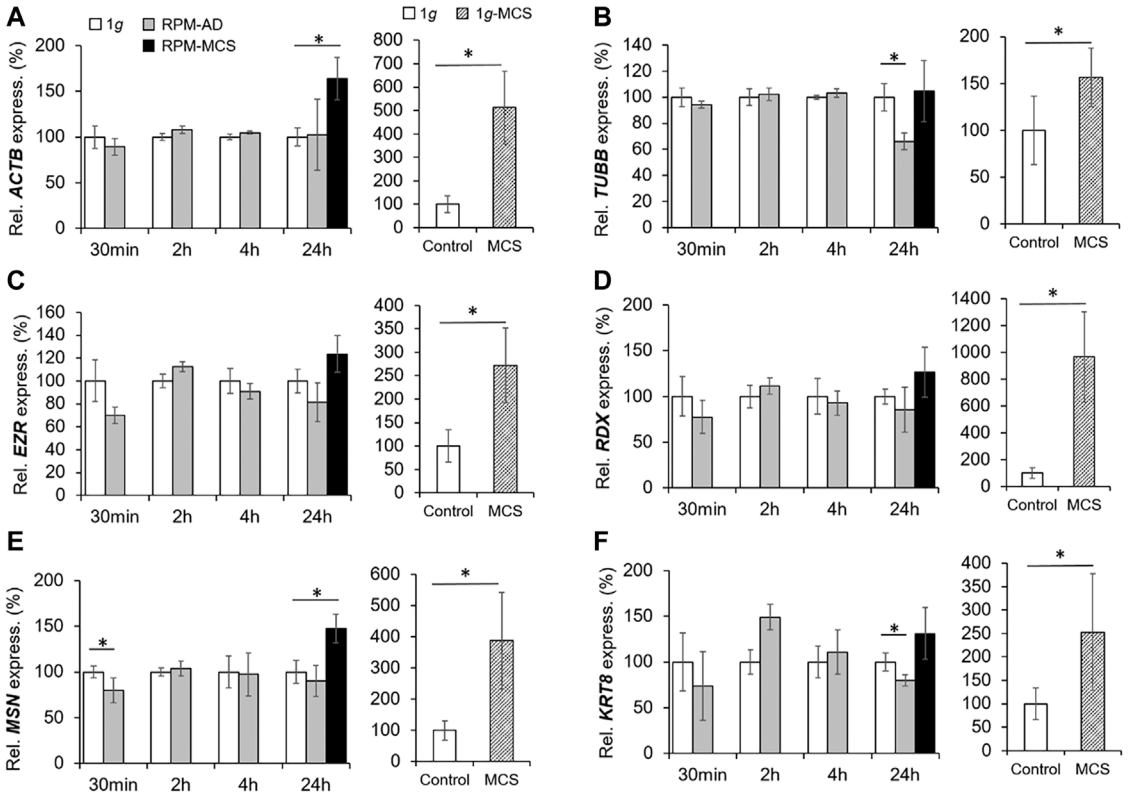

FIGURE 3 | Gene expression of **(A)** *ACTB*, **(B)** *TUBB*, **(C)** *EZR*, **(D)** *RDX*, **(E)** *MSN* and **(F)** *KRT8* of PC-3 cells exposed to the RPM for 30 min, 2, 4 and 24 h and 1*g*-MCS after 24 h. n = 5; *$p < 0.05$ vs. 1*g*.

Furthermore, the *SPP1* mRNA was not changed when the cells were exposed to the RPM and was not detectable by qPCR in 1*g*-MCS (**Figure 4D**). The release of osteopontin into the cell supernatant was reduced early, but remained later unchanged compared to 1*g* samples (**Table 3**).

Finally, the gene expression of *MMP9* was significantly increased in AD cells after a 24 h-RPM-exposure and was not detectable in 1*g*-MCS (**Figure 4E**), whereas *TIMP1* was elevated in RPM-MCS as well as in 1*g*-MCS (**Figure 4F**). The secretion of TIMP1 was not changed at any timepoint (**Table 1**). After 2 h, the release of MMP-2 protein in the supernatant was significantly lower in RPM cultures but remained unchanged in 4 and 24 h cell cultures exposed to 1*g*- or RPM-conditions (**Table 3**).

The Impact of Simulated Microgravity on Proinflammatory Cytokines

We focused on the expression and secretion of proliferation of proinflammatory cytokines known to be involved in tumor progression and metastasis. A significant upregulation of *IL6* was found already after 2 h in RPM samples. The *IL6* gene expression remained elevated after 4 and 24 h in RPM samples (**Figure 5A**). The release of IL-6 in the supernatant was significantly enhanced in all RPM samples after 2, 4 and 24 h (**Table 3**).

In parallel, the *CXCL8* mRNA was significantly upregulated already after 2 and 4 h in PC-3 cells exposed to the RPM. In addition, *CXCL8* was elevated in AD after 24 h compared to 1*g* cells (**Figure 5B**). The amount of released IL-8 protein in the supernatant was reduced after 2 h, but clearly elevated after 4 h in RPM samples compared to corresponding 1*g* samples (**Table 3**). After 24 h the cells secreted an equal amount of IL-8 in the supernatant, irrespective of RPM exposure or static 1*g* culture conditions (**Table 3**).

The *IL1B* mRNA expression was downregulated in RPM samples after 30 min, then upregulated after 2 and 4 h and finally downregulated in AD and MCS samples after 24 h (**Figure 5C**). The IL-1β protein release in the cell supernatant by the PC-3 cells was not significantly altered in this time course (**Table 3**).

In contrast to these findings, *TGFB1* was not differentially expressed in 1*g* and RPM samples at all time points (**Figure 5D**). IL-17 protein was secreted in a significantly reduced amount in RPM-exposed PC-3 cells compared with 1*g* samples after 2 h (**Table 3**). In addition, TNF-α was also released in a significantly decreased amount by RPM-exposed PC-3 cells after 2 h but was elevated after 4 h (**Table 3**). The expression of proinflammatory cytokines in 1*g*-MCS was, with the exception of *TGFB1*, highly upregulated (**Figures 5A–D**).

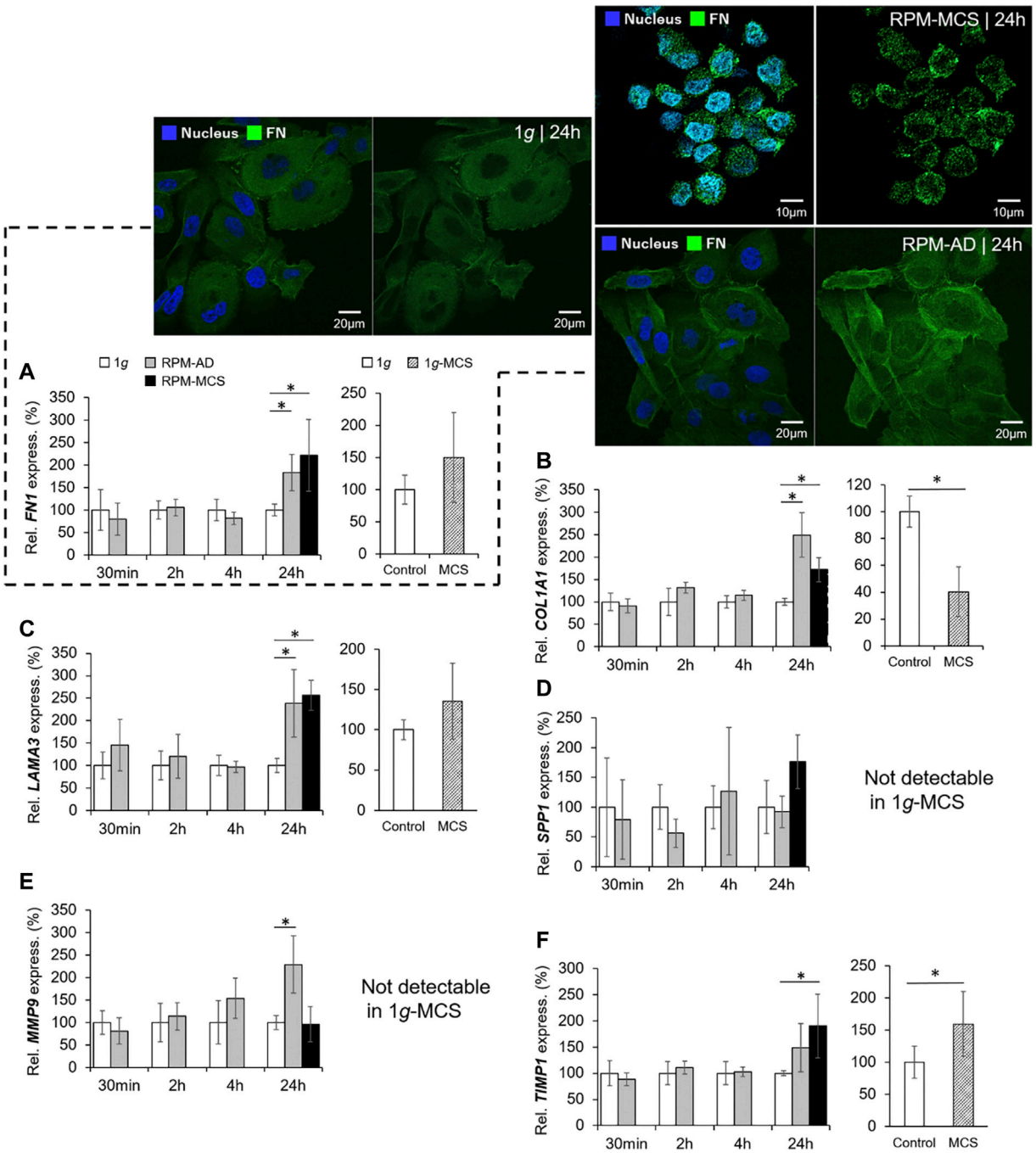

FIGURE 4 | Extracellular matrix: Gene expression of **(A)** *FN1* and immunofluorescence of fibronectin: left two images of the 1*g*/24 h sample (merged left picture and fibronectin (Alexa Fluor 488) right picture), top right two images of the RPM/24 h MCS samples (merged left picture and fibronectin right picture) and lower right two images of the RPM/24 h AD samples (merged left picture and fibronectin right picture), DAPI-stained nucleus (blue), **(B)** *COL1A1*, **(C)** *LAMA3*, **(D)** *SPP1*, **(E)** *MMP9,* and **(F)** *TIMP1* of PC-3 cells exposed to the RPM for 30 min, 2, 4 and 24 h and 1*g*-MCS after 24 h. n = 5; **p* < 0.05 vs. 1*g*.

Impact of Simulated Microgravity on Anti-inflammatory Cytokines

The gene expression of *IL1A* was elevated after 2 and 4 h in adherently growing cells exposed to the RPM compared to static control cells (**Figure 6A**). After 24 h, *IL1A* was significantly upregulated in MCS, but not in AD cells compared to 1*g* samples. The secretion of IL-1α in the cell supernatant was reduced in 2 h RPM-exposed samples compared to 1*g* (**Table 3**). In 1*g*-MCS a significant upregulation of *IL1A* was measured (**Figure 6A**).

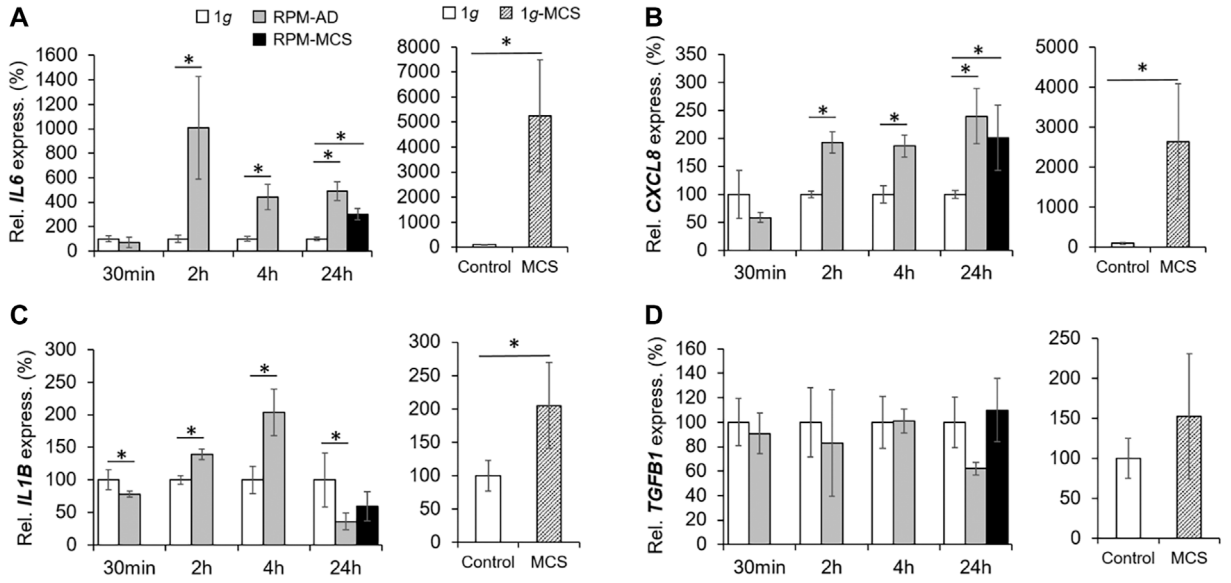

FIGURE 5 | Proinflammatory cytokines: Gene expression of **(A)** *IL6* and **(B)** *CXCL8* mRNA, **(C)** *IL1B*, and **(D)** *TGFB1* of PC-3 cells exposed to the RPM for 30 min, 2, 4 and 24 h and 1*g*-MCS after 24 h. n = 5; **p* < 0.05 vs. 1*g*.

TABLE 3 | Secreted proteins of PC-3 cells [pg/mL]. n = 5; **p* < 0.05 vs. 1*g*.

Protein	2 h		4 h		24 h	
	1*g*	RPM	1*g*	RPM	1*g*	RPM
IL-1α	22 ± 1	18 ± 2*	23 ± 2	25 ± 1	49 ± 8	42 ± 3
IL-1β	11 ± 1	10 ± 1	12 ± 2	15 ± 2*	22 ± 5	20 ± 2
IL-2	144 ± 2	132 ± 3*	146 ± 3	154 ± 3*	191 ± 13	184 ± 6
IL-6	13 ± 1	21 ± 3*	12 ± 3	58 ± 11*	59 ± 23	169 ± 42*
IL-7	14 ± 0	12 ± 0*	13 ± 1	15 ± 1*	21 ± 3	19 ± 2
IL-8	434 ± 65	195 ± 44*	519 ± 147	1,154 ± 208*	2,190 ± 1,059	3,097 ± 765
IL-17	39 ± 1	32 ± 4*	37 ± 5	40 ± 6	51 ± 7	48 ± 6
TNF-α	14 ± 1	11 ± 1*	14 ± 1	16 ± 1*	26 ± 4	23 ± 4
Fibronectin [ng/mL]	69 ± 2	58 ± 12	65 ± 13	65 ± 9	136 ± 31	97 ± 2*
Collagen I α1	125 ± 12	65 ± 11*	135 ± 33	138 ± 25	285 ± 101	163 ± 30*
Laminin	95 ± 9	145 ± 15*	88 ± 7	217 ± 34*	178 ± 17	233 ± 48
MMP-2	1854 ± 30	1786 ± 36*	1847 ± 39	1876 ± 45	2,149 ± 93	2068 ± 46
TIMP-1	1703 ± 208	1,334 ± 329	2,174 ± 695	1783 ± 372	9,245 ± 3,972	6,579 ± 1,086
Osteopontin	6,010 ± 154	5,441 ± 400*	5,928 ± 356	6,193 ± 260	7,287 ± 551	6,914 ± 537
EGF	13 ± 0	12 ± 2	12 ± 2	13 ± 2	15 ± 2	15 ± 2

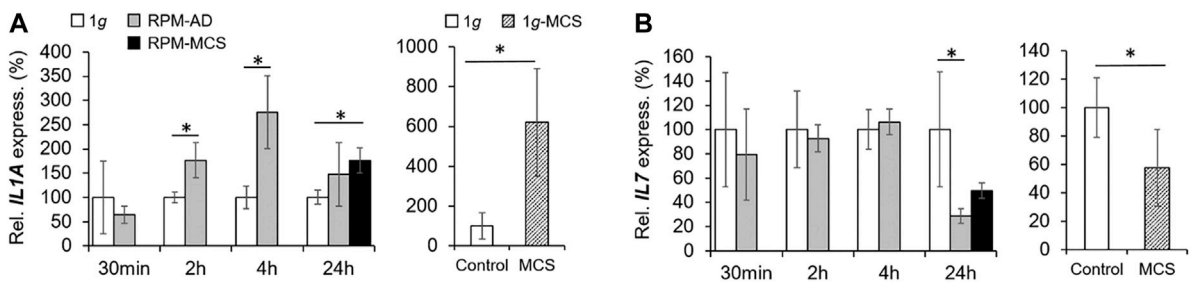

FIGURE 6 | Anti-inflammatory cytokines: Gene expression of **(A)** *IL1A* and **(B)** *IL17* of PC-3 cells exposed to the RPM for 30 min, 2, 4 and 24 h and 1*g*-MCS after 24 h. n = 5; **p* < 0.05 vs. 1*g*.

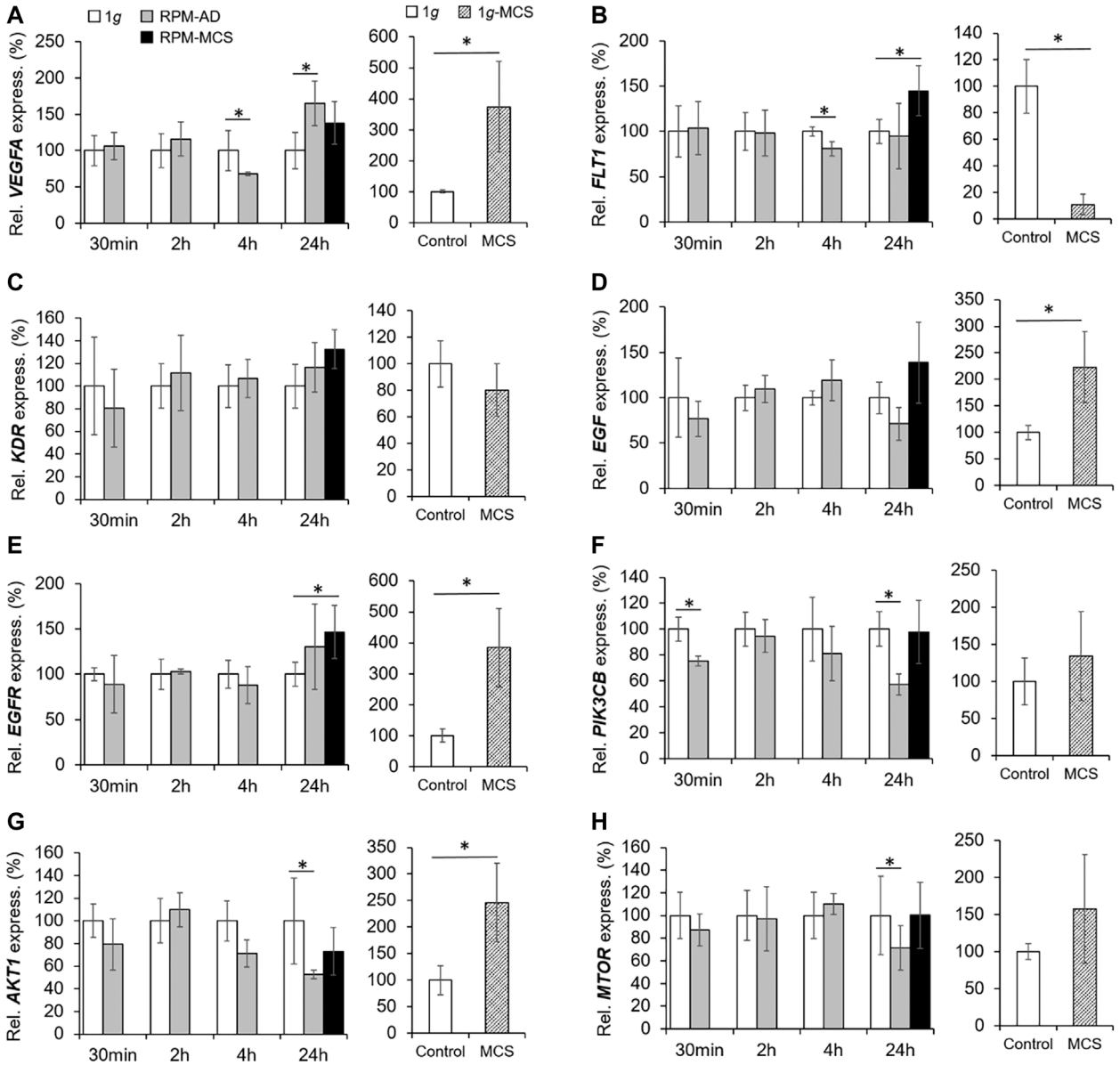

FIGURE 7 | VEGF, EGF and PAM signaling: Gene expression of **(A)** *VEGFA*, **(B)** *FLT1*, **(C)** *KDR*, **(D)** *EGF*, **(E)** *EGFR*, **(F)** *PIK3CB*, **(G)** *AKT1,* and **(H)** *MTOR* of PC-3 cells exposed to the RPM for 30min, 2, 4 and 24 h and 1*g*-MCS after 24 h. n = 5 $^{*}p < 0.05$ vs. 1*g*.

Furthermore, we measured the release of IL-2 and detected a reduced amount of this protein after a 2 h RPM exposure of the cells, whereas after 4 h the secretion was elevated in the RPM samples (**Table 3**). In contrast, the *IL7* gene expression was not changed in short-term cultures (30 min, 2 and 4 h). Interestingly, in 24 h RPM cultures the *IL7* mRNA was significantly downregulated in AD and MCS cells compared to the control group, which is similar in 1*g*-MCS (**Figure 6B**). The secretion of the IL-7 protein was reduced after 2 h and enhanced after 4 h of RPM exposure of the cells (**Table 3**). After 24 h, the secretion of IL-7 was similar in both groups.

Influence of Simulated Microgravity on VEGF, EGF and PI3K/AKT/mTOR (PAM) Signaling Pathways

The mRNA level of *VEGFA* was not changed in PC-3 cells exposed to the RPM for 30 min and 2 h. After 4 h the *VEGFA* mRNA was significantly downregulated in the AD group.

In contrast, the 24 h AD samples showed an increased level of *VEGFA* mRNA compared to 1*g*. RPM-MCS exhibited no change in *VEGFA*. In contrast, the gene expression of VEGF-A was elevated in 1*g*-MCS (**Figure 7A**). In parallel, we focused on the VEGF receptors *FLT1* and *KDR*. *FLT1* was significantly

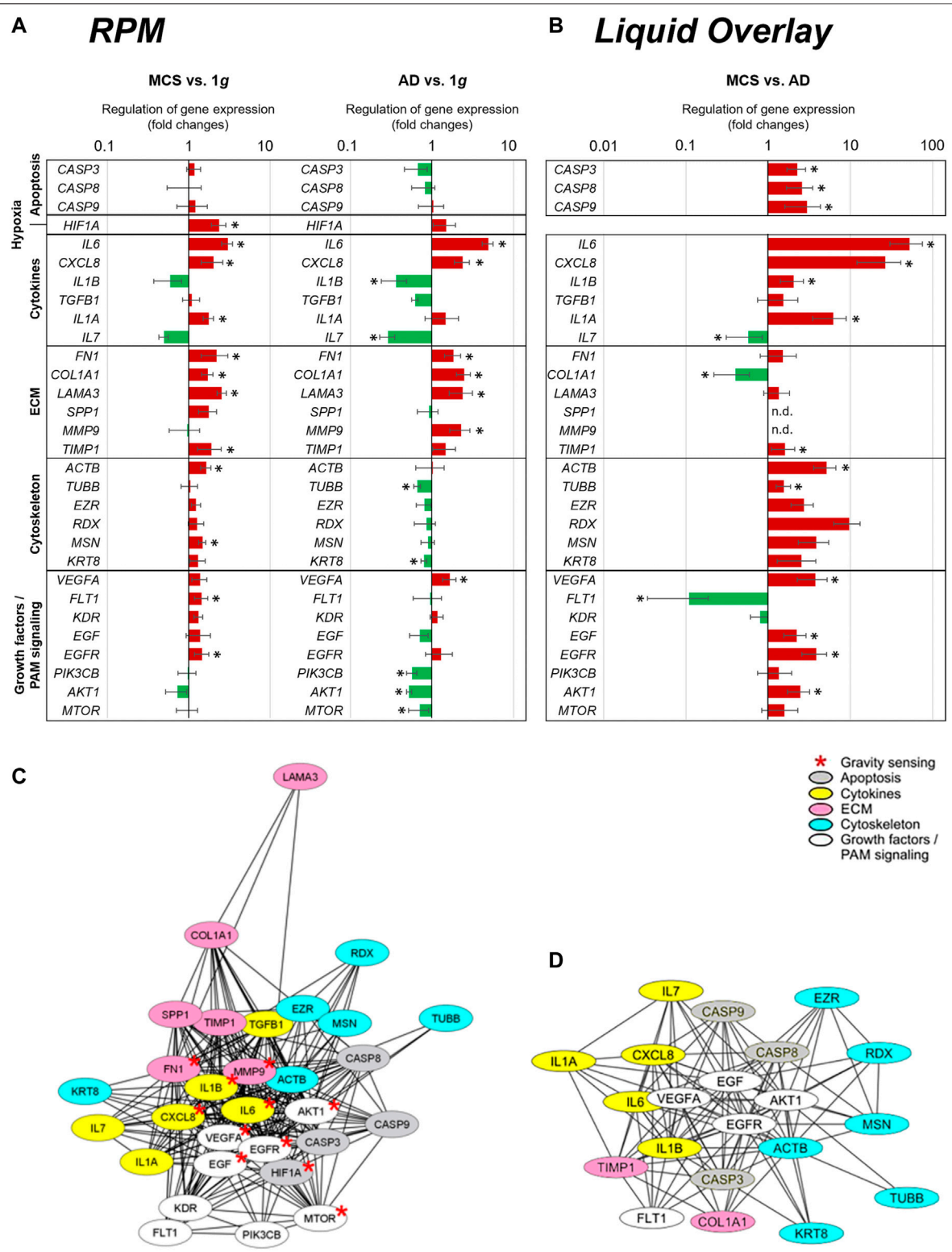

FIGURE 8 | qPCR expression changes of selected genes and their relationship in STRING protein-protein interaction networks. **(A)** qPCR gene expression fold changes of the 24 h RPM-exposed PC-3 samples (AD and MCS) in relation to 1*g*. The red and green colors indicate upregulated and downregulated genes in RPM-exposed samples respectively. Significant regulations are indicated by black asterisks ($p < 0.05$). **(B)** qPCR gene expression fold changes of liquid overlay derived MCS cell aggregates in relation to controls. **(C,D)** Network of the functional interaction of genes and their products **(C)** analyzed in this study and **(D)** differtially regulated in liquid overlay derived MCS cell aggregates. The analysis was performed by STRING 11.0 (https://string-db.org/) and combined scores are visualized by Cytoscape 3.8.2. Affiliation to functional gene groups is color-coded. Red asterisks indicate genes known to be involved in prostate cancer gravity sensing.

downregulated in AD cells after 4h, whereas after 24 h the *FLT1* mRNA was only upregulated in MCS. Contrary, *FLT1* is significantly downregulated in 1*g*-MCS (**Figure 7B**). The *KDR* mRNA expression was not altered over the entire time course using both methods (**Figure 7C**).

In addition, we investigated the *EGF* and *EGFR* gene expression in PC-3 cells exposed to s-μ*g* and in 1*g*-MCS. The *EGF* mRNA was not differentially displayed in PC-3 cells exposed to short-term microgravity. After 24 h, a non-significant increase in *EGF* was measured in MCS while a significant upregulation of *EGF* was measured in 1*g*-MCS (**Figure 7D**). After 24 h, a significant upregulation of the *EGFR* was detected in PC-3 cells growing in form of MCS using both methods (**Figure 7E**). The secretion of EGF protein was not changed in all groups (**Table 3**).

Furthermore, we studied key factors of the PAM pathway. The *PIK3CB* (Phosphatidylinositol-4,5-Bisphosphate 3-Kinase Catalytic Subunit Beta) gene was downregulated early in 30 min RPM exposed PC-3 cells (**Figure 7F**). After 24 h, RPM-exposed adherently growing PC-3 cells exhibited a downregulated *PIK3CB* mRNA expression. No expression changes were detectable in 1*g*-MCS (**Figure 7F**).

In parallel, the *AKT1* (RAC-alpha Serine/threonine-protein kinase 1) gene showed no altered expression in short-term samples but a significantly downregulated expression in 24 h AD RPM samples compared to 1*g*. Using the liquid overlay technique, the MCS group revealed a significantly upregulated *AKT1* (**Figure 7G**).

Finally, we studied the *MTOR* gene expression. The results were similar to the findings obtained for *AKT1*. *MTOR* was not differentially expressed in the short-term study, but the gene was downregulated in AD cells after a 24 h RPM exposure. In 1*g*-MCS no expression changes were measured for *MTOR* (**Figure 7H**).

Search Tool for the Retrieval of Interacting Genes/Proteins Analysis

Figure 8A presents a summary of the qPCR data, already demonstrated in **Figures 1**, **3–7**, and gives an interpretation of the results. The genes of interest were differentially regulated in RPM samples (AD and RPM).

The results indicate several interactions for VEGFA, EGF, EGFR, IL1B, CXCL8, IL6, MTOR, AKT1, MMP9, and FN1, which are known to be involved in gravisensing of PC-3 prostate cancer cells exposed to short-term r-μ*g* (**Figure 8C**). It became clear that these selected factors for which the expression pattern was measured are regulating each other very strongly.

The majority of the genes quantified in this study were upregulated in MCS with the exception of the downregulated *IL1B*, *IL7,* and *AKT1* mRNAs and *CASP3, CASP9, CASP8, MMP9, TUBB, EZR, RDX, KRT8, TGFB, SPP1, VEGFA, KDR, EGF, PIK3CB,* and *MTOR* which were not differentially displayed. A closer look at the 24 h AD samples revealed that the majority of cytoskeletal genes and PAM signaling factors were downregulated. In contrast, significant upregulations were found for ECM genes and proinflammatory cytokines such as among others *IL6*, *CXCL8*, and *VEGFA* and *FLT1*.

Figure 8B shows the summary of the qPCR data of the 1*g*-MCS vs. AD control cells (liquid-overlay engineered MCS), already given in **Figures 2–7**. The 1*g*-liquid overlay generated MCS cell aggregates show a different picture of gene regulation. Significant upregulations were measured for the following genes: *CASP3, CASP8, CASP9, IL6, CXCL8, IL1B, IL1A, TIMP1, ACTB, TUBB, EZR, RDX, MSN, KRT8, VEGFA, EGF, EGFR,* and *AKT1*. Significant downregulations were measured for *IL7, COL1A1,* and *FLT1*. In contrast to the RPM experiment, an upregulation of apoptosis-associated cysteine-aspartic acid proteases and a strong downregulation of the growth factor receptor FLT1 catch the eye (**Figure 8B**).

The various genes analyzed by qPCR were investigated with regard to possible interactions and mutual expression dependence of their corresponding proteins. A STRING/EMBL (European Molecular Biology Laboratory) analysis of the 30 qPCR items represented in this study are shown in **Figure 8C**. **Figure 8D** visualizes interactions of 21 proteins whose genes are significantly regulated in 1*g*-MCS compared to corresponding adherent controls. The STRING network shows a clear demarcation of cytokines from cytoskeletal genes.

DISCUSSION

For many years, it has been known that various cells exposed to r- and s-μ*g* exhibit a large number of morphological and molecular changes (Grimm et al., 2018; Grimm et al., 2020). Ingram et al. showed in 1997 that various tumor cell types, among them PC-3 cells, when exposed to s-μ*g* created by a NASA bioreactor grew in form of 3D aggregates (Ingram et al., 1997). The authors had used a NASA rotary cell culture system for the different spheroid cultures. They reported that the cell adhesion molecules CD44 and E-cadherin were upregulated in the 3D spheroids (Ingram et al., 1997). Furthermore, another group demonstrated the application of an s-μ*g* culture system to study growth and differentiation during a coculture of prostate stromal and epithelial cells on microcarrier beads (Zhau et al., 1997). The authors investigated the effects of an androgen (dihydrotestosterone) on growth and PSA expression by LNCaP prostate cancer cells grown alone or as coculture with prostate fibroblasts under s-μ*g* conditions (Zhau et al., 1997). The response was similar to that observed *in vivo*. Margolis et al. demonstrated that *ex vivo* integral prostatic tissue could be successfully cultured for 28 days on the NASA-designed Rotating Wall Vessel (RWV) (Margolis et al., 1999). The prostate tissue was still suitable for further investigations (Margolis et al., 1999). Another group used the high aspect rotating-wall vessel (HARV) to study the behavior of DU-145 human prostate carcinoma cells (Clejan et al., 2001). DU-145 cells exposed to HARV cultivation showed 3D growth as well as a less aggressive, slower growing, low proliferative, higher differentiated and less pliant cell than other techniques (Clejan et al., 2001).

The project Biotechnology Demonstration System-0, one of the 80 scientific experiments aboard Space Shuttle Columbia on flight STS-107, could show that in less than 1 day in space PCC had formed a tumor larger than one inch in diameter (Twombly,

2003). In a ground-based study under s-μ*g* conditions, the PCC and bone stroma formed small tissue aggregates (Twombly, 2003). On the space shuttle Columbia, the aggregates grew to the size of a golf ball by day 6. This data is in accordance with results obtained after the Shenzhou-8/SimBox Chinese-German space mission where follicular thyroid cancer cells (FTC-133 cell line) had been studied in space for 10 days (Pietsch et al., 2013). Interestingly, FTC-133 MCS grown in the flight sample in space ranged from 5 to 10 mm in diameter, while spheroids cultured on the RPM were significantly smaller at 2–3 mm in diameter, as observed in earlier experiments (Pietsch et al., 2010; Pietsch et al., 2013).

In a recent study, we investigated PC-3 cells for 3 and 5 days under s-μ*g* conditions using a desktop RPM without any scaffold (Hybel et al., 2020). The cells revealed changes in morphology, cytoskeleton, ECM, focal adhesion complex and growth behavior. In addition, a significant upregulation of genes belonging to the PAM pathway was demonstrated (Hybel et al., 2020).

PC-3 Cells Exposed to the RPM Exhibit Changes in Morphology, Cytoskeleton and Extracellular Matrix

PC-3 cells cultured under conditions of s-μ*g* showed changes in growth within 24 h. One part grew in form of 3D multicellular spheroids and the other one continued growing as adherent cells in a 2D monolayer. This is in accordance with other cell types, including human thyroid cancer cells and breast cancer cells (Pietsch et al., 2010; Pietsch et al., 2013; Masiello et al., 2014). We focused on signs of apoptosis and could show that the TUNEL staining revealed no apoptotic cells after 24 h. In addition, the *CASP3, CASP8,* and *CASP9* genes were not differentially displayed. These findings demonstrated in **Figure 1** show viable PC-3 after RPM exposure.

In addition, we have measured the gene expression of *HIF1A* after a 24-h exposure. Interestingly, there was no significant change in the adherently growing cells, but an increase in MCS (**Figure 1H**).

A significant *HIF1A* expression has been detected in a large number of cancers, which include among others prostate tumors (Zhong et al., 1999). Elevated HIF1A levels in several cancers have been associated with aggressive tumor progression, and thus has been implicated as a predictive and prognostic marker for resistance to therapy and increased mortality (Semenza, 2003). We do not expect hypoxia in the completely filled cell culture flasks because they have vented caps. The cells are viable and no apoptosis is detectable. The gas exchange has been studied earlier (Pietsch et al., 2012).

It is known that HIF1A is initiating angiogenesis through interactions with pro-angiogenic factors like VEGF-A (Birner et al., 2001). VEGF-A is elevated in RPM-exposed PC-3 cells after 24 h. HIF1A has a regulatory role in promoting tumor progression, likely through hypoxia-induced VEGF-A expression pathways (Powis and Kirkpatrick, 2004). HIF1A overexpression in tumors may also occur in a hypoxia-independent pathway. In hemangioblastoma, *HIF1A* expression is found in most cell samples from the well-vascularized tumor (Krieg et al., 2000). It will be of high interest to perform future long-term studies investigating this finding in detail.

A large number of studies have shown that r-μ*g* as well as s-μ*g* generated by an RPM has a major impact on the cytoskeleton (Vorselen et al., 2014; Corydon et al., 2016a; Chen et al., 2019; Nassef et al., 2019; Strube et al., 2020). Thereby it reacts on alterations of gravity with a bunch of rearrangements in the structure of the cytoskeleton. Moreover, it is suggested that the cytoskeleton may act as a direct sensor of gravity and displays the initial response to changed gravity levels (Vorselen et al., 2014; Häder et al., 2017). The cytoskeleton acts as a shape-giving structure providing the mechanical strength of cells. Thus, it works as a continuous pre-stressed lattice keeping cellular structural stability. It is composed of the actin and microtubule network, as well as intermediate filaments (Vorselen et al., 2014). F-actin belongs to the microfilaments and forms a large part of the cytoskeleton. In this study, we focused on the gene expression of β-actin (*ACTB*). β-actin is involved in forming the cell structure, cell motility and cell integrity. Short-term s-μ*g*-exposure induced no significant changes in the mRNA expression level (**Figure 3**). Remarkably, after 24 h an upregulation of *ACTB* was detectable in MCS samples but not in AD. This is in line with earlier studies finding that the mRNA level of ACTB was increased after cultivating PC-3 cells for 5 days on an RPM (Hybel et al., 2020). This supports the assumption that the actin-network is influenced by gravity changes and plays a critical role in 3D growth. Moreover, it is also suggested that actin itself can work as a mechanosensitive structure (Vorselen et al., 2014). The cytoskeleton of various cell types influenced by μ*g* reacts in a similar way, thus it can be assumed that the cytoskeleton acts as the general sensor of gravity and that the changes in the cytoskeleton become important for 3D growth (Grimm et al., 2018). Together with further morphogenetic events, these changes in the actin cytoskeleton promote the emergence of ordered structures and finally they result in the formation of MCS (Cui et al., 2017).

Moreover, we focused on the *TUBB* gene expression. β-tubulin belongs to the tubulin superfamily, that in turn contains six families (α, β, γ, δ, ε, and ζ tubulins). The most important families are the α- and β-tubulins as they form the major components of the microtubules. Short-term (30 min, 2 h, 4 h) RPM exposure showed no significant changes in the mRNA expression level compared to 1*g*. After a 24 h-exposure a significant downregulation was observed in AD samples but not in MCS samples. Previous research has clearly shown that microtubule self-organization is sensitive to the direction and the magnitude of gravity. The microtubules can respond to alteration of gravity by rearranging their structure and formation. Accordingly, they lose their radial organization, can be shortened, and can be more curved and bent (Lewis et al., 1998). But it was shown that these alterations are dependent on the type of cell and differ from cell to cell (Vorselen et al., 2014).

Furthermore, we investigated changes in the ECM. The ECM acts as a kind of sensor of alterations in gravity force. It is known that s-μ*g* exposure generated by an RPM, results in

changes in the ECM like the formation of long-chain fibers with multiple RGD motifs. The RGD motif is a tripeptide that consists of arginine, glycine, and aspartate and mediates cell attachment. These motifs can bind tightly to the integrins on the cell membrane surface and interact with the cytoskeleton in the way that dispersed cells in the cell culture flask initially are drawn closer to form loose aggregates (Cui et al., 2017). In this manner the ECM is also early involved in spheroid formation of different tumor types (Grimm et al., 2002; Marrero et al., 2009; Lin et al., 2020).

To investigate the ECM components, we measured the *FN1*, *COL1A1*, *LAMA3, SPP1, MMP9* and *TIMP1* gene expression. Short-term s-μ*g* exposure (30 min, 2 h, 4 h) did not alter the expression of the selected ECM genes. In contrast, after a 24-h RPM-exposure, the *FN1*, *COL1A1* and *LAMA3* genes were elevated in both AD and MCS samples (**Figures 4A–C**). This is in line with earlier studies on different cell types demonstrating that there is a general tendency of elevated ECM components when cancer cells but also stem cells and specialized cells were exposed to long-term s-μ*g* (Grimm et al., 2002; Kraus et al., 2017; Ebnerasuly et al., 2018). It has to be noted that this increase is dependent on the cell type. There were opposite results detectable when adult retinal epithelium cells (ARPE-19) were exposed to the RPM (Corydon et al., 2016b). The *FN1* expression and *LAMB2* expression was reduced after RPM exposure in AD and MCS of ARPE-19 cells (Corydon et al., 2016b).

When analyzing the presence of fibronectin in MCS obtained in s-μ*g*, a slightly different cytoplasmic distribution, exemplified by a dotted pattern, compared to 1*g* samples was observed. A likely explanation could be that the cells of the MCS are significantly smaller. The apparent shrinking of the cells and the accompanying compression of the cytoplasm may collectively result in an altered cytoplasmic distribution and reduced secretion of fibronectin, despite the increased expression of *FN1*. However, reduced gravitational conditions may also impact the cytoplasmic appearance of fibronectin in RPM-MCS (**Figure 4A**).

In addition, human mesenchymal stem cells exposed to 10 days s-μ*g* showed a decrease in collagen production, as well as a reduced expression of *TIMP1*, *TIMP3,* and *MMP11* genes, together with an elevated expression of tenascin and laminin subunit (Zhivodernikov et al., 2020).

The *SPP1* gene expression was not significantly changed in all groups of PC-3 exposed to s-μ*g* conditions. The expression of osteopontin is known to be cell type-dependent. Rat osteoblasts cultured for 4 or 5 days aboard the Space Shuttle revealed a reduced (30%) *SPP1* mRNA (osteopontin) in the flight samples (Kumei et al., 2006). In contrast, the *SPP1* mRNA was elevated in human fetal osteoblasts exposed to the RPM (Mann et al., 2019). A similar result was obtained for human primary chondrocytes (Wehland et al., 2020).

Simulated Microgravity Influences the Expression and Release of Inflammatory Cytokines in PC-3 Cells

We focused on the cytokine release pattern of PC-3 cells when exposed to the RPM. It is assumed that some cytokines play a major role in spheroid formation. *IL6* for example exhibits a higher expression in PC-3 cells as well as in other prostate cancer cell lines and plays a major role as a proliferative autocrine and paracrine factor in prostate cancer (Azevedo et al., 2011). Furthermore, Gopinathan et al. (Gopinathan et al., 2015) showed that *IL6* can directly generate the development of new blood vessels, the proliferation and migration of endothelial cells and has thereby a tumor promoting activity.

In the present study, the *IL6* gene expression increased very early with a 10-fold peak after 2 h of RPM-exposure. Afterwards, within 4 and 24 h (AD and MCS) it slightly decreased but still showed an about 5-fold elevation compared to 1*g* samples. This is in line with Grosse et al. (Grosse et al., 2012), who performed similar experiments with FTC-133 thyroid cancer cells and demonstrated that the tumor cells on the RPM released IL-6 in the supernatant. Svejgaard et al. (Svejgaard et al., 2015) demonstrated that both cytokines IL-6 and IL-8 improve 3D aggregation of the human thyroid cancer cell lines (ML-1 and RO-82-W-1) using the liquid overlay technique and that these cytokines induced the protein expression of β-actin, β_1-integrin, talin-1, and Ki-67. These findings implicate that IL-6 as well as IL-8 are involved in spheroid formation. The detailed mechanisms are still unknown and have to be investigated more precisely in future studies. Interestingly, the IL-6 release was significantly elevated in all RPM samples at all time points (**Table 3**).

Taken together, all these findings indicate that interleukin-6 might be an important factor for tumor cell growth, angiogenesis, metastasis and spheroid formation. The expression of *CXCL8* showed a similar pattern as *IL6* indicating a similar reaction of the anti-inflammatory cytokines to microgravity.

Singh et al. (Singh and Lokeshwar, 2009) showed that IL-8 is acting as a survival factor of cancer cells and in this context IL-8 interacts with Akt and NF-κB, and has thereby a control function on the apoptotic pathway. Moreover, IL-8 plays a role in PC-3 survival, invasion, and resistance to chemotherapeutic drugs in PC-3 cells. Wilson et al. (Waugh and Wilson, 2008) mentioned that IL-8 signaling is involved in PC-3 survival and acts as an intrinsic factor of chemoresistance in advanced prostate cancer. Besides, Waugh et al. (Waugh and Wilson, 2008) showed that *CXCL8* signaling regulates, among others, the transcriptional activity of the androgen receptor of PC-3 so that PC-3 proliferate androgen-independently. Therefore, taken these findings together, IL-8 is of special interest as it has an impact on PC-3 cells in many ways.

In the present study, we measured an upregulation of *CXCL8* in AD cells and 3D PC-3 MCS. The secretion of IL-8 was significantly elevated after 4 h, but similar after 24 h between the RPM and 1*g* group (**Table 3**). It is known that IL-8 increases the expression of several proteins of the cytoskeleton and focal adhesion complex. These proteins in turn play a major role in tumor progression and metastasis (Desiniotis and Kyprianou, 2011). Remarkably, these proteins belonging to the cytoskeleton and focal adhesion complex also

can sense gravity changes and therefore have a great impact on spheroid formation.

Simulated Microgravity has Impact on VEGF, EGF, and PAM Signaling

We studied factors of signaling pathways known to be involved in 3D growth (Krüger et al., 2019; Nassef et al., 2020). The expression of genes belonging to the *VEGF* signaling pathway were analyzed, showing that the gene expression of *VEGFA* was downregulated after 4 h and in contrast upregulated after 24 h of RPM exposure in AD samples compared to 1*g* (**Figure 7A**). In MCS samples, however, the *VEGFA* mRNA showed no significant change. One potential explanation for this finding could be that a less-aggressive phenotype developed when the cells merged into spheroid formation, which was found earlier in follicular thyroid cancer cells cultured in space (Ma et al., 2014). Furthermore, VEGF-A has various well-known effects in cancer. It is mediating increased vascular permeability, inducing angiogenesis, vasculogenesis and growth. In addition, VEGF-A promotes migration and progression. Within 24 h, the prostate cancer cells exposed to the RPM start to detach and to form MCS. A high amount of VEGF-A promotes spheroid formation which might explain the elevated level of *VEGFA* mRNA in 24 h AD samples.

The *KDR* gene was not differentially expressed in all groups, whereas *FLT1* was downregulated after 4 h in AD, unchanged after 24 h in AD, but elevated in MCS. As the VEGF-A pathway has been implicated in pathological angiogenesis and tumor development (Nagy et al., 2007), a lower expression of the pathway points towards a less-aggressive cancer growth behavior.

Furthermore, we investigated the gene expression of *EGF*. The EGF protein is a key player in cancer by enhancing cell proliferation, survival, invasion, and metastasis (Bhat et al., 2014). The expression of epidermal growth factor receptor (EGFR) in cancer is often associated with a more aggressive phenotype and predictive of poor prognosis (Bhat et al., 2014). The *EGFR* mRNA is upregulated in MCS compared to 1*g* control cells indicating its involvement in 3D spheroid formation (**Figure 7E**).

The PAM pathway is of special interest because it is often mutated in prostate cancer (Tee et al., 2018) and therefore involved in cancer growth and progression. It is also a frequent reason of drug-resistance especially to androgen-deprivation therapy in prostate cancer (Park et al., 2018). Regarding the PAM signaling pathway, the *PIK3CB* gene was downregulated after 30 min and finally, after 24 h also in AD samples. A similar result was obtained for the *AKT1* and *MTOR* mRNAs, which were both reduced in 24 h AD cells. In addition, these genes were not altered in MCS. This is an interesting result because downregulation of the PAM pathway can activate apoptosis in cancer (Yang et al., 2019). Apoptosis was not detected after RPM exposure, which is an interesting result and it can therefore be concluded that other signaling factors exhibited anti-apoptotic effects on the PC exposed to short-term μ*g*. Long-term s-μ*g*-exposure of PC-3 cells (5 days) resulted in a significant upregulation of *AKT* and *MTOR* mRNAs in both AD and MCS (Hybel et al., 2020).

Interaction Network of Selected Genes Evaluated by STRING Analysis and Cytoscape 3.8.2

The STRING analysis revealed an interaction network of VEGFA, FLT1, EGF, EGFR, IL1B, IL6, CXCL8, MTOR, AKT1, MMP9, and FN1. The interaction between the VEGF and EGFR pathway is well known and the rationale for a multi-target anticancer therapy (Ciardiello et al., 2006). EGF application is able to enhance VEGF-A production and to induce PI3K-dependent positive feedback on AKT and ERK via VEGFR2 in hematological malignancies (human monocytic leukemia THP1 cell line and Burkitt's lymphoma Raji cell line (Saryeddine et al., 2016). Both pathways are key players in cancer cell growth, progression, metastasis and angiogenesis. Multikinase inhibitor therapy targeting among other factors VEGF-A is applied today in different types of advanced metastatic cancers (Wehland et al., 2012; Ancker et al., 2017; Randrup Hansen et al., 2017; Sarkar et al., 2020). EGF mediates cellular proliferation, differentiation, and survival (Herbst, 2004) and is involved in spheroid formation of cancer cells exposed to r-μ*g* in space. The *EGF* gene expression was clearly upregulated in AD and MCS of FTC-133 follicular thyroid cancer cells in space during the Shenzhou-8 space mission (Pietsch et al., 2013). These results indicate the importance of EGF signaling for spheroid formation.

A further factor involved in spheroid formation and spreading of cancer cells is fibronectin. Proteome analyses revealed that surface proteins are binding fibronectin, and thus strengthening the 3D spheroid formation of thyroid cancer cells (Pietsch et al., 2011). This might be also important for other cancer types. Bioinformatic analyses have demonstrated that EGFR, KDR, FN1, TGFB1 as well as PCNA are interacting with VEGF-A and are involved in non-small cell lung cancer tumorigenesis (Wang et al., 2015). FN1 is involved in the occurrence and development of various tumors and is upregulated in multiple cancer types. *FN1* is able to promote cell proliferation and migration in gastric cancer cell lines (Sun et al., 2020). A recent study showed that both cell adhesion molecules and ECM components OPN (SPP1) and FN1 might work as biological markers of progression and prognosis in esophageal cancer (Li et al., 2020).

The functional roles of VEGF and OPN in angiogenesis and their clinical significance in tumor biology are well-described (Shijubo et al., 2000). In PC metastasis both protein synthesis and gene expression of *SPP1* were remarkably upregulated in metastatic castration-resistant PC (Pang et al., 2019).

Pro-inflammatory cytokines such as IL-1, IL-6, IL-17, and TNF-α promote proliferation and differentiation of cancer cells (Vendramini-Costa and Carvalho, 2012). The cytokines IL-6 and IL-8 (CXCL-8) are further key elements which are able to enhance 3D growth in PC-3 and have both already shown to

induce 3D growth in thyroid tumor cells grown under 1*g*-conditions using the liquid overlay technique (Svejgaard et al., 2015). Both cytokines were clearly elevated in PC-3 exposed to the RPM and may serve as key players for 3D aggregation. IL-6 is a key factor in the tumor microenvironment. IL-6 overexpression was demonstrated in almost all cancer types (Kumari et al., 2016). High levels of IL-6 advance tumorigenesis and regulate among others metabolism, angiogenesis, invasiveness, metastasis, apoptosis, and survival (Kumari et al., 2016). IL-6 can induce cell growth and VEGF synthesis in malignant mesotheliomas or gastric cancer (Huang et al., 2004; Adachi et al., 2006). Furthermore, EGFR signaling promotes induction of the IL-6 receptor controlled by mTOR (Garbers et al., 2013). An aberrant EGFR activation triggered IL-6 synthesis (Garbers et al., 2013).

The PI3K-AKT-mTOR signaling network is activated and during prostate tumorigenesis, PC progression and recurrence (Shorning et al., 2020). The mTOR pathway is involved in VEGF biosynthesis, and disruption of the VEGF/Neuroplin-1 (NRP1) axis. VEGF/NRP1 are promoting angiogenesis and pro-tumorigenic signaling in both endothelial and cancer cells (Pal et al., 2019). The *VEGFA* gene expression is enhanced in AD cells indicating signaling towards 3D formation of PC-3.

Even though there are various more convenient techniques to produce spheroids like the hanging drop technique (Timmins et al., 2004) or the liquid-overlay technique (Svejgaard et al., 2015), these methods introduce unfavorable aspects which are low quantity, poor nutrition exchange among others. In addition, the transition from 2D growth to 3D growth cannot be monitored in these experimental setups. We used the liquid-overlay technique and engineered MCS under 1*g*-conditions. After 24 h, the PC-3 cells formed loose 3D aggregates on agarose. Unfortunately, more dead cells were detected compared to RPM-engineered MCS (**Figure 2B**). The qPCR analysis revealed a strong up-regulation for proinflammatory cytokines like among others *IL6* and *CXCL8.* This finding might be explained by the higher amount of dead cells in 1*g*-engineered MCS. The opposite result was obtained for the expression of *VEGFA* and *FLT1* in 1*g*-MCS. *VEGFA* and *KDR* were both not differentially altered and *FLT1* was significantly elevated in RPM-MCS, whereas *VEGFA* was upregulated and *FLT1* down-regulated in 1*g*-MCS.

In addition, the ECM genes *FN1, COL1A1,* and *LAMA3* were all significantly up-regulated in RPM-MCS and differentially regulated in 1*g*-MCS. Taken together the results involving 1*g*-MCS engineered with the liquid-overlay technique are not suitable to study the early phases of tumor progression and metastasis in PC. The MCS formed with an RPM are rounder and compact, are created without agarose or a scaffold, do not show an increase in apoptosis and can grow for a longer time under s-μ*g* conditions as shown in an earlier study (Hybel et al., 2020).

Comparison Between Short-Term and Long-Term Changes in PC-3 Cells Exposed to the RPM

COL1A1, which encodes one part of the fibril-forming pro-alpha1 chains of type I collagen, *LAMA3,* encoding the alpha part of the heterotrimeric laminin molecule, and *FN1,* encoding fibronectin, which is involved in RET signaling and is part of the integrin pathway, are substantial components of the ECM. All three genes are upregulated in PC-3 after a 24-h RPM-exposure in AD as well as in MCS. In a previous study with long-term RPM-exposure of PC-3 cells, we found that the upregulation of *LAMA3* and *FN1* expression persists after 3 days of RPM exposure in AD and MCS but turns to depletion in AD at day five (Hybel et al., 2020). In contrast, the *COL1A1* gene is up-regulated after 5 days of RPM-exposure (Hybel et al., 2020).

ACTB and *TUBB* are encoding the β-actin and β-tubulin class I proteins, respectively. Both factors are substantial proteins of the cytoskeleton. While the *ACTB* expression is upregulated in PC-3 cells after a 24-h RPM-exposure only in MCS, the *TUBB* expression is depleted after 24 h in RPM-AD samples. However, after 5 days under RPM-conditions, both genes are upregulated in AD as well as in MCS samples (Hybel et al., 2020).

AKT1 encodes one of the three AKT serine-threonine protein kinases and participates in mTOR signaling. Both, *AKT1* and *MTOR* are depleted in AD under 24 h in s-μ*g,* but upregulated after 5 days in s-μ*g* (AD & MCS) (Hybel et al., 2020).

In contrast, *FLT1* and *VEGFA,* encoding the angiogenesis proteins vascular endothelial growth factor receptor 1 and the vascular endothelial growth factor 1, are both upregulated after 24 h s-μ*g*. The up-regulation of *FLT1* takes place in MCS and the up-regulation of *VEGFA* in AD. After 5 days of μg exposure *FLT1* is upregulated in AD and MCS and *VEGFA* expression is depleted in MCS (Hybel et al., 2020).

In general, compared to a short-term s-μ*g*-experiment, substantial changes in AD and MCS expression of cytoskeletal genes, extracellular matrix and PAM signaling can still be detected after three and 5 days of RPM-exposure, respectively. This suggests that in the future extended time course experiments may be appropriate. Recent studies have highlighted the existence of an integrated signaling network connecting mechanosensitive pathways to circadian gene regulation in *e.g.* human keratinocytes (Ranieri et al., 2015). Whether this is also the case in PC-3 prostate cancer cells awaits further studies.

In summary, this study focused on the early effects of s-μ*g* on PC-3 cells. Short-term s-μ*g* influenced the growth behavior of PC-3 cells towards a 3D phenotype. No signs of apoptosis were detectable. Changes in the expression of genes belonging to the cytoskeleton, ECM, cytokines, VEGF, EGFR, and PAM signaling were measured. This was accompanied by alterations of the secretion of the cytokines and ECM components. We observed significant increases in *IL6* and *CXCL8* gene expression after 2, 4 and 24 h in MCS, which hints towards a more aggressive phenotype in short-term microgravity. After 24 h *TIMP1* was elevated in MCS and *MMP9* in AD cells (**Figures 4E,F**). In addition, the release of IL-6 in the supernatant was elevated at all time points in RPM samples. These results fit to earlier short-term studies (parabolic flight experiments) which have already shown that thyroid cancer cells exhibit a more aggressive phenotype when cultured under r-μ*g* (Ma et al., 2014). This is a finding which should be studied in more detail in the future.

PC-3 exposed to s-μ*g* created by an RPM grew in form of two phenotypes: an adherent monolayer and as 3D aggregates. The

PC-3 cells started to aggregate 24 h following subjection to s-μg conditions. Moreover, the 24 h RPM exposure of PC-3 cells resulted in an early activation of the VEGF pathway, EGFR1 and a downregulation of PAM signaling. Moreover, the secretion and gene expression of proinflammatory cytokines *IL1B*, *IL6* and *CXCL8* were markedly upregulated and closely involved in the first phases of spheroid formation of PC-3 cultivated under conditions of s-μg. This makes them interesting targets for a possible suppression of the development of metastases. In fact, HuMax-IL-8 (BMS-986253), a novel fully human monoclonal anti-IL-8 antibody has recently been introduced in different phase I trials testing its anti-cancer potential [NCT02536469, NCT03689699] (Bilusic et al., 2019). These trials, however, were done on patients with advanced, already metastasized stages of cancer. Our results suggest that IL-6 or IL-8 inhibition might already be beneficial in early stages of cancer by preventing or slowing down metastasis. Both factors will be targeted in future short- and long-term experiments. Liquid-overlay engineered PC-3 MCS revealed apoptotic cells after 24 h, which may influence the expression of cytokines, cytoskeletal genes and other factors. Taken these findings together, multicellular spheroids engineered by microgravity represent a novel model for studying the early phases of metastasis *in vitro*. The present findings may thus provide additional insights in selecting new targets to impair prostate cancer progression.

DATA AVAILABILITY STATEMENT

The raw data supporting the conclusion of this article will be made available by the authors, without undue reservation.

AUTHOR CONTRIBUTIONS

Conceptualization, DG and SKo; methodology, DD, JS, TEH, DM, SB, BB, and RV; software, HS, and SKo; validation, MW, HS, DG, and MK; formal analysis, DD; investigation, DD, DM, TEH, JS, RV, and SKa; resources, DG; data curation, DD, DM, HS, and MW; writing—original draft preparation, DD, DG; writing—review and editing, DG, TJC, MK, BB, and SKo; visualization, MK, SKa; supervision, DG, MI, SB, and TJC; project administration, DG; funding acquisition, DG and SB; All authors have read and agreed to the published version of the manuscript.

FUNDING

This research was funded by Deutsches Zentrum für Luft-und Raumfahrt (DLR), BMWi project 50WB 1924. The research was supported by BELSPO PRODEX (IMPULSE Grant 4000109861).

REFERENCES

Adachi, Y., Aoki, C., Yoshio-Hoshino, N., Takayama, K., Curiel, D. T., and Nishimoto, N. (2006). Interleukin-6 Induces Both Cell Growth and VEGF Production in Malignant Mesotheliomas. *Int. J. Cancer* 119, 1303–1311. doi:10.1002/ijc.22006

Adekoya, T. O., and Richardson, R. M. (2020). Cytokines and Chemokines as Mediators of Prostate Cancer Metastasis. *Ijms* 21, 4449. doi:10.3390/ijms21124449

Ancker, O., Wehland, M., Bauer, J., Infanger, M., and Grimm, D. (2017). The Adverse Effect of Hypertension in the Treatment of Thyroid Cancer with Multi-Kinase Inhibitors. *Ijms* 18, 625. doi:10.3390/ijms18030625

Azevedo, A., Cunha, V., Teixeira, A. L., and Medeiros, R. (2011). IL-6/IL-6R as a Potential Key Signaling Pathway in Prostate Cancer Development. *Wjco* 2, 384–396. doi:10.5306/wjco.v2.i12.384

Becker, J. L., and Souza, G. R. (2013). Using Space-Based Investigations to Inform Cancer Research on Earth. *Nat. Rev. Cancer* 13, 315–327. doi:10.1038/nrc3507

Benavides Damm, T., Walther, I., Wüest, S. L., Sekler, J., and Egli, M. (2014). Cell Cultivation under Different Gravitational Loads Using a Novel Random Positioning Incubator. *Biotechnol. Bioeng.* 111, 1180–1190. doi:10.1002/bit.25179

Bhat, F. A., Sharmila, G., Balakrishnan, S., Singh, P. R., Srinivasan, N., and Arunakaran, J. (2014). Epidermal Growth Factor-Induced Prostate Cancer (PC3) Cell Survival and Proliferation Is Inhibited by Quercetin, a Plant Flavonoid through Apoptotic Machinery. *Biomed. Prev. Nutr.* 4, 459–468. doi:10.1016/j.bionut.2014.07.003

Bilusic, M., Heery, C. R., Collins, J. M., Donahue, R. N., Palena, C., Madan, R. A., et al. (2019). Phase I Trial of HuMax-IL8 (BMS-986253), an anti-IL-8 Monoclonal Antibody, in Patients with Metastatic or Unresectable Solid Tumors. *J. Immunotherapy Cancer* 7, 240. doi:10.1186/s40425-019-0706-x

Birner, P., Schindl, M., Obermair, A., Breitenecker, G., and Oberhuber, G. (2001). Expression of Hypoxia-Inducible Factor 1alpha in Epithelial Ovarian Tumors: its Impact on Prognosis and on Response to Chemotherapy. *Clin. Cancer Res.* 7, 1661–1668.

Bonnans, C., Chou, J., and Werb, Z. (2014). Remodelling the Extracellular Matrix in Development and Disease. *Nat. Rev. Mol. Cell Biol.* 15, 786–801. doi:10.1038/nrm3904

B. Vendramini-Costa, D., and E. Carvalho, J. (2012). Molecular Link Mechanisms between Inflammation and Cancer. *Cpd* 18, 3831–3852. doi:10.2174/138161212802083707

Chen, Z.-Y., Guo, S., Li, B.-B., Jiang, N., Li, A., Yan, H.-F., et al. (2019). Effect of Weightlessness on the 3D Structure Formation and Physiologic Function of Human Cancer Cells. *Biomed. Res. Int.* 2019, 1–17. doi:10.1155/2019/4894083

Ciardiello, F., Troiani, T., Bianco, R., Orditura, M., Morgillo, F., Martinelli, E., et al. (2006). Interaction between the Epidermal Growth Factor Receptor (EGFR) and the Vascular Endothelial Growth Factor (VEGF) Pathways: a Rational Approach for Multi-Target Anticancer Therapy. *Ann. Oncol.* 17 (Suppl. 7), vii109–vii114. doi:10.1093/annonc/mdl962

Clejan, S., O'connor, K., and Rosensweig, N. (2001). Tri-dimensional Prostate Cell Cultures in Simulated Microgravity and Induced Changes in Lipid Second Messengers and Signal Transduction. *J. Cell. Mol. Med.* 5, 60–73. doi:10.1111/j.1582-4934.2001.tb00138.x

Corydon, T. J., Kopp, S., Wehland, M., Braun, M., Schütte, A., Mayer, T., et al. (2016a). Alterations of the Cytoskeleton in Human Cells in Space Proved by Life-Cell Imaging. *Sci. Rep.* 6, 20043. doi:10.1038/srep20043

Corydon, T. J., Mann, V., Slumstrup, L., Kopp, S., Sahana, J., Askou, A. L., et al. (2016b). Reduced Expression of Cytoskeletal and Extracellular Matrix Genes in Human Adult Retinal Pigment Epithelium Cells Exposed to Simulated Microgravity. *Cell Physiol Biochem* 40, 1–17. doi:10.1159/000452520

Cui, X., Hartanto, Y., and Zhang, H. (2017). Advances in Multicellular Spheroids Formation. *J. R. Soc. Interf.* 14, 20160877. doi:10.1098/rsif.2016.0877

Desiniotis, A., and Kyprianou, N. (2011). Significance of Talin in Cancer Progression and Metastasis. *Int. Rev. Cell Mol. Biol.* 289, 117–147. doi:10.1016/B978-0-12-386039-2.00004-3

Dittrich, A., Grimm, D., Sahana, J., Bauer, J., Krüger, M., Infanger, M., et al. (2018). Key Proteins Involved in Spheroid Formation and Angiogenesis in Endothelial Cells after Long-Term Exposure to Simulated Microgravity. *Cell Physiol Biochem* 45, 429–445. doi:10.1159/000486920

Dranoff, G. (2004). Cytokines in Cancer Pathogenesis and Cancer Therapy. *Nat. Rev. Cancer* 4, 11–22. doi:10.1038/nrc1252

Ebnerasuly, F., Hajebrahimi, Z., Tabaie, S. M., and Darbouy, M. (2018). Simulated Microgravity Condition Alters the Gene Expression of Some ECM and Adhesion Molecules in Adipose Derived Stem Cells. *Int. J. Mol. Cell Med* 7, 146–157. doi:10.22088/IJMCM.BUMS.7.3.146

Gandaglia, G., Abdollah, F., Schiffmann, J., Trudeau, V., Shariat, S. F., Kim, S. P., et al. (2014). Distribution of Metastatic Sites in Patients with Prostate Cancer: A Population-Based Analysis. *Prostate* 74, 210–216. doi:10.1002/pros.22742

Garbers, C., Kuck, F., Aparicio-Siegmund, S., Konzak, K., Kessenbrock, M., Sommerfeld, A., et al. (2013). Cellular Senescence or EGFR Signaling Induces Interleukin 6 (IL-6) Receptor Expression Controlled by Mammalian Target of Rapamycin (mTOR). *Cell Cycle* 12, 3421–3432. doi:10.4161/cc.26431

Gopinathan, G., Milagre, C., Pearce, O. M. T., Reynolds, L. E., Hodivala-Dilke, K., Leinster, D. A., et al. (2015). Interleukin-6 Stimulates Defective Angiogenesis. *Cancer Res.* 75, 3098–3107. doi:10.1158/0008-5472.CAN-15-1227

Grimm, D., Bauer, J., Kossmehl, P., Shakibaei, M., Schönberger, J., Pickenhahn, H., et al. (2002). Simulated Microgravity Alters Differentiation and Increases Apoptosis in Human Follicular Thyroid Carcinoma Cells. *FASEB j.* 16, 604–606. doi:10.1096/fj.01-0673fje

Grimm, D., Egli, M., Krüger, M., Riwaldt, S., Corydon, T. J., Kopp, S., et al. (2018). Tissue Engineering under Microgravity Conditions-Use of Stem Cells and Specialized Cells. *Stem Cell Development* 27, 787–804. doi:10.1089/scd.2017.0242

Grimm, D., Wehland, M., Corydon, T. J., Richter, P., Prasad, B., Bauer, J., et al. (2020). The Effects of Microgravity on Differentiation and Cell Growth in Stem Cells and Cancer Stem Cells. *Stem Cell Transl Med* 9, 882–894. doi:10.1002/sctm.20-0084

Grosse, J., Wehland, M., Pietsch, J., Schulz, H., Saar, K., Hübner, N., et al. (2012). Gravity-sensitive Signaling Drives 3-dimensional Formation of Multicellular Thyroid Cancer Spheroids. *FASEB j.* 26, 5124–5140. doi:10.1096/fj.12-215749

Häder, D.-P., Braun, M., Grimm, D., and Hemmersbach, R. (2017). Gravireceptors in Eukaryotes-A Comparison of Case Studies on the Cellular Level. *NPJ Microgravity* 3, 13. doi:10.1038/s41526-017-0018-8

Herbst, R. S. (2004). Review of Epidermal Growth Factor Receptor Biology. *Int. J. Radiat. Oncology*Biology*Physics* 59, S21–S26. doi:10.1016/j.ijrobp.2003.11.041

Huang, S.-P., Wu, M.-S., Shun, C.-T., Wang, H.-P., Lin, M.-T., Kuo, M.-L., et al. (2004). Interleukin-6 Increases Vascular Endothelial Growth Factor and Angiogenesis in Gastric Carcinoma. *J. Biomed. Sci.* 11, 517–527. doi:10.1007/BF02256101

Hybel, T. E., Dietrichs, D., Sahana, J., Corydon, T. J., Nassef, M. Z., Wehland, M., et al. (2020). Simulated Microgravity Influences VEGF, MAPK, and PAM Signaling in Prostate Cancer Cells. *Ijms* 21, 1263. doi:10.3390/ijms21041263

Infanger, M., Kossmehl, P., Shakibaei, M., Bauer, J., Kossmehl-Zorn, S., Cogoli, A., et al. (2006). Simulated Weightlessness Changes the Cytoskeleton and Extracellular Matrix Proteins in Papillary Thyroid Carcinoma Cells. *Cell Tissue Res* 324, 267–277. doi:10.1007/s00441-005-0142-8

Ingram, M., Techy, G. B., Saroufeem, R., Yazan, O., Narayan, K. S., Goodwin, T. J., et al. (1997). Three-dimensional Growth Patterns of Various Human Tumor Cell Lines in Simulated Microgravity of a NASA Bioreactor. In Vitro *Cell.Dev.Biol.-Animal* 33, 459–466. doi:10.1007/s11626-997-0064-8

Kopp, S., Slumstrup, L., Corydon, T. J., Sahana, J., Aleshcheva, G., Islam, T., et al. (2016). Identifications of Novel Mechanisms in Breast Cancer Cells Involving Duct-like Multicellular Spheroid Formation after Exposure to the Random Positioning Machine. *Sci. Rep.* 6, 26887. doi:10.1038/srep26887

Kopp, S., Warnke, E., Wehland, M., Aleshcheva, G., Magnusson, N. E., Hemmersbach, R., et al. (2015). Mechanisms of Three-Dimensional Growth of Thyroid Cells during Long-Term Simulated Microgravity. *Sci. Rep.* 5, 16691. doi:10.1038/srep16691

Kraus, A., Luetzenberg, R., Abuagela, N., Hollenberg, S., and Infanger, M. (2017). Spheroid Formation and Modulation of Tenocyte-specific Gene Expression under Simulated Microgravity. *Mltj* 7, 411–417. doi:10.11138/mltj/2017.7.3.411

Krieg, M., Haas, R., Brauch, H., Acker, T., Flamme, I., and Plate, K. H. (2000). Up-regulation of hypoxia-inducible factors HIF-1α and HIF-2α under normoxic conditions in renal carcinoma cells by von Hippel-Lindau tumor suppressor gene loss of function. *Oncogene* 19, 5435–5443. doi:10.1038/sj.onc.1203938

Krüger, M., Melnik, D., Kopp, S., Buken, C., Sahana, J., Bauer, J., et al. (2019). Fighting Thyroid Cancer with Microgravity Research. *Ijms* 20, 2553. doi:10.3390/ijms20102553

Kumari, N., Dwarakanath, B. S., Das, A., and Bhatt, A. N. (2016). Role of Interleukin-6 in Cancer Progression and Therapeutic Resistance. *Tumor Biol.* 37, 11553–11572. doi:10.1007/s13277-016-5098-7

Kumei, Y., Morita, S., Katano, H., Akiyama, H., Hirano, M., Oyha, K., et al. (2006). Microgravity Signal Ensnarls Cell Adhesion, Cytoskeleton, and Matrix Proteins of Rat Osteoblasts: Osteopontin, CD44, Osteonectin, and -Tubulin. *Ann. New York Acad. Sci.* 1090, 311–317. doi:10.1196/annals.1378.034

Lewis, M. L., Reynolds, J. L., Cubano, L. A., Hatton, J. P., Lawless, B. D., and Piepmeier, E. H. (1998). Spaceflight Alters Microtubules and Increases Apoptosis in Human Lymphocytes (Jurkat). *FASEB j.* 12, 1007–1018. doi:10.1096/fasebj.12.11.1007

Li, M., Wang, K., Pang, Y., Zhang, H., Peng, H., Shi, Q., et al. (2020). SPP1 and FN1 Associated with Progression and Prognosis of Esophageal Cancer Identified by Integrated Expression Profiles Analysis. *Med. Sci. Monit.* 26, e920355. doi:10.12659/MSM.920355

Lin, X., Zhang, K., Wei, D., Tian, Y., Gao, Y., Chen, Z., et al. (2020). The Impact of Spaceflight and Simulated Microgravity on Cell Adhesion. *Ijms* 21, 3031. doi:10.3390/ijms21093031

Ma, X., Pietsch, J., Wehland, M., Schulz, H., Saar, K., Hübner, N., et al. (2014). Differential Gene Expression Profile and Altered Cytokine Secretion of Thyroid Cancer Cells in Space. *FASEB j.* 28, 813–835. doi:10.1096/fj.13-243287

Mann, V., Grimm, D., Corydon, T., Krüger, M., Wehland, M., Riwaldt, S., et al. (2019). Changes in Human Foetal Osteoblasts Exposed to the Random Positioning Machine and Bone Construct Tissue Engineering. *Ijms* 20, 1357. doi:10.3390/ijms20061357

Margolis, L., Hatfill, S., Chuaqui, R., Vocke, C., Emmert-Buck, M., Linehan, W. M., et al. (1999). Long Term Organ Culture of Human Prostate Tissue in a NASA-Designed Rotating wall Bioreactor. *J. Urol.* 161, 290–297. doi:10.1016/s0022-5347(01)62134-7

Marrero, B., Messina, J. L., and Heller, R. (2009). Generation of a Tumor Spheroid in a Microgravity Environment as a 3D Model of Melanoma. In Vitro *Cell.Dev.Biol.-Animal* 45, 523–534. doi:10.1007/s11626-009-9217-2

Masiello, M. G., Cucina, A., Proietti, S., Palombo, A., Coluccia, P., D'Anselmi, F., et al. (2014). Phenotypic Switch Induced by Simulated Microgravity on MDA-MB-231 Breast Cancer Cells. *Biomed. Res. Int.* 2014, 1–12. doi:10.1155/2014/652434

Mehta, G., Hsiao, A. Y., Ingram, M., Luker, G. D., and Takayama, S. (2012). Opportunities and Challenges for Use of Tumor Spheroids as Models to Test Drug Delivery and Efficacy. *J. Controlled Release* 164, 192–204. doi:10.1016/j.jconrel.2012.04.045

Nagy, J. A., Dvorak, A. M., and Dvorak, H. F. (2007). VEGF-A and the Induction of Pathological Angiogenesis. *Annu. Rev. Pathol. Mech. Dis.* 2, 251–275. doi:10.1146/annurev.pathol.2.010506.134925

Nassef, M. Z., Kopp, S., Wehland, M., Melnik, D., Sahana, J., Krüger, M., et al. (2019). Real Microgravity Influences the Cytoskeleton and Focal Adhesions in Human Breast Cancer Cells. *Ijms* 20, 3156. doi:10.3390/ijms20133156

Nassef, M. Z., Melnik, D., Kopp, S., Sahana, J., Infanger, M., Lützenberg, R., et al. (2020). Breast Cancer Cells in Microgravity: New Aspects for Cancer Research. *Ijms* 21, 7345. doi:10.3390/ijms21197345

Pal, K., Madamsetty, V. S., Dutta, S. K., Wang, E., Angom, R. S., and Mukhopadhyay, D. (2019). Synchronous Inhibition of mTOR and VEGF/NRP1 axis Impedes Tumor Growth and Metastasis in Renal Cancer. *Npj Precis. Onc.* 3, 31. doi:10.1038/s41698-019-0105-2

Pang, X., Xie, R., Zhang, Z., Liu, Q., Wu, S., and Cui, Y. (2019). Identification of SPP1 as an Extracellular Matrix Signature for Metastatic Castration-Resistant Prostate Cancer. *Front. Oncol.* 9, 924. doi:10.3389/fonc.2019.00924

Park, S., Kim, Y. S., Kim, D. Y., So, I., and Jeon, J.-H. (2018). PI3K Pathway in Prostate Cancer: All Resistant Roads lead to PI3K. *Biochim. Biophys. Acta (Bba) - Rev. Cancer* 1870, 198–206. doi:10.1016/j.bbcan.2018.09.001

Pietsch, J., Kussian, R., Sickmann, A., Bauer, J., Weber, G., Nissum, M., et al. (2010). Application of Free-Flow IEF to Identify Protein Candidates Changing under Microgravity Conditions. *Proteomics* 10, 904–913. doi:10.1002/pmic.200900226

Pietsch, J., Ma, X., Wehland, M., Aleshcheva, G., Schwarzwälder, A., Segerer, J., et al. (2013). Spheroid Formation of Human Thyroid Cancer Cells in an Automated Culturing System during the Shenzhou-8 Space mission. *Biomaterials* 34, 7694–7705. doi:10.1016/j.biomaterials.2013.06.054

Pietsch, J., Sickmann, A., Weber, G., Bauer, J., Egli, M., Wildgruber, R., et al. (2011). A Proteomic Approach to Analysing Spheroid Formation of Two Human Thyroid Cell Lines Cultured on a Random Positioning Machine. *Proteomics* 11, 2095–2104. doi:10.1002/pmic.201000817

Pietsch, J., Sickmann, A., Weber, G., Bauer, J., Egli, M., Wildgruber, R., et al. (2012). Metabolic Enzyme Diversity in Different Human Thyroid Cell Lines and Their Sensitivity to Gravitational Forces. *Proteomics* 12, 2539–2546. doi:10.1002/pmic.201200070

Powis, G., and Kirkpatrick, L. (2004). Hypoxia Inducible Factor-1alpha as a Cancer Drug Target. *Mol. Cancer Ther.* 3, 647–654.

Randrup Hansen, C., Grimm, D., Bauer, J., Wehland, M., and Magnusson, N. (2017). Effects and Side Effects of Using Sorafenib and Sunitinib in the Treatment of Metastatic Renal Cell Carcinoma. *Ijms* 18, 461. doi:10.3390/ijms18020461

Ranieri, D., Cucina, A., Bizzarri, M., Alimandi, M., and Torrisi, M. R. (2015). Microgravity Influences Circadian Clock Oscillation in Human Keratinocytes. *FEBS Open Bio* 5, 717–723. doi:10.1016/j.fob.2015.08.012

Riwaldt, S., Bauer, J., Wehland, M., Slumstrup, L., Kopp, S., Warnke, E., et al. (2016). Pathways Regulating Spheroid Formation of Human Follicular Thyroid Cancer Cells under Simulated Microgravity Conditions: A Genetic Approach. *Ijms* 17, 528. doi:10.3390/ijms17040528

Sarkar, C., Goswami, S., Basu, S., and Chakroborty, D. (2020). Angiogenesis Inhibition in Prostate Cancer: An Update. *Cancers* 12, 2382. doi:10.3390/cancers12092382

Saryeddine, L., Zibara, K., Kassem, N., Badran, B., and El-Zein, N. (2016). EGF-induced VEGF Exerts a PI3K-dependent Positive Feedback on ERK and AKT through VEGFR2 in Hematological *In Vitro* Models. *PLoS One* 11, e0165876. doi:10.1371/journal.pone.0165876

Semenza, G. L. (2003). Targeting HIF-1 for Cancer Therapy. *Nat. Rev. Cancer* 3, 721–732. doi:10.1038/nrc1187

Shijubo, N., Uede, T., Kon, S., Nagata, M., and Abe, S. (2000). Vascular Endothelial Growth Factor and Osteopontin in Tumor Biology. *Crit. Rev. Oncog* 11, 135–146.

Shorning, B. Y., Dass, M. S., Smalley, M. J., and Pearson, H. B. (2020). The PI3K-AKT-mTOR Pathway and Prostate Cancer: At the Crossroads of AR, MAPK, and WNT Signaling. *Ijms* 21, 4507. doi:10.3390/ijms21124507

Singh, R. K., and Lokeshwar, B. L. (2009). Depletion of Intrinsic Expression of Interleukin-8 in Prostate Cancer Cells Causes Cell Cycle Arrest, Spontaneous Apoptosis and Increases the Efficacy of Chemotherapeutic Drugs. *Mol. Cancer* 8, 57. doi:10.1186/1476-4598-8-57

Strube, F., Infanger, M., Wehland, M., Delvinioti, X., Romswinkel, A., Dietz, C., et al. (2020). Alteration of Cytoskeleton Morphology and Gene Expression in Human Breast Cancer Cells under Simulated Microgravity. *Cell J* 22, 106–114. doi:10.22074/cellj.2020.6537

Sun, Y., Zhao, C., Ye, Y., Wang, Z., He, Y., Li, Y., et al. (2020). High Expression of Fibronectin 1 Indicates Poor Prognosis in Gastric Cancer. *Oncol. Lett.* 19, 93–102. doi:10.3892/ol.2019.11088

Sung, H., Ferlay, J., Soerjomataram, I., Siegel, R. L., Laversanne, M., Soerjomataram, I., Jemal, A., et al. (2021). Global Cancer Statistics 2018: GLOBOCAN Estimates of Incidence and Mortality Worldwide for 36 Cancers in 185 Countries. *CA: A Cancer J. Clinicians* 71, 209–249. doi:10.3322/caac.21660

Svejgaard, B., Wehland, M., Ma, X., Kopp, S., Sahana, J., Warnke, E., et al. (2015). Common Effects on Cancer Cells Exerted by a Random Positioning Machine and a 2D Clinostat. *PLoS One* 10, e0135157. doi:10.1371/journal.pone.0135157

Tee, S. S., Suster, I., Truong, S., Jeong, S., Eskandari, R., Digialleonardo, V., et al. (2018). Targeted AKT Inhibition in Prostate Cancer Cells and Spheroids Reduces Aerobic Glycolysis and Generation of Hyperpolarized [1-13C] Lactate. *Mol. Cancer Res.* 16, 453–460. doi:10.1158/1541-7786.MCR-17-0458

Timmins, N., Dietmair, S., and Nielsen, L. (2004). Hanging-drop Multicellular Spheroids as a Model of Tumour Angiogenesis. *Angiogenesis* 7, 97–103. doi:10.1007/s10456-004-8911-7

Twombly, R. (2003). Prostate Modeling experiment success Becomes Part of Legacy of Shuttle Astronauts. *JNCI J. Natl. Cancer Inst.* 95, 505–507. doi:10.1093/jnci/95.7.505

Vorselen, D., Roos, W. H., Mackintosh, F. C., Wuite, G. J. L., and Loon, J. J. W. A. (2014). The Role of the Cytoskeleton in Sensing Changes in Gravity by Nonspecialized Cells. *FASEB j.* 28, 536–547. doi:10.1096/fj.13-236356

Wang, Y., Huang, L., Wu, S., Jia, Y., Yang, Y., Luo, L., et al. (2015). Bioinformatics Analyses of the Role of Vascular Endothelial Growth Factor in Patients with Non-small Cell Lung Cancer. *PLoS One* 10, e0139285. doi:10.1371/journal.pone.0139285

Waugh, D. J. J., and Wilson, C. (2008). The Interleukin-8 Pathway in Cancer. *Clin. Cancer Res.* 14, 6735–6741. doi:10.1158/1078-0432.CCR-07-4843

Wehland, M., Bauer, J., Infanger, M., and Grimm, D. (2012). Target-based Anti-angiogenic Therapy in Breast Cancer. *Curr. Pharm. Des.* 18, 4244–4257. doi:10.2174/138161212802430468

Wehland, M., Steinwerth, P., Aleshcheva, G., Sahana, J., Hemmersbach, R., Lützenberg, R., et al. (2020). Tissue Engineering of Cartilage Using a Random Positioning Machine. *Ijms* 21, 9596. doi:10.3390/ijms21249596

Yang, J., Nie, J., Ma, X., Wei, Y., Peng, Y., and Wei, X. (2019). Targeting PI3K in Cancer: Mechanisms and Advances in Clinical Trials. *Mol. Cancer* 18, 26. doi:10.1186/s12943-019-0954-x

Zhau, H. E., Goodwin, T. J., Chang, S.-M., Baker, T. L., and Chung, L. W. K. (1997). Establishment of a Three-Dimensional Human Prostate Organoid Coculture under Microgravity-Simulated Conditions: Evaluation of Androgen-Induced Growth and PSA Expression. In Vitro *Cell.Dev.Biol.-Animal* 33, 375–380. doi:10.1007/s11626-997-0008-3

Zhivodernikov, I. V., Ratushnyy, A. Y., Matveeva, D. K., and Buravkova, L. B. (2020). Extracellular Matrix Proteins and Transcription of Matrix-Associated Genes in Mesenchymal Stromal Cells during Modeling of the Effects of Microgravity. *Bull. Exp. Biol. Med.* 170, 230–232. doi:10.1007/s10517-020-05040-z

Zhong, H., De Marzo, A. M., Laughner, E., Lim, M., Hilton, D. A., Zagzag, D., et al. (1999). Overexpression of Hypoxia-Inducible Factor 1alpha in Common Human Cancers and Their Metastases. *Cancer Res.* 59, 5830–5835.

Conflict of Interest: The authors declare that the research was conducted in the absence of any commercial or financial relationships that could be construed as a potential conflict of interest.

Publisher's Note: All claims expressed in this article are solely those of the authors and do not necessarily represent those of their affiliated organizations, or those of the publisher, the editors and the reviewers. Any product that may be evaluated in this article, or claim that may be made by its manufacturer, is not guaranteed or endorsed by the publisher.

GLOSSARY

μg Microgravity
2D Two-dimensional
3D Three-dimensional
ACTB Beta-actin
AD Adherent Monolayer
AKT1 RAC-alpha Serine/Threonine-protein kinase 1
CASP3 Caspase-3
CASP8 Caspase-8
CASP9 Caspase-9
COL1A1 Collagen-1a1
CXCL8/IL-8 Interleukin-8
ECM Extracellular matrix
EGF Epidermal Growth Factor
EGFR1 Epidermal Growth Factor Receptor 1
EZR Ezrin
FLT1 Tyrosine kinase 1
FN1 Fibronectin
HARV High aspect rotating-wall vessel
HIF1A Hypoxia inducible factor 1A
IL-17 Interleukin-17
IL-1A Interleukin-1 Alpha
IL1B Interleukin-1 Beta
IL-2 Interleukin-2
IL-6 Interleukin-6
IL-7 Interleukin-7
KDR Kinase Insert Domain Receptor
KRT8 Kreatin 8
LAMA3 Laminin Subunit Alpha 3
LNCaP Lymph Node Carcinoma of the Prostate
MCP-1 Monocyte Chemoattractant Protein 1
MCS Multicellular Spheroid(s)
MMP11 Matrix Metalloproteinase-11
MMP2 Matrix Metallopeptidase-2
MMP9 Matrix Metalloproteinase-9
MSN Moesin
MTOR Mechanistic Target of Rapamycin kinase
NFKB Nuclear Factor kappa B
NRP1 Neuroplin-1
OPN/SPPI Osteopontin/Secreted Phosphoprotein 1
PAI-1 Plasminogen Activator Inhibitor-1
PCC Prostate Cancer Cells
PCNA Proliferating Cell Nuclear Antigen
PFA Paraformaldehyde
PIK3CB Phosphatidylinositol-4,5-bisphosphate 3-kinase Catalytic Subunit Beta
r-μg Real Microgravity
RDX Radixin
RPM Random Positioning Machine
RWV Rotating Wall Vessel
s-μg Simulated Microgravity
TGFB1 Transforming Growth Factor Beta 1
TIMP1 Tissue Inhibitor of Metalloproteinases/metallopeptidase Inhibitor 1
TIMP3 TIMP metallopeptidase Inhibitor 3
TNF-a Tumor Necrosis Factor Alpha
TUBB Tubulin Beta
VEGFA Vascular Endothelial Growth Factor A

13.3. Publikation 3

Schulz H[†], **Dietrichs D**[†], Wehland M, Corydon TJ, Hemmersbach R, Liemersdorf C, Melnik D, Hübner N, Saar K, Infanger M, Grimm D. In Prostate Cancer Cells Cytokines Are Early Responders to Gravitational Changes Occurring in Parabolic Flights. Int J Mol Sci. 23. 7876 (2022)

[†]These authors contributed equally to this work.

International Journal of
Molecular Sciences

MDPI

Article

In Prostate Cancer Cells Cytokines Are Early Responders to Gravitational Changes Occurring in Parabolic Flights

Herbert Schulz [1,2,3,†], Dorothea Dietrichs [1,2,†], Markus Wehland [1,2,3], Thomas J. Corydon [4,5], Ruth Hemmersbach [6], Christian Liemersdorf [6], Daniela Melnik [1,2,3], Norbert Hübner [7,8,9], Kathrin Saar [7], Manfred Infanger [1,2,3] and Daniela Grimm [1,2,3,4,*]

1 Department of Microgravity and Translational Regenerative Medicine, Medical Faculty, University Hospital Magdeburg, Otto von Guericke University, Universitätsplatz 2, 39106 Magdeburg, Germany; herbert.schulz@med.ovgu.de (H.S.); dorothea.dietrichs@st.ovgu.de (D.D.); markus.wehland@med.ovgu.de (M.W.); daniela.melnik@med.ovgu.de (D.M.); manfred.infanger@med.ovgu.de (M.I.)
2 Clinic for Plastic, Aesthetic and Hand Surgery, Medical Faculty, University Hospital Magdeburg, Otto von Guericke University, Leipziger Straße 44, 39120 Magdeburg, Germany
3 Research Group 'Magdeburger Arbeitsgemeinschaft für Forschung unter Raumfahrt- und Schwerelosigkeitsbedingungen' (MARS), Otto von Guericke University, Universitätsplatz 2, 39106 Magdeburg, Germany
4 Department of Biomedicine, The Faculty of Health, Aarhus University, Ole Worms Allé 4, 8000 Aarhus, Denmark; corydon@biomed.au.dk
5 Department of Ophthalmology, Aarhus University Hospital, Palle Juul-Jensens Blvd. 99, 8200 Aarhus, Denmark
6 Gravitational Biology, Institute of Aerospace Medicine, German Aerospace Center, Linder Höhe, 51147 Cologne, Germany; ruth.hemmersbach@dlr.de (R.H.); christian.liemersdorf@dlr.de (C.L.)
7 Cardiovascular and Metabolic Sciences, Max Delbrück Center for Molecular Medicine in the Helmholtz Association (MDC), 13125 Berlin, Germany; nhuebner@mdc-berlin.de (N.H.); ksaar@mdc-berlin.de (K.S.)
8 DZHK (German Centre for Cardiovascular Research), Partner Site Berlin, 10785 Berlin, Germany
9 Charité-Universitätsmedizin, 10117 Berlin, Germany
* Correspondence: daniela.grimm@med.ovgu.de
† These authors contributed equally to this work.

Abstract: The high mortality in men with metastatic prostate cancer (PC) establishes the need for diagnostic optimization by new biomarkers. Mindful of the effect of real microgravity on metabolic pathways of carcinogenesis, we attended a parabolic flight (PF) mission to perform an experiment with the PC cell line PC-3, and submitted the resulting RNA to next generation sequencing (NGS) and quantitative real-time PCR (qPCR). After the first parabola, alterations of the F-actin cytoskeleton-like stress fibers and pseudopodia are visible. Moreover, numerous significant transcriptional changes are evident. We were able to identify a network of relevant PC cytokines and chemokines showing differential expression due to gravitational changes, particularly during the early flight phases. Together with differentially expressed regulatory lncRNAs and micro RNAs, we present a portfolio of 298 potential biomarkers. Via qPCR we identified *IL6* and *PIK3CB* to be sensitive to vibration effects and hypergravity, respectively. Per NGS we detected five upregulated cytokines (*CCL2*, *CXCL1*, *IL6*, *CXCL2*, *CCL20*), one zink finger protein (*TNFAIP3*) and one glycoprotein (*ICAM1*) related to c-REL signaling and thus relevant for carcinogenesis as well as inflammatory aspects. We found regulated *miR-221* and the co-localized lncRNA *MIR222HG* induced by PF maneuvers. *miR-221* is related to the PC-3 growth rate and *MIR222HG* is a known risk factor for glioma susceptibility. These findings in real microgravity may further improve our understanding of PC and contribute to the development of new diagnostic tools.

Keywords: parabolic flight; microgravity; hypergravity; prostate cancer; PC-3; RNA sequencing; qPCR; cytokines; non-coding

Citation: Schulz, H.; Dietrichs, D.; Wehland, M.; Corydon, T.J.; Hemmersbach, R.; Liemersdorf, C.; Melnik, D.; Hübner, N.; Saar, K.; Infanger, M.; et al. In Prostate Cancer Cells Cytokines Are Early Responders to Gravitational Changes Occurring in Parabolic Flights. *Int. J. Mol. Sci.* **2022**, *23*, 7876. https://doi.org/10.3390/ijms23147876

Academic Editor: Jean-Pol Frippiat

Received: 24 June 2022
Accepted: 15 July 2022
Published: 17 July 2022

1. Introduction

Prostate cancer (PC) is the second leading cause of cancer death in the US male population after lung cancer. The American Cancer Society predicts 268,490 new cases of PC in the US in 2022, which is about 0.165% of the male population. The disease, which primarily occurs at an older age, has a predictable treatment prognosis. However, the 5-year survival prognosis is drastically reduced from 100% to 31% when metastases ensue (The American Cancer Society). Accordingly, early management of PC is a challenging matter in medicine. In the context of personalized medicine, transcriptional studies of factors influencing prostate carcinogenesis and progression may add new early-onset biomarkers to the diagnostic portfolio.

In general, cancer cells are characterized by uncontrolled proliferation, elevated survival and activated invasion potential. The genetic and epigenetic alterations lead to an impairment of the cell death mechanisms that are initiated upon sustained damage to the cell. As we know from previous studies, gravitational changes have a lasting effect on tumorigenesis [1,2] including cytoskeletal and focal adhesion changes and alterations in differentiation and proliferation [3–8], increased apoptosis [5,9,10], the release of cytokines [11], altered interleukin, OPN, TLN1, and CTGF signaling [9], and influenced PI3K/AKT/mTOR (PAM) signaling [7,8], to only name the most significant ones. Furthermore, a previous study by Corydon and coworkers also showed that gravitational changes have specific effects on the F-actin-cytoskeleton in non-carcinogenic epithelium cell lines [12].

In previous studies, DU-145 and PC-3 prostate carcinoma cell lines were exposed to simulated microgravity (s-μ*g*) for several days using a high aspect rotating-wall vessel (HARV) or random positioning machine (RPM), respectively [13–16]. DU-145 prostate cancer cultures revealed a slowed growth, an increase in cytokeratin 8 and 18, together with an increase in cell–cell and cell–matrix interactions, and ultimately an organotypic 3D spheroid organization after a few hours under HARF influence compared to the static 1*g* control [13,14]. Furthermore, significant changes in VEGF signaling were detected in aggressive PC-3 prostate carcinoma cells, resulting in early (4 h s-μ*g*) and late (3 days to 5 days s-μ*g*) downregulation of *VEGFA* expression [15,16], indicating attenuation of PC-3 aggressiveness [15]. In contrast, a significant increase in *IL6* and *CXCL8* gene expression in the first 24 h of s-μ*g* hints towards a more aggressive phenotype of PC-3 [16]. Moreover, substantial components of PAM signaling were deregulated after a 5-day RPM exposure and *AKT1* was upregulated in multi-cellular spheroids, but even more in adherent cells [15]. Consequently, AKT kinase inhibitors are already being assessed in phase 3 clinical trials and seem to be particularly effective in castration-resistant metastatic prostate cancer [17,18], which supports the idea that μ*g*-based research is relevant for increasing the current knowledge about cancer progression and metastases on Earth.

In summary, it was found in previous studies that crucial key positions of carcinogenesis are influenced by microgravity and various *g* sensitive key players tend to promote a milder progression. Since the s-μ*g* influence on already known major actors of prostate carcinogenesis have been investigated, the idea of our current study was to identify transcriptome-wide early responders to gravitational changes in PC-3 using a parabolic flight scenario. Parabolic flights are a cost-effective and proven approach to briefly expose cell lines to gravitational changes. During a parabolic flight (PF), which typically consists of 31 parabolas, samples experience repeating phases of free fall and hypergravity [19]. In a PF, each parabola consists of short periods (22 s) of ~0.01*g* (microgravity), encased by 1.8*g* (hypergravity) phases. These alterations allow tracking of dynamic transcriptional responses of known biomarkers of prostate cancer development and identification of, for the first time in prostate carcinoma cells, novel μ*g* related biomarkers by transcription-wide RNA sequencing. To distinguish microgravity from other influences occurring during parabolic flight, the expression of key genes of the extracellular matrix, focal adhesion, PAM signal transduction, cell growth and apoptosis were additionally studied under hypergravity conditions (1.8*g*) and vibrations as they occur during a typical parabolic flight.

Focusing on early responders reduces the accumulation of secondary expression changes. Finally, both transcriptional primary effects and secondary effects are relevant to research. In a biomedical context, early responses to the gravitational stimulus are closer to the cause, i.e., genetic epigenetic constitution, and subsequent secondary effects are closer to physiological, morphological changes, e.g., progression of cancer. In particular, the study of the first parabola opens the possibility to observe the primary transcriptional response to gravitational changes before the point of divergence of related signaling pathways, mostly unaffected by later secondary regulatory responses, to unravel the origin of gravitational metabolic networks. In conclusion, the knowledge of the primary transcriptional responses to gravitational changes is essential for assessing subsequent synergistic and competitive effects of prostate carcinogenesis under μ*g*.

2. Results

2.1. Gravitational Changes of the F-Actin Cytoskeleton

When comparing the F-actin staining under 1*g*, first parabola (1P) and 31st parabola (31P) conditions, it is noticeable that stress fibers appear already after the first parabola, but formation of pseudopodia can be observed only sporadically (Figure S1A,B). Nevertheless, the observed effects after 1P are more pronounced than in our previous PF experiment with human chondrocytes [20]. After 31 parabolas the stress fibers are more frequent and more pronounced; the most striking change though is an increase of pseudopoidia and lamellipodia (Figure S1C).

2.2. qPCR Results

To isolate μ*g*-related expression changes, the main intention of the qPCR analysis was to compare RNA expression changes in PF with those under hypergravity (1.8*g*) and vibration. Additionally, corresponding results of the RNAseq experiment (control vs. 1P and control vs. 31P) were added to check the validity of the qPCR results. Non-concordant results between qPCR and RNAseq are significantly enriched in genes with weak regulation (<2-fold) [21]. In contrast to Section 2.3, the candidate gene approach in this section also considers the differential expression with less than two-fold difference. Accordingly, a cross-validation of qPCR results with RNAseq results seemed appropriate. First, it should be noted that under hypergravity (*PIK3CB*) and vibration (*IL6*) exposure, only 1 of the 32 investigated genes was differentially expressed (Figure 1).

2.2.1. Cytokines

The qPCR study served to assess the influence of PF and its sub-aspects, vibration and hypergravity, on key players of carcinogenesis. Strikingly, the cytokines *IL6* and *CXCL8* were markedly upregulated as measured after the 1P and 31P (RNAseq and qPCR, Figure 1). However, the more moderate but significant upregulation of *IL6* in the vibration experiment indicates that IL6 regulation is at least in part due to aircraft vibration.

2.2.2. Cytoskeleton

Of the six cytoskeletal genes tested via qPCR, only radixin (*RDX*) and tubulin, beta class I (*TUBB*), are differentially expressed between the 1*g* control and 1P. *TUBB* is additionally differentially expressed between control and 31P. However, *TUBB* qPCR results cannot be confirmed by RNAseq results, but *TUBB* is in RNAseq nominally significant between 1P and 31P (p = 0.009). TUBB is a structural component of microtubules and forms a dimer with alpha tubulin in this function. In RNAseq, two components of alpha tubulin *TUBA4A* and *TUBA1B* are significant differentially expressed after multiple testing corrections in comparison between 1P and 31P (P_{adj} = 0.004 and 0.023 respectively). RDX probably possesses a role in coupling actin to the plasma membrane. Actin itself is not differentially expressed in the RNAseq experiment.

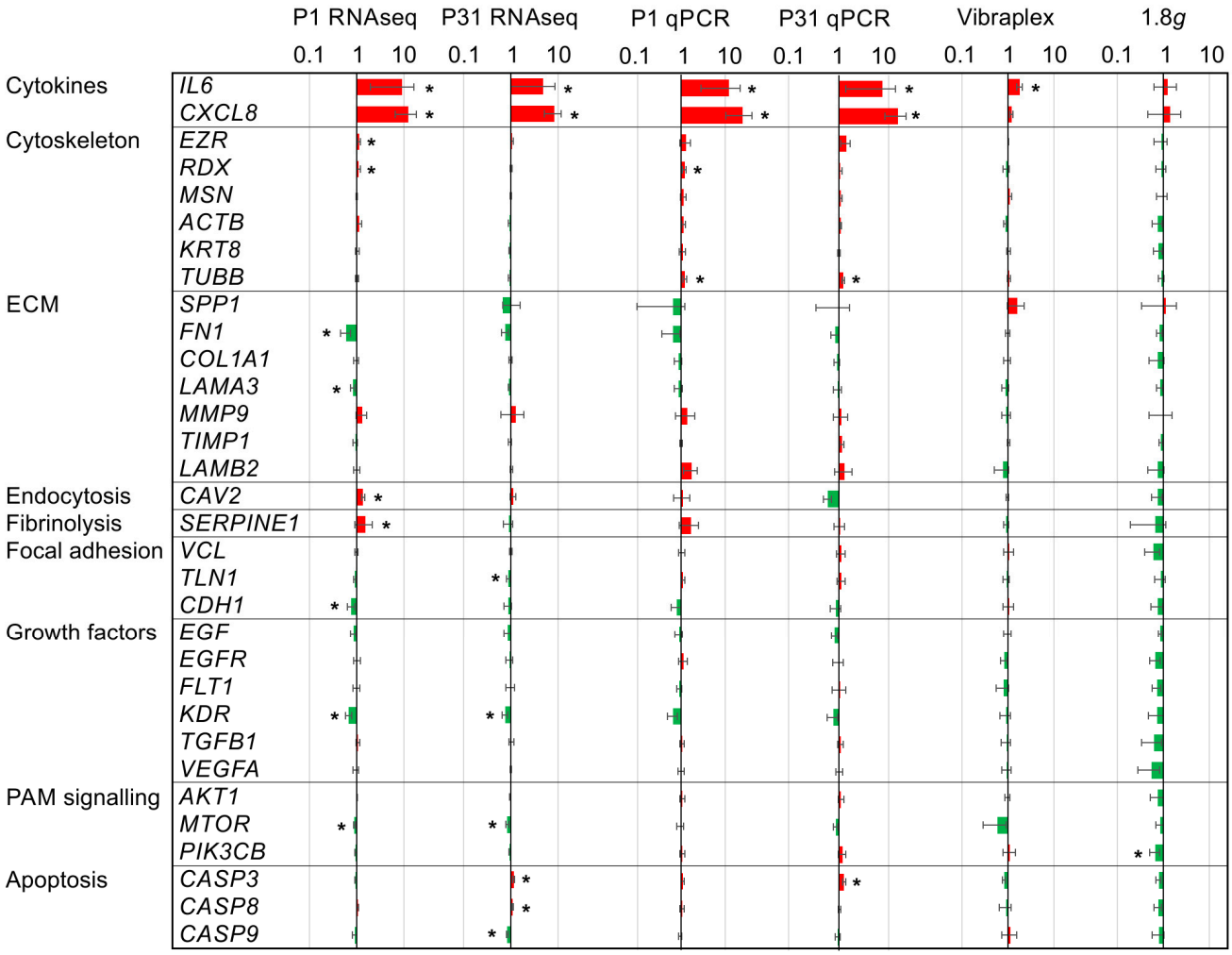

Figure 1. Gene expression ratios of 32 key players of carcinogenesis in PC-3 prostate cancer cells under altered gravitational conditions measured by qPCR and RNAseq: Results determined after P1, after P31, after vibration-exposure and after hypergravity (1.8*g*)-exposure in relation to the respective 1*g* control samples. The red color indicates upregulated genes and the green color downregulated genes. Significant changes (nominal $p < 0.05$) are indicated by asterisks. The ratios are given on a logarithmic scale.

2.2.3. PI3K/AKT/mTOR (PAM) Signaling

The phosphoinositide-3-kinase, catalytic, beta polypeptide (*PIK3CB*) is a catalytic subunit of phosphoinositide 3-kinase (*PI3K*). *PIK3CB* is not regulated in PF, but four genes encoding catalytic subunits of PI3K are deregulated between 1*g* and 1P (PIK3CA, $P_{adj} = 2.8 \times 10^{-5}$; *PIK3R3*, $P_{adj} = 2.8 \times 10^{-5}$; *PIK3R1*, $P_{adj} = 1.9 \times 10^{-4}$; *PIK3C2A* $P_{adj} = 2.8 \times 10^{-3}$). It should be noted that the phosphoinositide 3-kinase expression is modulated by hypergravity (at least in one subunit) whereas the gene expression of other subunits is susceptible to gravitational changes in PF.

2.2.4. Apoptosis

The qPCR assessment measuring significant *CASP3* upregulation after 31P is confirmed by RNAseq and complemented by a significant upregulation of *CASP8* and significant downregulation of *CASP9* in the RNAseq analysis. Regulations of the CASP genes are moderate and do not reach a two-fold upregulation or downregulation, respectively. Additionally, two upstream key genes of the apoptosis cascade, namely the gene coding

the Tumor Necrosis Factor Receptor Type 1 (*TRADD*, $P_{adj} > 0.7$) and the gene coding the Fas Associated Via Death Domain (*FADD*, $P_{adj} > 0.1$), are not regulated by PF in PC-3 cells.

2.2.5. RNAseq to qPCR Comparison

As expected, additional genes could be detected in the RNAseq experiment as being regulated in PF due to the increased sensitivity (Figure 1). However, more importantly, apart from TUBB, all other qPCR PF findings could be confirmed. Apart from the cytokines *IL6* and *CXCL8*, none of the remaining 30 qPCR-tested genes achieved an adjusted significant two-fold change in the RNAseq control to 1P comparison or in the RNAseq control to 31P comparison. The genes *RDX*, *SERPINE1*, *CDH1* and *MTOR* are only nominally significant in the control to 1P comparison, as is *KDR* in the control to 31P comparison.

2.3. RNAseq Analysis

2.3.1. QC

Demultiplexed FASTQ files are used to process the 10 PF and 5 control samples individually in the secondary analysis using STAR. Fortunately, all samples exceeded a mean quality score of 35; the ratio of Q30 bases was, with one exception, >93% and the ratio of perfect barcodes >98% (Table S1). No significant difference between controls and PF samples for any of the parameters was observed.

2.3.2. General Expression Profile Reveals a Potential Habituation Effect

The general expression profile was determined using principal component analysis on the read counts. We found a high proportion of variance in the first two principal components (PCs, 65% of the variance in PC #1 and 18% of the variance in PC #2, Figure 2). This is due to the low sample number (n = 15) and to a strong effect of microgravity on the PC-3 cells. This strong effect is understandable if one considers the changes of the F-actin cytoskeleton during the PF as shown in Figure S1. The three conditions are incompletely separated in PC #1 with a tending intermediate position of the measurements after 31P. This suggests a habituation effect of the PC-3 cells to the alternating gravitational conditions during the flight.

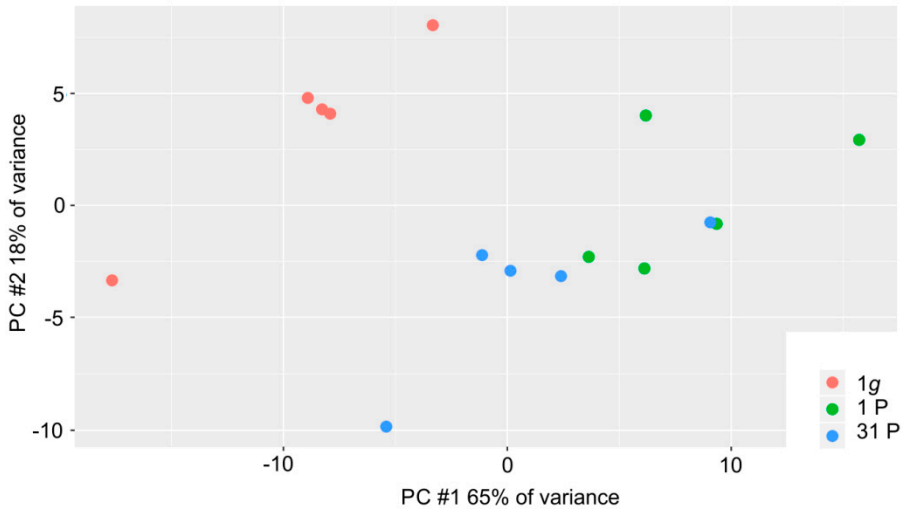

Figure 2. Distribution of the 15 PC-3 samples in the first two principal components; 1*g* control samples, 1P and 31P inflight samples are color-coded in red, green and blue, respectively.

2.3.3. Differential Expression Analyses Reveal Expression Difference in Cytokines and Genes of the NFκB System Induced by Gravitational Changes

By comparing the number of genes significantly expressed until the end of 1P with the number of genes significantly expressed after 31P, the data, in terms of both stringency and fold change, reveal that the strongest changes occur in the early flight phase. DESeq2

results for the set of 298 differentially expressed genes and their dotplot visualization can be downloaded (Table S2, Figure S2). The total sum of 298 two-fold differentially expressed genes (DEGs) at P_{adj} less than 0.05 is divided (with overlaps) into 208 DEGs between 1*g* and post 1P, 129 DEGs between 1*g* and post 31P, 47 DEGs between post 1P and post 31P. In addition to the chemokine encoding *CXCL2*, a significant > two-fold upregulation after P1 is followed by a significant > two-fold downregulation after P31 for another eight genes (*ATOH8*, *AC107308.1*, *AC018628.2*, *KRTAP1-5*, *MIR221*, *CCN2*, *ZEB2*, *AC008264.2*). Even though the applied RNAseq method enriches coding genes by a poly-A selection step, we found that the DEG set contains a considerable number of long non-coding RNAs (23.9% lncRNAs) and micro RNAs (2.46% miRNAs) in addition to 65.5% coding genes (Figure 3A).

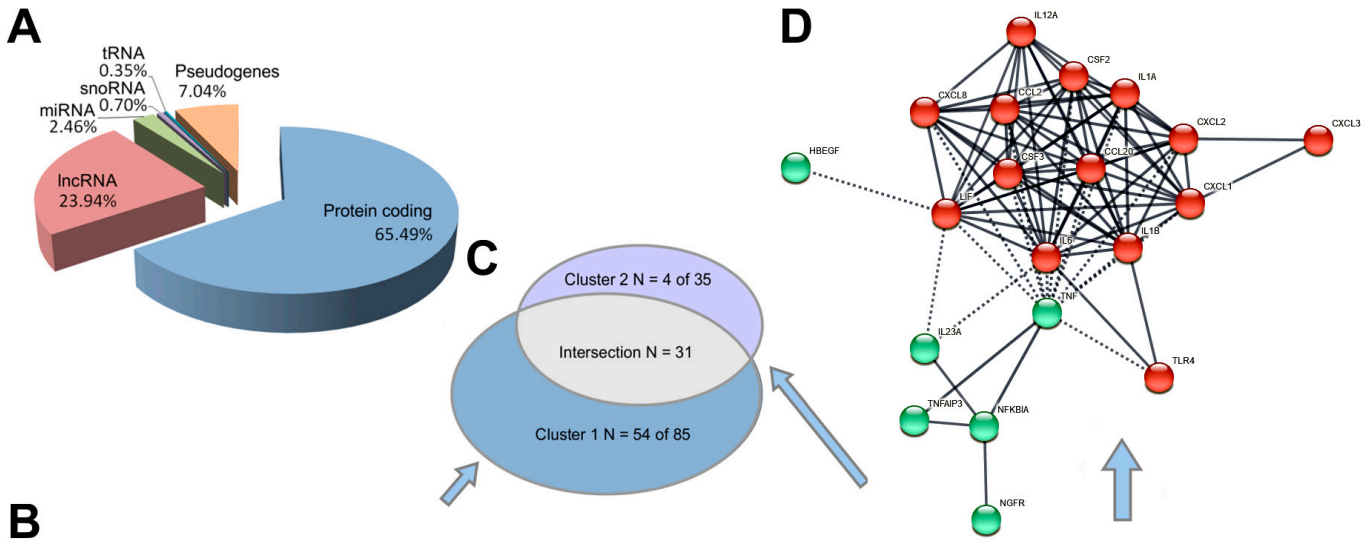

B

Annotation Cluster 1 (Content: Inflamation; DAVID Enrichment Score: 6.12, 85 genes)

Category	Term	Count	%	FDR
GOTERM_BP_DIRECT	GO:0006954~inflammatory response	29	13.00	3.88E-14
UP_KEYWORDS	Cytokine	18	8.07	5.06E-10
GOTERM_BP_DIRECT	GO:0006955~immune response	23	10.31	6.73E-08
KEGG_PATHWAY	hsa05323:Rheumatoid arthritis	14	6.28	1.01E-08
KEGG_PATHWAY	hsa04060:Cytokine-cytokine receptor interaction	20	8.97	3.92E-08
UP_KEYWORDS	Inflammatory response	14	6.28	1.85E-07
GOTERM_CC_DIRECT	GO:0005576~extracellular region	36	16.14	4.71E-04
GOTERM_CC_DIRECT	GO:0005615~extracellular space	31	13.90	8.54E-04
KEGG_PATHWAY	hsa05132:Salmonella infection	9	4.04	2.93E-04
UP_KEYWORDS	Secreted	35	15.70	0.01099
UP_SEQ_FEATURE	disulfide bond	45	20.18	0.36482
UP_SEQ_FEATURE	signal peptide	48	21.52	0.53819
UP_KEYWORDS	Disulfide bond	49	21.97	0.06028
UP_KEYWORDS	Signal	54	24.22	0.18369
UP_KEYWORDS	Glycoprotein	55	24.66	0.44494
UP_SEQ_FEATURE	glycosylation site:N-linked (GlcNAc...)	47	21.08	1.00000

Annotation Cluster 2 (Content: Cyto/chemokine, Enrichment Score: 5.1, 35 genes)

Category	Term	Count	%	FDR
UP_KEYWORDS	Cytokine	18	8.07	5.06E-10
KEGG_PATHWAY	hsa04060:Cytokine-cytokine receptor interaction	20	8.97	3.92E-08
UP_KEYWORDS	Inflammatory response	14	6.28	1.85E-07
GOTERM_BP_DIRECT	GO:0006935~chemotaxis	10	4.48	4.44E-04
INTERPRO	IPR001811:Chemokine interleukin-8-like domain	7	3.14	5.59E-04
INTERPRO	IPR001089:CXC chemokine	5	2.24	5.59E-04
INTERPRO	IPR018048:CXC chemokine, conserved site	5	2.24	5.59E-04
GOTERM_BP_DIRECT	GO:0070098~chemokine-mediated signaling	8	3.59	6.97E-04
SMART	SM00199:SCY	7	3.14	5.52E-04
GOTERM_MF_DIRECT	GO:0008009~chemokine activity	7	3.14	0.00110
UP_KEYWORDS	Chemotaxis	8	3.59	0.00240
GOTERM_BP_DIRECT	GO:0030593~neutrophil chemotaxis	7	3.14	0.00383
GOTERM_BP_DIRECT	GO:0090023~pos. regulation of neutrop. chemotaxis	5	2.24	0.00428
GOTERM_MF_DIRECT	GO:0045236~CXCR chemokine receptor binding	4	1.79	0.00700
GOTERM_BP_DIRECT	GO:0060326~cell chemotaxis	6	2.69	0.02041
KEGG_PATHWAY	hsa04062:Chemokine signaling pathway	9	4.04	0.02777
BBID	109.Chemokine_families	4	1.79	0.55933
GOTERM_BP_DIRECT	GO:0007186~G-protein coupled receptor signaling	12	5.38	0.96825

Figure 3. Results of the post hoc analyses on 298 genes. (**A**) Functional assembly of differentially expressed genes. (**B**) Result of the annotation clustering. The two most stringent clusters with an enrichment score > 5 are shown. (**C**) Venn diagram of the two functional enrichment clusters. (**D**) STRING protein–protein interactions of annotation cluster 2 genes.

The functional enrichment analyses over the annotations included in DAVID (GO, KEGG, Interpro, Smart, etc.) revealed two annotation clusters with an enrichment score of >5. The gene clusters comprise 85 genes (cluster 1) and 35 genes (cluster 2) with a strong overlap of 31 genes between the two clusters (Figure 3B,C). The annotations suggest a strong (over-)representation of cytokines (both clusters, FDR = 5.06×10^{-10}) in those interactions (hsa04060; both clusters, FDR = 3.92×10^{-8}), inflammatory genes (GO:0006954; cluster 1, FDR 3.88×10^{-14}), chemokines and chemotaxis (IPR001089 and GO0006953; cluster 2, FDR = 5.59×10^{-4}, FDR = 4.48×10^{-4} respectively). Visualization of the pairwise protein interaction of cluster 2 using the EMBL STRING database with the highest confidence

(score > 0.9) reveals a core with C-X-C motif and C-C motif chemokines surrounded by interleukins and other cytokines.

3. Discussion

A PF is a long-established platform acknowledged by NASA (National Aeronautics and Space Administration), ESA (European Space Agency) and other national space agencies for studying molecular changes under the influence of gravitational changes. This platform to study the early effects of real microgravity has been used for molecular studies on, among others, Euglena gracilis [22], mouse stem cells [23] and human cardiomyocytes [24], chondrocytes [20,25], endothelial cells [26,27], but especially in cancer cells [6,8,28,29]. The parabolic flight campaign opened-up the possibility for us to generate a list of 298 gravisensitive PC-3 genes and categorize them by subsequent enrichment and interaction network analyses. However, the specific carcinogenesis reference is crucial for the usability of the study. We were able to determine an accumulation of cytokines (DAVID FDR 5.06×10^{-10}, Figure 3) and, in particular, chemokines (DAVID FDR 5.59×10^{-4}). These are, in turn, partially integrated into the portfolio of genes of the inflammatory response (DAVID FDR = 3.88×10^{-14}, Figure 4).

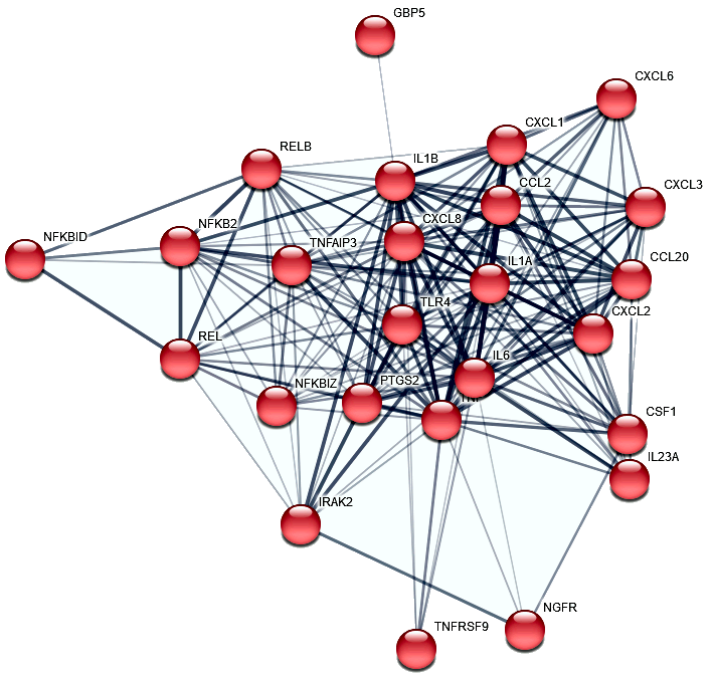

Figure 4. STRING protein–protein interactions of PC-3 PF differential expressed genes. The 23 protein to protein interactors (confidence > 0.4) annotated in cluster 1 and involved in the inflammatory response (GO:0006954) are shown.

3.1. NF-kB Signaling and Chemokines

Because the post parabola showed one significant upregulation of the *RELB* proto-oncogene NF-KB subunit (P_{adj} to $1g = 1.3 \times 10^{-37}$), which is accompanied by the regulation of NF-KB-related inflammatory genes, a detailed consideration of these relationships is appropriate. de Jesús and Ramakrishnan have shown that a c-Rel knockout in mouse embryonic fibroblasts (MEF) leads to an upregulation of *CCL2*, *CCL7*, *IP-10* (*CXCL10*), *CXCL1*, *A20* (*TNFAIP3*), *IL-6*, *CXCL2*, *CCL20*, and *ZFP36* by maintaining the expression kinetics [30]. Additionally, they found *ICAM1* and *VCAM1* upregulated with slowed kinetics. The gene *REL* encodes c-REL and was significantly upregulated after parabola one (P_{adj} to $1g = 7.7 \times 10^{-16}$) in our PF RNAseq experiment. Notably, seven of the eleven genes mentioned by de Jesús and Ramakrishnan as c-REL knock-out-dependently upregulated [30] are also highly significant and more than two-fold upregulated after P1 in our PC-3 PF

(Figure 5): *CCL2* (P_{adj} to $1g = 5.0 \times 10^{-49}$), *CXCL1* (P_{adj} to $1g = 2.8 \times 10^{-50}$), *TNFAIP3* (P_{adj} to $1g = 9.5 \times 10^{-23}$), *IL6* (P_{adj} to $1g = 4.0 \times 10^{-6}$), *CXCL2* (P_{adj} to $1g = 5.2 \times 10^{-33}$), *CCL20* (P_{adj} to $1g = 3.1 \times 10^{-17}$), and *ICAM1* (P_{adj} to $1g = 1.7 \times 10^{-52}$), whereas the joint significant upregulation of *CCL2* and *RELB* after the first parabola is in concordance with the *CCL2* expression depletion described by de Jesús and Ramakrishnan in the RELB MEF knock out experiment [30].

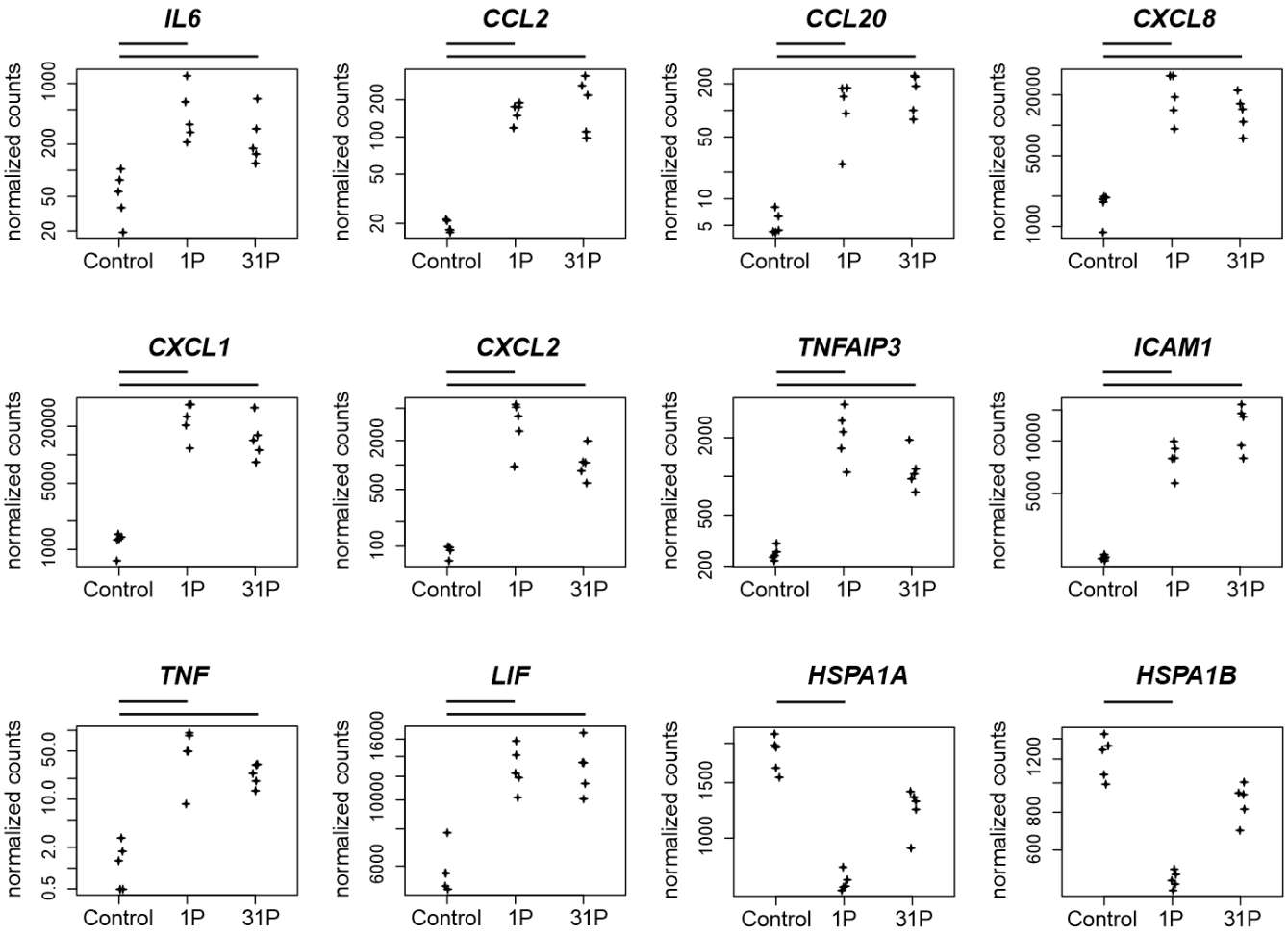

Figure 5. Normalized PF RNAseq counts of twelve candidate genes over the conditions control, 1P and 31P. Normalized mapped RNAseq read counts to the genes encodes the cytokine *IL6*, two C-C motif chemokines (*CCL2*, *CCL20*), three C-X-C motif chemokines (*CXCL8*, *CXCL1*, *CXCL2*), the zinc finger protein *TNFAIP3*, the glycoprotein *ICAM1*, the proinflammatory cytokine *TNF*, the pleiotropic cytokine *LIF* and the heat shock 70 kDa protein (*HSPA1A*, *HSPA1B*). Bars on top of the graph indicate two-fold significant ($P_{adj} < 0.05$) differential expression between the conditions.

In conclusion, although c-Rel and RELB are important factors in the regulatory cascade, the presence of other regulatory key players must be assumed. Furthermore, we were able to demonstrate the activation of genes relevant to inflammation by the gravitational change in PC-3.

3.2. Cytokines and Chemokines

The inflammatory cytokines TNF-α and LIF influence the CXCL-8 expression in pancreatic cancer progression [31]. CXCL-8 has been detected in prostate epithelium and stroma, is involved in multiple intracellular signaling [32] and upregulates the activity of Akt kinase [33]. *TNF*, *LIF* and *CXCL8* are upregulated after parabola one in our PC-3 PF (P_{adj} to $1g = 8.6 \times 10^{-12}$, 1.9×10^{-15} and 2.0×10^{-22}, respectively). In PC-3 cells, migration and

proliferation are stimulated by *CXCL3* overexpression [34]. In general, a highly increased secretion of the chemokine CXCL3 can be detected in PC-3 while an elevated expression of *CXCR2* was observed in the PC cell lines DU145, LNCaP and exogenous CXCL3, which does not affect proliferation but migration [35]. The experimental autoimmune prostatitis (EAP) mice are a model for the autoimmune dysfunction of chronic prostatitis. In EAP prostate, the proinflammatory cytokine interleukin 17 and the chemokine ligands *CXCL1* and *CXCL2* are upregulated. These findings suggest that IL-17 promotes the production of *CXCL1* and *CXCL2* [36]. In support of this notion, we find *CXCL1* and *CXCL2* to be upregulated after P1 (P_{adj} to $1g = 2.8 \times 10^{-50}$ and 5.2×10^{-33}, respectively).

3.3. Protein Transport

The two 70 kDa heat shock protein coding genes *HSPA1A* and *HSPA1B* are both downregulated after P1 (P_{adj} to $1g = 4.6 \times 10^{-43}$ and 2.5×10^{-33} respectively, Figure 5). The proteins have chaperone and lipid-binding functions and are involved in protein stabilization and folding. The gene *HspA1B* is one of the most prominent biomarkers for PC [37] and *HSPA1A* and *HSPA1B* upregulation is associated with a poor survival in colon cancer [38]. Furthermore, HspA1A specifically inhibits the malignant progression of Arid2-deficient lung cancer [39]. The known translocation of HspA1A toward the plasma membrane and the resulting presentation at the cell surface [40] are possible targets of gravitational variation in our PF experiment.

3.4. Non-Coding RNA

Although the applied RNAseq method is targeted towards coding genes by poly-A filtering, 23.9% and 25% of significantly and two-fold regulated genes are lncRNAs and miRNAs, respectively (Figure 3A). miRNAs and lncRNAs are important regulators of translation and transcription, respectively, so it is interesting to investigate whether expression of the non-coding genes were altered early on by microgravity.

The role of *miR-221/222* in PC remains controversial but upregulation of *miR-221/222* in CRPC is associated with an androgene receptor modulation during cancer development [41]. It has been shown that elimination of *miR-221* by CRISPR in PC-3 cells led to a reduced growth rate and expression of cell-cycle genes [42] through post transcriptional inhibition of *CDKN1B*/p27 [43]. In cells fixed after P1, we found a significantly increased miR-221 expression ($q = 1.65 \times 10^{-5}$) and at the same time expression depletion of *CDKN1B* (P_{adj} to $1g = 5.07 \times 10^{-5}$). Upstream of *miR221/222 MIR222HG*, a long non-coding RNA (lncRNA), is located. *MIR222HG* is associated with PC progression to CRPC, increases androgen-independent cell growth and represses the expression of *TMPRSS2* and *FKBP5* in hormone-sensitive prostate cancer [44]. We found a significant increase in *MIR222HG* expression in cells fixed after first parabola (P_{adj} to $1g = 1.47 \times 10^{-9}$), but no corresponding expression depletion in *TMPRSS2* and *FKBP5* (Figure 6).

MIR3142HG, a long non-coding RNA (lncRNA) associated with genomic instability, is upregulated in PC-3 cells in PF after the first parabola (P_{adj} to $1g = 3.7 \times 10^{-34}$, Figure 6). Its role in cancer progression is unclear. *MIR3142HG* is propagated as a risk factor for glioma susceptibility in the Chinese Han population [45], but it is also assumed to serve as a protective factor for head and neck squamous cell carcinoma (HNSCC) because the upregulated expression of *MIR3142HG* was associated with better survival outcomes [46].

The lncRNA *LINC02605* is involved in the antiviral immune response and its knock-down leads to an increased viral replication [47]. *LINC02605* is upregulated in PC-3 cells after the first parabola (P_{adj} to $1g = 2.9 \times 10^{-6}$) and even more after parabola 31 (P_{adj} to $1g = 1.9 \times 10^{-16}$). It has an effect on *hsa-miR-107* regulation on the protein expression of phosphatase and tensin homolog (PTEN) [47,48]. Both miR-107 and *PTEN* are important players in carcinogenesis. miR-107 has a potential role in regulating NEDD9 in the invasion, migration and proliferation of breast cancer [49]. Additionally, miR-107 is hypothesized to deactivate the phosphatidylinositol 3-kinase (PI3K)/Akt pathway in a hypopharyngeal

squamous cell carcinoma (HSCC) study [48]. Downregulation of *miR-107* by the potential therapeutic target LINC-DUBR suppressed malignant progression of ovarian cancer [50].

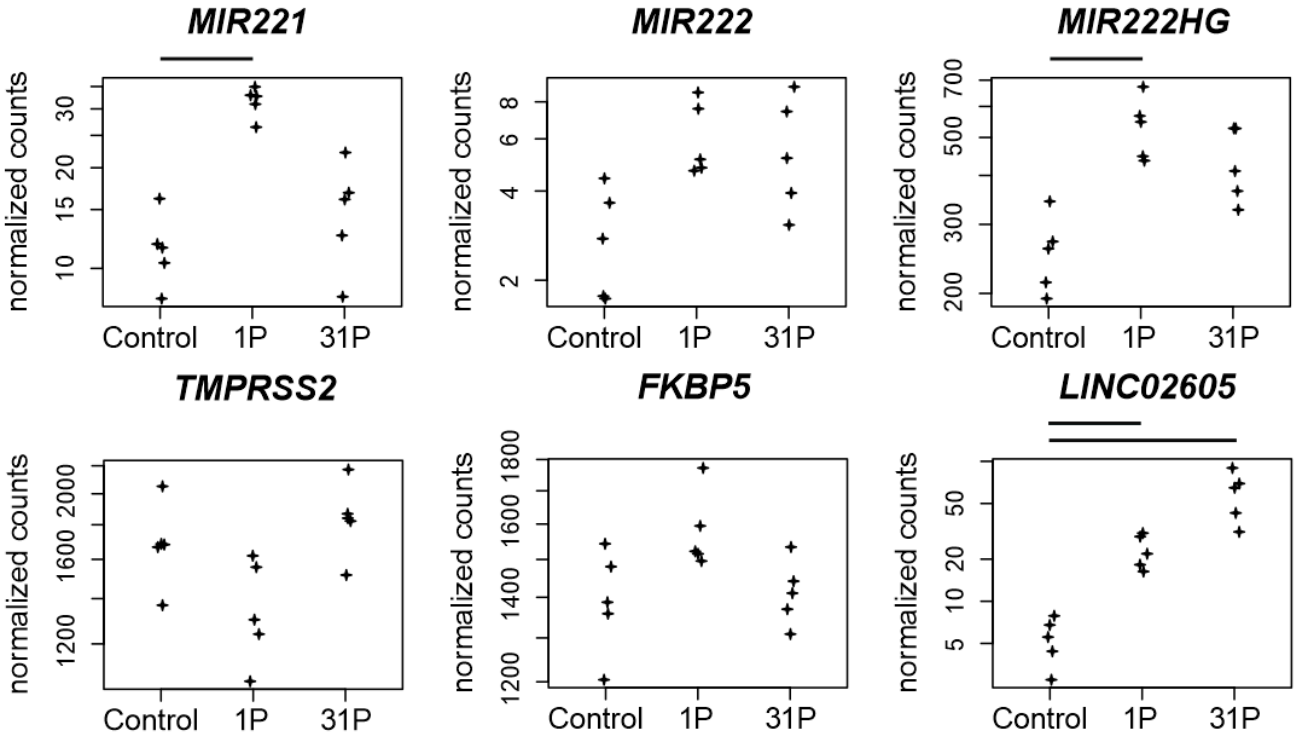

Figure 6. Normalized PF RNAseq counts of four non-coding RNAs and two protein coding RNAs. Expressions of the micro RNAs *miR-221* and *miR-222*, of the lncRNA *MIR222HG*, of the serine protease encoding *TMPRSS2* gene, of the Peptidyl-Prolyl Cis-Trans Isomerase encoding gene FKBP5 and of the lncRNA *LINC02605* are given. Bars on top of the graph indicate two-fold significant ($P_{adj} < 0.05$) differential expression between the conditions.

3.5. qPCR: Apoptosis, Hypogravity, and Vibration

The set of genes to be validated by qPCR shows that a substantial fraction of PC key players is unaffected by the gravitational influence of PF. However, it should be noted that the cytokine interleukin 6 is at least partially upregulated due to the vibration effect. Since cytokines play a major role in early PF-induced regulation, *IL6* requires further investigation. Furthermore, apoptotic processes seem to start at 31P. Although the effects on *CASP3, CASP8*, and *CASP9* are at the limit of detection even with RNAseq, mutual validation of RNAseq and qPCR for upregulation of *CASP3* indicates an albeit weak but stable finding (Figure 7A). Since more than 31P are not performed for technical reasons, it should be sufficient to keep an eye on the apoptosis problem. The downregulation of *PIK3CB* after 24 h of simulated microgravity obtained by random positioning published in our recent paper [16] does not technically match the downregulation measured in the present study under hypergravity (Figure 7B). *PIK3CB* following regulation cascades should therefore be kept in mind at least for long-term experiments with preceding hypergravity (e.g., rocket launch during ISS missions). It remains to be verified whether *PIK3CB* is subject to a general sensitivity to gravitational changes.

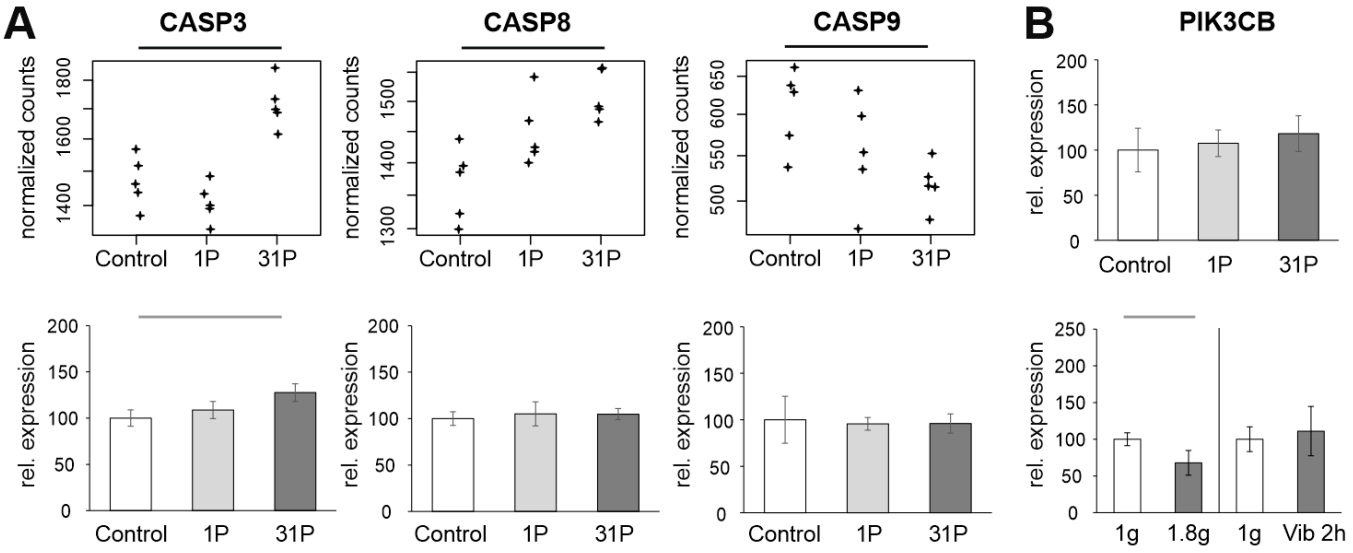

Figure 7. Analysis of apoptosis-related genes in PF samples. (**A**): Normalized PF RNAseq counts and qPCR ratios of the three apoptosis-related genes *CASP3*, *CASP8* and *CASP9*. (**B**): *PIK3CB* qPCR expression relative to the controls of the PF, hypergravity and Vibraplex experiment. Black and grey bars on top of the graph indicate adjusted and nominal significant ($p < 0.05$) differential expression, respectively.

4. Materials and Methods

4.1. Cell Culturing

The PC-3 cell line (ECACC 90112714) was purchased from the European Collection of Authenticated Cell Cultures (ECACC). The cells originated from a 62-year-old male Caucasian who suffered from a grade 4 prostate adenocarcinoma.

During cell cultivation, Ham's F-12 Nutrient Mixture (F-12) medium (Gibco, Fisher Scientific, Schwerte, Germany) was used and was supplemented with 10% FCS (Sigma Aldrich, Steinheim, Germany) and 1% penicillin/streptomycin (Life Technologies, New York, USA). The cells were cultured in T75 cm^2 flasks (Sarstedt, Nümbrecht, Germany). Every 3–4 days the medium was changed. The cells were split using 0.05% trypsin-EDTA (Gibco, Life Technologies, Paisley, UK).

4.2. Parabolic Flight Campaign

The 34th PF campaign was organized by the French company Novespace at the Bordeaux-Mérignac airport on behalf of the DLR (Deutsches Zentrum für Luft- und Raumfahrt) as part of their scientific and technological research programs.

The PF campaign consisted of a total of three flight days with the same experimental setup. The PF was carried out with the Airbus A310 ZERO G (Figure S3A,B) and took about two hours. When the flight altitude was reached, a total of 31 parabolas were flown. A parabola consists of a 20-s climb phase during which the acceleration due to gravity is almost twice as high (1.8*g*). This is followed by the actual 22-s-long μ*g*-phase. In the nosedive, a 20-s phase of hyper-*g* (1,8*g*) follows again. During the PF, the PC-3 cells were fixed after the first and after the 31st parabola using RNAlater (Invitrogen by Thermo Fischer Scientific, Vilnius, Lithuania), thus stabilizing the RNA until isolation.

T75 cm^2 flasks (Sarstedt, Nümbrecht, Germany) were placed on board in an incubator preheated to 37 °C 1 h before take-off. This was secured inside the so-called flight rack (Figure S3C). The flasks were connected to syringes via a flexible tube and a three-way valve (Figure S3D). The syringes contained 50 mL RNAlater. At the time points mentioned above, the syringes were manually actuated so that the culture flasks were filled with RNAlater at a ratio of approximately 4:1 (RNAlater:medium). Post-flight, the cells were transferred into 15 mL Falcon™ tubes (Sarstedt, Nümbrecht, Germany) by scratching the

cells with 25 cm cell scrapers (Sarstedt, Nümbrecht, Germany) and stored suspended in RNAlater at 4 °C until RNA isolation.

For F-actin staining, 200,000 cells were pipetted into eight slideflasks (Thermo Scientific, Waltham, MA, USA) and were incubated for 1.5 days. Of these, four slideflasks remained under 1*g* conditions and served as ground controls. The other four flasks were on board the aircraft in the incubator. Cells were fixed at the designated times using 4% paraformaldehyde (PFA, Sigma-Aldrich, St. Louis, MO, USA) in phosphate buffered saline (PBS; Gibco, Life Technologies, Paisley, UK). The 1*g* ground controls were also fixed at approximately the same times using 4% PFA. The slideflasks remained in 4% PFA until staining.

4.3. RNA Isolation

The cell suspension in the 15 mL Falcon™ tubes was diluted 1:5 with PBS. After centrifuging the dilution, the supernatant was discarded. Then, the RNA was isolated using the RNeasy Mini Kit (Qiagen, Hilden, Germany). Then, RTL lysis buffer was added, and the cell pellet was dissolved by pipetting up and down with a syringe. Afterwards, 350 µL of a 70% ethanol dilution was added, 700 µL of the solution was transferred to RNeasy Mini spin column, and the column was centrifuged for 15 s at 8000× *g*. Next, 700 µL RW1 buffer and 500 µL RPE buffer were added and centrifuged in between. Then, 35 µL RNAse-free water was pipetted directly to the spin column membrane and the column was put into a new Eppendorf tube. Finally, the spin column was centrifuged again to detach the RNA from the membrane.

The quality and the concentration of the RNA of each sample was evaluated by the Nanodrop technique and a spectrophotometer.

4.4. Quantitative Real-Time Polymerase Chain Reaction

A 7500 Fast Real-Time PCR System (Applied Biosystems, Darmstadt, Germany) was used both for cDNA synthesis and the following quantitative real time polymerase chain reaction (qPCR).

First, the RNA was converted into cDNA with the High-Capacity cDNA reverse Transcription Kit (Applied Biosystems, Darmstadt, Germany) on a 96-well plate. Then, 2 µL RT buffer, 0.8 µL dNTP mix, 2 µL RT random primer, 1 µL reverse transcriptase and 4.2 µL nuclease free water were added to each well. In the end, the RNA of each sample was added to get a total amount of 1 µg RNA in 20 µL solution.

The qPCR was performed with FAST SYBR™ Green Master Mix (Applied Biosystems, Foster City, CA, USA) on a 96-well plate. Every sample was measured in triplicate. Each well contained 1 µL cDNA of the corresponding sample, 7.5 µL SYBR Green Master Mix, 0.042 µL primer forward, 0.042 µL primer reverse and 6.41 µL water (Table S3). The plate was placed in the qPCR instrument and went through the following thermal cycles: 95 °C for 20 s, 95 °C for 3 s, and 60 °C for 30 s.

The samples were analyzed with the comparative threshold cycle ($\Delta\Delta C_T$) method, using the 18 s housekeeping gene as a reference.

4.5. F-Actin Staining

F-actin was visualized by means of rhodamine-phalloidin staining (Molecular Probes®, Eugene, OR, USA). Moreover, the nuclei were stained with 4′,6-diamidino-2-phenylindole (DAPI, Sigma-Aldrich, Merck Life Science A/S, Søborg, Denmark). The protocol was published earlier in [20].

4.6. Microscopy

The slideflasks were investigated using confocal laser scanning microscopy. The observations were made with a Leica DM 2000 microscope and an objective with a 400× magnification. The microscope was also connected to an external light source Leica EL 6000 (Leica Microsystems GmbH, Wetzlar, Germany).

4.7. Hypergravity

The hyper-*g* experiments were performed using the DLR Multi-Sample Incubator Centrifuge (MuSIC, DLR, Department of Gravitational Biology) as already described by Aleshcheva et al. [20]. For this purpose, four T75 cell culture flasks were placed on the MuSIC in a 37 °C incubator (Figure S3E,F). For two hours, 1.8*g* gravitational load was then applied to the cell cultures, which corresponds to the hyper-*g*-phases during the PF. At the end of the run, the samples were fixed with RNAlater for RNA isolation. The 1*g* control samples were cultured in parallel and also fixed using RNAlater.

4.8. Vibration Experiment

T75 flasks containing subconfluent PC-3 cells were attached to the Vibraplex device (DLR, Cologne, Germany Figure S3G) and placed on the device in a 37 °C incubator in line with the protocol published earlier by Lützenberg et al. [51]. Vibrations between 0.2 and 14 Hz were transmitted via the Vibraplex using a connected loudspeaker for about 2 h. This procedure corresponds to frequencies generated during the PF. At the end of the two hours, the samples were fixed with RNAlater for RNA isolation. Static control samples were cultured and fixed with RNAlater in parallel.

4.9. RNA Sequencing

Extracted RNA was checked for quantity and quality as described in Section 4.3. Sufficient quality RNA was converted to libraries using the TruSeq™ RNA Library Prep Kit v2 (Illumina, San Diego, CA, USA) as directed by standard protocols. Libraries were sequenced on Illumina's novaseq 6000 with paired-end 100 base pair reads and a sequencing depth of >20 milion pairs. For all sequencing data, reads were quality checked for read counts and quality values. The unaligned reads were mapped on the hg38 genome using STAR 2.6.1a [52] and the ENSEMBL v.99 [53] annotation. A maximum of ten mismatches and a multimapping to up to 10 different positions was allowed. Secondary alignments were filtered out.

4.10. Transcriptomic Analyses

We used the Bioconductor R package DESeq2 to capture differentially expressed genes (DEG). DESeq2 relies on a negative binomial generalized linear model (GLM) and uses the uniquely mapped RNAseq counts to an exon [54]. For integrated post hoc analysis for enrichments and networks of differentially expressed genes, we used the Database for Annotation, Visualization and Integrated Discovery (DAVID v. 6.8) [55] and the protein-to-protein interaction database STRING v. 11.5 [56], respectively.

4.11. Statistical Analysis

The statistics were performed using the GraphPad Prism 7.01 software (GraphPad Software, Inc., San Diego, CA, USA) and the stats package of R 3.4.3. The sample and the related control were analyzed with the Mann–Whitney U-test at a significance level of $p * < 0.05$.

5. Conclusions

The objective behind our PF experiment was to identify early responses to the alternating gravitational stimulus and to put them into context with carcinogenesis and cancer progression in order to finally obtain new and fast expression-altering biomarkers for PC diagnosis. In general, we observed that the highly differential genes, which include some cytokines and especially chemokines, on the one hand provide a stable expression and are therefore robust for a diagnostic approach, and on the other hand are already related to the disease. Notably, the NGS analysis identified five cytokines (*CCL2*, *CXCL1*, *IL6*, *CXCL2*, *CCL20*), one zink finger protein (*TNFAIP3*), one glycoprotein (*ICAM1*) related to c-REL signaling, and the microRNA (*miR-221*) to be differentially regulated during PFs. Since these factors are relevant in cancer as well as inflammatory aspects, the presented

findings may thus contribute to the development of improved diagnostic tools relevant to PC. CCL2/CCR2 have been associated with PC advancement, metastasis and relapse [57]. A similar action is known for IL6, which plays a key role in cancer progression [58]. In particular, non-coding RNAs and micro-RNAs have recently been increasingly used in cancer medicine as diagnostic, prognostic and therapeutic biomarkers [59–62] and cytokines are well established in cancer immunotherapy [63–66].

Supplementary Materials: The following supporting information can be downloaded at: https://www.mdpi.com/article/10.3390/ijms23147876/s1.

Author Contributions: Conceptualization H.S., D.G.; methodology, H.S. and D.D.; software H.S. and M.W.; validation D.G., H.S., T.J.C. and M.W.; formal analysis H.S. and D.D.; investigation H.S., D.D., M.W., T.J.C., R.H., C.L., K.S., N.H. and D.M.; resources M.I., R.H. and D.G.; writing—original draft preparation, H.S.; writing—review and editing, D.G., T.J.C., R.H. and M.W.; visualization, H.S., T.J.C. and D.G.; supervision, D.G.; project administration, D.G.; funding acquisition, D.G. and M.I. All authors have read and agreed to the published version of the manuscript.

Funding: This research was funded by Deutsches Zentrum für Luft- und Raumfahrt (DLR) projects 50WB2219 and 50WB1924 (D.G.).

Institutional Review Board Statement: Not applicable.

Informed Consent Statement: Not applicable.

Data Availability Statement: Not applicable.

Acknowledgments: The authors express their thanks to Yale T. Kozinski for his thorough language review of the manuscript.

Conflicts of Interest: The authors declare no conflict of interest.

Abbreviations

PF	parabolic flight,
PC	prostate cancer
HNSCC	head and neck squamous cell carcinoma
HSCC	hypopharyngeal squamous cell carcinoma
PCA	principal component analysis
µ*g*	Microgravity
s-µ*g*	simulated microgravity
p	probability-value
P_{adj}	adjusted probability-value
1P	one parabola
31P	31 parabolas
NGS	next generation sequencing
qPCR	quantitative real-time PCR
RPM	random positioning machine
HARV	high aspect rotating-wall vessel
PAM	PI3K/AKT/mTOR

References

1. Grimm, D.; Schulz, H.; Krüger, M.; Cortés-Sánchez, J.L.; Egli, M.; Kraus, A.; Sahana, J.; Corydon, T.J.; Hemmersbach, R.; Wise, P.M.; et al. The Fight against Cancer by Microgravity: The Multicellular Spheroid as a Metastasis Model. *Int. J. Mol. Sci.* **2022**, *23*, 3073. [CrossRef] [PubMed]
2. Pietsch, J.; Kussian, R.; Sickmann, A.; Bauer, J.; Weber, G.; Nissum, M.; Westphal, K.; Egli, M.; Grosse, J.; Schönberger, J.; et al. Application of free-flow IEF to identify protein candidates changing under microgravity conditions. *Proteomics* **2010**, *10*, 904–913. [CrossRef] [PubMed]
3. Nassef, M.Z.; Kopp, S.; Wehland, M.; Melnik, D.; Sahana, J.; Krüger, M.; Corydon, T.J.; Oltmann, H.; Schmitz, B.; Schütte, A.; et al. Real Microgravity Influences the Cytoskeleton and Focal Adhesions in Human Breast Cancer Cells. *Int. J. Mol. Sci.* **2019**, *20*, 3156. [CrossRef] [PubMed]

4. Häder, D.P.; Braun, M.; Grimm, D.; Hemmersbach, R. Gravireceptors in eukaryotes-a comparison of case studies on the cellular level. *NPJ Microgravity* **2017**, *3*, 13. [CrossRef]
5. Grimm, D.; Bauer, J.; Kossmehl, P.; Shakibaei, M.; Schöberger, J.; Pickenhahn, H.; Schulze-Tanzil, G.; Vetter, R.; Eilles, C.; Paul, M.; et al. Simulated microgravity alters differentiation and increases apoptosis in human follicular thyroid carcinoma cells. *FASEB J.* **2002**, *16*, 604–606. [CrossRef]
6. Corydon, T.J.; Kopp, S.; Wehland, M.; Braun, M.; Schütte, A.; Mayer, T.; Hülsing, T.; Oltmann, H.; Schmitz, B.; Hemmersbach, R.; et al. Alterations of the cytoskeleton in human cells in space proved by life-cell imaging. *Sci. Rep.* **2016**, *6*, 20043. [CrossRef]
7. Tan, X.; Xu, A.; Zhao, T.; Zhao, Q.; Zhang, J.; Fan, C.; Deng, Y.; Freywald, A.; Genth, H.; Xiang, J. Simulated microgravity inhibits cell focal adhesions leading to reduced melanoma cell proliferation and metastasis via FAK/RhoA-regulated mTORC1 and AMPK pathways. *Sci. Rep.* **2018**, *8*, 3769. [CrossRef]
8. Nassef, M.Z.; Kopp, S.; Melnik, D.; Corydon, T.J.; Sahana, J.; Krüger, M.; Wehland, M.; Bauer, T.J.; Liemersdorf, C.; Hemmersbach, R.; et al. Short-Term Microgravity Influences Cell Adhesion in Human Breast Cancer Cells. *Int. J. Mol. Sci.* **2019**, *20*, 5730. [CrossRef]
9. Grosse, J.; Wehland, M.; Pietsch, J.; Schulz, H.; Saar, K.; Hübner, N.; Eilles, C.; Bauer, J.; Abou-El-Ardat, K.; Baatout, S.; et al. Gravity-sensitive signaling drives 3-dimensional formation of multicellular thyroid cancer spheroids. *FASEB J.* **2012**, *26*, 5124–5140. [CrossRef]
10. Kossmehl, P.; Shakibaei, M.; Cogoli, A.; Infanger, M.; Curcio, F.; Schönberger, J.; Eilles, C.; Bauer, J.; Pickenhahn, H.; Schulze-Tanzil, G.; et al. Weightlessness induced apoptosis in normal thyroid cells and papillary thyroid carcinoma cells via extrinsic and intrinsic pathways. *Endocrinology* **2003**, *144*, 4172–4179. [CrossRef]
11. Warnke, E.; Pietsch, J.; Kopp, S.; Bauer, J.; Sahana, J.; Wehland, M.; Krüger, M.; Hemmersbach, R.; Infanger, M.; Lützenberg, R.; et al. Cytokine Release and Focal Adhesion Proteins in Normal Thyroid Cells Cultured on the Random Positioning Machine. *Cell Physiol. Biochem.* **2017**, *43*, 257–270. [CrossRef] [PubMed]
12. Corydon, T.J.; Mann, V.; Slumstrup, L.; Kopp, S.; Sahana, J.; Askou, A.L.; Magnusson, N.E.; Echegoyen, D.; Bek, T.; Sundaresan, A.; et al. Reduced Expression of Cytoskeletal and Extracellular Matrix Genes in Human Adult Retinal Pigment Epithelium Cells Exposed to Simulated Microgravity. *Cell Physiol. Biochem.* **2016**, *40*, 1–17. [CrossRef] [PubMed]
13. Clejan, S.; O'Connor, K.C.; Cowger, N.L.; Cheles, M.K.; Haque, S.; Primavera, A.C. Effects of simulated microgravity on DU 145 human prostate carcinoma cells. *Biotechnol. Bioeng.* **1996**, *50*, 587–597. [CrossRef]
14. Clejan, S.; O'Connor, K.; Rosensweig, N. Tri-dimensional prostate cell cultures in simulated microgravity and induced changes in lipid second messengers and signal transduction. *J. Cell Mol. Med.* **2001**, *5*, 60–73. [CrossRef]
15. Hybel, T.E.; Dietrichs, D.; Sahana, J.; Corydon, T.J.; Nassef, M.Z.; Wehland, M.; Krüger, M.; Magnusson, N.E.; Bauer, J.; Utpatel, K.; et al. Simulated Microgravity Influences VEGF, MAPK, and PAM Signaling in Prostate Cancer Cells. *Int. J. Mol. Sci.* **2020**, *21*, 1263. [CrossRef]
16. Dietrichs, D.; Grimm, D.; Sahana, J.; Melnik, D.; Corydon, T.J.; Wehland, M.; Krüger, M.; Vermeesen, R.; Baselet, B.; Baatout, S.; et al. Three-Dimensional Growth of Prostate Cancer Cells Exposed to Simulated Microgravity. *Front. Cell Dev. Biol.* **2022**, *10*, 841017. [CrossRef]
17. Gasmi, A.; Roubaud, G.; Dariane, C.; Barret, E.; Beauval, J.B.; Brureau, L.; Créhange, G.; Fiard, G.; Fromont, G.; Gauthé, M.; et al. Overview of the Development and Use of Akt Inhibitors in Prostate Cancer. *J. Clin. Med.* **2021**, *11*, 160. [CrossRef]
18. Bachmann, S.; Iding, H.; Lautz, C.; Thomé-Pfeiffer, I.; Maierhofer, C.; Mondière, R.; Schmidt, P.; Strasser, C.; Bär, T.; Aebi, A.; et al. Development of the Commercial Manufacturing Process for Ipatasertib. *Chimia* **2021**, *75*, 605–613. [CrossRef]
19. Riwaldt, S.; Corydon, T.J.; Pantalone, D.; Sahana, J.; Wise, P.; Wehland, M.; Krüger, M.; Melnik, D.; Kopp, S.; Infanger, M.; et al. Role of Apoptosis in Wound Healing and Apoptosis Alterations in Microgravity. *Front. Bioeng. Biotechnol.* **2021**, *9*, 679650. [CrossRef]
20. Aleshcheva, G.; Wehland, M.; Sahana, J.; Bauer, J.; Corydon, T.J.; Hemmersbach, R.; Frett, T.; Egli, M.; Infanger, M.; Grosse, J.; et al. Moderate alterations of the cytoskeleton in human chondrocytes after short-term microgravity produced by parabolic flight maneuvers could be prevented by up-regulation of BMP-2 and SOX-9. *FASEB J.* **2015**, *29*, 2303–2314. [CrossRef]
21. Everaert, C.; Luypaert, M.; Maag, J.L.V.; Cheng, Q.X.; Dinger, M.E.; Hellemans, J.; Mestdagh, P. Benchmarking of RNA-sequencing analysis workflows using whole-transcriptome RT-qPCR expression data. *Sci. Rep.* **2017**, *7*, 1559. [CrossRef] [PubMed]
22. Kruger, J.; Richter, P.; Stoltze, J.; Strauch, S.M.; Kruger, M.; Daiker, V.; Prasad, B.; Sonnewald, S.; Reid, S.; Lebert, M. Changes of Gene Expression in Euglena gracilis Obtained During the 29(th) DLR Parabolic Flight Campaign. *Sci. Rep.* **2019**, *9*, 14260. [CrossRef] [PubMed]
23. Acharya, A.; Brungs, S.; Henry, M.; Rotshteyn, T.; Singh Yaduvanshi, N.; Wegener, L.; Jentzsch, S.; Hescheler, J.; Hemmersbach, R.; Boeuf, H.; et al. Modulation of Differentiation Processes in Murine Embryonic Stem Cells Exposed to Parabolic Flight-Induced Acute Hypergravity and Microgravity. *Stem. Cells Dev.* **2018**, *27*, 838–847. [CrossRef] [PubMed]
24. Acharya, A.; Brungs, S.; Lichterfeld, Y.; Hescheler, J.; Hemmersbach, R.; Boeuf, H.; Sachinidis, A. Parabolic, Flight-Induced, Acute Hypergravity and Microgravity Effects on the Beating Rate of Human Cardiomyocytes. *Cells* **2019**, *8*, 352. [CrossRef] [PubMed]
25. Wehland, M.; Aleshcheva, G.; Schulz, H.; Saar, K.; Hubner, N.; Hemmersbach, R.; Braun, M.; Ma, X.; Frett, T.; Warnke, E.; et al. Differential gene expression of human chondrocytes cultured under short-term altered gravity conditions during parabolic flight maneuvers. *Cell Commun. Signal.* **2015**, *13*, 18. [CrossRef] [PubMed]

26. Grosse, J.; Wehland, M.; Pietsch, J.; Ma, X.; Ulbrich, C.; Schulz, H.; Saar, K.; Hubner, N.; Hauslage, J.; Hemmersbach, R.; et al. Short-term weightlessness produced by parabolic flight maneuvers altered gene expression patterns in human endothelial cells. *FASEB J.* **2012**, *26*, 639–655. [CrossRef]
27. Wehland, M.; Ma, X.; Braun, M.; Hauslage, J.; Hemmersbach, R.; Bauer, J.; Grosse, J.; Infanger, M.; Grimm, D. The impact of altered gravity and vibration on endothelial cells during a parabolic flight. *Cell Physiol. Biochem.* **2013**, *31*, 432–451. [CrossRef]
28. Ulbrich, C.; Pietsch, J.; Grosse, J.; Wehland, M.; Schulz, H.; Saar, K.; Hubner, N.; Hauslage, J.; Hemmersbach, R.; Braun, M.; et al. Differential gene regulation under altered gravity conditions in follicular thyroid cancer cells: Relationship between the extracellular matrix and the cytoskeleton. *Cell Physiol. Biochem.* **2011**, *28*, 185–198. [CrossRef]
29. Ma, X.; Pietsch, J.; Wehland, M.; Schulz, H.; Saar, K.; Hubner, N.; Bauer, J.; Braun, M.; Schwarzwalder, A.; Segerer, J.; et al. Differential gene expression profile and altered cytokine secretion of thyroid cancer cells in space. *FASEB J.* **2014**, *28*, 813–835. [CrossRef]
30. de Jesús, T.J.; Ramakrishnan, P. NF-κB c-Rel Dictates the Inflammatory Threshold by Acting as a Transcriptional Repressor. *iScience* **2020**, *23*, 100876. [CrossRef]
31. Kamohara, H.; Takahashi, M.; Ishiko, T.; Ogawa, M.; Baba, H. Induction of interleukin-8 (CXCL-8) by tumor necrosis factor-alpha and leukemia inhibitory factor in pancreatic carcinoma cells: Impact of CXCL-8 as an autocrine growth factor. *Int. J. Oncol.* **2007**, *31*, 627–632. [PubMed]
32. Liu, Q.; Li, A.; Tian, Y.; Wu, J.D.; Liu, Y.; Li, T.; Chen, Y.; Han, X.; Wu, K. The CXCL8-CXCR1/2 pathways in cancer. *Cytokine Growth Factor Rev.* **2016**, *31*, 61–71. [CrossRef] [PubMed]
33. Culig, Z. CXCL8, an underestimated "bad guy" in prostate cancer. *Eur. Urol.* **2013**, *64*, 189–190. [CrossRef] [PubMed]
34. Xin, H.; Cao, Y.; Shao, M.L.; Zhang, W.; Zhang, C.B.; Wang, J.T.; Liang, L.C.; Shao, W.W.; Qi, Y.L.; Li, Y.; et al. Chemokine CXCL3 mediates prostate cancer cells proliferation, migration and gene expression changes in an autocrine/paracrine fashion. *Int. Urol. Nephrol.* **2018**, *50*, 861–868. [CrossRef]
35. Gui, S.L.; Teng, L.C.; Wang, S.Q.; Liu, S.; Lin, Y.L.; Zhao, X.L.; Liu, L.; Sui, H.Y.; Yang, Y.; Liang, L.C.; et al. Overexpression of CXCL3 can enhance the oncogenic potential of prostate cancer. *Int. Urol. Nephrol.* **2016**, *48*, 701–709. [CrossRef]
36. Zhang, C.; Chen, J.; Wang, H.; Chen, J.; Zheng, M.J.; Chen, X.G.; Zhang, L.; Liang, C.Z.; Zhan, C.S. IL-17 exacerbates experimental autoimmune prostatitis via CXCL1/CXCL2-mediated neutrophil infiltration. *Andrologia* **2022**, e14455. [CrossRef]
37. Zhou, K.; Arslanturk, S.; Craig, D.B.; Heath, E.; Draghici, S. Discovery of primary prostate cancer biomarkers using cross cancer learning. *Sci. Rep.* **2021**, *11*, 10433. [CrossRef]
38. Guan, Y.; Zhu, X.; Liang, J.; Wei, M.; Huang, S.; Pan, X.X. Upregulation of HSPA1A/HSPA1B/HSPA7 and Downregulation of HSPA9 Were Related to Poor Survival in Colon Cancer. *Front. Oncol.* **2021**, *11*, 749673. [CrossRef]
39. Wang, X.; Wang, Y.; Fang, Z.; Wang, H.; Zhang, J.; Zhang, L.; Huang, H.; Jiang, Z.; Jin, Y.; Han, X.; et al. Targeting HSPA1A in ARID2-deficient lung adenocarcinoma. *Natl. Sci. Rev.* **2021**, *8*, nwab014. [CrossRef]
40. Smulders, L.; Daniels, A.J.; Plescia, C.B.; Berger, D.; Stahelin, R.V.; Nikolaidis, N. Characterization of the Relationship between the Chaperone and Lipid-Binding Functions of the 70-kDa Heat-Shock Protein, HspA1A. *Int. J. Mol. Sci.* **2020**, *21*, 5995. [CrossRef]
41. Gui, B.; Hsieh, C.L.; Kantoff, P.W.; Kibel, A.S.; Jia, L. Androgen receptor-mediated downregulation of microRNA-221 and -222 in castration-resistant prostate cancer. *PLoS ONE* **2017**, *12*, e0184166. [CrossRef] [PubMed]
42. Dart, D.A.; Koushyar, S.; Lanning, B.E.; Jiang, W. MiR-221 Is Specifically Elevated in PC3 Cells and its Deletion Reduces Adhesion, Motility and Growth. *Anticancer Res.* **2019**, *39*, 5311–5327. [CrossRef] [PubMed]
43. Fornari, F.; Gramantieri, L.; Ferracin, M.; Veronese, A.; Sabbioni, S.; Calin, G.A.; Grazi, G.L.; Giovannini, C.; Croce, C.M.; Bolondi, L.; et al. MiR-221 controls CDKN1C/p57 and CDKN1B/p27 expression in human hepatocellular carcinoma. *Oncogene* **2008**, *27*, 5651–5661. [CrossRef] [PubMed]
44. Sun, T.; Du, S.Y.; Armenia, J.; Qu, F.; Fan, J.; Wang, X.; Fei, T.; Komura, K.; Liu, S.X.; Lee, G.M.; et al. Expression of lncRNA MIR222HG co-transcribed from the miR-221/222 gene promoter facilitates the development of castration-resistant prostate cancer. *Oncogenesis* **2018**, *7*, 30. [CrossRef] [PubMed]
45. Feng, J.; Ouyang, Y.; Xu, D.; He, Q.; Liu, D.; Fan, X.; Xu, P.; Mo, Y. Genetic variants in MIR17HG affect the susceptibility and prognosis of glioma in a Chinese Han population. *BMC Cancer* **2020**, *20*, 976. [CrossRef] [PubMed]
46. Chen, Y.; Zhao, Y.; Lu, R.; Zhao, H.; Guo, Y. Identification and Validation of a Novel Genomic Instability-Associated Long Non-Coding RNA Prognostic Signature in Head and Neck Squamous Cell Carcinoma. *Front. Cell Dev. Biol.* **2021**, *9*, 787766. [CrossRef]
47. Xu, R.; Yu, S.S.; Yao, R.R.; Tang, R.C.; Liang, J.W.; Pang, X.; Zhang, J. Interferon-Inducible LINC02605 Promotes Antiviral Innate Responses by Strengthening IRF3 Nuclear Translocation. *Front. Immunol.* **2021**, *12*, 755512. [CrossRef]
48. Gao, X.; Fan, X.; Zeng, W.; Liang, J.; Guo, N.; Yang, X.; Zhao, Y. Overexpression of microRNA-107 suppressed proliferation, migration, invasion, and the PI3K/Akt signaling pathway and induced apoptosis by targeting Nin one binding (NOB1) protein in a hypopharyngeal squamous cell carcinoma cell line (FaDu). *Bioengineered* **2022**, *13*, 7881–7893. [CrossRef]
49. Zhou, J.; Sun, X.; Zhang, X.; Yang, H.; Jiang, Z.; Luo, Q.; Liu, Y.; Wang, G. miR-107 is involved in the regulation of NEDD9-mediated invasion and metastasis in breast cancer. *BMC Cancer* **2022**, *22*, 533. [CrossRef]
50. Han, Z.; Li, D.; Yang, Y.; Zhang, H. LINC-DUBR Suppresses Malignant Progression of Ovarian Cancer by Downregulating miR-107 to Induce SMAC Expression. *J. Healthc. Eng.* **2022**, *2022*, 4535655. [CrossRef]

51. Lützenberg, R.; Wehland, M.; Solano, K.; Nassef, M.Z.; Buken, C.; Melnik, D.; Bauer, J.; Kopp, S.; Krüger, M.; Riwaldt, S.; et al. Beneficial Effects of Low Frequency Vibration on Human Chondrocytes in Vitro. *Cell Physiol. Biochem.* **2019**, *53*, 623–637. [PubMed]
52. Dobin, A.; Davis, C.A.; Schlesinger, F.; Drenkow, J.; Zaleski, C.; Jha, S.; Batut, P.; Chaisson, M.; Gingeras, T.R. STAR: Ultrafast universal RNA-seq aligner. *Bioinformatics* **2013**, *29*, 15–21. [CrossRef] [PubMed]
53. Yates, A.D.; Achuthan, P.; Akanni, W.; Allen, J.; Allen, J.; Alvarez-Jarreta, J.; Amode, M.R.; Armean, I.M.; Azov, A.G.; Bennett, R.; et al. Ensembl 2020. *Nucleic Acids Res.* **2020**, *48*, D682–D688. [CrossRef] [PubMed]
54. Love, M.I.; Huber, W.; Anders, S. Moderated estimation of fold change and dispersion for RNA-seq data with DESeq2. *Genome Biol.* **2014**, *15*, 550. [CrossRef] [PubMed]
55. Dennis, G.; Sherman, B.T.; Hosack, D.A.; Yang, J.; Gao, W.; Lane, H.C.; Lempicki, R.A. DAVID: Database for Annotation, Visualization, and Integrated Discovery. *Genome Biol.* **2003**, *4*, P3. [CrossRef]
56. Szklarczyk, D.; Gable, A.L.; Nastou, K.C.; Lyon, D.; Kirsch, R.; Pyysalo, S.; Doncheva, N.T.; Legeay, M.; Fang, T.; Bork, P.; et al. The STRING database in 2021: Customizable protein-protein networks, and functional characterization of user-uploaded gene/measurement sets. *Nucleic Acids. Res.* **2021**, *49*, D605–D612. [CrossRef]
57. Hao, Q.; Vadgama, J.V.; Wang, P. CCL2/CCR2 signaling in cancer pathogenesis. *Cell Commun. Signal.* **2020**, *18*, 82. [CrossRef]
58. Smith, P.C.; Hobisch, A.; Lin, D.L.; Culig, Z.; Keller, E.T. Interleukin-6 and prostate cancer progression. *Cytokine Growth Factor Rev.* **2001**, *12*, 33–40. [CrossRef]
59. Tornesello, M.L.; Faraonio, R.; Buonaguro, L.; Annunziata, C.; Starita, N.; Cerasuolo, A.; Pezzuto, F.; Tornesello, A.L.; Buonaguro, F.M. The Role of microRNAs, Long Non-coding RNAs, and Circular RNAs in Cervical Cancer. *Front. Oncol.* **2020**, *10*, 150. [CrossRef]
60. Casarotto, M.; Fanetti, G.; Guerrieri, R.; Palazzari, E.; Lupato, V.; Steffan, A.; Polesel, J.; Boscolo-Rizzo, P.; Fratta, E. Beyond MicroRNAs: Emerging Role of Other Non-Coding RNAs in HPV-Driven Cancers. *Cancers* **2020**, *12*, 1246. [CrossRef]
61. Zheng, J.; Chen, L. Non-coding RNAs-EZH2 regulatory mechanisms in cervical cancer: The current state of knowledge. *Biomed. Pharmacother.* **2022**, *146*, 112123. [CrossRef] [PubMed]
62. Razavi, Z.S.; Tajiknia, V.; Majidi, S.; Ghandali, M.; Mirzaei, H.R.; Rahimian, N.; Hamblin, M.R.; Mirzaei, H. Gynecologic cancers and non-coding RNAs: Epigenetic regulators with emerging roles. *Crit. Rev. Oncol. Hematol.* **2021**, *157*, 103192. [CrossRef] [PubMed]
63. Lippitz, B.E. Cytokine patterns in patients with cancer: A systematic review. *Lancet Oncol.* **2013**, *14*, e218–e228. [CrossRef]
64. Rallis, K.S.; Corrigan, A.E.; Dadah, H.; George, A.M.; Keshwara, S.M.; Sideris, M.; Szabados, B. Cytokine-based Cancer Immunotherapy: Challenges and Opportunities for IL-10. *Anticancer Res.* **2021**, *41*, 3247–3252. [CrossRef]
65. Bonati, L.; Tang, L. Cytokine engineering for targeted cancer immunotherapy. *Curr. Opin. Chem. Biol.* **2021**, *62*, 43–52. [CrossRef]
66. Conlon, K.C.; Miljkovic, M.D.; Waldmann, T.A. Cytokines in the Treatment of Cancer. *J. Interferon Cytokine Res.* **2019**, *39*, 6–21. [CrossRef]

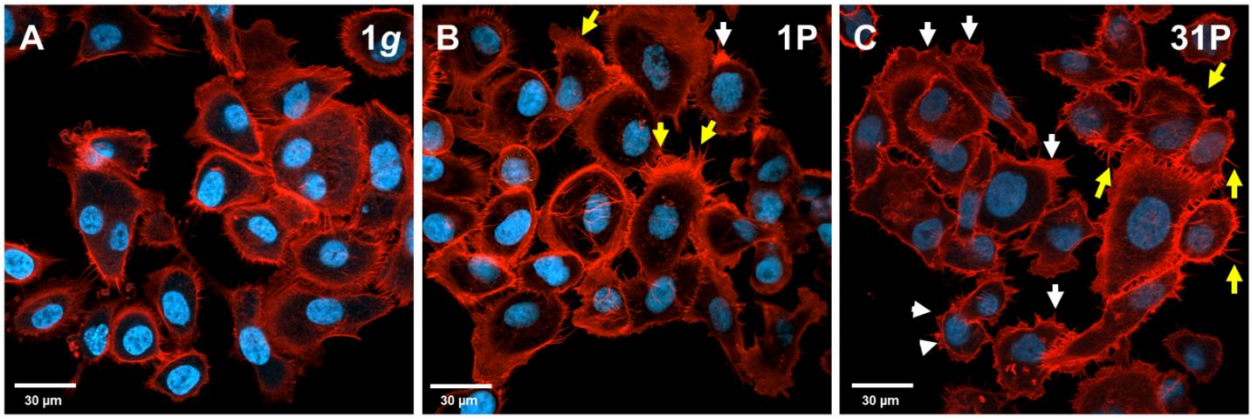

Figure S1: Impact of altered gravity on intracellular organization of F-actin: *Confocal laser scanning microscopy of TRITC-conjugated phalloidin stained (F-actin) samples.* ***A-C:*** *PC-3 cells cultivated under altered gravity conditions.* ***A:*** *Static 1g ground control.* ***B:*** *After the first parabola (1P).* ***C:*** *After the 31st parabola (31P). The white arrows show psudopoida and lamellipodia and yellow arrows indicate stress fibers. Scale bars represent 30 µm.*

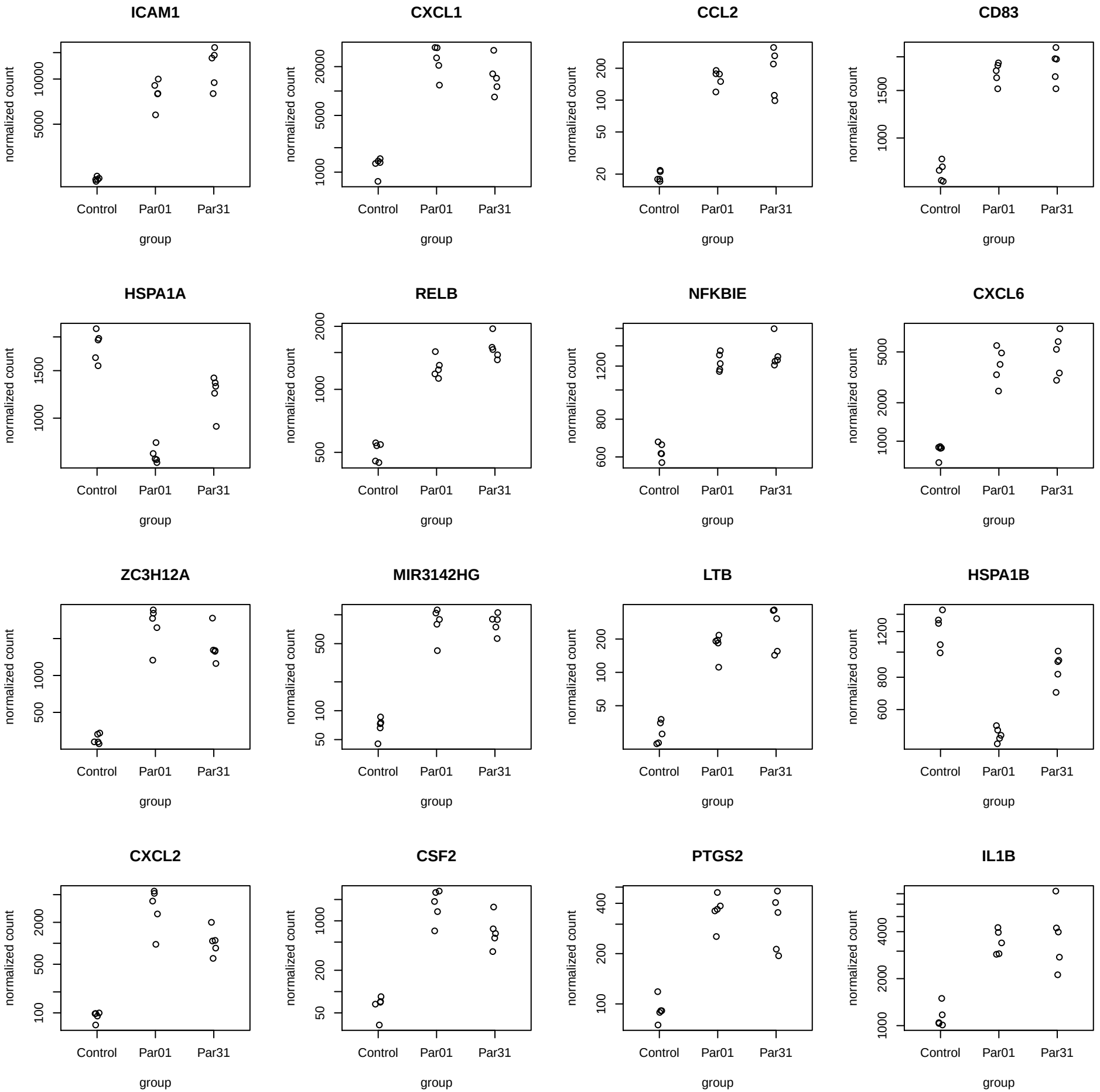
ICAM1
CXCL1
CCL2
CD83
HSPA1A
RELB
NFKBIE
CXCL6
ZC3H12A
MIR3142HG
LTB
HSPA1B
CXCL2
CSF2
PTGS2
IL1B
normalized count
group
Control
Par01
Par31

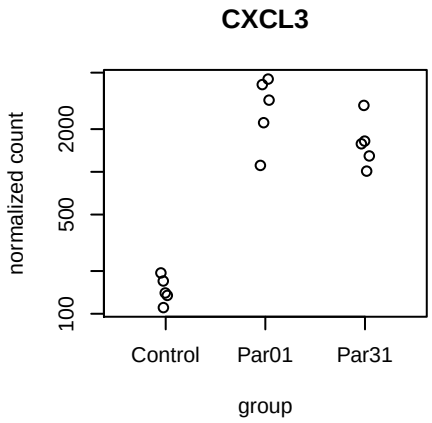
CXCL3
normalized count
100
500
2000
Control
Par01
Par31
group

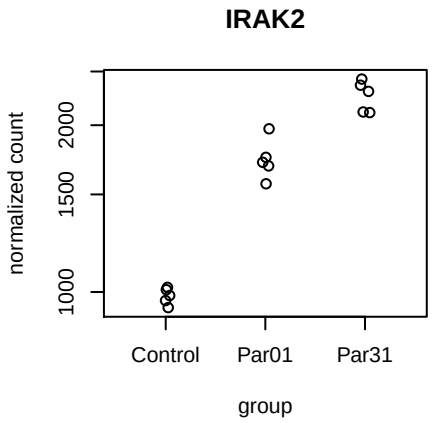
IRAK2
normalized count
1000
1500
2000
Control
Par01
Par31
group

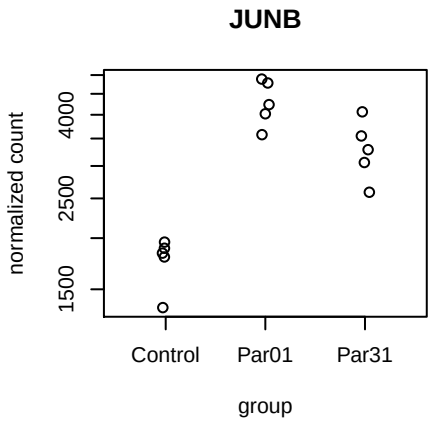
JUNB
normalized count
1500
2500
4000
Control
Par01
Par31
group

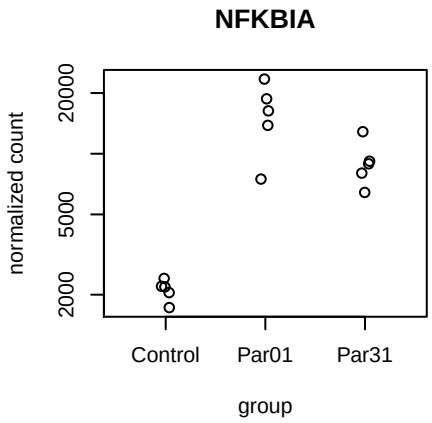
NFKBIA
normalized count
2000
5000
20000
Control
Par01
Par31
group

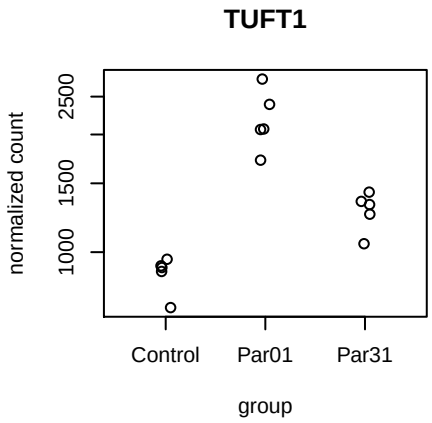
TUFT1
normalized count
1000
1500
2500
Control
Par01
Par31
group

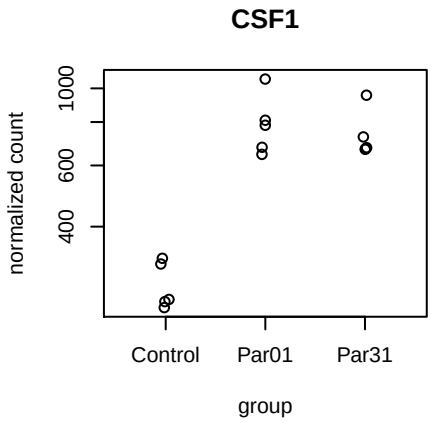
CSF1
normalized count
400
600
1000
Control
Par01
Par31
group

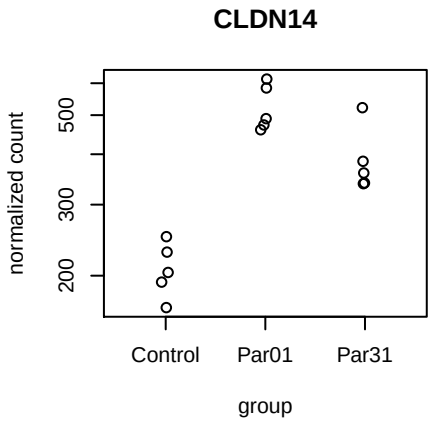
CLDN14
normalized count
200
300
500
Control
Par01
Par31
group

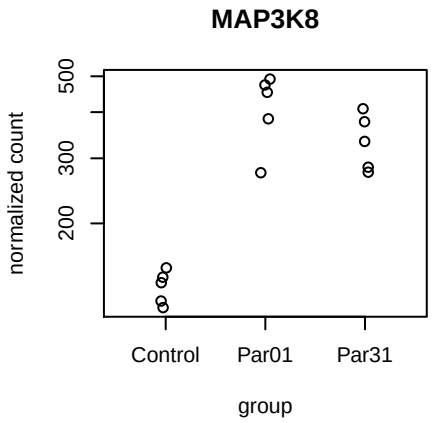
MAP3K8
normalized count
200
300
500
Control
Par01
Par31
group

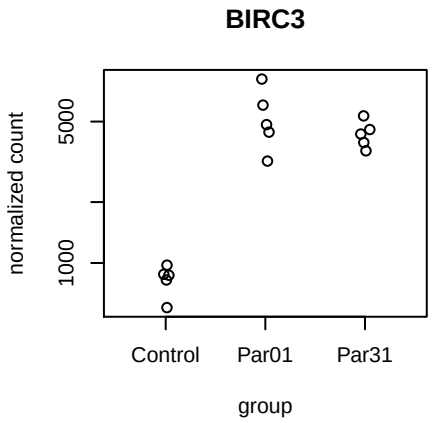
BIRC3
normalized count
1000
5000
Control
Par01
Par31
group

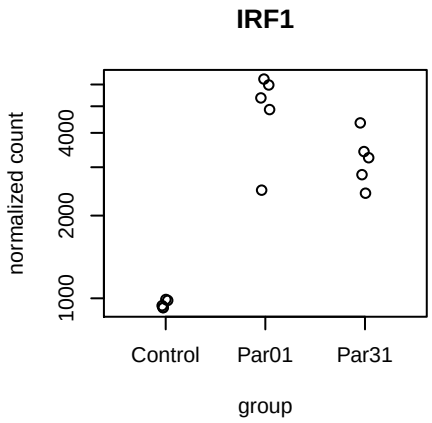
IRF1
normalized count
1000
2000
4000
Control
Par01
Par31
group

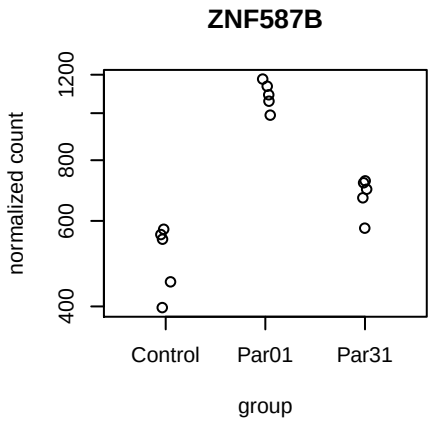
ZNF587B
normalized count
400
600
800
1200
Control
Par01
Par31
group

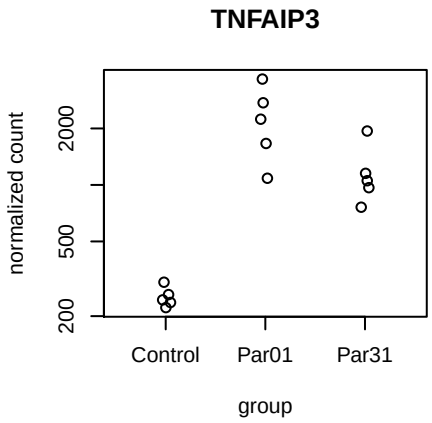
TNFAIP3
normalized count
200
500
2000
Control
Par01
Par31
group

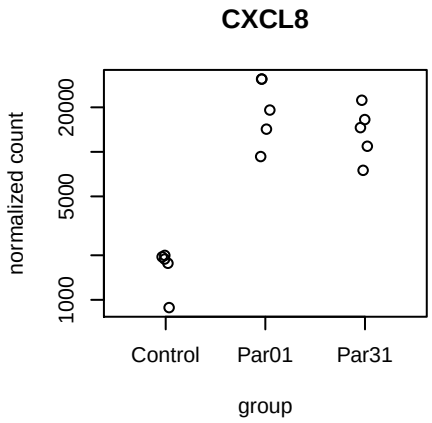
CXCL8
normalized count
1000
5000
20000
Control
Par01
Par31
group

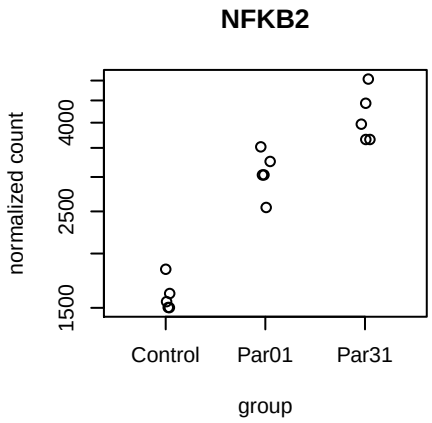
NFKB2
normalized count
1500
2500
4000
Control
Par01
Par31
group

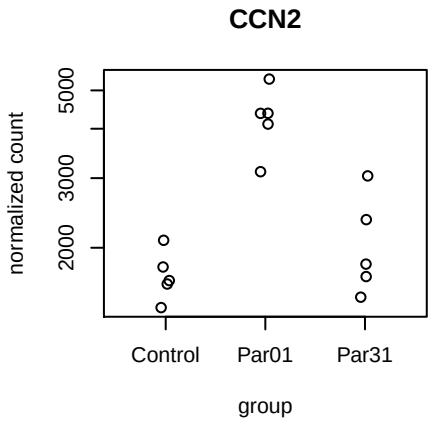
CCN2
normalized count
2000
3000
5000
Control
Par01
Par31
group

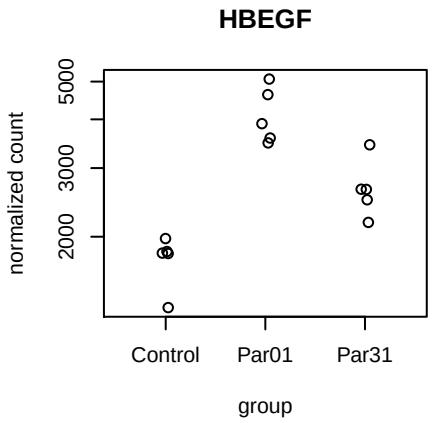
HBEGF
normalized count
2000
3000
5000
Control
Par01
Par31
group

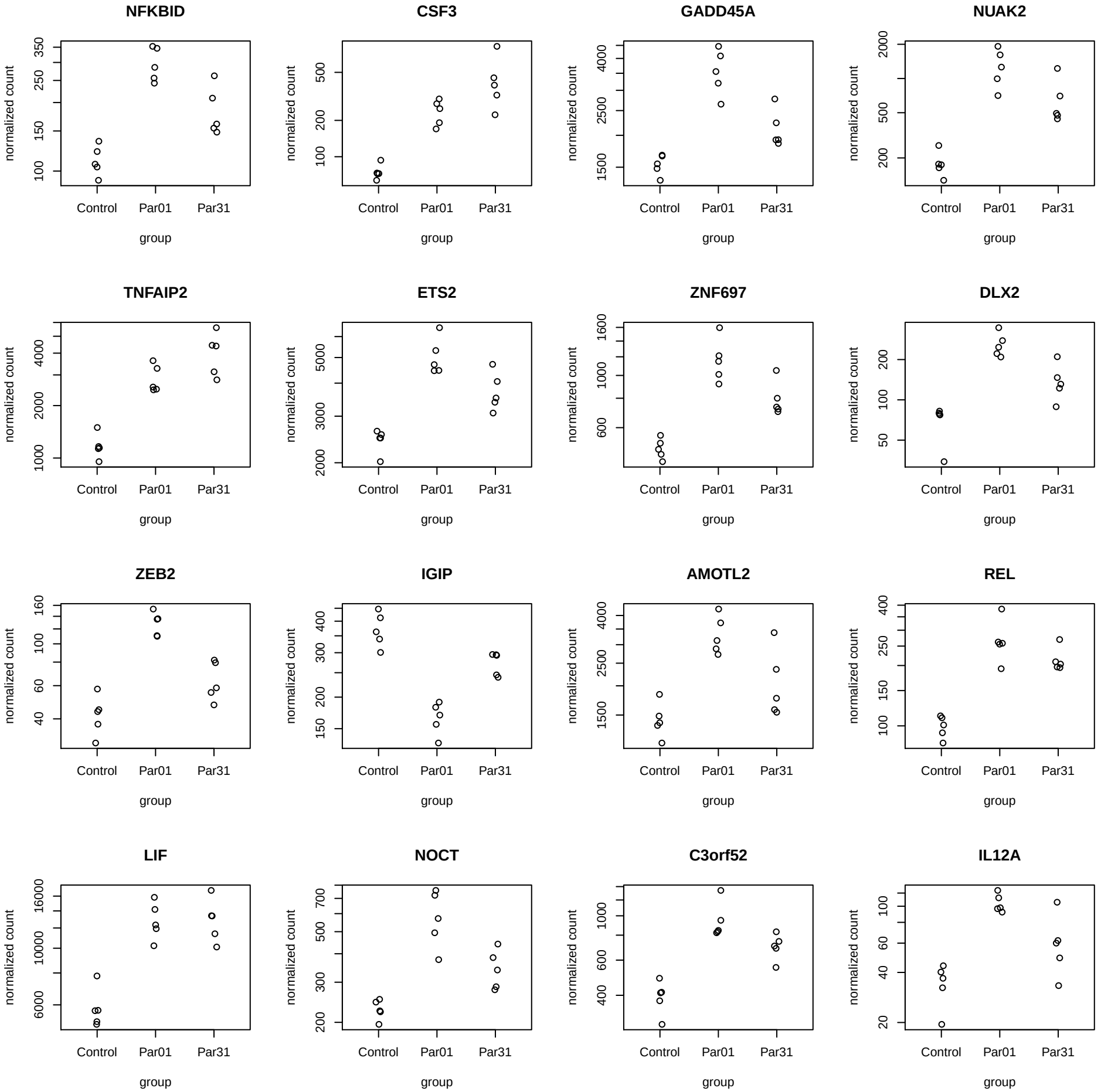
NFKBID
CSF3
GADD45A
NUAK2
TNFAIP2
ETS2
ZNF697
DLX2
ZEB2
IGIP
AMOTL2
REL
LIF
NOCT
C3orf52
IL12A
normalized count
group
Control
Par01
Par31

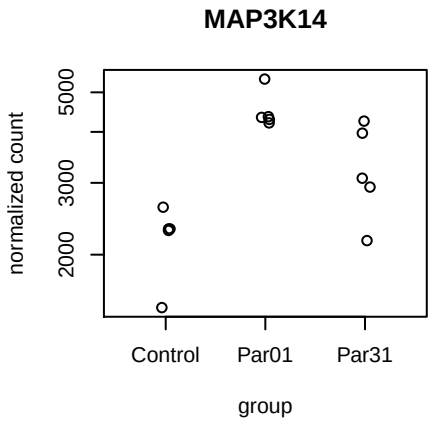
MAP3K14
normalized count
2000
3000
5000
Control
Par01
Par31
group

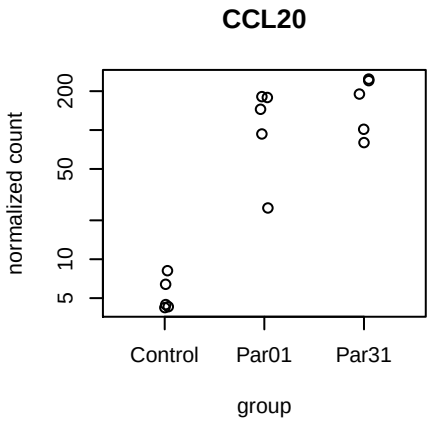
CCL20
normalized count
5
10
50
200
Control
Par01
Par31
group

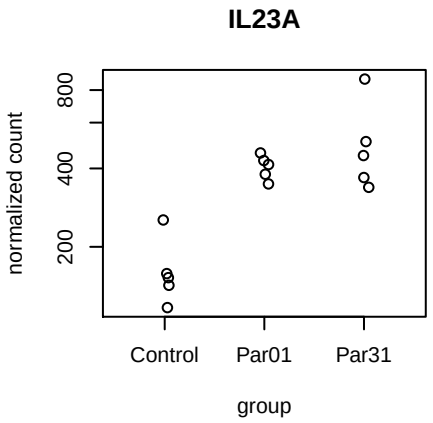
IL23A
normalized count
200
400
800
Control
Par01
Par31
group

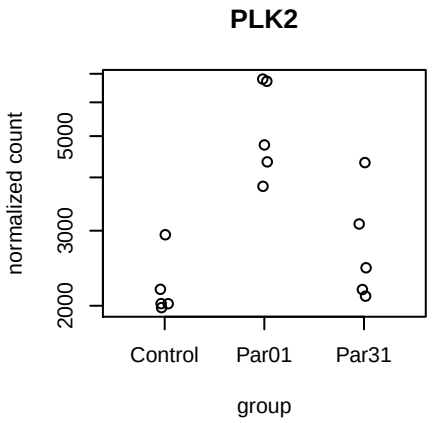
PLK2
normalized count
2000
3000
5000
Control
Par01
Par31
group

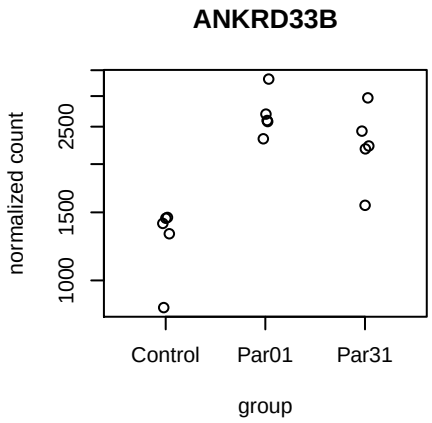
ANKRD33B
normalized count
1000
1500
2500
Control
Par01
Par31
group

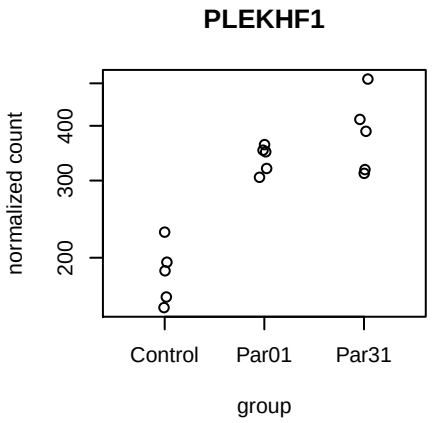
PLEKHF1
normalized count
200
300
400
Control
Par01
Par31
group

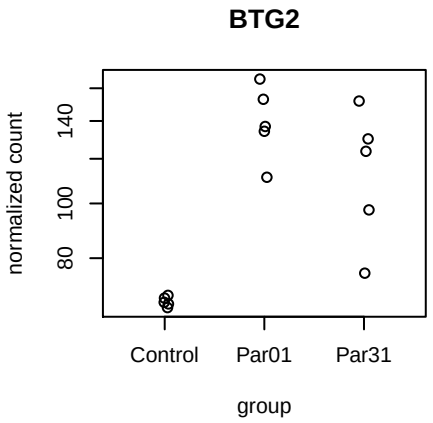
BTG2
normalized count
80
100
140
Control
Par01
Par31
group

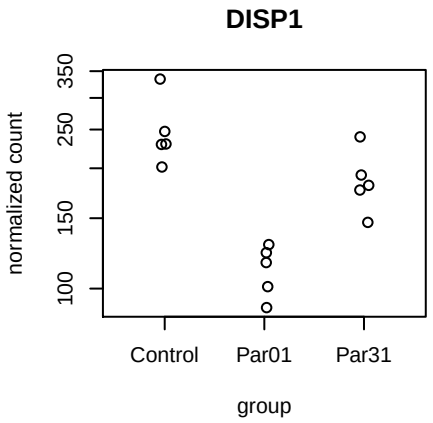
DISP1
normalized count
100
150
250
350
Control
Par01
Par31
group

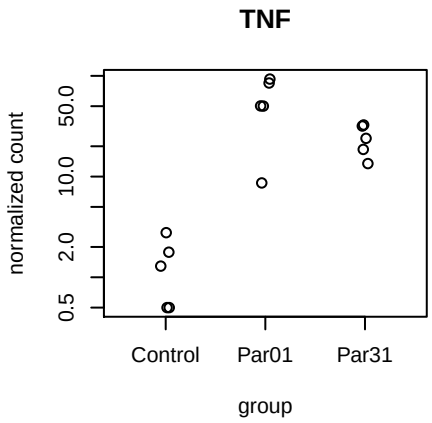
TNF
normalized count
0.5
2.0
10.0
50.0
Control
Par01
Par31
group

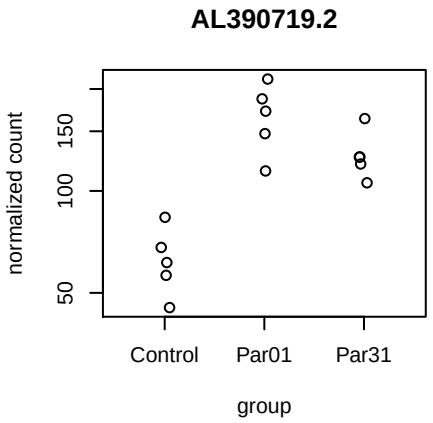
AL390719.2
normalized count
50
100
150
Control
Par01
Par31
group

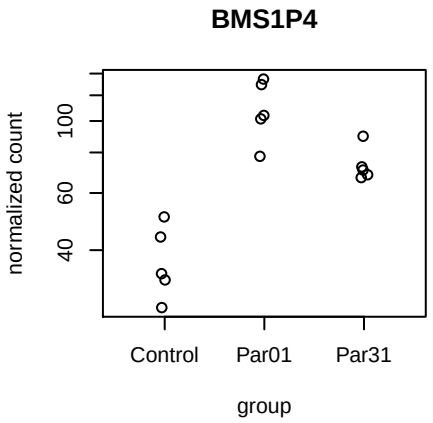
BMS1P4
normalized count
40
60
100
Control
Par01
Par31
group

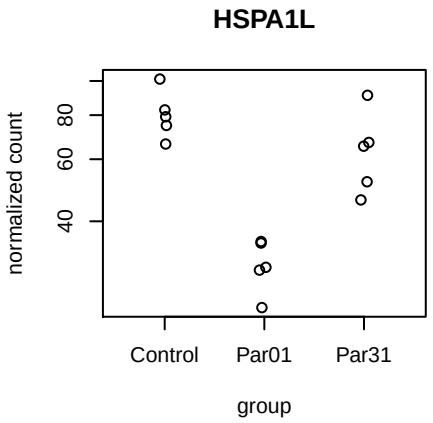
HSPA1L
normalized count
40
60
80
Control
Par01
Par31
group

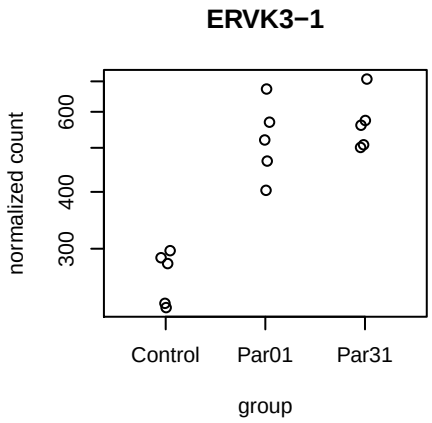
ERVK3−1
normalized count
300
400
600
Control
Par01
Par31
group

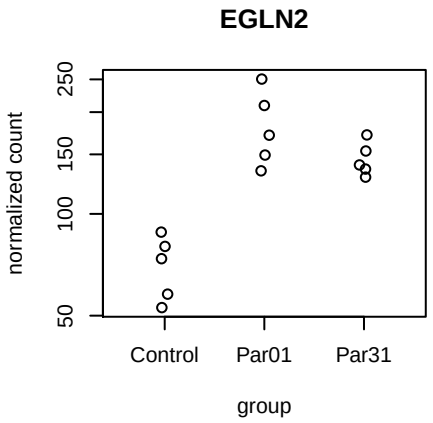
EGLN2
normalized count
50
100
150
250
Control
Par01
Par31
group

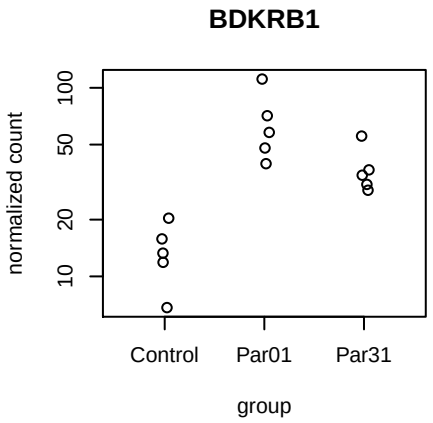
BDKRB1
normalized count
10
20
50
100
Control
Par01
Par31
group

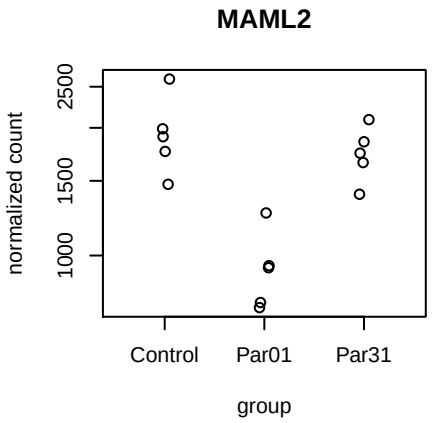
MAML2
normalized count
1000
1500
2500
Control
Par01
Par31
group

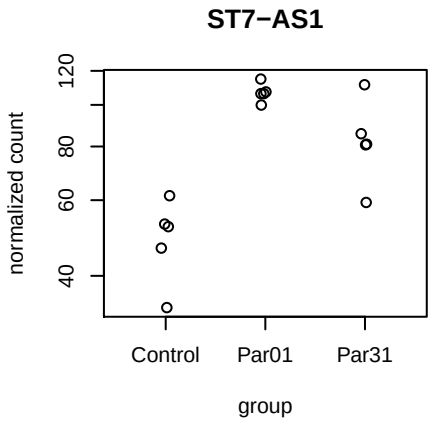
ST7−AS1
normalized count
40
60
80
120
Control
Par01
Par31
group

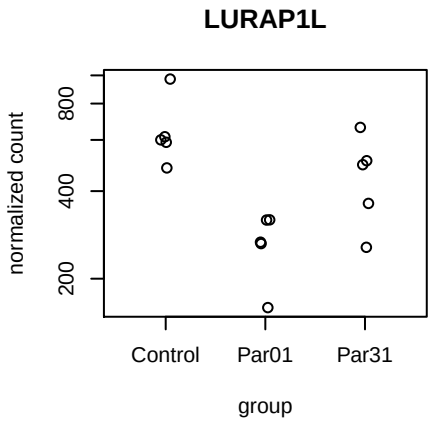
LURAP1L
normalized count
200
400
800
Control
Par01
Par31
group

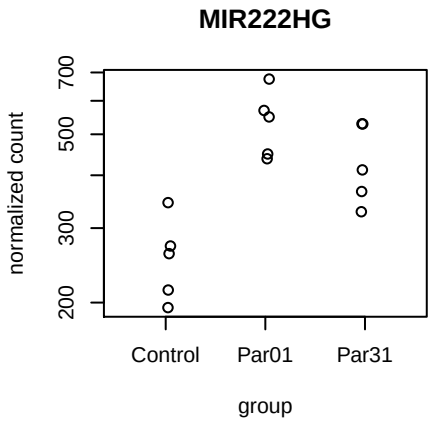
MIR222HG
normalized count
200
300
500
700
Control
Par01
Par31
group

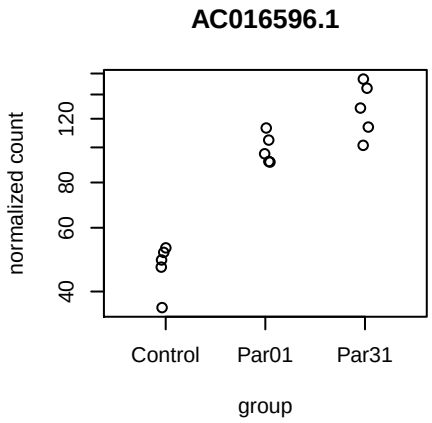
AC016596.1
normalized count
40
60
80
120
Control
Par01
Par31
group

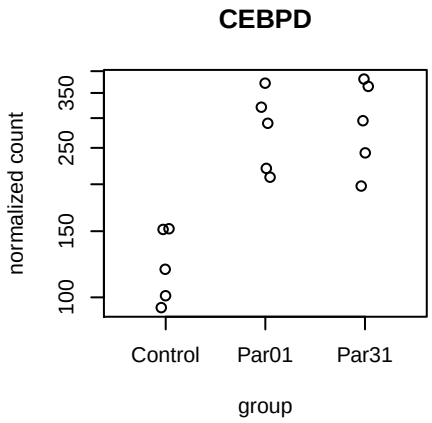
CEBPD
normalized count
100
150
250
350
Control
Par01
Par31
group

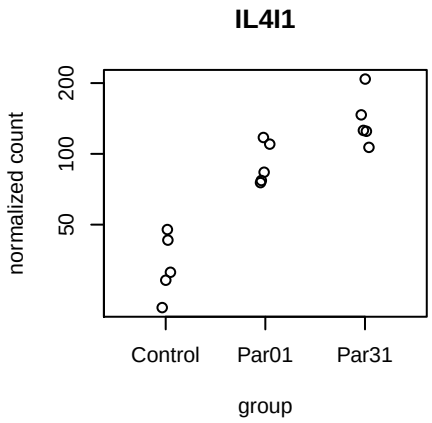
IL4I1
normalized count
50
100
200
Control
Par01
Par31
group

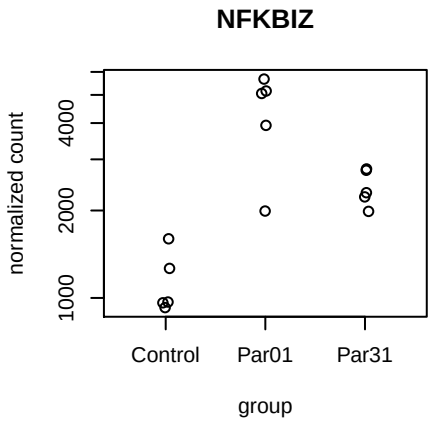
NFKBIZ
normalized count
1000
2000
4000
Control
Par01
Par31
group

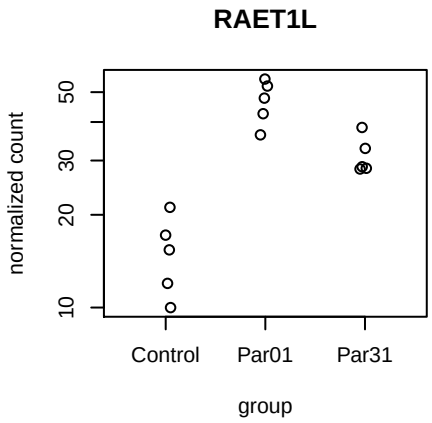
RAET1L
normalized count
10
20
30
50
Control
Par01
Par31
group

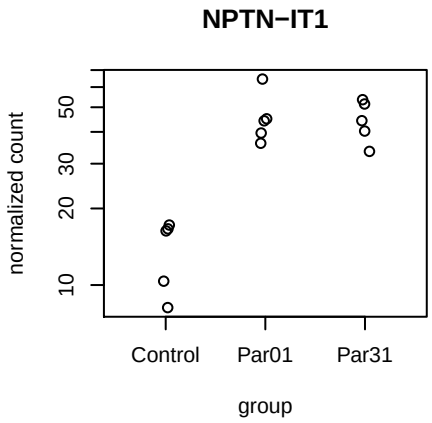
NPTN−IT1
normalized count
10
20
30
50
Control
Par01
Par31
group

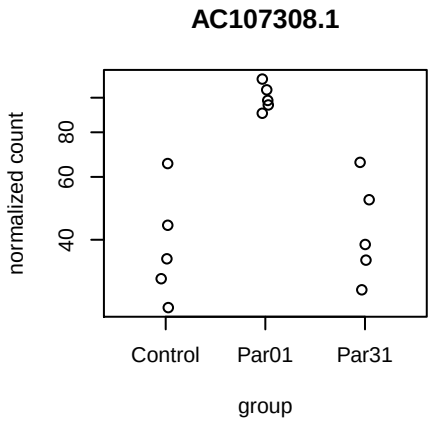
AC107308.1
normalized count
40
60
80
Control
Par01
Par31
group

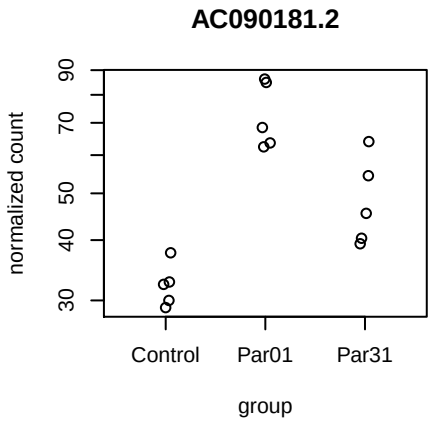
AC090181.2
normalized count
30
40
50
70
90
Control
Par01
Par31
group

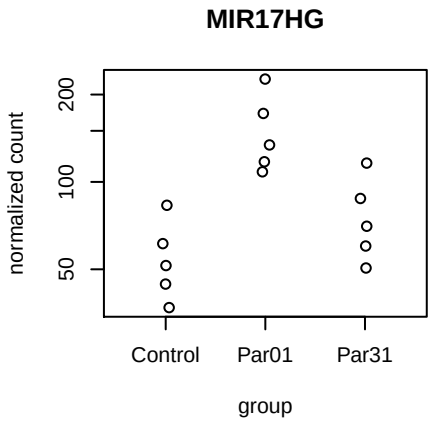
MIR17HG
normalized count
50
100
200
Control
Par01
Par31
group

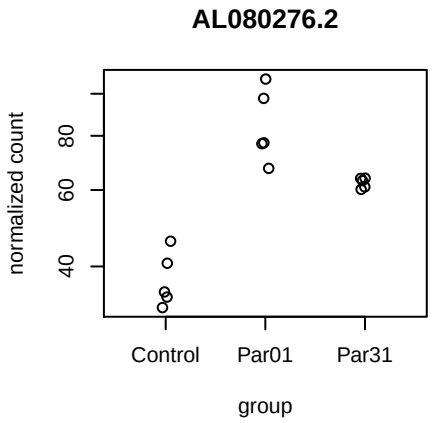
AL080276.2
normalized count
40
60
80
Control
Par01
Par31
group

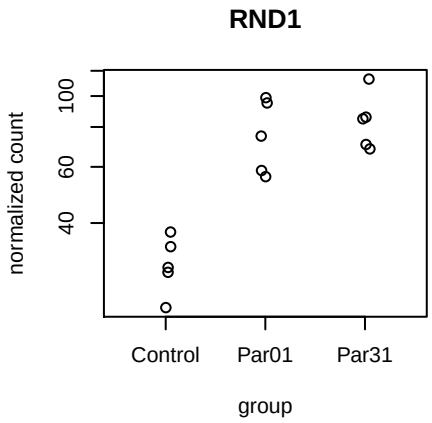
RND1
normalized count
40
60
100
Control
Par01
Par31
group

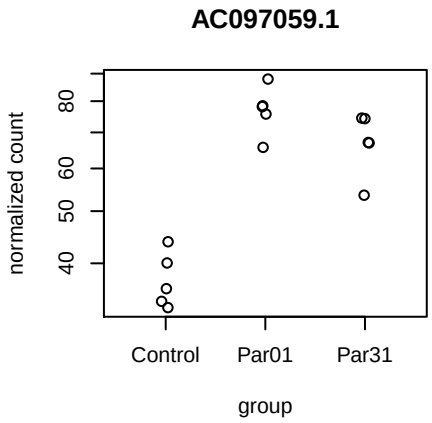
AC097059.1
normalized count
40
50
60
80
Control
Par01
Par31
group

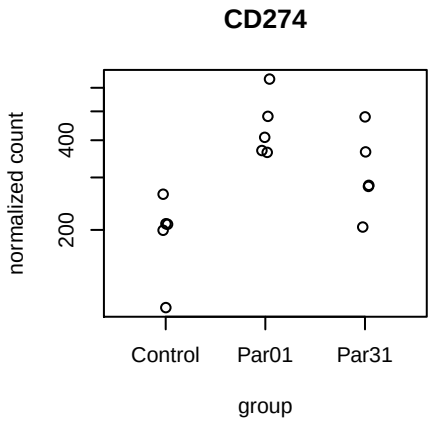
CD274
normalized count
200
400
Control
Par01
Par31
group

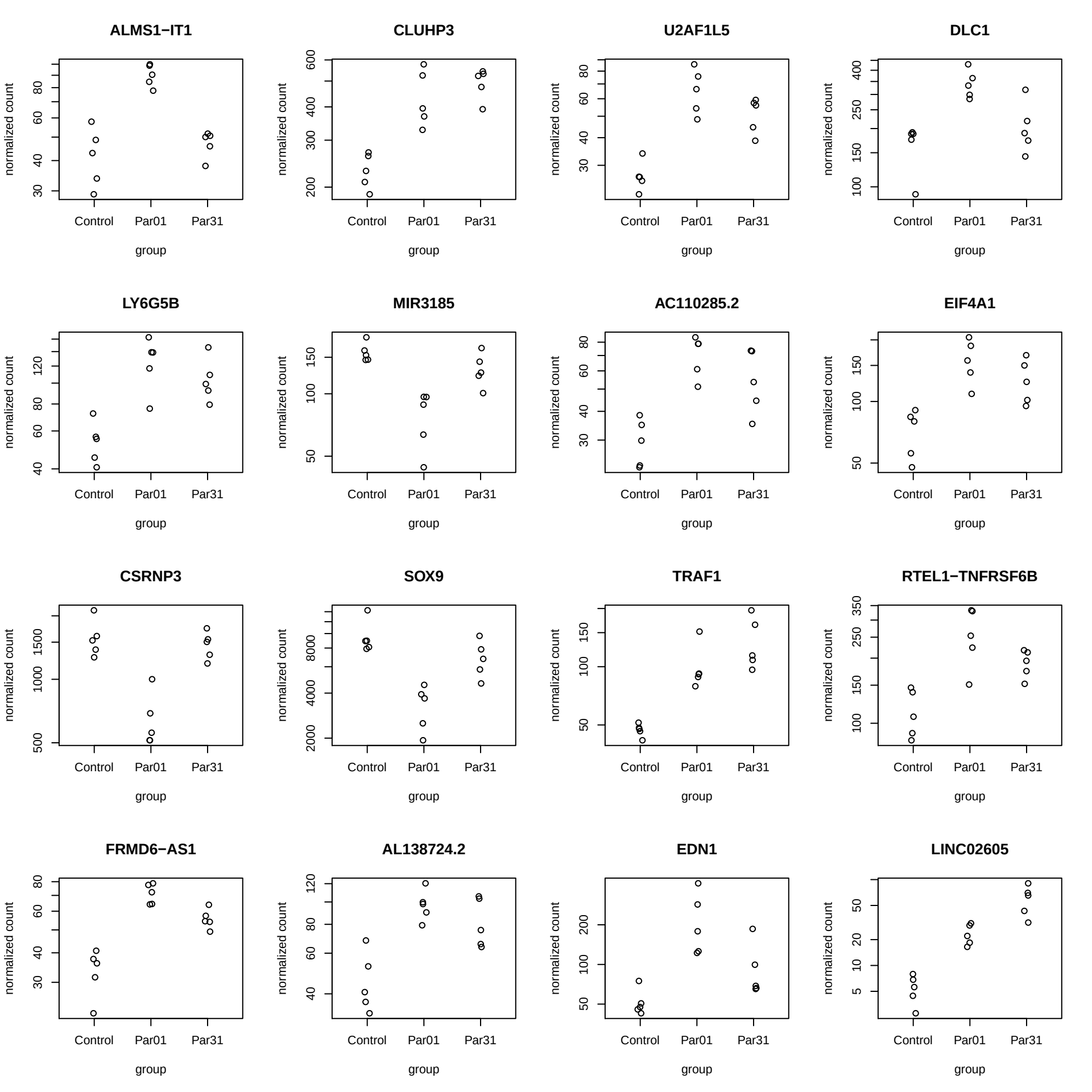
ALMS1−IT1
CLUHP3
U2AF1L5
DLC1
LY6G5B
MIR3185
AC110285.2
EIF4A1
CSRNP3
SOX9
TRAF1
RTEL1−TNFRSF6B
FRMD6−AS1
AL138724.2
EDN1
LINC02605
normalized count
group
Control
Par01
Par31

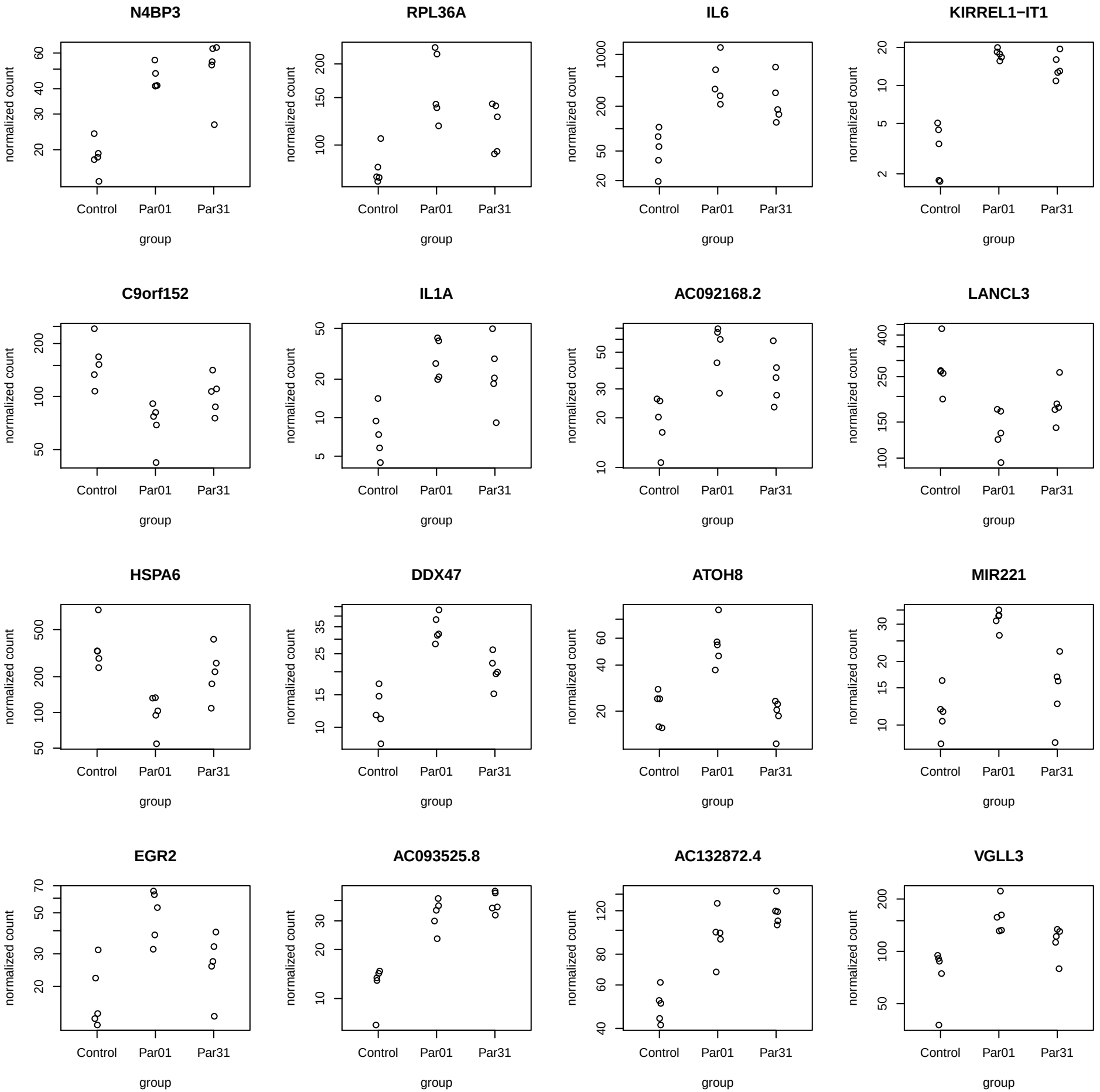
N4BP3
RPL36A
IL6
KIRREL1−IT1
C9orf152
IL1A
AC092168.2
LANCL3
HSPA6
DDX47
ATOH8
MIR221
EGR2
AC093525.8
AC132872.4
VGLL3
normalized count
Control
Par01
Par31
group

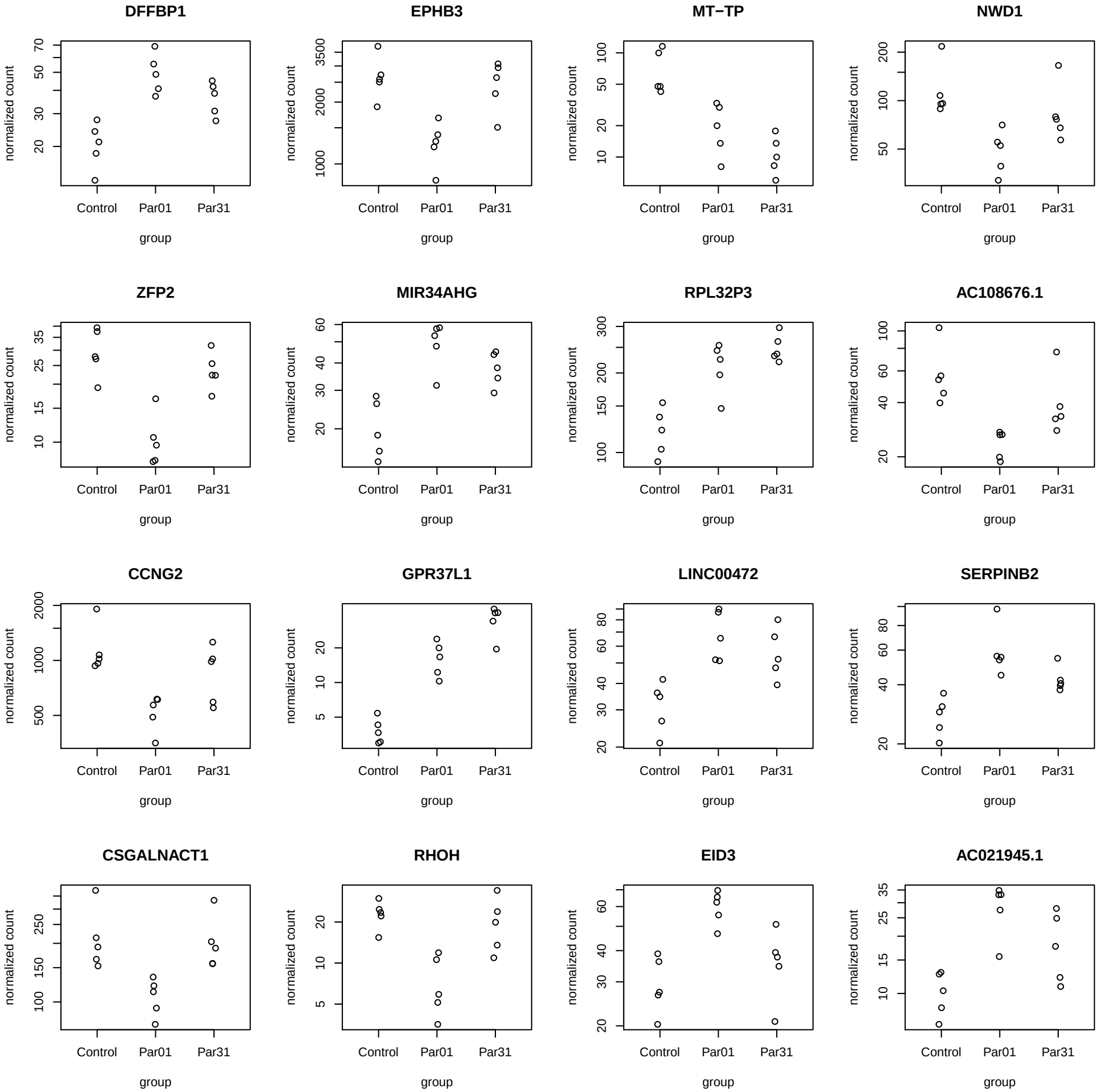
DFFBP1
EPHB3
MT−TP
NWD1
ZFP2
MIR34AHG
RPL32P3
AC108676.1
CCNG2
GPR37L1
LINC00472
SERPINB2
CSGALNACT1
RHOH
EID3
AC021945.1
normalized count
group
Control
Par01
Par31

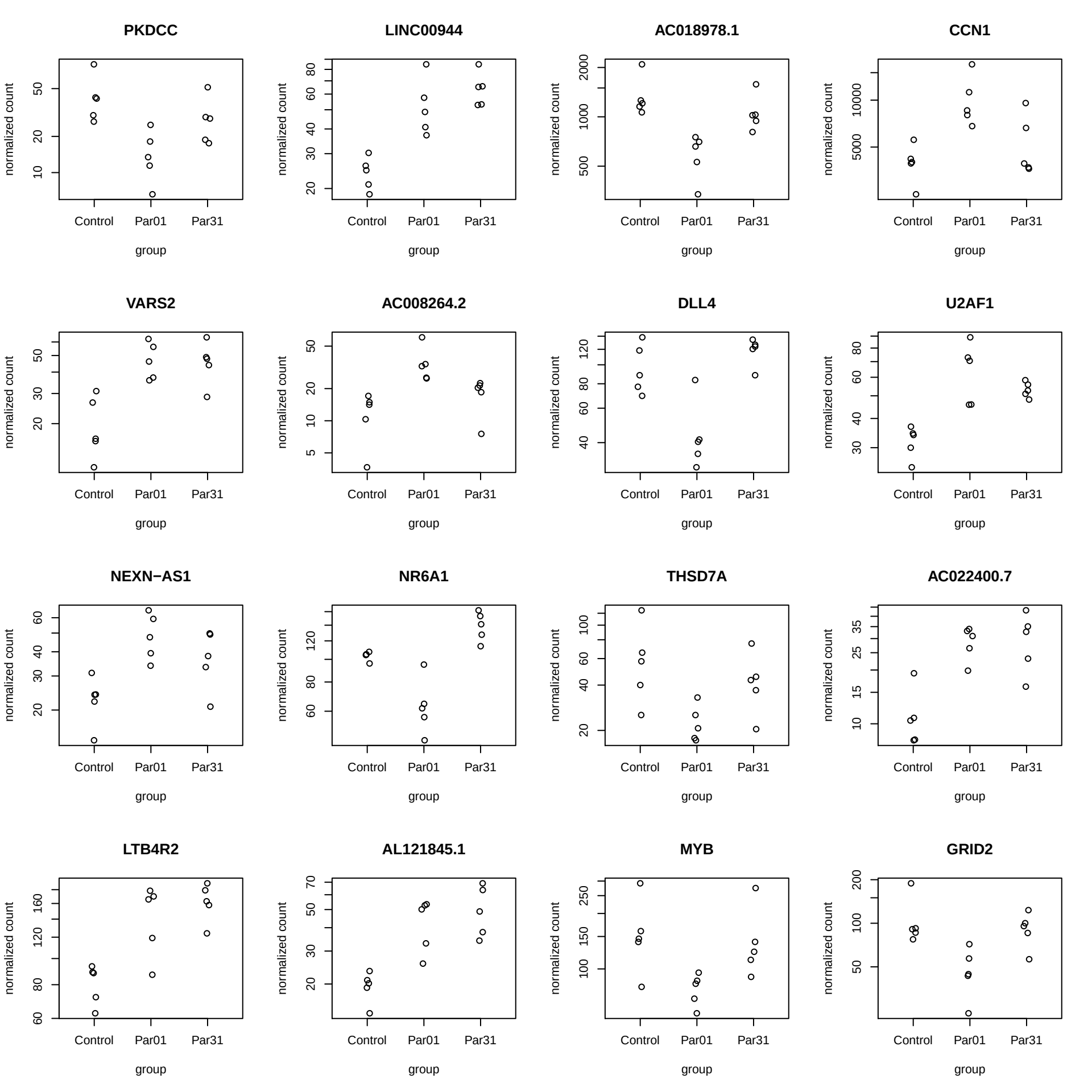
PKDCC
LINC00944
AC018978.1
CCN1
VARS2
AC008264.2
DLL4
U2AF1
NEXN−AS1
NR6A1
THSD7A
AC022400.7
LTB4R2
AL121845.1
MYB
GRID2
normalized count
Control
Par01
Par31
group

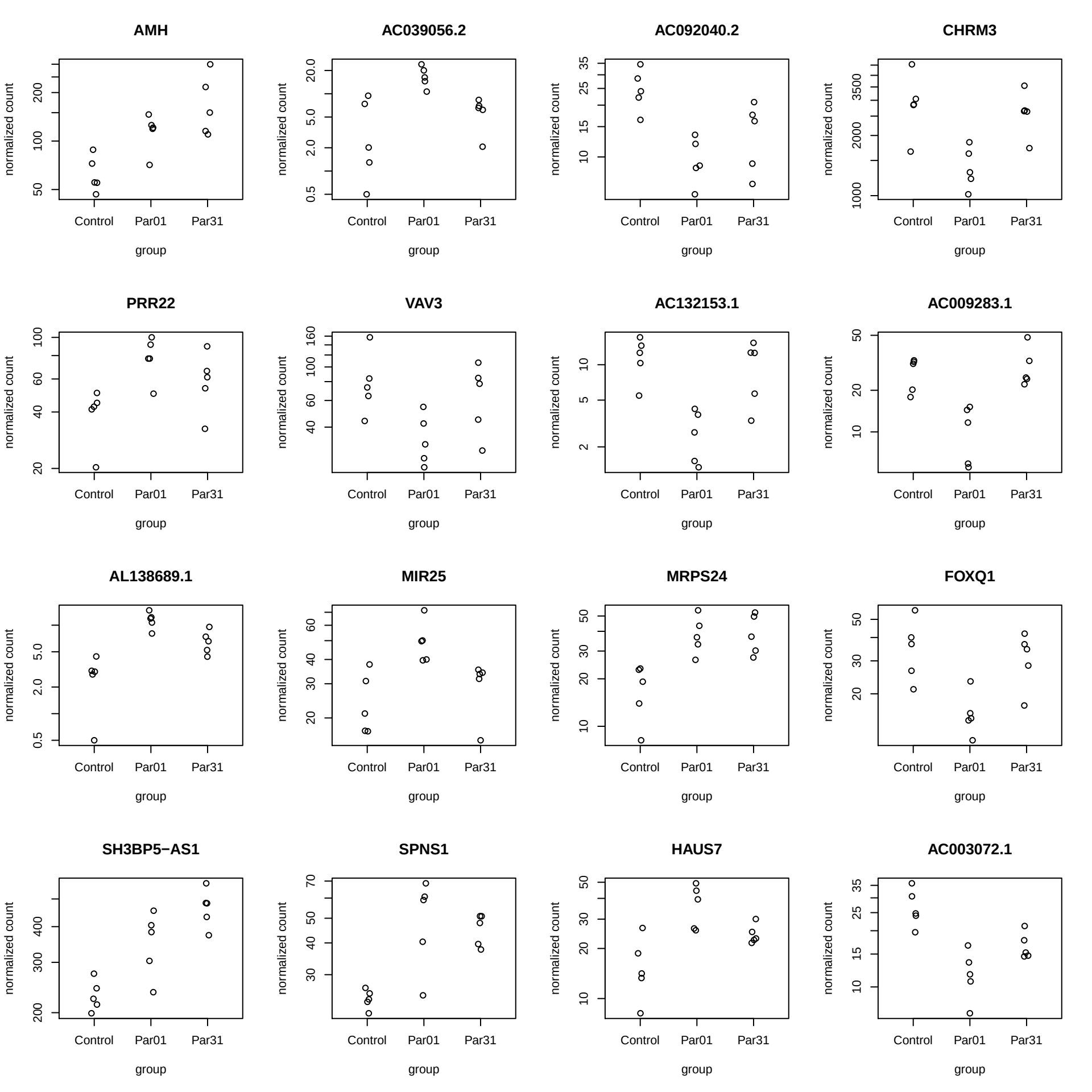
AMH
AC039056.2
AC092040.2
CHRM3
PRR22
VAV3
AC132153.1
AC009283.1
AL138689.1
MIR25
MRPS24
FOXQ1
SH3BP5−AS1
SPNS1
HAUS7
AC003072.1
normalized count
group
Control
Par01
Par31

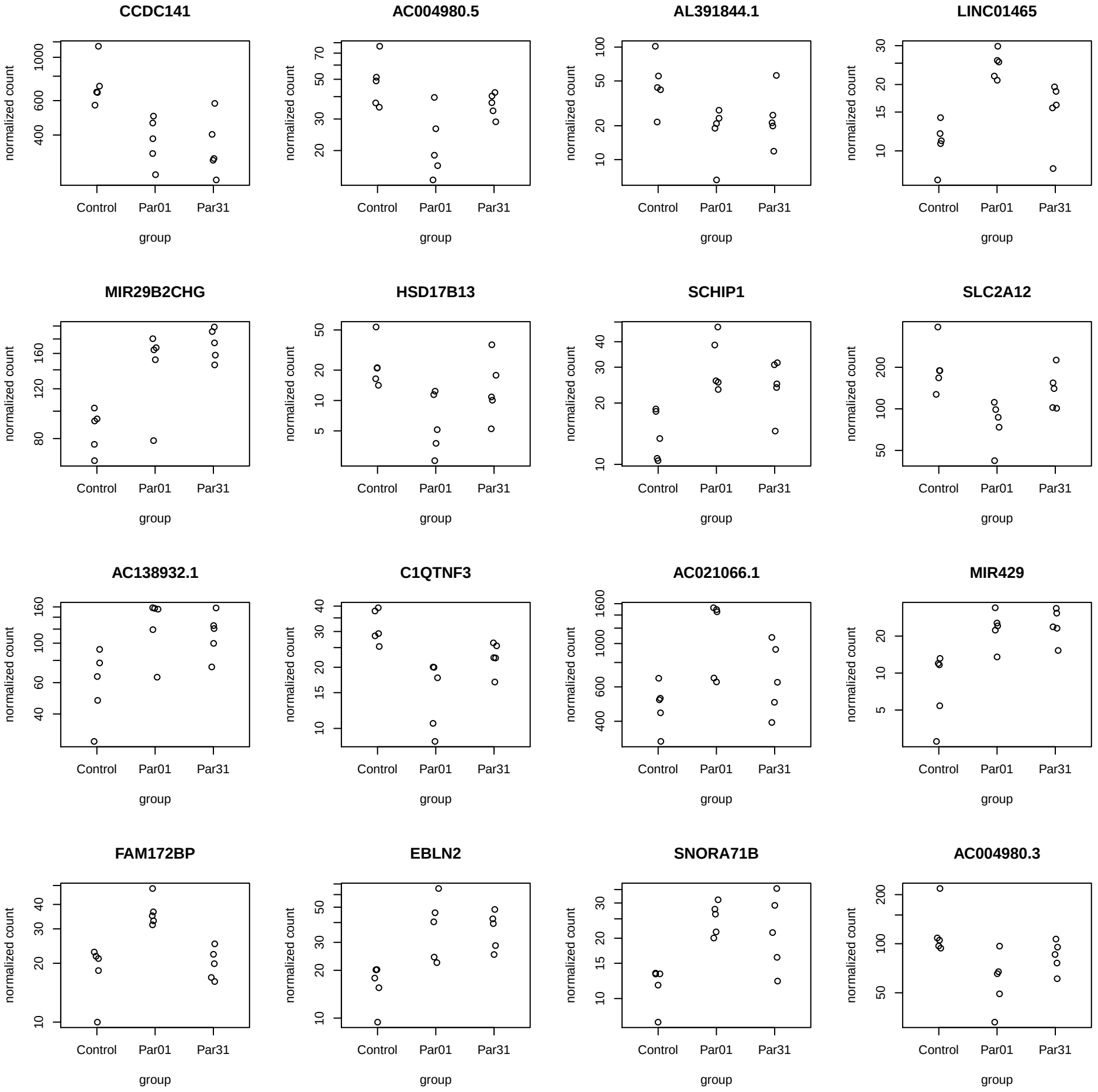
CCDC141
AC004980.5
AL391844.1
LINC01465
MIR29B2CHG
HSD17B13
SCHIP1
SLC2A12
AC138932.1
C1QTNF3
AC021066.1
MIR429
FAM172BP
EBLN2
SNORA71B
AC004980.3
normalized count
group
Control
Par01
Par31

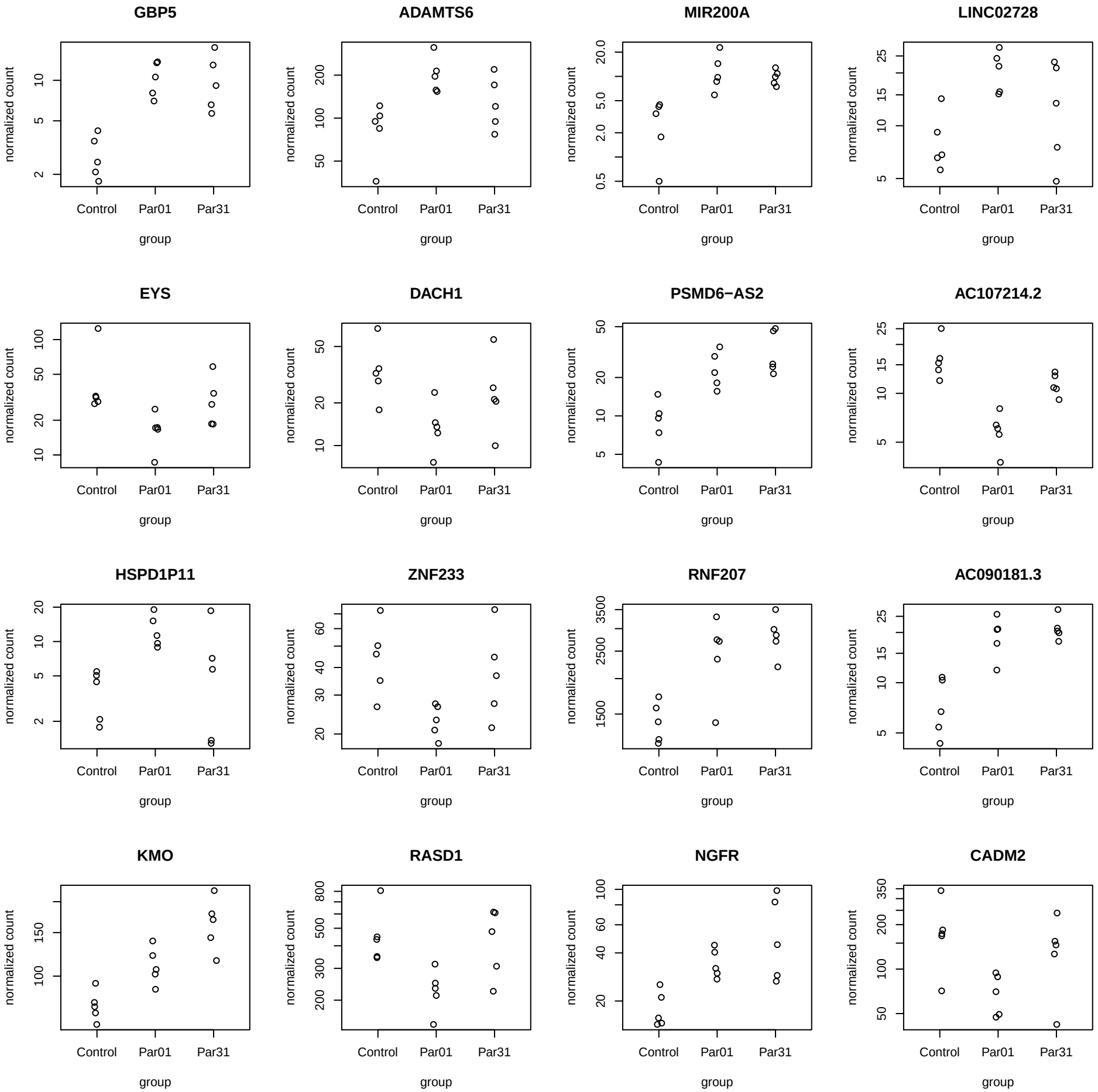
GBP5
ADAMTS6
MIR200A
LINC02728
EYS
DACH1
PSMD6−AS2
AC107214.2
HSPD1P11
ZNF233
RNF207
AC090181.3
KMO
RASD1
NGFR
CADM2
normalized count
Control
Par01
Par31
group

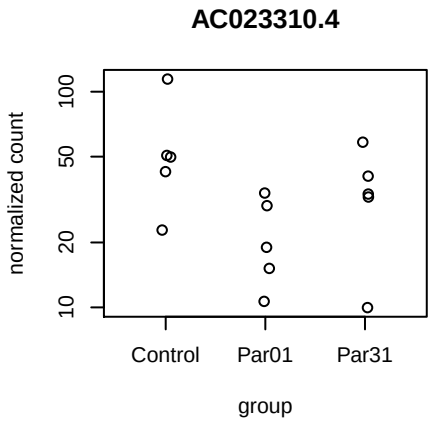
AC023310.4
normalized count
10
20
50
100
Control
Par01
Par31
group

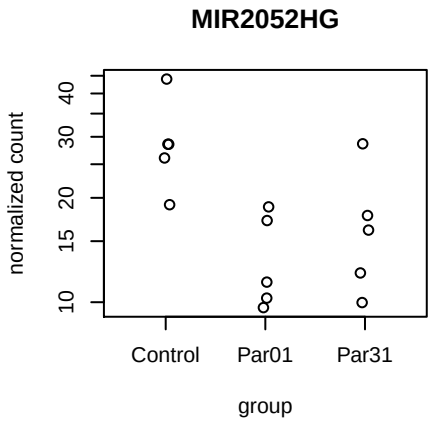
MIR2052HG
normalized count
10
15
20
30
40
Control
Par01
Par31
group

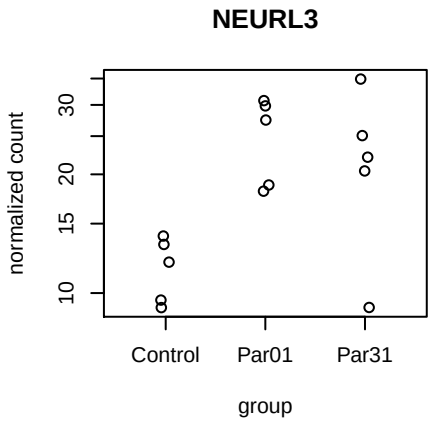
NEURL3
normalized count
10
15
20
30
Control
Par01
Par31
group

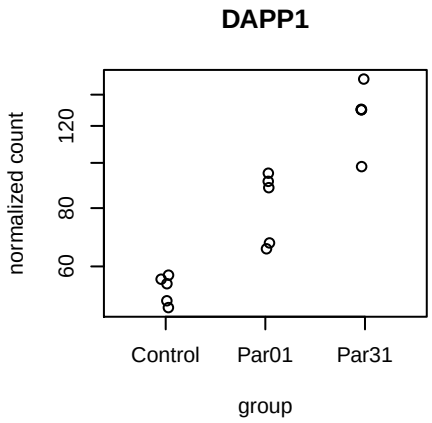
DAPP1
normalized count
60
80
120
Control
Par01
Par31
group

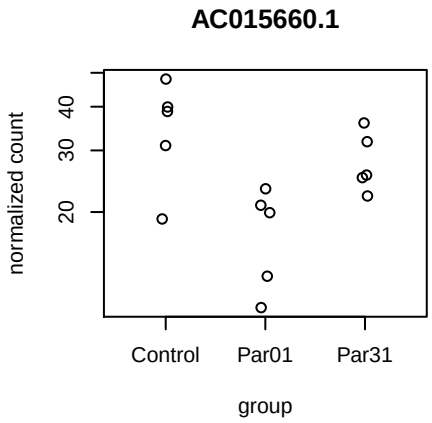
AC015660.1
normalized count
20
30
40
Control
Par01
Par31
group

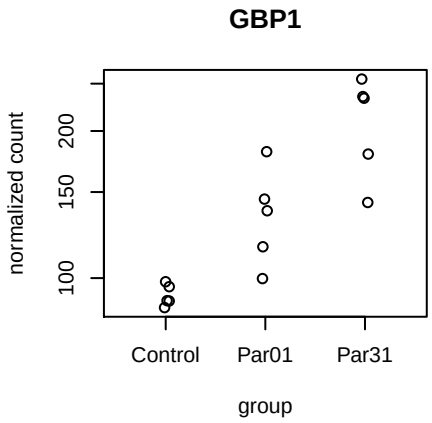
GBP1
normalized count
100
150
200
Control
Par01
Par31
group

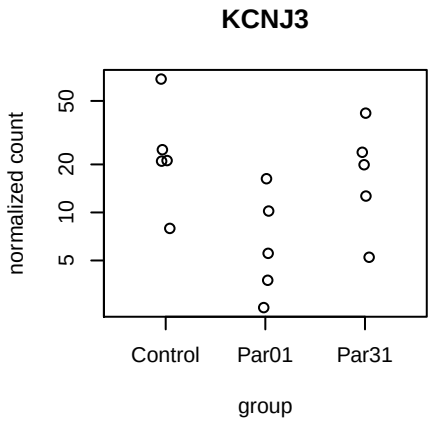
KCNJ3
normalized count
5
10
20
50
Control
Par01
Par31
group

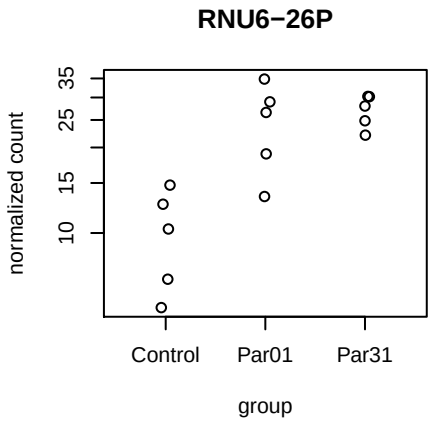
RNU6−26P
normalized count
10
15
25
35
Control
Par01
Par31
group

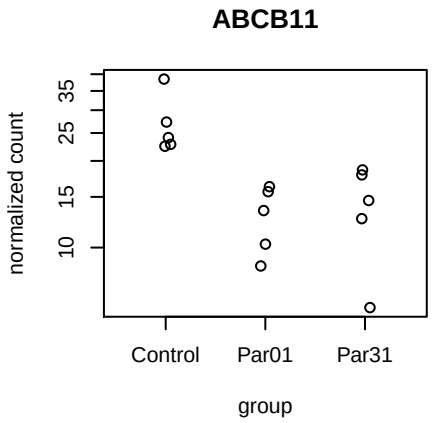
ABCB11
normalized count
10
15
25
35
Control
Par01
Par31
group

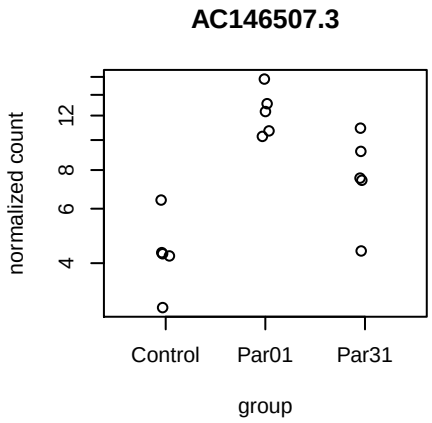
AC146507.3
normalized count
4
6
8
12
Control
Par01
Par31
group

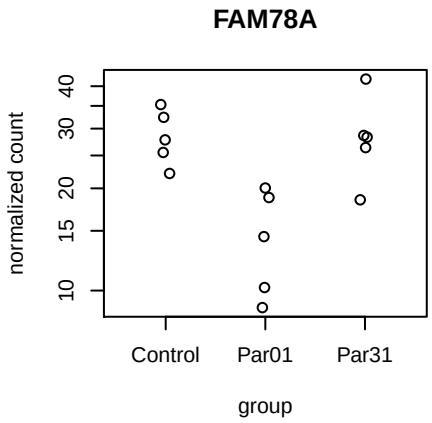
FAM78A
normalized count
10
15
20
30
40
Control
Par01
Par31
group

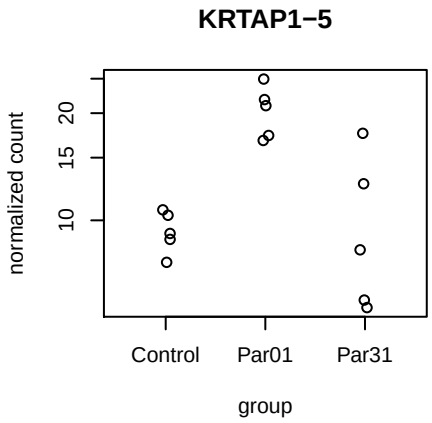
KRTAP1−5
normalized count
10
15
20
Control
Par01
Par31
group

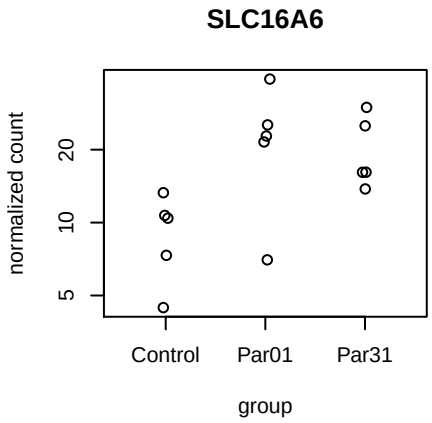
SLC16A6
normalized count
5
10
20
Control
Par01
Par31
group

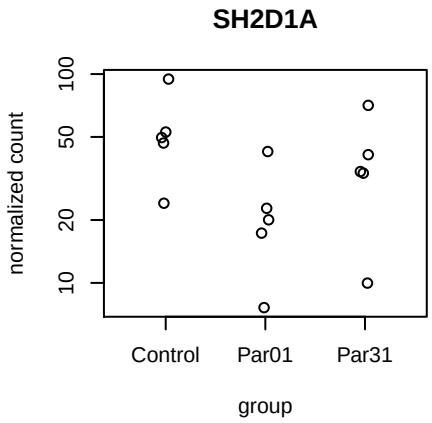
SH2D1A
normalized count
10
20
50
100
Control
Par01
Par31
group

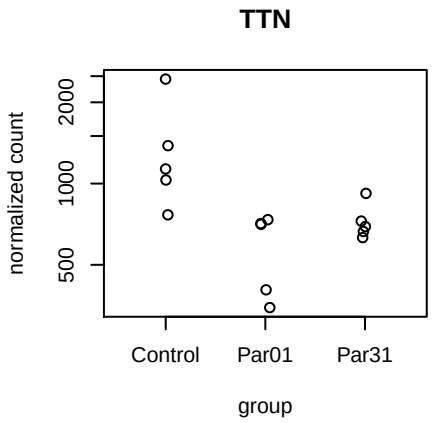
TTN
normalized count
500
1000
2000
Control
Par01
Par31
group

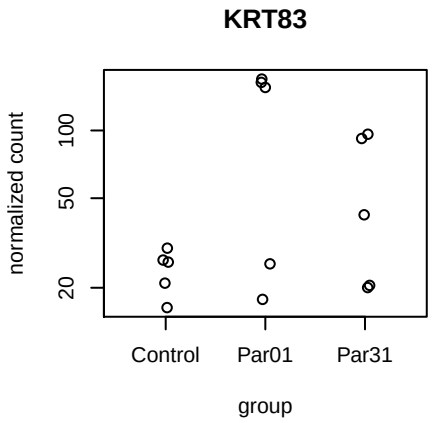
KRT83
normalized count
20
50
100
Control
Par01
Par31
group

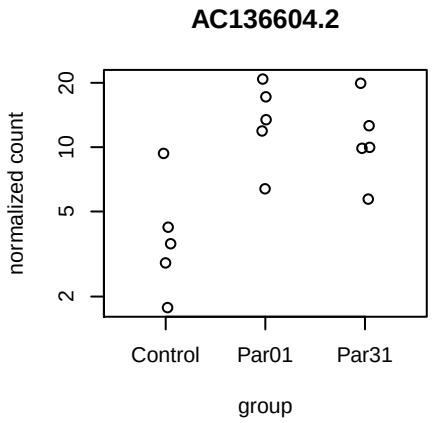
AC136604.2
normalized count
2
5
10
20
Control
Par01
Par31
group

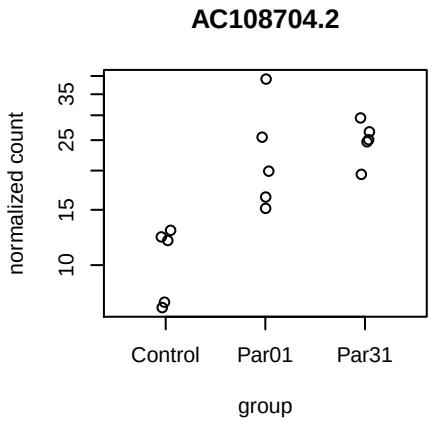
AC108704.2
normalized count
10
15
25
35
Control
Par01
Par31
group

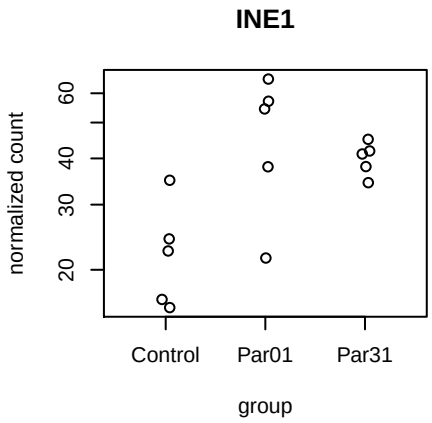
INE1
normalized count
20
30
40
60
Control
Par01
Par31
group

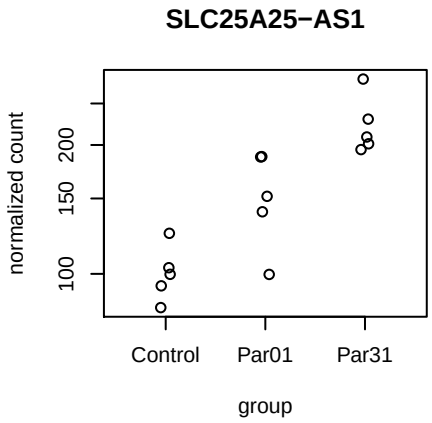
SLC25A25−AS1
normalized count
100
150
200
Control
Par01
Par31
group

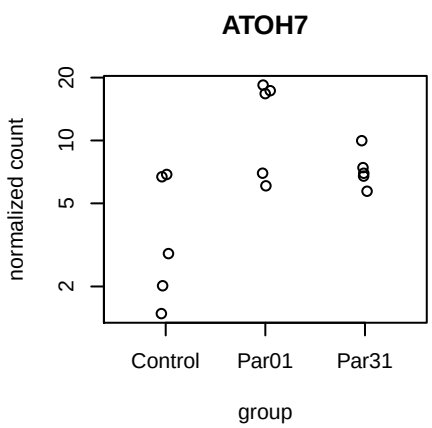
ATOH7
normalized count
2
5
10
20
Control
Par01
Par31
group

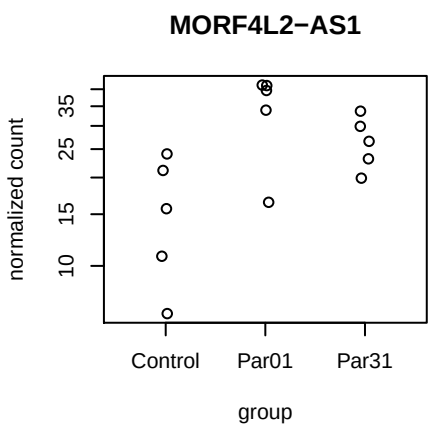
MORF4L2−AS1
normalized count
10
15
25
35
Control
Par01
Par31
group

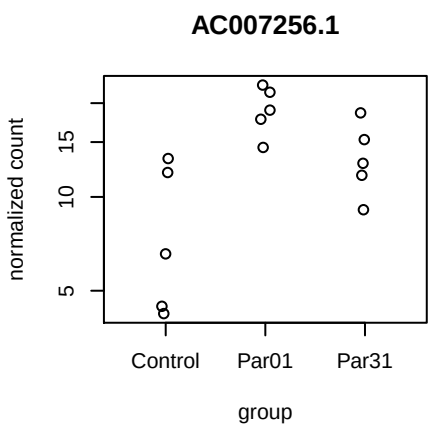
AC007256.1
normalized count
5
10
15
Control
Par01
Par31
group

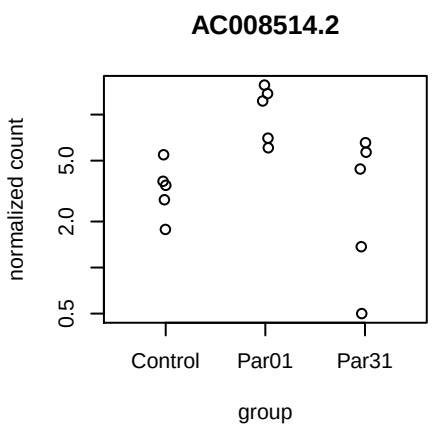
AC008514.2
normalized count
0.5
2.0
5.0
Control
Par01
Par31
group

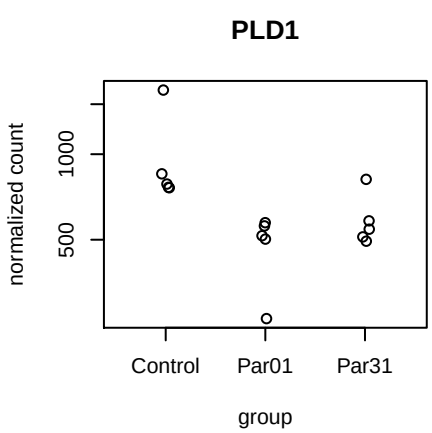
PLD1
normalized count
500
1000
Control
Par01
Par31
group

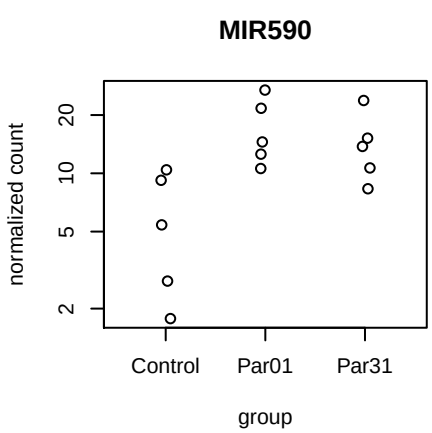
MIR590
normalized count
2
5
10
20
Control
Par01
Par31
group

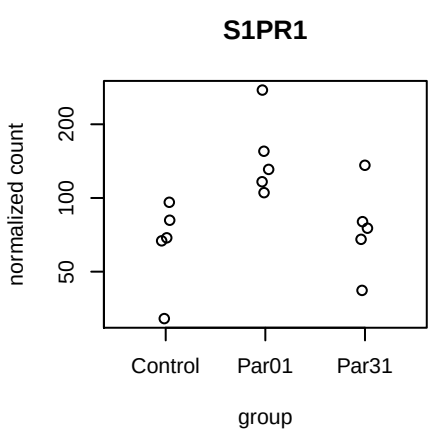
S1PR1
normalized count
50
100
200
Control
Par01
Par31
group

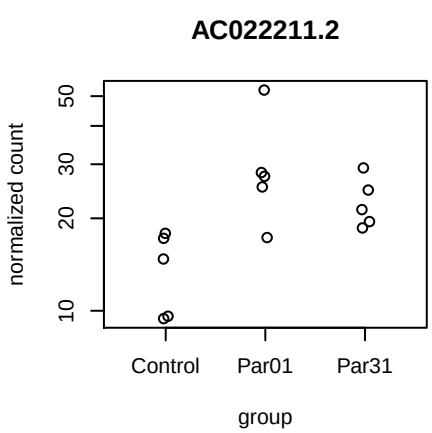
AC022211.2
normalized count
10
20
30
50
Control
Par01
Par31
group

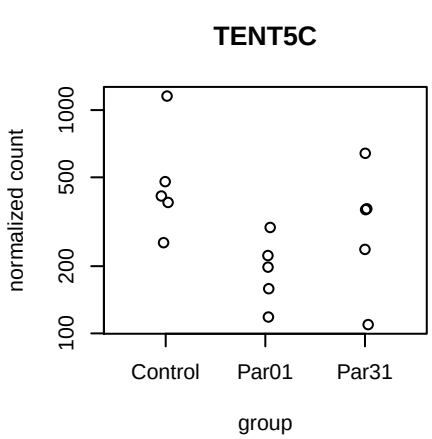
TENT5C
normalized count
100
200
500
1000
Control
Par01
Par31
group

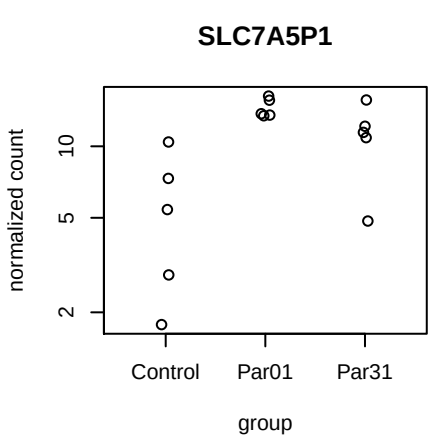
SLC7A5P1
normalized count
2
5
10
Control
Par01
Par31
group

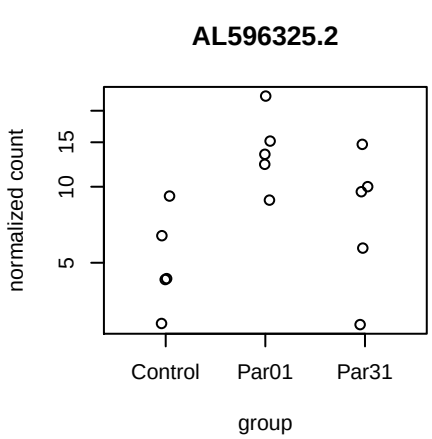
AL596325.2
normalized count
5
10
15
Control
Par01
Par31
group

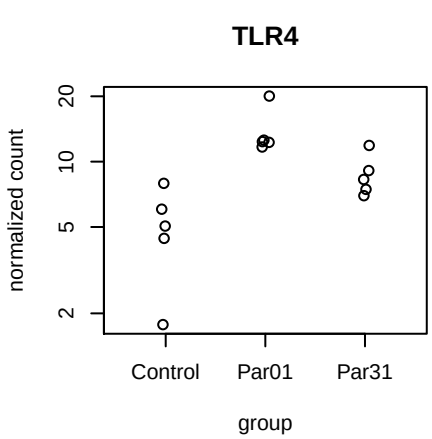
TLR4
normalized count
2
5
10
20
Control
Par01
Par31
group

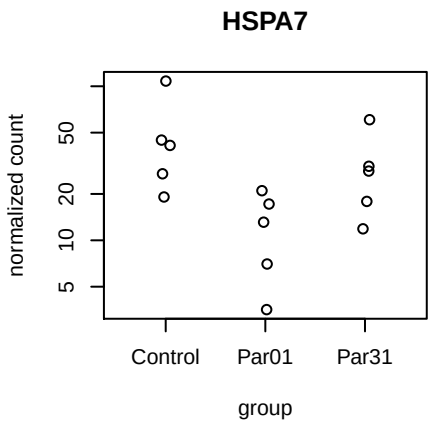
HSPA7
normalized count
5
10
20
50
Control
Par01
Par31
group

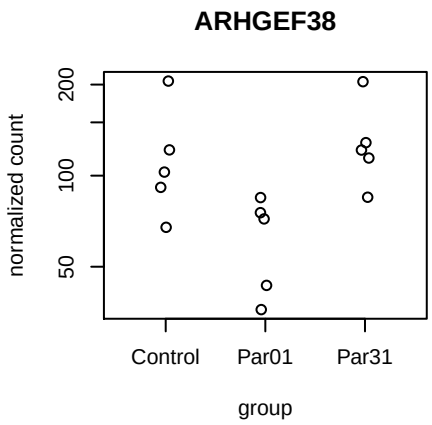
ARHGEF38
normalized count
50
100
200
Control
Par01
Par31
group

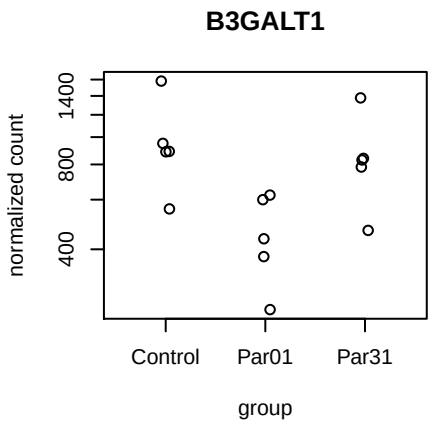
B3GALT1
normalized count
400
800
1400
Control
Par01
Par31
group

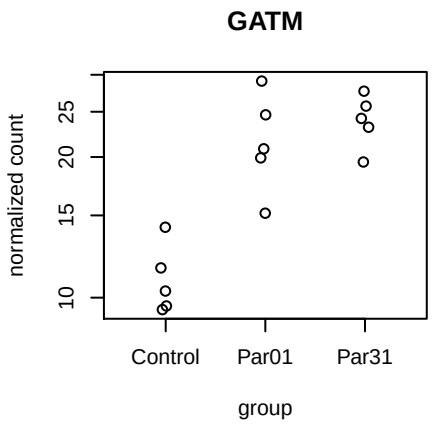
GATM
normalized count
10
15
20
25
Control
Par01
Par31
group

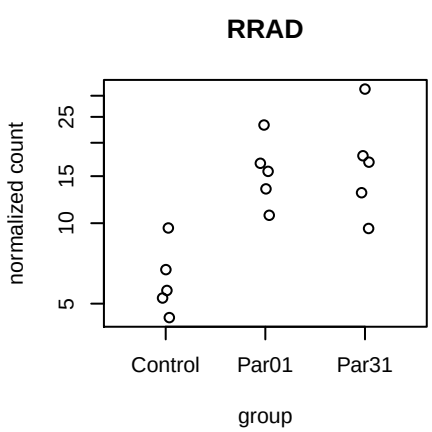
RRAD
normalized count
5
10
15
25
Control
Par01
Par31
group

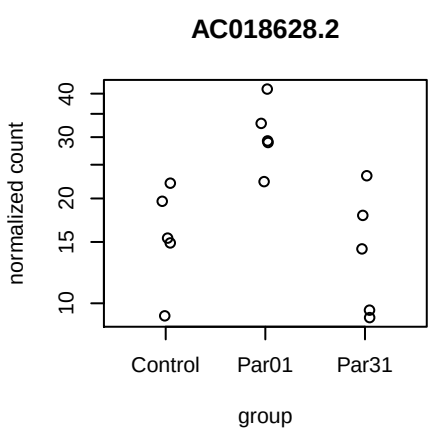
AC018628.2
normalized count
10
15
20
30
40
Control
Par01
Par31
group

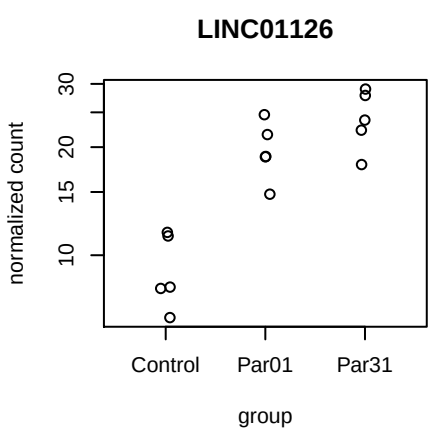
LINC01126
normalized count
10
15
20
30
Control
Par01
Par31
group

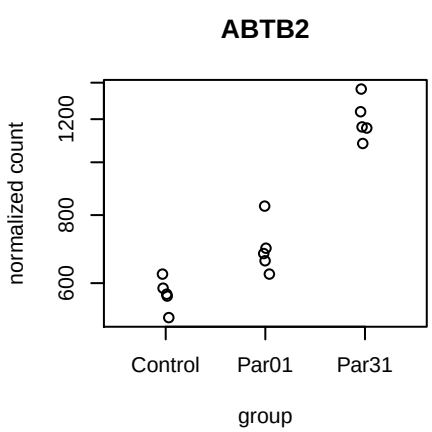
ABTB2
normalized count
600
800
1200
Control
Par01
Par31
group

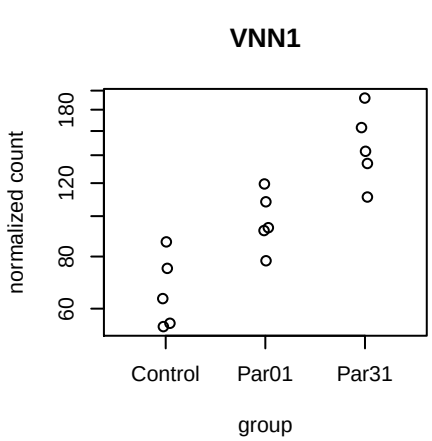
VNN1
normalized count
60
80
120
180
Control
Par01
Par31
group

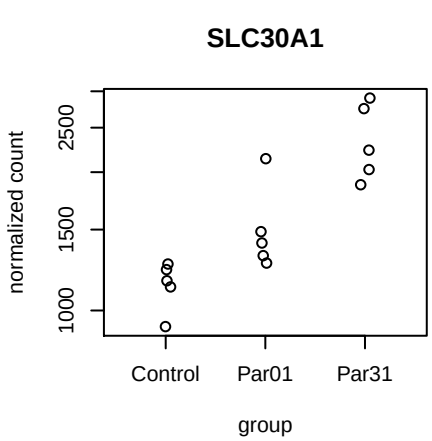
SLC30A1
normalized count
1000
1500
2500
Control
Par01
Par31
group

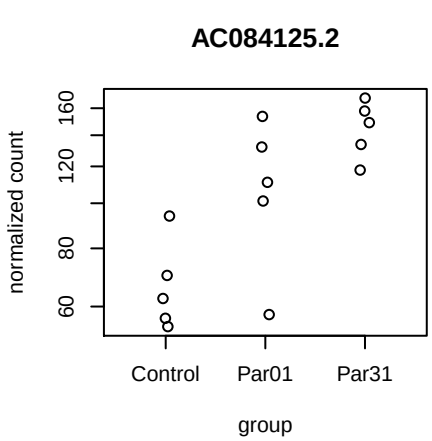
AC084125.2
normalized count
60
80
120
160
Control
Par01
Par31
group

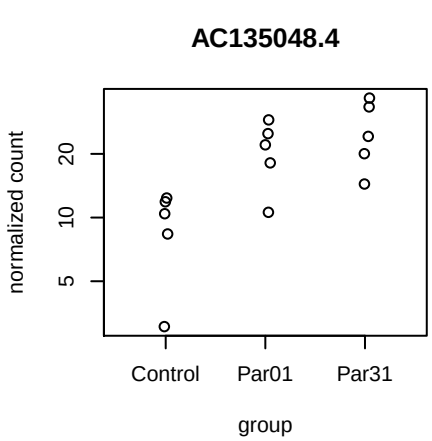
AC135048.4
normalized count
5
10
20
Control
Par01
Par31
group

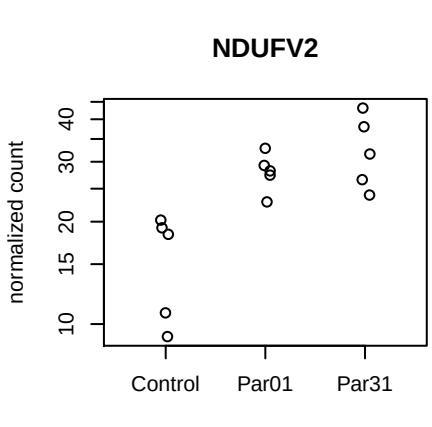
NDUFV2
normalized count
10
15
20
30
40
Control
Par01
Par31
group

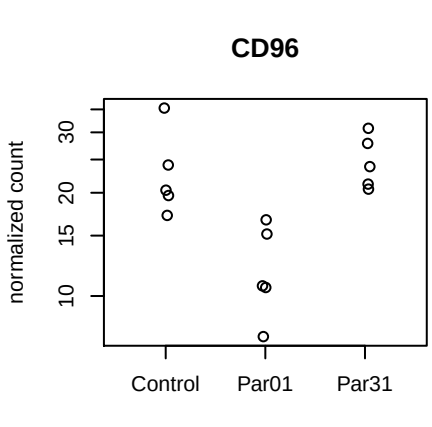
CD96
normalized count
10
15
20
30
Control
Par01
Par31
group

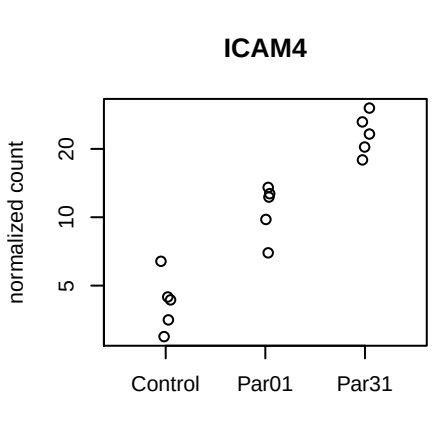
ICAM4
normalized count
5
10
20
Control
Par01
Par31
group

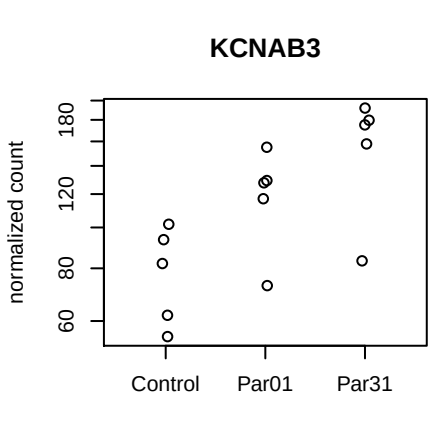
KCNAB3
normalized count
60
80
120
180
Control
Par01
Par31
group

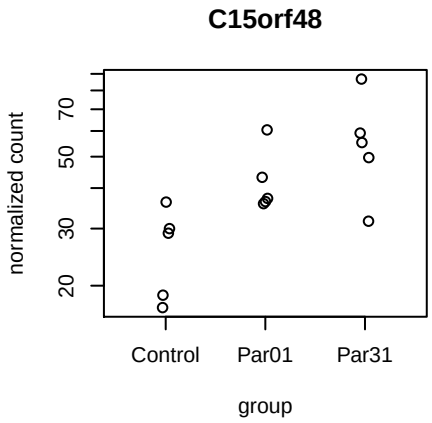
C15orf48
normalized count
20
30
50
70
Control
Par01
Par31
group

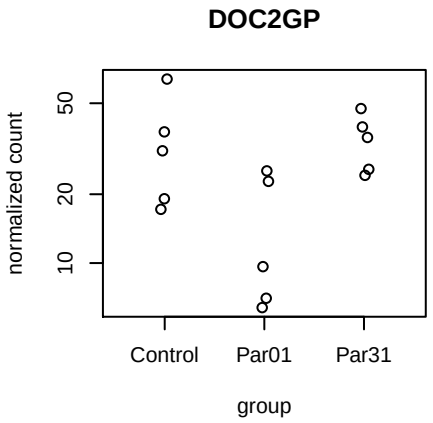
DOC2GP
normalized count
10
20
50
Control
Par01
Par31
group

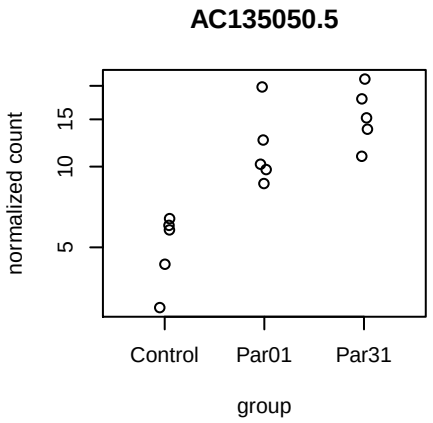
AC135050.5
normalized count
5
10
15
Control
Par01
Par31
group

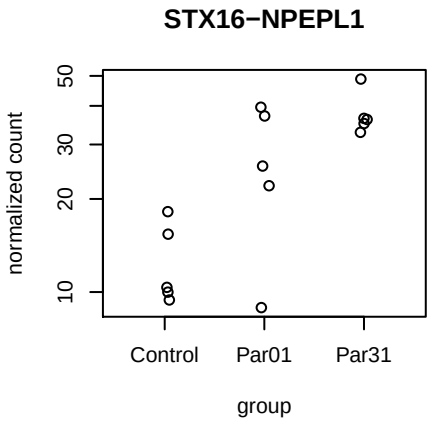
STX16−NPEPL1
normalized count
10
20
30
50
Control
Par01
Par31
group

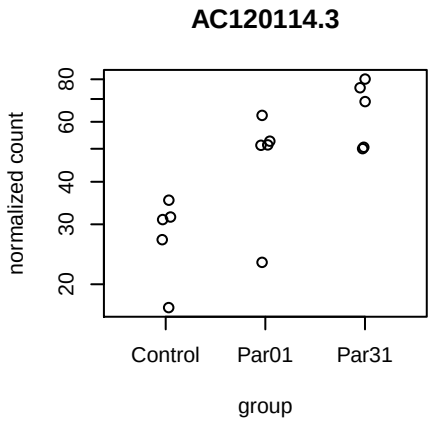
AC120114.3
normalized count
20
30
40
60
80
Control
Par01
Par31
group

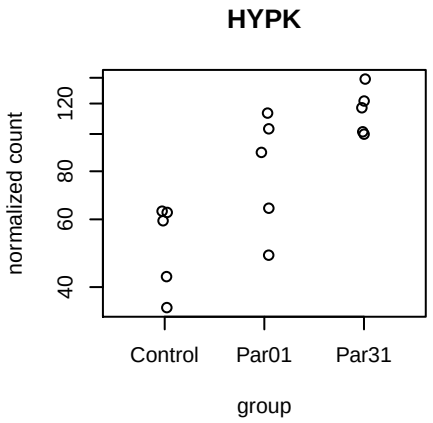
HYPK
normalized count
40
60
80
120
Control
Par01
Par31
group

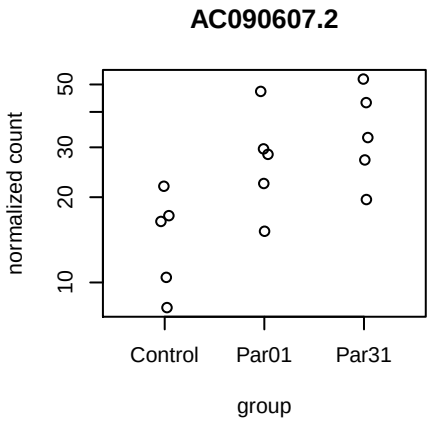
AC090607.2
normalized count
10
20
30
50
Control
Par01
Par31
group

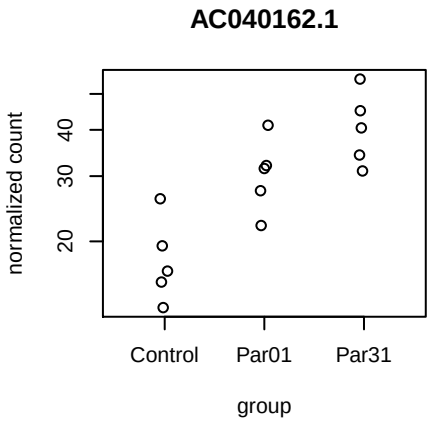
AC040162.1
normalized count
20
30
40
Control
Par01
Par31
group

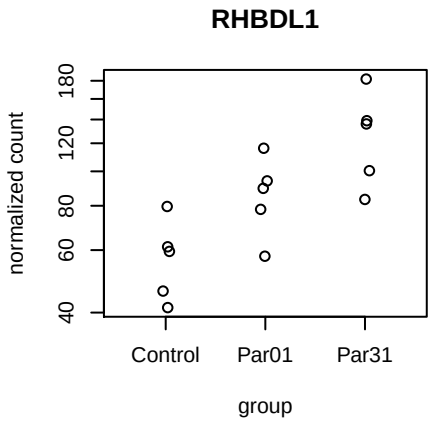
RHBDL1
normalized count
40
60
80
120
180
Control
Par01
Par31
group

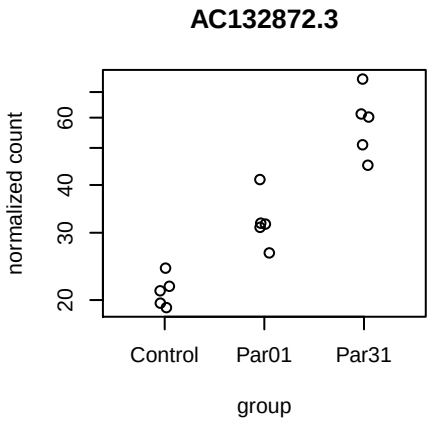
AC132872.3
normalized count
20
30
40
60
Control
Par01
Par31
group

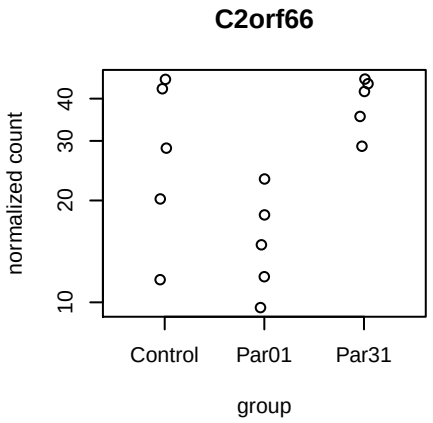
C2orf66
normalized count
10
20
30
40
Control
Par01
Par31
group

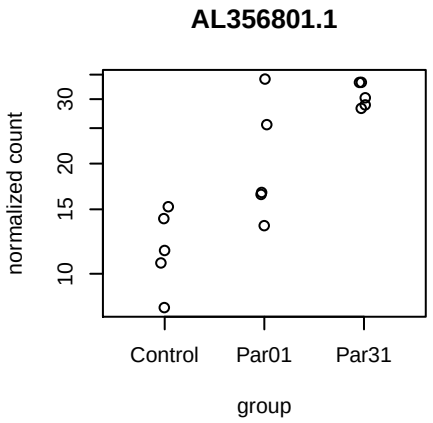
AL356801.1
normalized count
10
15
20
30
Control
Par01
Par31
group

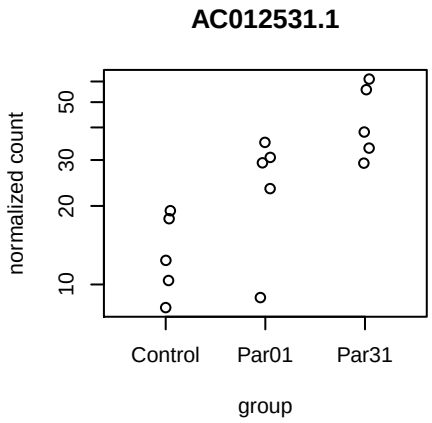
AC012531.1
normalized count
10
20
30
50
Control
Par01
Par31
group

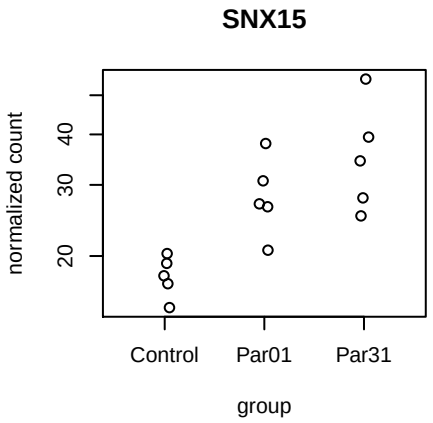
SNX15
normalized count
20
30
40
Control
Par01
Par31
group

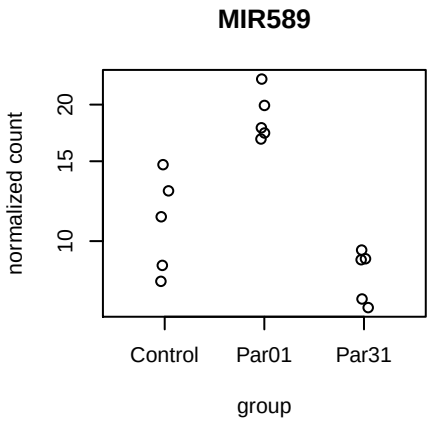
MIR589
normalized count
10
15
20
Control
Par01
Par31
group

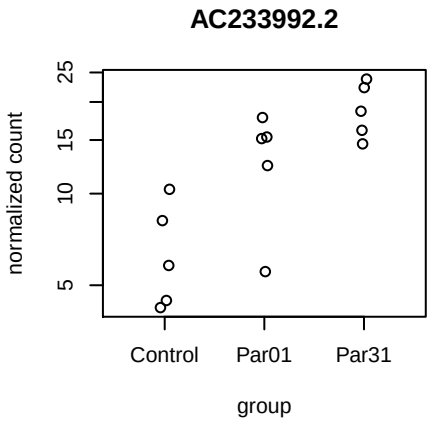
AC233992.2
normalized count
5
10
15
25
Control
Par01
Par31
group

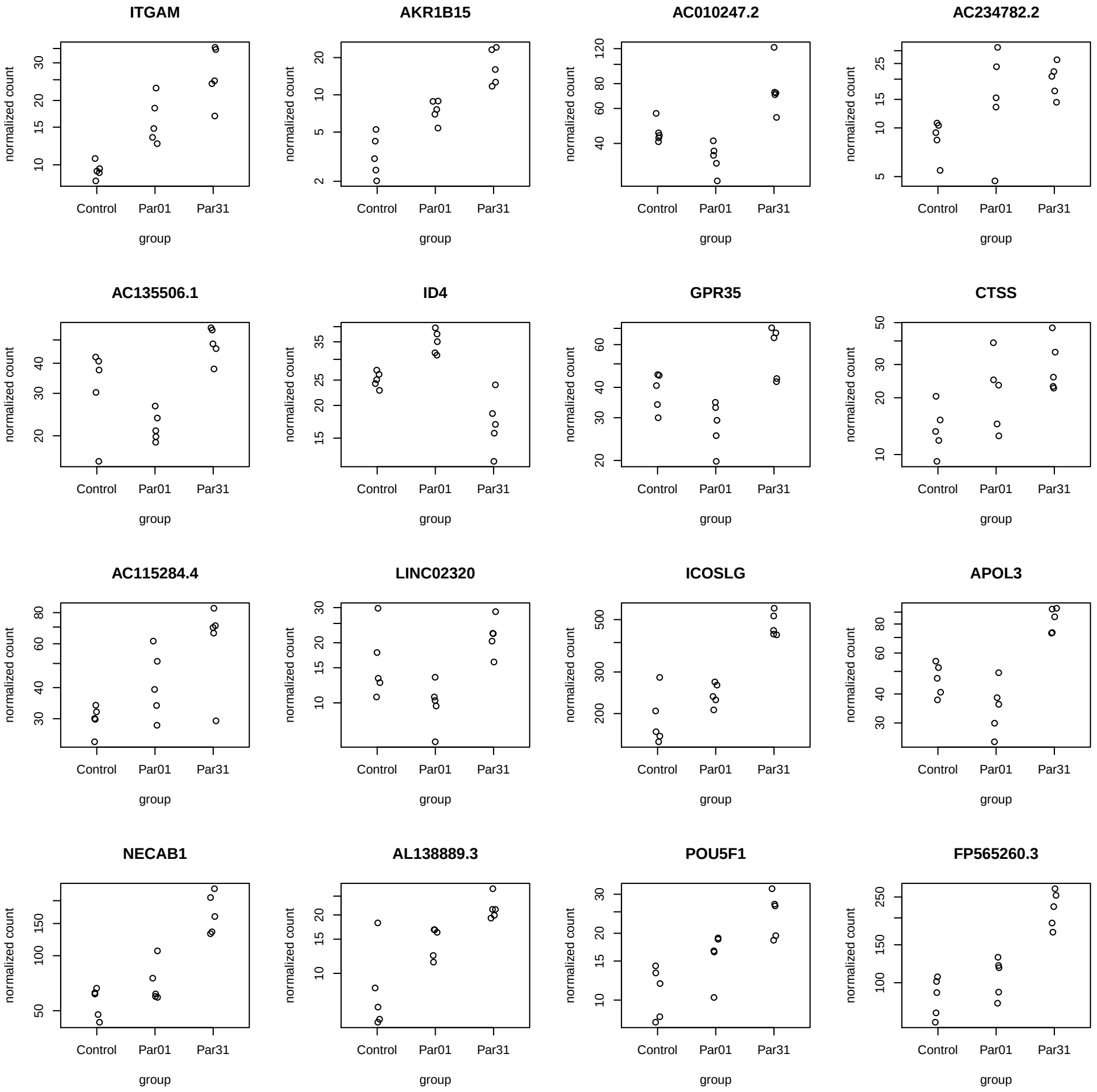
ITGAM
AKR1B15
AC010247.2
AC234782.2
AC135506.1
ID4
GPR35
CTSS
AC115284.4
LINC02320
ICOSLG
APOL3
NECAB1
AL138889.3
POU5F1
FP565260.3
normalized count
group
Control
Par01
Par31

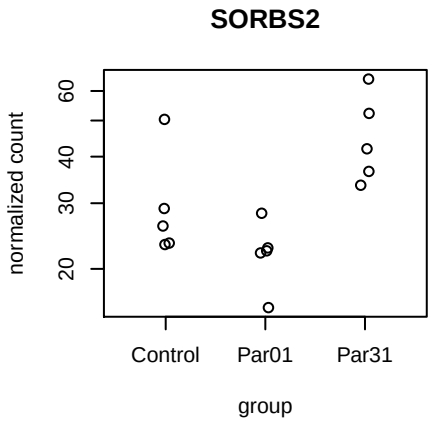
SORBS2
normalized count
20
30
40
60
Control
Par01
Par31
group

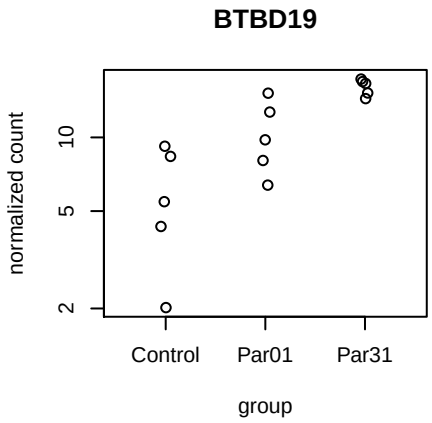
BTBD19
normalized count
2
5
10
Control
Par01
Par31
group

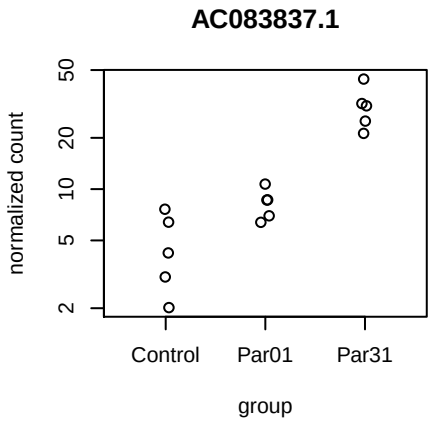
AC083837.1
normalized count
2
5
10
20
50
Control
Par01
Par31
group

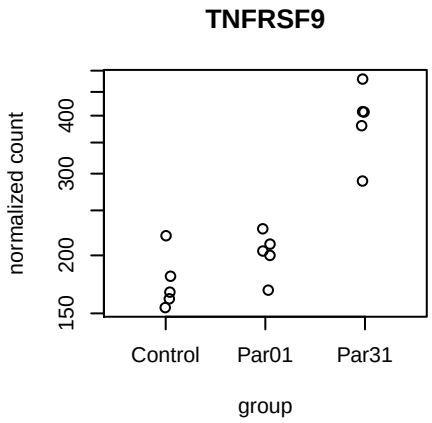
TNFRSF9
normalized count
150
200
300
400
Control
Par01
Par31
group

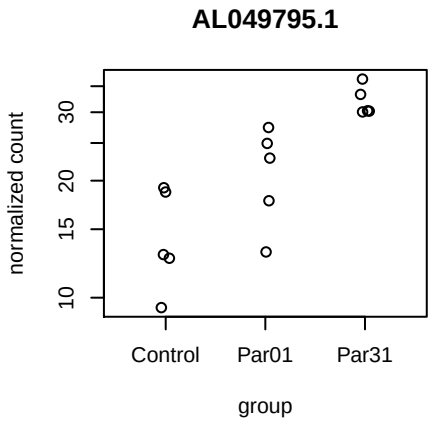
AL049795.1
normalized count
10
15
20
30
Control
Par01
Par31
group

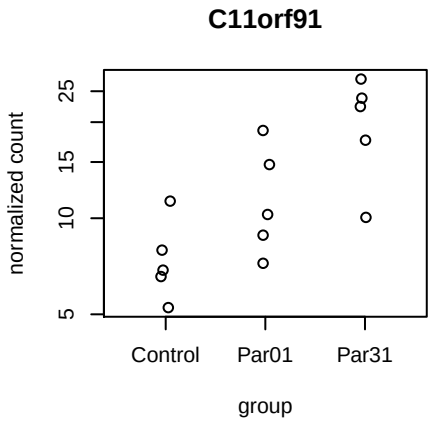
C11orf91
normalized count
5
10
15
25
Control
Par01
Par31
group

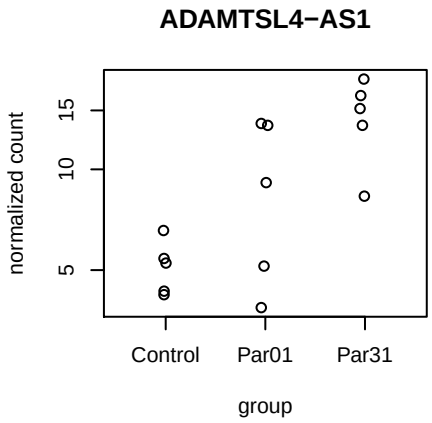
ADAMTSL4−AS1
normalized count
5
10
15
Control
Par01
Par31
group

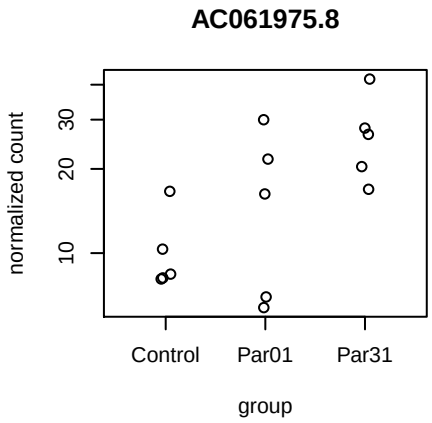
AC061975.8
normalized count
10
20
30
Control
Par01
Par31
group

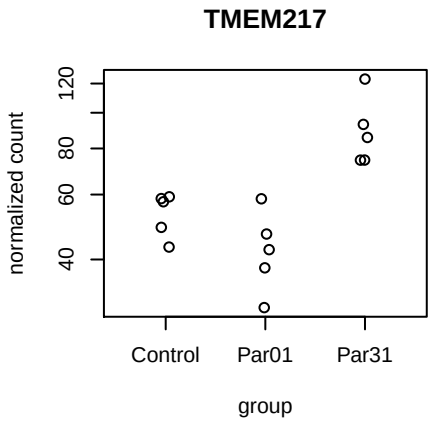
TMEM217
normalized count
40
60
80
120
Control
Par01
Par31
group

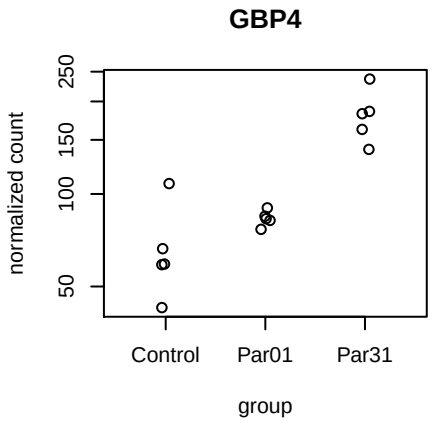
GBP4
normalized count
50
100
150
250
Control
Par01
Par31
group

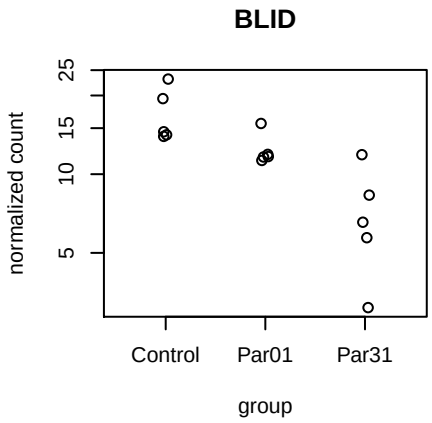
BLID
normalized count
5
10
15
25
Control
Par01
Par31
group

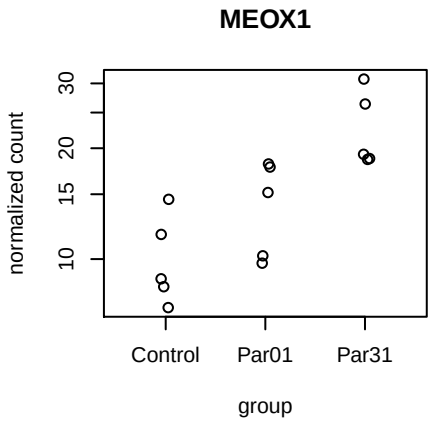
MEOX1
normalized count
10
15
20
30
Control
Par01
Par31
group

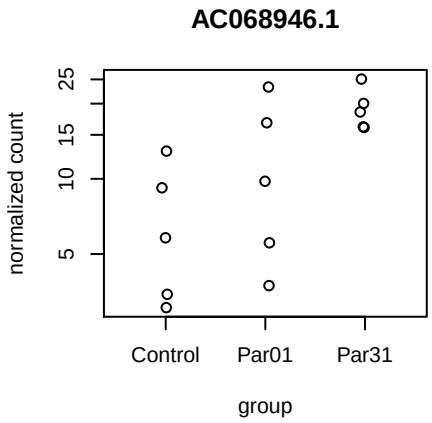
AC068946.1
normalized count
5
10
15
25
Control
Par01
Par31
group

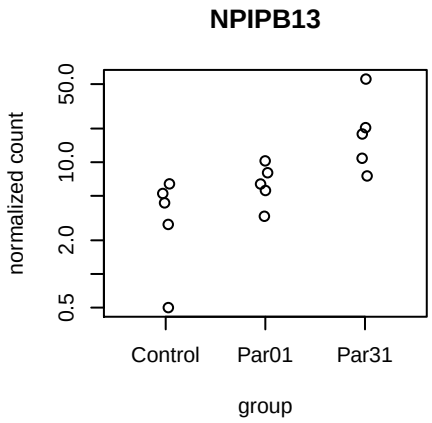
NPIPB13
normalized count
0.5
2.0
10.0
50.0
Control
Par01
Par31
group

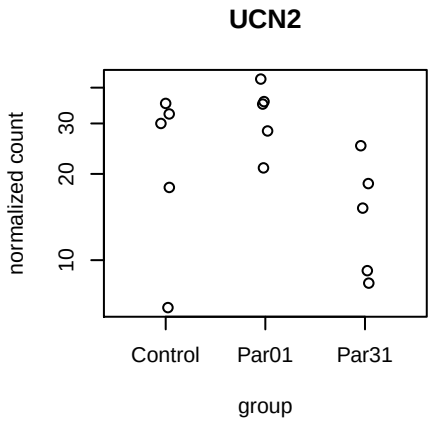
UCN2
normalized count
10
20
30
Control
Par01
Par31
group

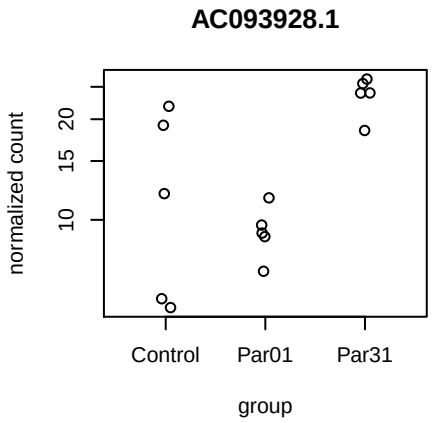
AC093928.1
normalized count
10
15
20
Control
Par01
Par31
group

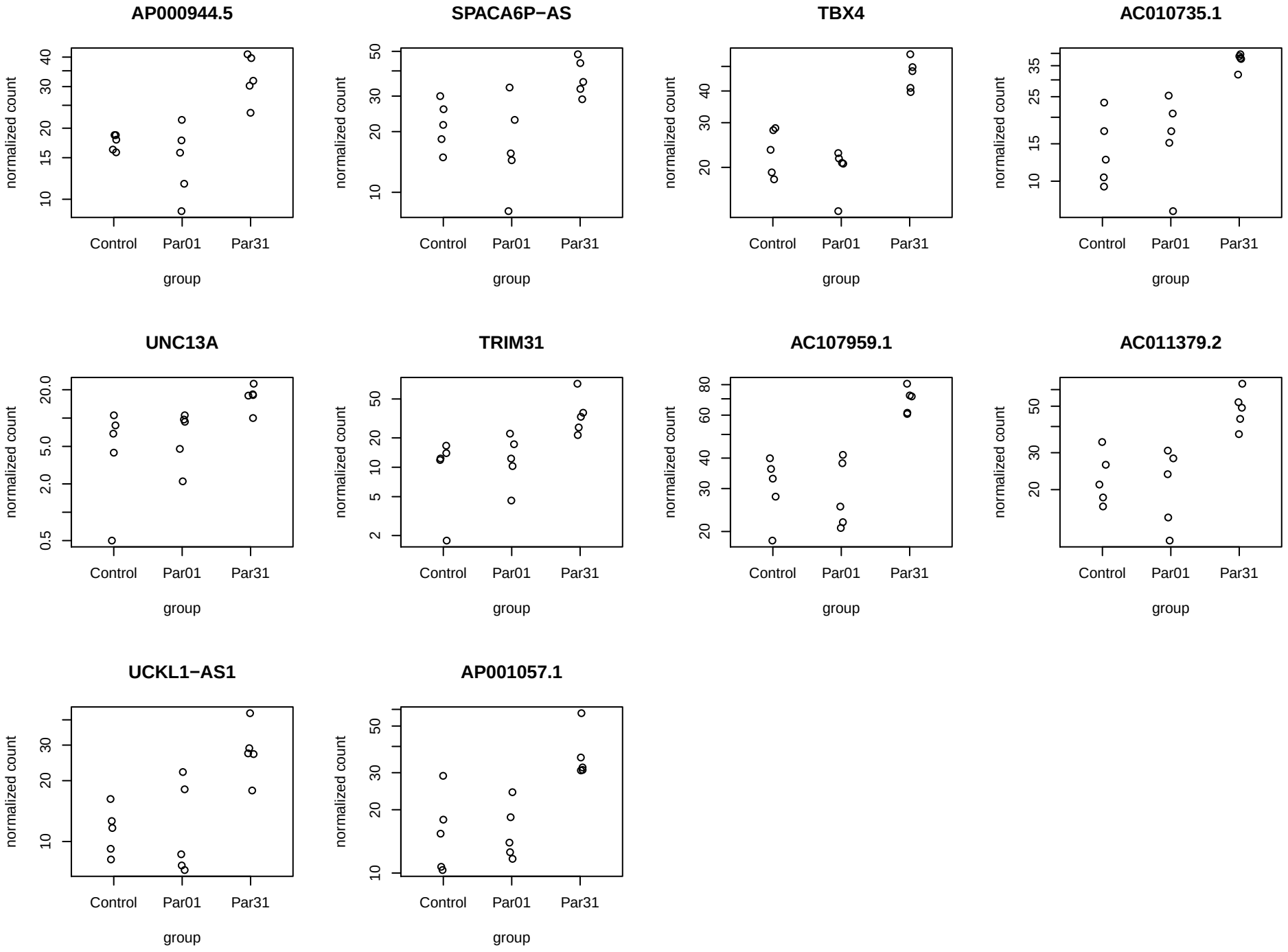

Figure S2: Boxplots of all 298 genes differentially expressed in the PC-3 PF RNAseq experiment.

Figure S3. Experiment hardware setup. A: Airbus 310 aircraft used for the 34th DLR parabolic flight campaign. **B:** View in the aircraft, equipped with the experiment racks of several science teams. **C:** The rack with the incubator used for the experiment. **D:** Inside of the incubator prior to take off of the flight. **E:** The Multi Sample Incubator Centrifuge (MuSIC) of DLR (Gravitational Biology) Cologne, placed in an incubator on ground. **F:** Samples within the swing-out device on the MuSIC centrifuge during acceleration. **G**: The Vibraplex device built by DLR (Gravitational Biology), Cologne, Germany.

Table S1 Demultiplexing statistic of the 10 PF and 5 control samples.

Sample	Barcode sequence	PF Clusters	% Perfect barcode	% One mismatch barcode	Yield (Mbases)	% PF Clusters	% >= Q30 bases	Mean Quality Score
1P 1	GCCAAT	54,026,813	98.33	1.67	10,913	100	93.96	35.94
1P 2	CAGATC	65,954,683	98.59	1.41	13,323	100	93.68	35.87
1P 3	ACTTGA	59,237,051	98.95	1.05	11,966	100	93.85	35.92
1P 4	GATCAG	50,967,453	98.98	1.02	10,295	100	94.05	35.95
1P 5	TAGCTT	32,965,164	98.95	1.05	6,659	100	93.54	35.85
31P 1	GGCTAC	61,988,136	99.24	0.76	12,522	100	93.25	35.8
31P 2	CTTGTA	42,205,855	98.4	1.6	8,526	100	93.36	35.82
31P 3	AGTCAA	67,427,596	98.51	1.49	13,620	100	93.49	35.86
31P 4	AGTTCC	64,146,346	98.84	1.16	12,958	100	93.37	35.81
31P 5	ATGTCA	56,824,184	98.38	1.62	11,478	100	93.14	35.79
Control 1	ACAGTG	42,430,335	98.87	1.13	8,571	100	93.92	35.93
Control 2	ATCACG	58,111,319	98.8	1.2	11,738	100	91.96	35.49
Control 3	CGATGT	82,935,298	98.83	1.17	16,753	100	94.14	35.98
Control 4	TTAGGC	42,112,474	99.13	0.87	8,507	100	93.29	35.82
Control 5	TGACCA	67,660,339	98.73	1.27	13,667	100	93.53	35.85

Table S3. Primer selection for the 32 genes and the housekeeper gene 18S in qPCR

Factor	Primer Name	Sequence 5′–3′
18S rRNA	18s-F	GGAGCCTGCGGCTTAATTT
	18s-R	CAACTAAGAACGGCCATGCA
Actin beta (*ACTB*)	ACTB-F	TGCCGACAGGATGCAGAAG
	ACTB-R	GCCGATCCACACGGAGTACT
RAC alpha serine / threonine protein kinase (*AKT1*)	AKT1-F	CTTCTATGGCGCTGAGATTGTG
	AKT1-R	CAGCATGAGGTTCTCCAGCTT
Caspase 3 (*CASP3*)	CASP3-F	CTCCAACATCGACTGTGAGAAGTT
	CASP3-R	GCGCCAGCTCCAGCAA
Caspase 8 (*CASP8*)	CASP8-F	TGCAAAAGCACGGGAGAAAG
	CASP8-R	CTCTTCAAAGGTCGTGGTCAAAG
Caspase 9 (*CASP9*)	CASP9-F	CTCCAACATCGACTGTGAGAAGTT
	CASP9-R	GCGCCAGCTCCAGCAA
Caveolin 2 (*CAV2*)	CAV2-F	GATCCCCACCGGCTCAAC
	CAV2-R	CACCGGCTCTGCGATCA
Cadherin-1 (*CDH1*)	CDH1-F	GCTGGACCGAGAGAGTTTCC
	CDH1-R	CAGCTGTTGCTGTTGTGCTT
Collagen 1 alpha 1 (*COL1A1*)	COL1A1-F	ACGAAGACATCCCACCAATCAC
	COL1A1-R	CGTTGTCGCAGACGCAGAT
Endothelial growth factor (*EGF*)	EGF-F	TGCCAGCTGCACAAATACAGA
	EGF-R	TCTTACGGAATAGTGGTGGTCATC
Endothelial growth factor receptor (*EGFR*)	EGFR-F	TTGCCGCAAAGTGTGTAACG
	EGFR-R	GAGATCGCCACTGATGGAGG
Ezrin (*EZR*)	EZR-F	GCAATCCAGCCAAATACAACTG
	EZR-R	CCACATAGTGGAGGCCAAAGTAC
Vascular endothelial growth factor receptor 2 (*FLK1*)	FLK1-F	TCTTCTGGCTACTTCTTGTCATCATC
	FLK1-R	GATGGACAAGTAGCCTGTCTTCAGT
Vascular endothelial growth factor receptor 1 (*FLT1*)	FLT1-F	CCCTCGCCGGAAGTTGTAT
	FLT1-R	GATAATTAACGAGTAGCCACGAGTCAA
Fibronectin (*FN1*)	FN1-F	AGATCTACCTGTACACCTTGAATGACA
	FN1-R	CATGATACCAGCAAGGAATTGG
Interleukin 6 (*IL6*)	IL6-F	CGGGAACGAAAGAGAAGCTCTA
	IL6-R	GAGCAGCCCCAGGGAGAA
Interleukin 8 (*CXCL8*)	IL8-F	TGGCAGCCTTCCTGATTTCT
	IL8-R	GGGTGGAAAGGTTTGGAGTATG
Cytokeratin 8 (*KRT8*)	KRT8-F	GATCTCTGAGTGAACCGGAACA
	KRT8-R	GCTCGGCATCTGCAATGG
Laminin alpha 3 (*LAMA3*)	LAMA3-F	AAAGCAAGAAGTCAGTCCAGC
	LAMA3-R	TCCCATGAAGACCATCTCGG
Laminin beta 2 (*LAMB2*)	LAMB2-F	TGCTCATGGTCAATGCTAATCTG
	LAMB2-R	TCTATCAATCCTCTTCCTTGGACAA
Matrix metalloproteinase 9 (*MMP9*)	MMP9-F	CCTGGAGACCTGAGAACCAATC
	MMP9-R	TTCGACTCTCCACGCATCTCT
Moesin (*MSN*)	MSN-F	GAAATTTGTCATCAAGCCCATTG
	MSN-R	CCATGCACAAGGCCAAGAT
Mechanistic target of	MTOR-F	ATCTTGGCCATAGCTAGCCTC

rapamycin (*MTOR*)	MTOR-R	ACAACTGGGTCATTGGAGGG
Osteopontin (*OPN*/*SPP1*)	OSP-F	CGAGGTGATAGTGTGGTTTATGGA
	OSP-R	CGTCTGTAGCATCAGGGTACTG
Plasminogen activator inhibitor 1 (*PAI1*)	PAI1-F	AGGCTGACTTCACGAGTCTTTCA
	PAI1-R	CACTCTCGTTCACCTCGATCTTC
Phosphatidylinositol 4,5 bisphosphate 3 kinase catalytic subunit beta (*PIK3CB*)	PIK3CB-F	AGAAAAGTTTGGCCGGTTCC
	PIK3CB-R	GCAGTCAACATCAGCGCAAA
Radexin (*RDX*)	RDX-F	GAAAATGCCGAAACCAATCAA
	RDX-R	GTATTGGGCTGAATGGCAAATT
Transforming growth factor beta (*TGFB1*)	TGFB1-F	CACCCGCGTGCTAATGGT
	TGFB1-R	AGAGCAACACGGGTTCAGGTA
TIMP metallopeptidase inhibitor 1 (TIMP1)	TIMP1-F	GCCATCGCCGCAGATC
	TIMP1-R	GCTATCAGCCACAGCAACAACA
Talin 1 (*TLN1*)	TLN1-F	GATGGCTATTACTCAGTACAGACAACTGA
	TLN1-R	CATAGTAGACTCCTCATCTCCTTCCA
Tubulin beta (*TUBB*)	TUBB-F	CTGGACCGCATCTCTGTGTACTAC
	TUBB-R	GACCTGAGCGAACAGAGTCCAT
Vinculin (*VCL*)	VCL-F	GTCTCGGCTGCTCGTATCTT
	VCL-R	GTCCACCAGCCCTGTCATTT
Vascular Endothelial Growth Factor A (*VEGFA*)	VEGFA	CTACCTCCACCATGCCAAGTG
	VEGFA	GCGCTGATAGACATCCATGAAC

OrderP1	OrderP31	ENSGv99	Symbol	min(padj)	ctr-p01-p31_baseMean	ctr-p01-p31_log2FoldChange
1	4	ENSG00000090339	ICAM1	7,82540E-57	7564,839166	2,520315681
2	22	ENSG00000163739	CXCL1	2,75523E-50	14343,21916	3,730535615
3	16	ENSG00000108691	CCL2	5,00619E-49	127,1777507	3,42259496
4	10	ENSG00000112149	CD83	2,52094E-46	1452,725128	1,309628949
5	93	ENSG00000204389	HSPA1A	4,62131E-43	1279,267811	-0,577208278
6	5	ENSG00000104856	RELB	5,65992E-53	1122,562101	1,643319196
7	11	ENSG00000146232	NFKBIE	5,01498E-37	1061,531488	1,072354485
8	19	ENSG00000124875	CXCL6	3,65222E-36	3320,548829	2,573177891
9	14	ENSG00000163874	ZC3H12A	6,69578E-36	1589,522227	2,560852589
10	1	ENSG00000253522	MIR3142HG	1,23755E-86	584,4641492	3,601834013
11	24	ENSG00000227507	LTB	8,73658E-34	157,9463094	3,213125447
12	130	ENSG00000204388	HSPA1B	2,51082E-33	861,1193196	-0,488711969
13	13	ENSG00000081041	CXCL2	5,21558E-33	1638,140412	3,650255696
14	30	ENSG00000164400	CSF2	3,97722E-32	890,1324632	3,59989956
15	40	ENSG00000073756	PTGS2	6,71685E-32	261,7209052	1,824592969
16	80	ENSG00000125538	IL1B	2,83663E-30	2896,463085	1,822506716
17	12	ENSG00000163734	CXCL3	3,16207E-29	1624,911284	3,504876925
18	2	ENSG00000134070	IRAK2	4,72462E-83	1660,576447	1,200868916
19	50	ENSG00000171223	JUNB	2,50578E-28	3126,011385	0,905968724
20	6	ENSG00000100906	NFKBIA	1,30743E-42	9051,001776	2,103005069
21	81	ENSG00000143367	TUFT1	2,98033E-25	1453,765592	0,537926773
22	15	ENSG00000184371	CSF1	2,36737E-26	601,7820614	1,44202745
23	65	ENSG00000159261	CLDN14	5,92917E-25	373,2739148	0,907128608
24	21	ENSG00000107968	MAP3K8	6,12352E-25	294,6982755	1,317838273
25	3	ENSG00000023445	BIRC3	6,58673E-75	3500,0636	2,391298311
26	7	ENSG00000125347	IRF1	9,75466E-42	3064,187912	1,770466612
27	147	ENSG00000269343	ZNF587B	7,57428E-23	758,0840767	0,418996477
28	26	ENSG00000118503	TNFAIP3	9,53549E-23	1235,197449	2,215922474
29	20	ENSG00000169429	CXCL8	2,02868E-22	12345,75532	3,082675707
30	8	ENSG00000077150	NFKB2	6,59649E-41	2944,336077	1,372892658
31	242	ENSG00000118523	CCN2	3,02216E-21	2685,008422	0,282238897
32	95	ENSG00000113070	HBEGF	1,41626E-20	2854,254447	0,614826959
33	114	ENSG00000167604	NFKBID	1,87468E-20	198,0580043	0,738320919
34	46	ENSG00000108342	CSF3	2,04928E-20	251,0649633	2,567179047
35	116	ENSG00000116717	GADD45A	2,63149E-20	2423,94	0,478835792
36	75	ENSG00000163545	NUAK2	7,14050E-20	714,8254812	1,896706007

37	17	ENSG00000185215	TNFAIP2	2,19780E-24	2709,765137	1,791053976
38	78	ENSG00000157557	ETS2	3,37909E-19	3756,362144	0,624099497
39	72	ENSG00000143067	ZNF697	5,61165E-19	822,1696639	0,710816334
40	126	ENSG00000115844	DLX2	2,86031E-18	156,2657044	1,002811362
41	187	ENSG00000169554	ZEB2	4,65269E-17	78,15971057	0,603181948
42	142	ENSG00000182700	IGIP	1,15635E-16	270,2365309	-0,453789183
43	208	ENSG00000114019	AMOTL2	2,95565E-16	2302,195597	0,560785093
44	32	ENSG00000162924	REL	7,66947E-16	194,3269981	1,107343387
45	36	ENSG00000128342	LIF	1,85620E-15	10600,58589	1,148463931
46	103	ENSG00000151014	NOCT	1,24909E-14	385,8048571	0,601997814
47	69	ENSG00000114529	C3orf52	2,04269E-14	685,2149807	0,836704683
48	183	ENSG00000168811	IL12A	2,66179E-14	66,60364549	0,869663296
49	167	ENSG00000006062	MAP3K14	1,39575E-13	3333,200917	0,57431262
50	18	ENSG00000115009	CCL20	6,52559E-24	100,2884951	5,124737425
51	85	ENSG00000110944	IL23A	3,97360E-13	359,4506166	1,636609192
52	232	ENSG00000145632	PLK2	9,35033E-13	3452,390573	0,348545161
53	91	ENSG00000164236	ANKRD33B	2,30701E-12	2091,264699	0,813828145
54	53	ENSG00000166289	PLEKHF1	8,02867E-13	303,4139888	1,072138304
55	109	ENSG00000159388	BTG2	5,73243E-12	107,1878624	0,780169319
56	192	ENSG00000154309	DISP1	8,30096E-12	182,0293735	-0,411000111
57	68	ENSG00000232810	TNF	8,56870E-12	27,11423061	4,64241201
58	74	ENSG00000272141	AL390719.2	1,82719E-11	118,9024211	1,030877428
59	87	ENSG00000242338	BMS1P4	1,93412E-11	73,02804455	0,986841507
60	219	ENSG00000204390	HSPA1L	3,59419E-11	57,94499918	-0,345978477
61	23	ENSG00000142396	ERVK3-1	1,81618E-18	452,6830322	1,119870253
62	58	ENSG00000269858	EGLN2	1,26262E-10	132,5429546	1,044273258
63	94	ENSG00000100739	BDKRB1	1,36149E-10	38,3105742	1,524351581
64	252	ENSG00000184384	MAML2	6,23764E-10	1542,471995	-0,156162823
65	143	ENSG00000227199	ST7-AS1	9,33466E-10	79,42833612	0,774837298
66	221	ENSG00000153714	LURAP1L	1,29039E-09	457,3568547	-0,512856027
67	104	ENSG00000270069	MIR222HG	1,46896E-09	408,3295477	0,754763775
68	29	ENSG00000227908	AC016596.1	2,41058E-17	91,24425117	1,461389666
69	57	ENSG00000221869	CEBPD	3,47317E-09	233,5835777	1,266771373
70	25	ENSG00000104951	IL4I1	2,13854E-18	89,3936645	2,051734053
71	51	ENSG00000144802	NFKBIZ	8,68805E-11	2637,710728	1,075067712
72	139	ENSG00000155918	RAET1L	1,57327E-08	30,58658403	1,062858083
73	66	ENSG00000281183	NPTN-IT1	6,91000E-09	34,25608253	1,723169704
74	275	ENSG00000277945	AC107308.1	3,20078E-08	61,11931286	0,145639166
75	186	ENSG00000269951	AC090181.2	4,36165E-08	50,89415184	0,598857245
76	218	ENSG00000215417	MIR17HG	5,65653E-08	94,18725841	0,484017943
77	122	ENSG00000227627	AL080276.2	5,94417E-08	61,25700655	0,736730013
78	52	ENSG00000172602	RND1	1,03089E-10	63,22894259	1,526476944
79	98	ENSG00000236098	AC097059.1	8,47427E-08	60,10558884	0,855198653
80	200	ENSG00000120217	CD274	1,33956E-07	324,0871495	0,704784926
81	261	ENSG00000230002	ALMS1-IT1	2,17359E-07	59,49507098	0,175853614
82	27	ENSG00000131797	CLUHP3	1,00684E-16	387,3735426	1,087759359
83	110	ENSG00000275895	U2AF1L5	2,81182E-07	47,59118032	0,926670779
84	235	ENSG00000164741	DLC1	3,47522E-07	238,5493522	0,325565777
85	97	ENSG00000240053	LY6G5B	3,86306E-07	94,83869341	0,974198915
86	215	ENSG00000263602	MIR3185	5,80344E-07	122,3296072	-0,274287573

87	160	ENSG00000262877	AC110285.2	7,72307E-07	51,70314787	0,915312076
88	131	ENSG00000161960	EIF4A1	8,42889E-07	119,2912043	0,83434733
89	260	ENSG00000178662	CSRNP3	8,42889E-07	1231,707018	-0,118013911
90	216	ENSG00000125398	SOX9	8,53980E-07	6630,378336	-0,475855703
91	48	ENSG00000056558	TRAF1	2,46375E-11	94,05913419	1,543870303
92	107	ENSG00000026036	RTEL1-TNFRSF6B	1,06780E-06	186,7211837	0,74396039
93	152	ENSG00000273888	FRMD6-AS1	1,07380E-06	53,11820508	0,700611998
94	141	ENSG00000272269	AL138724.2	1,14474E-06	75,02134518	0,873590376
95	173	ENSG00000078401	EDN1	1,27716E-06	124,3687377	0,90514704
96	28	ENSG00000261618	LINC02605	2,99806E-17	29,20611025	3,618009245
97	82	ENSG00000145911	N4BP3	3,61628E-07	38,21484924	1,488960293
98	177	ENSG00000241343	RPL36A	4,03063E-06	123,2025143	0,526505696
99	137	ENSG00000136244	IL6	4,03063E-06	294,4969462	2,28514012
100	285	ENSG00000226520	KIRREL1-IT1	6,54492E-06	11,30460871	2,179962229
101	182	ENSG00000188959	C9orf152	8,08279E-06	111,8176074	-0,632199693
102	151	ENSG00000115008	IL1A	8,55374E-06	20,67881392	1,729817928
103	180	ENSG00000232034	AC092168.2	8,87441E-06	36,19168757	0,903973042
104	178	ENSG00000147036	LANCL3	9,28563E-06	202,6153399	-0,60030332
105	227	ENSG00000173110	HSPA6	1,02549E-05	240,4435201	-0,703610275
106	207	ENSG00000213782	DDX47	1,07071E-05	22,10880366	0,721107494
107	269	ENSG00000168874	ATOH8	1,37790E-06	32,18253189	-0,167126353
108	251	ENSG00000207870	MIR221	1,64971E-05	19,04555538	0,408432433
109	223	ENSG00000122877	EGR2	2,04729E-05	31,77660459	0,611114607
110	71	ENSG00000279520	AC093525.8	3,56942E-08	27,7525032	1,646317936
111	42	ENSG00000280407	AC132872.4	3,51694E-13	88,18348455	1,249381306
112	193	ENSG00000206538	VGLL3	3,26544E-05	117,3455797	0,589723013
113	175	ENSG00000232303	DFFBP1	3,37952E-05	35,47081697	0,818972575
114	274	ENSG00000182580	EPHB3	3,72090E-05	2145,337257	-0,122215181
115	49	ENSG00000210196	MT-TP	3,71992E-11	33,70839809	-2,72211031
116	248	ENSG00000188039	NWD1	4,51615E-05	86,2459969	-0,442072854
117	246	ENSG00000198939	ZFP2	4,51786E-05	21,03163274	-0,325207431
118	166	ENSG00000228526	MIR34AHG	4,63456E-05	35,57973314	0,874053519
119	47	ENSG00000251474	RPL32P3	1,22603E-11	194,3290065	1,04285757
120	225	ENSG00000244675	AC108676.1	5,26368E-05	41,27095069	-0,527692747
121	237	ENSG00000138764	CCNG2	6,77379E-05	862,25456	-0,421967153
122	44	ENSG00000170075	GPR37L1	1,85422E-12	18,19592751	3,346456449
123	168	ENSG00000233237	LINC00472	9,55083E-05	52,21794943	0,815615685
124	184	ENSG00000197632	SERPINB2	1,06342E-04	43,61365406	0,643358269
125	282	ENSG00000147408	CSGALNACT1	1,07650E-04	177,9117807	-0,077876337
126	270	ENSG00000168421	RHOH	1,16384E-04	16,49490577	-0,181847703
127	255	ENSG00000255150	EID3	1,22089E-04	41,64690028	0,290454005
128	203	ENSG00000279347	AC021945.1	1,58601E-04	18,7501475	0,906564133
129	222	ENSG00000162878	PKDCC	1,64391E-04	28,7667214	-0,616176685
130	61	ENSG00000256128	LINC00944	8,20562E-09	46,95154131	1,451190861
131	239	ENSG00000287023	AC018978.1	1,91705E-04	1009,416259	-0,332394508
132	244	ENSG00000142871	CCN1	2,13980E-04	6618,696022	0,444198354
133	123	ENSG00000137411	VARS2	2,30591E-04	37,62495297	1,240736348
134	234	ENSG00000273489	AC008264.2	2,43606E-04	21,33291746	0,623441889
135	233	ENSG00000128917	DLL4	2,27287E-08	87,2418342	0,278511005
136	145	ENSG00000160201	U2AF1	2,85058E-04	49,51154483	0,725364731

137	195	ENSG00000235927	NEXN-AS1	4,00702E-04	36,29783142	0,758900596
138	172	ENSG00000148200	NR6A1	1,97161E-08	102,1045257	0,425644204
139	256	ENSG00000005108	THSD7A	4,27643E-04	42,81885643	-0,517516772
140	129	ENSG00000272916	AC022400.7	4,32153E-04	22,91895311	1,428205061
141	62	ENSG00000213906	LTB4R2	9,62852E-09	128,8145663	1,00966746
142	84	ENSG00000229299	AL121845.1	1,13177E-05	37,23203044	1,398662187
143	277	ENSG00000118513	MYB	6,60233E-04	129,5564321	-0,144232552
144	259	ENSG00000152208	GRID2	6,95054E-04	81,98882426	-0,223602135
145	77	ENSG00000104899	AMH	7,70215E-07	119,024056	1,490388976
146	286	ENSG00000278493	AC039056.2	7,68881E-04	8,584605282	0,67116522
147	201	ENSG00000241111	AC092040.2	7,75280E-04	15,85465365	-0,819551835
148	266	ENSG00000133019	CHRM3	7,81823E-04	2346,012336	-0,177118738
149	211	ENSG00000212123	PRR22	7,87882E-04	59,40497175	0,609450697
150	265	ENSG00000134215	VAV3	8,37580E-04	62,0497733	-0,314798154
151	268	ENSG00000285755	AC132153.1	9,37174E-04	7,713549301	-0,274081729
152	272	ENSG00000273576	AC009283.1	4,17107E-04	22,10487537	0,157766395
153	287	ENSG00000274204	AL138689.1	9,90516E-04	6,473965771	1,481903438
154	258	ENSG00000207547	MIR25	1,16737E-03	34,53868471	0,288415146
155	135	ENSG00000062582	MRPS24	1,18095E-03	31,37268578	1,164484407
156	267	ENSG00000164379	FOXQ1	1,18095E-03	27,43891417	-0,179918089
157	34	ENSG00000224660	SH3BP5-AS1	3,77449E-14	351,1780294	1,017739631
158	119	ENSG00000169682	SPNS1	7,08517E-04	39,58044295	0,918587774
159	213	ENSG00000213397	HAUS7	1,38869E-03	25,39882429	0,617766741
160	188	ENSG00000250318	AC003072.1	1,42926E-03	18,0549495	-0,740319363
161	156	ENSG00000163492	CCDC141	1,47840E-03	498,0885762	-1,041675446
162	217	ENSG00000250778	AC004980.5	1,64060E-03	35,87495198	-0,452184408
163	204	ENSG00000287661	AL391844.1	1,66915E-03	32,5267514	-0,989546934
164	236	ENSG00000221949	LINC01465	1,70235E-03	16,65298302	0,514291894
165	54	ENSG00000203709	MIR29B2CHG	3,62198E-10	135,7085087	1,004140387
166	238	ENSG00000170509	HSD17B13	1,90994E-03	15,56592947	-0,675217274
167	198	ENSG00000151967	SCHIP1	1,92211E-03	23,3131276	0,788790502
168	230	ENSG00000146411	SLC2A12	2,04956E-03	146,2526048	-0,560289123
169	169	ENSG00000183458	AC138932.1	2,06204E-03	102,3051447	0,896657175
170	210	ENSG00000082196	C1QTNF3	2,08522E-03	22,87960736	-0,53065659
171	224	ENSG00000170442	AC021066.1	2,13794E-03	784,4659909	0,523326556
172	133	ENSG00000198976	MIR429	5,99118E-04	18,92562109	1,587695821
173	278	ENSG00000175841	FAM172BP	2,23825E-03	24,75243322	0,107139462
174	128	ENSG00000255423	EBLN2	1,39894E-03	30,54405363	1,139552535
175	190	ENSG00000235408	SNORA71B	2,36830E-03	19,53321199	0,958697432
176	206	ENSG00000230305	AC004980.3	2,47399E-03	90,11603054	-0,557550376
177	288	ENSG00000154451	GBP5	2,55837E-03	7,427587701	2,116815156
178	229	ENSG00000049192	ADAMTS6	2,57642E-03	143,373648	0,637015613
179	289	ENSG00000207607	MIR200A	2,68442E-03	7,850670061	1,995282237
180	231	ENSG00000251323	LINC02728	2,97926E-03	14,00095214	0,758513226
181	249	ENSG00000188107	EYS	2,99288E-03	31,99485801	-0,652617801
182	254	ENSG00000276644	DACH1	3,19382E-03	25,20298721	-0,447552213
183	92	ENSG00000239653	PSMD6-AS2	1,80864E-05	21,62136972	1,836117046
184	226	ENSG00000272744	AC107214.2	3,23464E-03	10,8125727	-0,566769187
185	290	ENSG00000251348	HSPD1P11	3,26337E-03	7,298628569	0,861380524
186	271	ENSG00000159915	ZNF233	3,27287E-03	36,1409055	-0,182908241

187	43	ENSG00000158286	RNF207	1,62017E-12	2255,644768	1,000959891
188	121	ENSG00000278991	AC090181.3	4,67116E-04	15,56317342	1,500935655
189	63	ENSG00000117009	KMO	2,83887E-09	117,3000551	1,141951632
190	281	ENSG00000108551	RASD1	3,69509E-03	384,4032533	-0,09318208
191	106	ENSG00000064300	NGFR	6,68152E-05	35,98471692	1,658624913
192	262	ENSG00000175161	CADM2	3,89875E-03	132,5365509	-0,405612912
193	241	ENSG00000278626	AC023310.4	3,93971E-03	37,07408872	-0,693782473
194	202	ENSG00000254349	MIR2052HG	3,94164E-03	19,3939086	-0,796594182
195	194	ENSG00000163121	NEURL3	4,57341E-03	19,14475646	0,971449409
196	39	ENSG00000070190	DAPP1	1,19488E-13	87,21421768	1,252751313
197	240	ENSG00000259341	AC015660.1	4,65780E-03	26,51549257	-0,353028981
198	45	ENSG00000117228	GBP1	5,29600E-12	145,3037887	1,191417102
199	264	ENSG00000162989	KCNJ3	4,99001E-03	18,51716116	-0,482709535
200	105	ENSG00000206712	RNU6-26P	3,06615E-04	20,05011865	1,411405504
201	174	ENSG00000073734	ABCB11	5,46766E-03	17,45400643	-0,999806827
202	291	ENSG00000286634	AC146507.3	5,69239E-03	7,751428729	0,956212046
203	284	ENSG00000126882	FAM78A	5,72019E-03	23,45832849	0,015283567
204	292	ENSG00000221852	KRTAP1-5	5,73632E-03	12,74623087	0,117877663
205	176	ENSG00000108932	SLC16A6	6,38931E-03	17,03049222	1,202618478
206	257	ENSG00000183918	SH2D1A	6,57532E-03	37,36023925	-0,504775607
207	181	ENSG00000155657	TTN	6,80942E-03	885,473926	-0,894693792
208	185	ENSG00000170523	KRT83	6,85749E-03	60,99468328	1,193995269
209	293	ENSG00000244945	AC136604.2	7,05318E-03	9,473597313	1,490259116
210	112	ENSG00000279500	AC108704.2	5,74515E-04	19,07393911	1,355432089
211	170	ENSG00000224975	INE1	7,16297E-03	36,24425664	0,805301801
212	38	ENSG00000234771	SLC25A25-AS1	7,83166E-14	158,9326361	1,14551877
213	294	ENSG00000179774	ATOH7	7,30891E-03	7,655224361	1,094772941
214	197	ENSG00000231154	MORF4L2-AS1	7,31158E-03	25,11846242	0,794910843
215	220	ENSG00000213090	AC007256.1	7,51377E-03	13,08494124	0,780632246
216	295	ENSG00000253966	AC008514.2	7,58991E-03	5,520225384	0,118727987
217	191	ENSG00000075651	PLD1	7,85202E-03	680,2639896	-0,71783879
218	189	ENSG00000207741	MIR590	7,93849E-03	12,00806137	1,32517555
219	263	ENSG00000170989	S1PR1	7,98011E-03	101,4704704	0,22324701
220	199	ENSG00000263786	AC022211.2	7,99156E-03	21,68880226	0,758494949
221	245	ENSG00000183508	TENT5C	8,41969E-03	358,9414593	-0,655283097
222	296	ENSG00000260727	SLC7A5P1	8,53745E-03	9,859328696	1,050985362
223	297	ENSG00000272574	AL596325.2	8,69375E-03	9,000875675	0,740999724
224	298	ENSG00000136869	TLR4	8,79664E-03	8,690009559	0,847697776
225	247	ENSG00000225217	HSPA7	9,04852E-03	29,57179464	-0,702350951
226	276	ENSG00000236699	ARHGEF38	5,32634E-04	103,1147773	0,149456105
227	273	ENSG00000172318	B3GALT1	9,19332E-03	762,3632899	-0,178807635
228	140	ENSG00000171766	GATM	1,99474E-03	18,49791466	1,164163101
229	161	ENSG00000166592	RRAD	3,27233E-03	12,87310646	1,561980425
230	279	ENSG00000279133	AC018628.2	9,54888E-03	20,17107241	-0,105897071
231	108	ENSG00000279873	LINC01126	2,24307E-04	17,19507239	1,429102956
232	9	ENSG00000166016	ABTB2	6,47827E-39	823,5562139	1,063664908
233	64	ENSG00000112299	VNN1	3,24236E-09	104,1580227	1,15390348
234	33	ENSG00000170385	SLC30A1	2,63371E-14	1672,746209	1,049034582
235	60	ENSG00000255182	AC084125.2	8,00279E-09	107,4644714	1,10901202
236	136	ENSG00000279196	AC135048.4	1,86100E-03	18,13346008	1,469120742

237	154	ENSG00000178127	NDUFV2	2,09683E-03	24,94251318	1,07050615
238	280	ENSG00000153283	CD96	8,96558E-03	19,60412797	0,084549716
239	70	ENSG00000105371	ICAM4	5,81840E-08	12,50122803	2,571422909
240	101	ENSG00000170049	KCNAB3	2,93578E-04	118,4380141	1,007817976
241	132	ENSG00000166920	C15orf48	7,07441E-04	41,26528593	1,155010895
242	283	ENSG00000231793	DOC2GP	8,38388E-03	26,95579711	0,026012431
243	134	ENSG00000262766	AC135050.5	1,73479E-03	10,5352983	1,6656779
244	73	ENSG00000254995	STX16-NPEPL1	4,21889E-07	25,23068078	1,631973541
245	83	ENSG00000279789	AC120114.3	9,55452E-06	46,69961575	1,187941481
246	67	ENSG00000242028	HYPK	2,56240E-08	83,5420095	1,143973528
247	157	ENSG00000259562	AC090607.2	5,37186E-03	25,59437596	1,207097304
248	102	ENSG00000261884	AC040162.1	1,94891E-04	29,54380821	1,167129046
249	88	ENSG00000103269	RHBDL1	1,95965E-05	90,44557492	1,152247434
250	59	ENSG00000275888	AC132872.3	2,07634E-09	36,92833097	1,480322841
251	243	ENSG00000187944	C2orf66	6,99721E-05	27,68619295	0,394434202
252	90	ENSG00000259318	AL356801.1	2,58864E-05	20,84904983	1,429543247
253	79	ENSG00000260597	AC012531.1	2,72677E-06	27,04935984	1,716070575
254	149	ENSG00000110025	SNX15	2,55997E-03	27,08223289	1,021858195
255	253	ENSG00000207973	MIR589	8,50076E-03	12,36167634	-0,4373619
256	124	ENSG00000271698	AC233992.2	1,02785E-03	12,47543403	1,610442274
257	99	ENSG00000169896	ITGAM	7,33964E-05	17,16778074	1,564112086
258	89	ENSG00000227471	AKR1B15	2,52046E-05	9,002317808	2,563955998
259	164	ENSG00000259436	AC010247.2	1,66874E-05	52,17845733	0,765358914
260	165	ENSG00000234345	AC234782.2	8,11503E-03	15,09669512	1,211685971
261	209	ENSG00000270441	AC135506.1	2,76426E-05	34,14883067	0,556747074
262	214	ENSG00000172201	ID4	2,25625E-03	25,37880593	-0,547877486
263	196	ENSG00000178623	GPR35	4,40469E-04	41,09647383	0,55037812
264	148	ENSG00000163131	CTSS	3,55687E-03	21,99030055	1,193240875
265	117	ENSG00000287707	AC115284.4	6,76544E-04	45,07462659	1,098956316
266	250	ENSG00000258404	LINC02320	8,31910E-03	15,78723789	0,380172649
267	35	ENSG00000160223	ICOSLG	5,23237E-16	304,1622603	1,295161908
268	86	ENSG00000128284	APOL3	1,47841E-08	54,83226232	0,859267392
269	31	ENSG00000123119	NECAB1	8,32165E-15	100,5273252	1,641868818
270	155	ENSG00000287089	AL138889.3	2,61238E-03	14,66876346	1,332095244
271	144	ENSG00000204531	POU5F1	1,99730E-03	16,87340327	1,200104309
272	41	ENSG00000277117	FP565260.3	1,94530E-13	138,8431008	1,345473817
273	212	ENSG00000154556	SORBS2	1,07679E-03	32,31352535	0,580483328
274	158	ENSG00000222009	BTBD19	4,22364E-03	10,29366245	1,526065747
275	55	ENSG00000285744	AC083837.1	1,17536E-09	14,02525151	2,84416782
276	37	ENSG00000049249	TNFRSF9	1,44630E-15	256,856284	1,152201989
277	118	ENSG00000224066	AL049795.1	7,08305E-04	22,12099908	1,140163196
278	146	ENSG00000205177	C11orf91	3,44480E-03	12,76453318	1,48778169
279	163	ENSG00000203804	ADAMTSL4-AS1	7,75688E-03	9,062502528	1,530617489
280	127	ENSG00000287721	AC061975.8	1,38879E-03	17,27779932	1,424753783
281	120	ENSG00000172738	TMEM217	2,10527E-05	61,73821012	0,752372903
282	56	ENSG00000162654	GBP4	1,84111E-11	110,0641644	1,425751857
283	171	ENSG00000259571	BLID	7,69537E-03	11,69271536	-1,298061058
284	150	ENSG00000005102	MEOX1	4,06729E-03	15,21598066	1,232653359
285	138	ENSG00000280537	AC068946.1	2,58237E-03	12,12631056	1,542651629
286	111	ENSG00000198064	NPIPB13	2,72146E-04	10,49690586	2,681642486

287	228	ENSG00000145040	UCN2	6,31692E-03	23,60797182	-0,703421648
288	205	ENSG00000286952	AC093928.1	1,06688E-03	14,76727102	0,881318045
289	153	ENSG00000285816	AP000944.5	1,38732E-03	21,4369823	0,944983367
290	179	ENSG00000269959	SPACA6P-AS	8,20439E-03	25,73736667	0,775110554
291	100	ENSG00000121075	TBX4	1,53015E-05	29,54255617	1,024321944
292	96	ENSG00000261379	AC010735.1	5,47777E-05	22,484625	1,33685419
293	162	ENSG00000130477	UNC13A	7,45539E-03	9,696791818	1,574155991
294	115	ENSG00000204616	TRIM31	6,47471E-04	20,19697283	1,763927489
295	76	ENSG00000245025	AC107959.1	5,26452E-07	42,76005875	1,131565182
296	113	ENSG00000254363	AC011379.2	3,45563E-04	30,87637021	1,060653872
297	125	ENSG00000280213	UCKL1-AS1	1,09814E-03	17,23035963	1,344845944
298	159	ENSG00000232124	AP001057.1	9,82788E-04	22,87694557	1,154951488

ctr-p01-p31_lfcSE	ctr-p01-p31_stat	ctr-p01-p31_pvalue	ctr-p01-p31_padj	ctr-p01-p31_twofold-padj1e-2	p01-p31_baseMean	p01-p31_log2FoldChange
0,159218317	15,8293074	1,95360E-56	1,67648E-52	1	10233,04757	0,600979842
0,370593512	10,06638134	7,77876E-24	8,34418E-21	1	20821,01446	-0,624637131
0,283324623	12,08011831	1,34526E-33	2,30887E-30	1	180,8237835	0,305728107
0,095531124	13,70892436	8,97789E-43	3,85219E-39	1	1796,838193	0,091129826
0,107139462	-5,387447958	7,14652E-08	5,78564E-06	0	984,772265	0,77600027
0,104282382	15,75835886	6,01754E-56	3,44264E-52	1	1425,157364	0,315966002
0,083370611	12,86250008	7,31712E-38	1,79405E-34	1	1274,422312	0,087862817
0,26190882	9,824708829	8,81283E-23	7,96077E-20	1	4540,132777	0,316898957
0,258205846	9,917872229	3,48098E-23	3,31911E-20	1	2224,267582	-0,575189691
0,265102311	13,58658098	4,81032E-42	1,37599E-38	1	839,3447614	-0,045109345
0,314844541	10,20543484	1,87479E-24	2,29836E-21	1	221,8047506	0,56687672
0,109955239	-4,444644701	8,80372E-06	3,61479E-04	0	675,5655362	0,867320583
0,419788357	8,695466747	3,45407E-18	1,79643E-15	1	2403,475006	-1,713238898
0,416604582	8,641046483	5,57004E-18	2,81173E-15	1	1297,973683	-1,208037957
0,255653718	7,13697022	9,54105E-13	2,30638E-10	1	345,2402297	-0,162564492
0,290062499	6,283151816	3,31777E-10	4,48369E-08	1	3756,554465	0,229389387
0,368522399	9,510621157	1,89527E-21	1,62643E-18	1	2354,15805	-0,840445321
0,066663557	18,01387408	1,51635E-72	2,60251E-68	1	1992,459157	0,377501678
0,120816913	7,498691204	6,44582E-14	1,84111E-11	0	3792,550956	-0,378884002
0,247248114	8,505646545	1,80586E-17	8,85544E-15	1	12475,5374	-0,81424021
0,116979147	4,598484296	4,25576E-06	1,96348E-04	0	1733,887622	-0,784965771
0,141507194	10,19048862	2,18662E-24	2,50194E-21	1	764,1480864	-0,110280519
0,135751991	6,682249002	2,35303E-11	3,88317E-09	0	454,4009795	-0,435058563
0,151090816	8,72216001	2,72944E-18	1,46392E-15	1	373,540642	-0,311610856
0,219786872	10,88007801	1,43440E-27	2,14476E-24	1	4817,917334	-0,289686008
0,218893697	8,088248485	6,05288E-16	2,36104E-13	1	4105,49572	-0,619532964
0,100966874	4,149841037	3,32706E-05	1,04392E-03	0	880,7502637	-0,68626717
0,312903577	7,081806141	1,42288E-12	3,25611E-10	1	1720,211716	-0,957282273
0,352986983	8,733114398	2,47754E-18	1,43855E-15	1	17607,5972	-0,544395612
0,100954974	13,59905917	4,05618E-42	1,37599E-38	1	3602,796781	0,430909737
0,201138196	1,403208847	1,60555E-01	4,32454E-01	0	3160,888054	-1,035529865
0,131206518	4,685948275	2,78667E-06	1,37042E-04	0	3394,517897	-0,626962434
0,166327915	4,43894771	9,03998E-06	3,68535E-04	0	240,5498042	-0,672725228
0,308373519	8,324901095	8,43992E-17	3,71421E-14	1	338,1150984	0,895651739
0,13122024	3,649100096	2,63161E-04	5,27576E-03	0	2856,788728	-0,746078714
0,337492339	5,619997222	1,90961E-08	1,80080E-06	1	979,0876991	-0,962495387

0,195917172	9,141893777	6,13681E-20	4,05100E-17	1	3463,912855	0,500695818
0,120915812	5,161438233	2,45060E-07	1,73800E-05	0	4402,261183	-0,439782866
0,137705833	5,161846222	2,44526E-07	1,73800E-05	0	985,1164782	-0,557527444
0,22611981	4,434867352	9,21290E-06	3,74694E-04	1	198,7944197	-0,908092897
0,194681135	3,098307123	1,94630E-03	2,43117E-02	0	95,8276065	-1,026699602
0,119211966	-3,806574119	1,40905E-04	3,28135E-03	0	218,5547424	0,7249108
0,235527357	2,380976462	1,72668E-02	1,09332E-01	0	2723,567124	-0,654571459
0,15757179	7,02754846	2,10194E-12	4,50945E-10	1	241,1511205	-0,344240356
0,141518686	8,115281203	4,84661E-16	1,93447E-13	1	12918,20345	0,01345778
0,166643622	3,612486383	3,03275E-04	5,89376E-03	0	463,2289651	-0,762988028
0,149756702	5,587093394	2,30902E-08	2,11923E-06	0	827,7172978	-0,447335666
0,257718288	3,374472575	7,39573E-04	1,17967E-02	0	82,58842937	-0,769874062
0,156838889	3,661799849	2,50450E-04	5,09901E-03	0	3884,791564	-0,463381386
0,558455451	9,1766271	4,44805E-20	3,05368E-17	1	147,4197006	0,465454409
0,265310389	6,168658528	6,88718E-10	8,41486E-08	1	455,5788922	0,325752074
0,239907349	1,452832364	1,46270E-01	4,09617E-01	0	4050,102353	-0,89943824
0,153401432	5,305218701	1,12538E-07	8,73977E-06	0	2480,358104	-0,248493654
0,135338407	7,921907251	2,33895E-15	8,02867E-13	1	361,3366851	0,197940338
0,169062615	4,614676762	3,93708E-06	1,84623E-04	0	127,0486073	-0,299119101
0,150401939	-2,73267828	6,28217E-03	5,61567E-02	0	148,5084172	0,756289443
0,77199155	6,013552878	1,81501E-09	2,02279E-07	1	40,09175802	-1,277346414
0,18321978	5,626452704	1,83953E-08	1,74430E-06	1	146,6098373	-0,39385093
0,197126023	5,006145276	5,55309E-07	3,49112E-05	0	90,73291927	-0,588002765
0,183635141	-1,884053751	5,95577E-02	2,43726E-01	0	46,57397006	1,100212458
0,134512532	8,325397143	8,40465E-17	3,71421E-14	1	546,137367	0,112134525
0,177073532	5,897398943	3,69276E-09	3,88828E-07	1	163,1914291	-0,340374367
0,324734825	4,69414262	2,67727E-06	1,32421E-04	1	50,71891915	-0,845456238
0,14865698	-1,050491027	2,93492E-01	5,91778E-01	0	1336,146424	0,906789648
0,177030595	4,376855287	1,20404E-05	4,63339E-04	0	94,42531185	-0,363082121
0,265061128	-1,934859449	5,30075E-02	2,28241E-01	0	359,4435615	0,785503684
0,165760527	4,553338427	5,28012E-06	2,31180E-04	0	482,4055806	-0,309948597
0,158656656	9,211020236	3,23040E-20	2,41058E-17	1	113,1383001	0,367617618
0,195217361	6,489030312	8,63906E-11	1,30063E-08	1	287,8774202	0,066217943
0,216495841	9,477013716	2,61664E-21	2,13854E-18	1	116,6065477	0,617653932
0,252974837	4,249702161	2,14055E-05	7,26052E-04	1	3372,933363	-0,856155205
0,252978481	4,201377447	2,65296E-05	8,71280E-04	1	38,42660719	-0,618600158
0,261523154	6,588975685	4,42871E-11	6,91000E-09	1	44,60876398	-0,058433581
0,239036104	0,609276858	5,42341E-01	7,92239E-01	0	71,52617934	-1,187257008
0,197524141	3,031817994	2,43086E-03	2,87730E-02	0	60,20470585	-0,597964866
0,255795546	1,892206297	5,84635E-02	2,41320E-01	0	113,4047451	-0,985852915
0,179836086	4,096675084	4,19127E-05	1,26201E-03	0	73,13724499	-0,464011369
0,217539192	7,017020372	2,26650E-12	4,80245E-10	1	79,81993628	0,125903571
0,168901086	5,063310577	4,12038E-07	2,69916E-05	0	71,46706417	-0,221052856
0,262687726	2,682976237	7,29702E-03	6,21532E-02	0	385,9042474	-0,49304715
0,182907708	0,961433592	3,36334E-01	6,31772E-01	0	68,0378684	-0,92297662
0,148045905	7,347446442	2,02029E-13	5,33450E-11	1	463,8152681	0,163496099
0,215752909	4,295055789	1,74649E-05	6,15505E-04	0	57,95502167	-0,383358498
0,20334552	1,60104721	1,09366E-01	3,48313E-01	0	273,7527066	-0,71983416
0,213036077	4,572929286	4,80952E-06	2,14405E-04	0	115,1550481	-0,264964676
0,17188229	-1,595787284	1,10536E-01	3,50254E-01	0	103,9674272	0,772803986

0,236697139	3,867017914	1,10174E-04	2,71246E-03	0	62,6600789	-0,331964025
0,208894893	3,994101137	6,49401E-05	1,81144E-03	0	142,8629982	-0,323325091
0,167118715	-0,706168132	4,80084E-01	7,49776E-01	0	1053,135662	1,157011909
0,266623264	-1,784749376	7,43020E-02	2,78073E-01	0	5108,785443	1,061704088
0,214637105	7,192932956	6,34141E-13	1,57736E-10	1	117,3807922	0,43235077
0,198818919	3,741899385	1,82635E-04	4,00336E-03	0	222,9578281	-0,447053587
0,179318913	3,907072514	9,34211E-05	2,38245E-03	0	62,88429639	-0,367285816
0,20618369	4,236951897	2,26575E-05	7,56557E-04	0	89,34183584	-0,242443312
0,402177761	2,250614349	2,44100E-02	1,38403E-01	0	160,0986884	-1,217760265
0,393989802	9,183002277	4,19236E-20	2,99806E-17	1	41,15726372	1,373899199
0,251923313	5,910371203	3,41338E-09	3,61628E-07	1	48,06810889	0,183832911
0,194821482	2,702503288	6,88195E-03	5,95037E-02	0	143,1641788	-0,514220674
0,610090249	3,745577191	1,79979E-04	3,98065E-03	1	410,7788793	-0,907268051
0,458363099	4,755972353	1,97493E-06	1,02096E-04	1	15,50687204	-0,31803744
0,217482655	-2,906897072	3,65033E-03	3,84832E-02	0	87,3827745	0,534380048
0,4352322	3,97447139	7,05357E-05	1,91723E-03	1	27,05184237	-0,261300947
0,297721476	3,03630445	2,39497E-03	2,84653E-02	0	44,51645845	-0,572875928
0,199393669	-3,010643831	2,60694E-03	3,01910E-02	0	161,965029	0,437470481
0,391645171	-1,796550365	7,24070E-02	2,74210E-01	0	168,5894548	1,192608366
0,289114683	2,494191881	1,26244E-02	8,92167E-02	0	27,03370794	-0,758750228
0,29740277	-0,561952914	5,74148E-01	8,10637E-01	0	37,66448969	-1,599097884
0,310164868	1,31682365	1,87898E-01	4,68557E-01	0	22,91719377	-1,051031328
0,32017904	1,90866525	5,63053E-02	2,36029E-01	0	38,4039394	-0,898502276
0,26045431	6,320947176	2,59965E-10	3,56942E-08	1	35,5315404	0,206227505
0,171237476	7,29619087	2,96029E-13	7,47168E-11	1	107,2298955	0,298833141
0,213216536	2,76584088	5,67762E-03	5,22001E-02	0	137,2247606	-0,486842872
0,250539891	3,268831055	1,07993E-03	1,57208E-02	0	42,86086288	-0,443949294
0,225854946	-0,541122444	5,88423E-01	8,18940E-01	0	1867,461805	0,950120797
0,39311079	-6,924537252	4,37403E-12	8,53085E-10	1	15,43981746	-0,937843925
0,349099485	-1,266323422	2,05397E-01	4,91459E-01	0	68,87612829	0,854313453
0,267190117	-1,217138701	2,23551E-01	5,13767E-01	0	16,66526896	1,278317803
0,248149113	3,522291533	4,27833E-04	7,77850E-03	0	43,17950082	-0,382018462
0,154154898	6,764997936	1,33311E-11	2,40844E-09	1	230,2249695	0,230972204
0,294359163	-1,792683269	7,30236E-02	2,75498E-01	0	32,1517335	0,830143146
0,279334226	-1,510617439	1,30886E-01	3,84196E-01	0	701,4011814	0,739403865
0,428360462	7,812244	5,61787E-15	1,85422E-12	1	25,51447947	1,102439454
0,240713016	3,388332296	7,03190E-04	1,13750E-02	0	62,36949998	-0,27338635
0,239202978	2,689591392	7,15396E-03	6,12691E-02	0	51,42408617	-0,522869592
0,282494756	-0,275673568	7,82799E-01	9,13718E-01	0	156,8260482	0,965409312
0,338504709	-0,537208783	5,91123E-01	8,20245E-01	0	13,39826804	1,574397422
0,242561055	1,197446989	2,31132E-01	5,23253E-01	0	47,64354347	-0,721459699
0,353355854	2,56558402	1,03002E-02	7,81533E-02	0	23,18215041	-0,613493766
0,353366332	-1,743733428	8,12056E-02	2,92739E-01	0	21,36470285	1,029692186
0,2440969	5,945142532	2,76216E-09	2,98157E-07	1	58,39738827	0,261729165
0,261387816	-1,271652646	2,03497E-01	4,89047E-01	0	833,6102016	0,854441723
0,354156257	1,254243983	2,09753E-01	4,96833E-01	0	7882,089828	-0,911589386
0,280759997	4,419206309	9,90640E-06	3,99116E-04	1	46,4404155	-0,046713605
0,386867836	1,611511299	1,07068E-01	3,44768E-01	0	26,14002445	-1,022836648
0,219363972	1,26962966	2,04217E-01	4,89658E-01	0	81,67158283	1,430716707
0,21059167	3,444413218	5,72300E-04	9,58282E-03	0	58,30133427	-0,28161258

0,277162947	2,738102634	6,17948E-03	5,54097E-02	0	43,02155849	-0,362429228
0,146361346	2,908173607	3,63546E-03	3,84209E-02	0	101,2334607	1,147292686
0,354362442	-1,460416543	1,44176E-01	4,06120E-01	0	32,96355211	1,009702611
0,32501349	4,394294714	1,11133E-05	4,32153E-04	1	28,86388289	0,053728424
0,184932149	5,459664358	4,77036E-08	4,09368E-06	1	152,3876253	0,180123542
0,272412817	5,134347936	2,83124E-07	1,92828E-05	1	46,16778062	0,246838192
0,352000872	-0,409750554	6,81989E-01	8,70194E-01	0	112,4170704	0,927303211
0,267071548	-0,837236824	4,02459E-01	6,91363E-01	0	69,42273891	0,945968028
0,258055035	5,775469473	7,67388E-09	7,70215E-07	1	146,4439856	0,61405094
0,588339136	1,140779491	2,53962E-01	NA	0	11,02900169	-1,616429325
0,329947951	-2,483882181	1,29959E-02	9,08917E-02	0	11,42440333	0,606620663
0,254057746	-0,697159371	4,85703E-01	7,52969E-01	0	2016,945376	0,915471093
0,265501094	2,295473394	2,17060E-02	1,27889E-01	0	69,15230964	-0,392309577
0,410035087	-0,767734675	4,42645E-01	7,22475E-01	0	50,89553021	0,972634592
0,460332505	-0,595399468	5,51576E-01	NA	0	5,793876631	2,180441879
0,295270838	0,53431079	5,93127E-01	8,20954E-01	0	19,90506429	1,593948715
0,587545659	2,522192814	1,16626E-02	NA	0	8,557330543	-0,883406808
0,280237771	1,029180129	3,03395E-01	6,00665E-01	0	39,51075723	-0,770676865
0,285394261	4,08026568	4,49843E-05	1,33807E-03	1	38,43523711	-0,005980861
0,280083166	-0,642373805	5,20631E-01	7,76454E-01	0	23,27918529	1,079039494
0,152671666	6,666198487	2,62514E-11	4,25050E-09	1	410,2032533	0,393610962
0,250553615	3,666232372	2,46150E-04	5,01743E-03	0	47,40420698	-0,154016301
0,291063794	2,122444474	3,38004E-02	1,71126E-01	0	30,16324932	-0,593331077
0,277664006	-2,666241743	7,67045E-03	6,44386E-02	0	13,78983666	0,513895875
0,274796149	-3,790720679	1,50211E-04	3,45123E-03	1	371,7918521	-0,074246687
0,259023487	-1,745727433	8,08583E-02	2,91978E-01	0	29,10641305	0,73238693
0,408457888	-2,422641264	1,54081E-02	1,01716E-01	0	22,54906224	0,494963208
0,322426405	1,595067541	1,10697E-01	3,50534E-01	0	19,62141525	-0,683585481
0,184171813	5,452193627	4,97522E-08	4,24825E-06	1	160,0673035	0,22555526
0,50031164	-1,349593375	1,77146E-01	4,55550E-01	0	10,95116711	1,222768446
0,305978055	2,577931615	9,93937E-03	7,63947E-02	0	27,97468563	-0,390144707
0,343250335	-1,632304664	1,02615E-01	3,35656E-01	0	112,7850907	0,816560137
0,331395778	2,705698852	6,81608E-03	5,91129E-02	0	122,244871	-0,176612338
0,254581252	-2,08442918	3,71211E-02	1,81203E-01	0	18,47463718	0,59552193
0,343617703	1,522990673	1,27761E-01	3,79312E-01	0	927,6453335	-0,709985495
0,369020992	4,302453945	1,68917E-05	5,99118E-04	1	24,05067676	0,055890525
0,27320769	0,392153902	6,94945E-01	8,76703E-01	0	27,87568082	-0,910067348
0,313863883	3,630722091	2,82629E-04	5,58201E-03	1	37,61271769	-0,113795166
0,326707425	2,934421927	3,34170E-03	3,63020E-02	0	23,54169348	-0,198357704
0,255001168	-2,18646205	2,87818E-02	1,54249E-01	0	72,9555601	0,47447724
0,560072481	3,77953788	1,57120E-04	NA	0	9,94904227	-0,034066927
0,353918043	1,799895837	7,18771E-02	2,72787E-01	0	170,5658134	-0,601595393
0,580409898	3,437712286	5,86651E-04	NA	0	10,54783156	-0,365084888
0,43236579	1,754332197	7,93736E-02	2,88437E-01	0	16,94559178	-0,611269667
0,418790612	-1,55833914	1,19153E-01	3,64966E-01	0	23,61883829	0,954197855
0,40271493	-1,111337525	2,66423E-01	5,63351E-01	0	19,92713281	0,92695855
0,356517773	5,150141694	2,60290E-07	1,80864E-05	1	27,93570249	0,488297283
0,338256386	-1,675560936	9,38242E-02	3,19127E-01	0	8,156729013	0,962481579
0,660680188	1,303778349	1,92309E-01	NA	0	9,284858919	-1,04595605
0,306146743	-0,59745284	5,50205E-01	7,96690E-01	0	31,34130903	0,837979939

0,203547599	4,917571586	8,76244E-07	5,20380E-05	1	2662,966845	0,187812814
0,343140918	4,374108643	1,21930E-05	4,67116E-04	1	19,76436138	0,11263034
0,169513695	6,736633461	1,62098E-11	2,83887E-09	1	137,543122	0,575107019
0,326073413	-0,285770246	7,75054E-01	9,10594E-01	0	337,5197839	0,952766826
0,341394224	4,858385979	1,18347E-06	6,68152E-05	1	44,97342791	0,691301828
0,440484344	-0,92083389	3,57137E-01	6,51287E-01	0	105,0067409	1,020716548
0,492550739	-1,408550264	1,58968E-01	4,30275E-01	0	27,73773548	0,694550699
0,319098254	-2,496391541	1,25464E-02	8,90763E-02	0	14,66124419	0,353340623
0,340557326	2,852528299	4,33730E-03	4,34819E-02	0	23,094932	-0,156287608
0,156189681	8,020704712	1,05140E-15	3,83941E-13	1	103,8631278	0,6537492
0,261179662	-1,351671022	1,76481E-01	4,54522E-01	0	22,26928383	0,725794169
0,167555661	7,110575064	1,15560E-12	2,71694E-10	1	171,5149972	0,629091375
0,661440249	-0,729785549	4,65521E-01	7,38496E-01	0	13,6463852	1,474735462
0,320896372	4,398321789	1,09091E-05	4,27473E-04	1	25,23421827	0,140725732
0,30817187	-3,244315675	1,17733E-03	1,68388E-02	0	12,86672127	0,091252121
0,473218731	2,02065553	4,33154E-02	NA	0	9,632835656	-0,680631908
0,265132549	0,057645003	9,54031E-01	9,83367E-01	0	21,04798137	1,059644456
0,381457809	0,309018876	7,57307E-01	9,02904E-01	0	14,65286072	-1,052378238
0,397315604	3,026859417	2,47109E-03	2,91286E-02	0	21,09570181	-0,240381468
0,512983523	-0,983999649	3,25116E-01	6,20377E-01	0	29,4021131	0,800562073
0,305139544	-2,932080776	3,36699E-03	3,64361E-02	0	651,1353366	0,324694582
0,652199556	1,830720763	6,71422E-02	2,62736E-01	0	79,4937168	-0,981914554
0,513278425	2,903412734	3,69120E-03	3,87474E-02	0	12,24061819	-0,311906462
0,327190744	4,142635791	3,43337E-05	1,07140E-03	1	23,56414677	0,097318759
0,278557412	2,890972441	3,84052E-03	3,98759E-02	0	43,05546385	-0,246028009
0,16284023	7,03461772	1,99808E-12	4,34089E-10	1	187,5225148	0,553405982
0,554902636	1,972909968	4,85058E-02	NA	0	9,706905756	-0,861290948
0,315282035	2,521269069	1,16932E-02	8,51468E-02	0	29,97023364	-0,356128706
0,379347237	2,057830321	3,96064E-02	1,88353E-01	0	15,7728327	-0,537873803
0,653912622	0,181565523	8,55924E-01	NA	0	6,793976783	-1,739285008
0,269856154	-2,660079376	7,81222E-03	6,52463E-02	0	534,2424792	0,28847223
0,461154394	2,873604951	4,05816E-03	4,14516E-02	0	15,2496631	-0,286947616
0,37296426	0,598574807	5,49456E-01	7,96271E-01	0	117,5508882	-0,973641466
0,325218131	2,332265263	1,96867E-02	1,19732E-01	0	25,80922133	-0,403483221
0,473472015	-1,383995413	1,66360E-01	4,40351E-01	0	269,0668112	0,778671619
0,443375392	2,370418793	1,77679E-02	1,11745E-01	0	12,21569623	-0,439290143
0,505562479	1,465693668	1,42732E-01	NA	0	11,00482657	-0,814377411
0,445327308	1,903538723	5,69703E-02	NA	0	10,72731537	-0,644850521
0,575540058	-1,220333738	2,22338E-01	5,12489E-01	0	20,5096447	1,287365431
0,335234746	0,445825223	6,55724E-01	8,55512E-01	0	95,72545749	1,089203932
0,337822862	-0,529294062	5,96601E-01	8,23109E-01	0	655,1978344	0,915128972
0,293790654	3,962560024	7,41504E-05	1,99474E-03	1	22,40872	0,091859479
0,410191795	3,807927035	1,40137E-04	3,27233E-03	1	16,34673092	0,204903488
0,324534907	-0,3263041	7,44194E-01	8,97899E-01	0	22,3079521	-1,056586027
0,31331085	4,561294173	5,08393E-06	2,24307E-04	1	21,38632669	0,313329756
0,085481644	12,44319663	1,52285E-35	3,26709E-32	1	945,219812	0,78043344
0,171930461	6,711454587	1,92694E-11	3,24236E-09	1	122,5943916	0,608334634
0,142978063	7,337031718	2,18383E-13	5,59419E-11	1	1932,501545	0,629252031
0,208599253	5,316471689	1,05799E-07	8,25374E-06	1	127,2935329	0,406486695
0,36868625	3,984745142	6,75526E-05	1,86100E-03	1	22,76034665	0,309062121

0,271251915	3,946538594	7,92891E-05	2,09683E-03	1	29,7855849	0,205266919
0,275961604	0,306382173	7,59314E-01	9,03533E-01	0	17,93714842	1,101142566
0,412081102	6,24008938	4,37321E-10	5,81840E-08	1	16,77442699	1,131219033
0,226573835	4,448077489	8,66423E-06	3,59189E-04	1	137,9517836	0,389088351
0,271301869	4,257290598	2,06919E-05	7,07441E-04	1	48,87213566	0,406532442
0,381166343	0,068244302	9,45591E-01	9,80245E-01	0	23,74296216	1,290033189
0,41579679	4,005990281	6,17582E-05	1,73479E-03	1	13,44822196	0,353050884
0,329474535	4,953261529	7,29798E-07	4,44167E-05	1	31,65253425	0,553882907
0,248852412	4,773678783	1,80891E-06	9,45263E-05	1	55,90538959	0,43775136
0,21405822	5,344216762	9,08088E-08	7,18227E-06	1	98,91601487	0,47711107
0,335390094	3,599084543	3,19339E-04	6,14442E-03	1	31,11641055	0,258132585
0,253661588	4,601126463	4,20212E-06	1,94891E-04	1	35,34484047	0,402986966
0,224584871	5,130565691	2,88873E-07	1,95965E-05	1	106,7614213	0,569569701
0,218030633	6,789517682	1,12509E-11	2,07634E-09	1	44,89081309	0,85001126
0,301676841	1,307472598	1,91052E-01	4,72510E-01	0	26,80170587	1,360022431
0,29570766	4,834312542	1,33607E-06	7,37328E-05	1	25,4556278	0,526026738
0,340079582	5,046085289	4,50954E-07	2,93171E-05	1	33,90437643	0,784627242
0,262953131	3,886084908	1,01874E-04	2,55997E-03	1	31,82960008	0,359482256
0,357511156	-1,223351756	2,21197E-01	5,11198E-01	0	13,15184378	-1,220170385
0,392697656	4,100972464	4,11418E-05	1,24316E-03	1	15,60989513	0,553452955
0,323413214	4,836265237	1,32301E-06	7,33964E-05	1	21,20248172	0,738206409
0,490186223	5,230575395	1,68983E-07	NA	0	12,01212378	1,24421378
0,209979129	3,644928517	2,67466E-04	5,33782E-03	0	55,39642397	1,216799888
0,399861205	3,03026639	2,44338E-03	2,88416E-02	0	18,40704462	0,229055862
0,237244789	2,346719929	1,89395E-02	1,16523E-01	0	34,68208397	1,175751652
0,248777005	-2,20228347	2,76453E-02	1,50103E-01	0	25,6607105	-1,025551874
0,211200711	2,605948237	9,16203E-03	7,22840E-02	0	42,27664244	1,037726338
0,339616673	3,51349321	4,42256E-04	7,93149E-03	1	26,15392631	0,434396058
0,261982854	4,194764267	2,73156E-05	8,87911E-04	1	52,65646935	0,586607148
0,321073924	1,184065786	2,36387E-01	5,29526E-01	0	15,45197892	1,193983526
0,146458539	8,84319835	9,30169E-19	5,91277E-16	1	358,2700127	0,987437371
0,174390952	4,927247544	8,33961E-07	4,96988E-05	0	59,05698369	1,272597828
0,200379919	8,19377923	2,53149E-16	1,03448E-13	1	122,4389461	1,266472406
0,343315171	3,880094317	1,04416E-04	2,61238E-03	1	17,71808664	0,603982833
0,302941407	3,961506359	7,44784E-05	1,99730E-03	1	19,91475752	0,599109815
0,16804104	8,006816782	1,17716E-15	4,20907E-13	1	164,3586311	1,042939217
0,260423704	2,228995742	2,58142E-02	1,43461E-01	0	33,39435686	1,077515519
0,40972841	3,724578795	1,95642E-04	4,22364E-03	1	12,71011458	0,700450268
0,413742559	6,874245244	6,23189E-12	1,17536E-09	1	18,89436102	1,973260353
0,132025404	8,727123379	2,61232E-18	1,44630E-15	1	296,2046734	0,951688375
0,270613914	4,213246758	2,51726E-05	8,30840E-04	1	26,05550691	0,627903578
0,39305435	3,785180578	1,53597E-04	3,50557E-03	1	15,54634274	0,784474652
0,450643354	3,39651628	6,82495E-04	NA	0	11,2256672	0,743594201
0,406703927	3,503171935	4,59753E-04	8,16846E-03	1	20,92944502	0,742199732
0,185614084	4,053425734	5,04730E-05	1,46577E-03	0	65,90018485	1,05268455
0,190183492	7,496717225	6,54359E-14	1,84111E-11	1	131,383233	1,135754215
0,368200462	-3,525419421	4,22813E-04	7,69537E-03	1	9,238536234	-0,830009763
0,329917762	3,736244309	1,86789E-04	4,06729E-03	1	17,92658702	0,694743246
0,455016463	3,390320473	6,98110E-04	1,13141E-02	0	14,94878955	0,783552324
0,593779087	4,51622926	6,29505E-06	2,72146E-04	1	14,01798819	1,862582948

0,381735034	-1,842696073	6,53734E-02	2,58151E-01	0	23,34460202	-1,153446301
0,348001237	2,532514119	1,13248E-02	8,29566E-02	0	15,91326807	1,372676096
0,265797789	3,55527174	3,77589E-04	6,95338E-03	0	23,59259639	1,218390707
0,291328905	2,66060298	7,80009E-03	6,51767E-02	0	27,69231264	1,083064311
0,222649758	4,6005976	4,21281E-06	1,94891E-04	1	32,73615013	1,252111082
0,296521867	4,508450607	6,53028E-06	2,80198E-04	1	26,56726999	1,154566
0,45157198	3,485947009	4,90398E-04	8,54488E-03	1	11,68492598	1,255575282
0,425015788	4,150263448	3,32093E-05	1,04390E-03	1	24,81540518	1,533076656
0,215388155	5,253609154	1,49147E-07	1,11710E-05	1	48,70341991	1,283861205
0,267360162	3,967135067	7,27418E-05	1,96300E-03	1	34,82730064	1,224788782
0,353535239	3,803994045	1,42382E-04	3,30676E-03	1	20,2329666	1,199837634
0,314327909	3,674352345	2,38453E-04	4,91306E-03	1	26,14587118	1,260945977

p01-p31_lfcSE	p01-p31_stat	p01-p31_pvalue	p01-p31_padj	p01-p31_twofold-padj1e-2	ctr-p01_baseMean	ctr-p01_log2FoldChange
0,220400477	2,726762896	6,39590E-03	5,22157E-02	0	5006,112014	1,919171875
0,430716236	-1,450228894	1,46995E-01	3,62766E-01	0	12896,14532	4,353968006
0,340998994	0,89656601	3,69951E-01	6,05367E-01	0	87,77211998	3,118443572
0,098982576	0,920665332	3,57225E-01	5,93025E-01	0	1211,834296	1,218929846
0,105829428	7,332556625	2,25803E-13	1,24064E-10	0	1256,646929	-1,354531156
0,103739197	3,045772575	2,32083E-03	2,67513E-02	0	864,3697936	1,325625804
0,087612476	1,002857361	3,15930E-01	5,54222E-01	0	905,3699441	0,983636053
0,312092379	1,015401136	3,09915E-01	5,48199E-01	0	2380,32371	2,255757686
0,30939575	-1,859074309	6,30166E-02	2,19884E-01	0	1443,289368	3,135496529
0,273613773	-0,164865038	8,69050E-01	9,43833E-01	0	448,1900537	3,645613079
0,325936613	1,739223817	8,19954E-02	2,58805E-01	0	100,9355233	2,65309144
0,100305758	8,646767643	5,29787E-18	9,70275E-15	0	828,8720208	-1,357022083
0,489592524	-3,499315892	4,66454E-04	8,59823E-03	1	1836,708679	5,362429929
0,471740767	-2,560808904	1,04429E-02	7,17644E-02	0	913,4028504	4,807220751
0,283213372	-0,574000058	5,65968E-01	7,61248E-01	0	222,359805	1,989926924
0,336477335	0,681738004	4,95405E-01	7,09158E-01	0	2241,50412	1,592986123
0,408560303	-2,057090018	3,96776E-02	1,65918E-01	0	1543,066822	4,344295168
0,074089831	5,095188789	3,48394E-07	3,19032E-05	0	1320,196277	0,822528922
0,115932107	-3,268154202	1,08251E-03	1,57823E-02	0	2943,954755	1,283562171
0,292532598	-2,783417012	5,37896E-03	4,65903E-02	0	8767,408747	2,916085583
0,11760073	-6,674837557	2,47506E-11	9,27192E-09	0	1495,340912	1,32123308
0,136228167	-0,809528027	4,18211E-01	6,47266E-01	0	517,6697172	1,551158798
0,129010873	-3,37226277	7,45533E-04	1,21838E-02	0	354,9827671	1,342199159
0,150972496	-2,064024007	3,90154E-02	1,64224E-01	0	266,4093092	1,629331062
0,245733867	-1,178860739	2,38454E-01	4,73546E-01	0	2982,263788	2,679402757
0,26455012	-2,341835889	1,91892E-02	1,05713E-01	0	2883,561762	2,389408223
0,080628142	-8,511509123	1,71684E-17	2,35822E-14	0	774,7012372	1,103709493
0,373903103	-2,560241588	1,04599E-02	7,18380E-02	0	1227,987863	3,172161028
0,394725396	-1,379175542	1,67841E-01	3,89944E-01	0	10990,64486	3,625566941
0,104910302	4,107411063	4,00119E-05	1,35147E-03	0	2271,447985	0,940707335
0,227104933	-4,559697804	5,12273E-06	2,72380E-04	1	2898,724176	1,317345202
0,126069658	-4,973142968	6,58760E-07	5,38417E-05	0	2854,549233	1,240122378
0,162066359	-4,15092455	3,31135E-05	1,14666E-03	0	197,8361448	1,410067586
0,348575076	2,569465806	1,01855E-02	7,05413E-02	0	151,2094283	1,680162595
0,13752951	-5,424862742	5,79991E-08	6,78013E-06	0	2488,432944	1,223626879
0,373785835	-2,574991607	1,00243E-02	6,98351E-02	0	716,8222232	2,858520087

0,214145336	2,338112173	1,93814E-02	1,06382E-01	0	1968,001534	1,290111862
0,124657928	-3,527917352	4,18843E-04	8,04637E-03	0	3647,643354	1,062305838
0,142548201	-3,911150319	9,18576E-05	2,59706E-03	0	808,274468	1,267239095
0,191257929	-4,748001303	2,05437E-06	1,33842E-04	0	159,8884193	1,909775349
0,170213322	-6,031840451	1,62103E-09	3,25846E-07	1	82,714081	1,628718594
0,119469998	6,067722554	1,29737E-09	2,74160E-07	0	260,9481527	-1,178128422
0,248880404	-2,630064269	8,53687E-03	6,29871E-02	0	2320,257323	1,214529494
0,153666946	-2,240171778	2,50798E-02	1,25803E-01	0	178,9099819	1,450399013
0,133174832	0,101053477	9,19508E-01	9,66906E-01	0	9109,656571	1,134375481
0,172132171	-4,432570759	9,31161E-06	4,42867E-04	0	393,8920736	1,364140792
0,138592474	-3,227705333	1,24787E-03	1,74311E-02	0	655,9418307	1,281853234
0,231759074	-3,321872363	8,94156E-04	1,38259E-02	0	67,08761305	1,650394448
0,144410246	-3,208784685	1,33297E-03	1,81882E-02	0	3260,961972	1,036051038
0,534596887	0,870664271	3,83937E-01	6,18043E-01	0	62,65781283	4,658550575
0,262724447	1,239900121	2,15012E-01	4,46973E-01	0	276,4441945	1,315209273
0,269328861	-3,339553866	8,39131E-04	1,31728E-02	0	3647,855578	1,246998125
0,137057056	-1,813067206	6,98215E-02	2,34488E-01	0	1939,568196	1,060647836
0,128962757	1,53486435	1,24817E-01	3,30912E-01	0	253,3631655	0,875624983
0,172612176	-1,732896877	8,31140E-02	2,60844E-01	0	100,1293233	1,085180706
0,150673665	5,019387057	5,18366E-07	4,49696E-05	0	174,3576474	-1,167141063
0,539102192	-2,369395697	1,78172E-02	1,00714E-01	0	28,02678731	5,925133852
0,161459959	-2,439310234	1,47153E-02	9,00679E-02	0	111,1012717	1,422230899
0,16904838	-3,478310562	5,04585E-04	9,01091E-03	0	70,85020404	1,571047435
0,226293675	4,861878969	1,16277E-06	8,33300E-05	1	53,43277401	-1,447489367
0,132644783	0,845374561	3,97902E-01	6,30212E-01	0	382,4384369	1,006695619
0,158927407	-2,1416971	3,22179E-02	1,46053E-01	0	122,4729585	1,382358891
0,270000059	-3,131318711	1,74023E-03	2,18297E-02	0	37,95009236	2,362954052
0,135425139	6,695873878	2,14387E-11	8,21799E-09	0	1397,407761	-1,063261725
0,158140118	-2,295952003	2,16786E-02	1,14433E-01	0	75,29005843	1,13763375
0,28643452	2,742349924	6,10013E-03	5,04835E-02	0	444,3206441	-1,301516953
0,149682327	-2,070709369	3,83860E-02	1,62586E-01	0	384,5649416	1,063842416
0,145657503	2,523849513	1,16078E-02	7,71806E-02	0	70,58136409	1,092269095
0,185388716	0,357184325	7,20954E-01	8,64543E-01	0	196,5433865	1,200434571
0,188645144	3,274157592	1,05977E-03	1,55853E-02	0	61,29659747	1,432736713
0,267359805	-3,202258483	1,36355E-03	1,84375E-02	0	2670,041876	1,931060612
0,209598091	-2,951363516	3,16374E-03	3,27769E-02	0	29,58789805	1,676392126
0,213173394	-0,274112916	7,83998E-01	9,01167E-01	0	28,44519965	1,779097546
0,192599151	-6,16439379	7,07537E-10	1,59951E-07	1	67,81106772	1,335184638
0,187425533	-3,190413051	1,42070E-03	1,89768E-02	0	50,6888867	1,196031954
0,232048414	-4,248479431	2,15226E-05	8,49803E-04	0	99,99499329	1,469479938
0,16669704	-2,783560933	5,37658E-03	4,65903E-02	0	59,12490363	1,198816982
0,197706885	0,636819355	5,24243E-01	7,31924E-01	0	51,26704137	1,397862255
0,157416883	-1,40425126	1,60244E-01	3,80628E-01	0	55,10612546	1,074647314
0,257702159	-1,913244155	5,57168E-02	2,04767E-01	0	315,5891703	1,197262921
0,161963876	-5,698657275	1,20755E-08	1,79315E-06	0	63,92758243	1,099010372
0,145668428	1,122385279	2,61699E-01	4,97759E-01	0	324,8358753	0,923527962
0,200329446	-1,913640287	5,56661E-02	2,04641E-01	0	44,67615569	1,309794025
0,178025031	-4,043443523	5,26718E-05	1,68254E-03	0	246,3711436	1,044381293
0,199840006	-1,325884046	1,84878E-01	4,09369E-01	0	87,20520348	1,238458249
0,199659912	3,870601651	1,08567E-04	2,97261E-03	0	114,4169838	-1,049351174

0,218706873	-1,517849071	1,29052E-01	3,36975E-01	0	48,32785715	1,245040445
0,189871495	-1,702862726	8,85938E-02	2,70575E-01	0	111,8082132	1,156690877
0,210564012	5,494822671	3,91103E-08	4,74011E-06	1	1085,312218	-1,275663555
0,275471482	3,854134298	1,16140E-04	3,12799E-03	1	6288,358681	-1,538223462
0,214868553	2,012164013	4,42027E-02	1,77989E-01	0	71,19118196	1,111707624
0,182780866	-2,445844566	1,44513E-02	8,89290E-02	0	179,7727237	1,190764653
0,162565589	-2,259308491	2,38642E-02	1,21982E-01	0	50,491039	1,070317167
0,179696137	-1,349184884	1,77278E-01	4,01052E-01	0	69,2582272	1,115373895
0,454863764	-2,677197796	7,42408E-03	5,74701E-02	0	134,0557579	2,122145992
0,291940667	4,706090492	2,52512E-06	1,58257E-04	1	13,56896526	2,242660566
0,227247918	0,808953115	4,18542E-01	6,47581E-01	0	30,60565546	1,304070808
0,193932163	-2,651549215	8,01234E-03	6,03875E-02	0	121,6749924	1,040452128
0,6313924	-1,436932169	1,50737E-01	3,67810E-01	0	289,327686	3,190512237
0,314217807	-1,012156002	3,11463E-01	5,49549E-01	0	9,708318199	2,504252668
0,207367412	2,576972158	9,96700E-03	6,94655E-02	0	112,4234082	-1,16689074
0,374658373	-0,697437894	4,85529E-01	7,01953E-01	0	18,02492354	2,00247598
0,269376281	-2,126675464	3,34471E-02	1,49568E-01	0	34,98726657	1,475715568
0,182989081	2,390691717	1,68167E-02	9,76362E-02	0	204,2701296	-1,037427757
0,384823928	3,099101382	1,94109E-03	2,34384E-02	0	235,8171645	-1,895832118
0,253090602	-2,997939164	2,71812E-03	2,96315E-02	0	22,42351745	1,480310701
0,27809679	-5,750148654	8,91650E-09	1,37790E-06	1	37,69763631	1,430352102
0,277865288	-3,782521142	1,55248E-04	3,90084E-03	1	20,5684421	1,457589063
0,27760986	-3,23656471	1,20978E-03	1,70580E-02	0	33,00370136	1,507136139
0,219196521	0,940833843	3,46790E-01	5,83161E-01	0	21,69780397	1,440578046
0,163755554	1,824873312	6,80201E-02	2,30268E-01	0	70,6915279	0,952416337
0,172244955	-2,82645649	4,70661E-03	4,26728E-02	0	114,9744085	1,071754737
0,221682507	-2,00263566	4,52164E-02	1,80242E-01	0	34,0290369	1,264149302
0,23983995	3,96147846	7,44871E-05	2,21220E-03	0	1924,367095	-1,07318785
0,421630366	-2,224327282	2,61264E-02	1,29051E-01	0	43,93731302	-1,785607167
0,281105588	3,039119422	2,37271E-03	2,70863E-02	0	82,47795547	-1,296654742
0,334760488	3,818604192	1,34209E-04	3,51137E-03	1	19,29189427	-1,605750027
0,21937225	-1,741416531	8,16106E-02	2,58342E-01	0	33,58718784	1,259866505
0,142321518	1,622890254	1,04613E-01	2,98586E-01	0	161,9583278	0,811897724
0,300125072	2,765990662	5,67502E-03	4,82918E-02	0	40,09506303	-1,358990252
0,270642659	2,732030001	6,29454E-03	5,15927E-02	0	827,894695	-1,16168383
0,300479738	3,668931093	2,43567E-04	5,42528E-03	1	9,462247053	2,242031516
0,225568478	-1,211988276	2,25517E-01	4,59992E-01	0	48,53974383	1,086717282
0,223544552	-2,338995012	1,93357E-02	1,06230E-01	0	42,89600153	1,161527725
0,206307398	4,679470159	2,87617E-06	1,76238E-04	0	158,2449479	-1,041592218
0,441815618	3,563471636	3,65982E-04	7,24188E-03	1	14,32351757	-1,766442873
0,224705936	-3,210683758	1,32420E-03	1,81135E-02	0	43,0781697	1,009349676
0,320224183	-1,915825844	5,53873E-02	2,04011E-01	0	18,46268764	1,517367424
0,376435454	2,73537515	6,23092E-03	5,12496E-02	0	28,0686201	-1,647000157
0,228348015	1,14618542	2,51718E-01	4,87853E-01	0	37,35133648	1,186386933
0,253371246	3,372291597	7,45455E-04	1,21838E-02	0	946,907983	-1,187110981
0,396567221	-2,298700792	2,15219E-02	1,13929E-01	0	6967,839642	1,353771268
0,233925733	-0,19969417	8,41720E-01	9,31329E-01	0	32,36986997	1,281805971
0,325962071	-3,137900816	1,70162E-03	2,14361E-02	0	22,53408824	1,639649846
0,219436329	6,519962817	7,03248E-11	2,27287E-08	1	69,59766325	-1,140072503
0,203365686	-1,384759572	1,66126E-01	3,87937E-01	0	46,50800241	1,009468682

0,257994433	-1,404794759	1,60082E-01	3,80628E-01	0	34,52502688	1,120047556
0,175174787	6,549416743	5,77622E-11	1,97161E-08	1	81,145236	-0,724455625
0,316889586	3,186291548	1,44109E-03	1,91406E-02	0	41,05745304	-1,520260663
0,279569075	0,192183001	8,47599E-01	9,33702E-01	0	19,01721939	1,372870638
0,181850472	0,990503576	3,21928E-01	5,60019E-01	0	108,765748	0,82893781
0,256653545	0,961756411	3,36172E-01	5,73853E-01	0	29,84142569	1,149951829
0,252314765	3,675184098	2,37678E-04	5,35128E-03	0	116,8549099	-1,07305364
0,250346903	3,778628842	1,57694E-04	3,93829E-03	0	74,84422554	-1,168803286
0,325490901	1,886537957	5,92225E-02	2,12718E-01	0	86,96395944	0,872760966
0,432813509	-3,734701646	1,87938E-04	NA	0	9,816087434	2,276868415
0,408586918	1,484679601	1,37629E-01	NA	0	16,46447644	-1,436543474
0,219523852	4,170257962	3,04255E-05	1,08551E-03	0	2131,495498	-1,092741967
0,240818118	-1,629070024	1,03298E-01	2,96425E-01	0	57,30845433	1,00010135
0,324019211	3,001780629	2,68406E-03	2,94157E-02	0	57,40736663	-1,291428236
0,667011568	3,268971609	1,07939E-03	NA	0	6,654704504	-2,466519503
0,358275254	4,448950073	8,62911E-06	4,17107E-04	1	17,66233654	-1,434635262
0,431528172	-2,04715906	4,06425E-02	NA	0	6,442913228	2,357697859
0,251476796	-3,064604276	2,17958E-03	2,54795E-02	0	35,91569424	1,056795254
0,251271681	-0,023802367	9,81010E-01	9,92124E-01	0	26,80815164	1,166769607
0,298901346	3,61001885	3,06175E-04	6,38012E-03	1	24,75489552	-1,253984773
0,156120213	2,52120437	1,16954E-02	7,76067E-02	0	284,3807671	0,623160718
0,246097381	-0,625834785	5,31423E-01	7,37327E-01	0	35,83095222	1,074113271
0,25484431	-2,328210026	1,99010E-02	1,08331E-01	0	25,34723705	1,2137193
0,344118486	1,49336899	1,35341E-01	3,46078E-01	0	18,41672045	-1,251811862
0,287676959	-0,258090487	7,96337E-01	9,08627E-01	0	548,7550788	-0,96729651
0,27323461	2,680432504	7,35271E-03	5,71536E-02	0	34,81157391	-1,174435159
0,409862348	1,207632781	2,27189E-01	4,61631E-01	0	34,59485977	-1,484947594
0,296615927	-2,304614881	2,11882E-02	1,13097E-01	0	16,8882923	1,196610663
0,182156289	1,23825129	2,15623E-01	4,47678E-01	0	113,605367	0,779599408
0,560082815	2,183192223	2,90217E-02	NA	0	15,16891363	-1,89555117
0,282285233	-1,38209393	1,66943E-01	3,88716E-01	0	21,98546939	1,178957046
0,246666404	3,310382456	9,31686E-04	1,41800E-02	0	142,9289016	-1,373893976
0,23105869	-0,764361374	4,44652E-01	6,69932E-01	0	93,12888356	1,072087101
0,313697507	1,898395481	5,76440E-02	2,08830E-01	0	22,55030528	-1,124643597
0,382044266	-1,858385422	6,31143E-02	2,20031E-01	0	798,6511917	1,229919585
0,288781708	0,193539006	8,46537E-01	9,33187E-01	0	15,49813904	1,518231998
0,249141254	-3,652816754	2,59379E-04	5,70503E-03	0	26,5366241	1,013372837
0,293664618	-0,387500433	6,98386E-01	8,51883E-01	0	26,86866245	1,255023832
0,302896473	-0,65486964	5,12552E-01	7,22640E-01	0	17,59189012	1,159492778
0,232375798	2,041853085	4,11661E-02	1,70129E-01	0	90,15561866	-1,02502921
0,422609691	-0,080610853	9,35751E-01	NA	0	6,011272119	2,147974478
0,331777118	-1,813251606	6,97930E-02	2,34440E-01	0	142,6438679	1,236874434
0,423364847	-0,862341052	3,88500E-01	NA	0	6,885450941	2,348855518
0,395465457	-1,545696737	1,22178E-01	3,27084E-01	0	13,80618199	1,372722972
0,360614363	2,64603397	8,14416E-03	6,11573E-02	0	31,55241736	-1,592893399
0,424340648	2,184467959	2,89279E-02	1,37174E-01	0	23,99760224	-1,376284557
0,307548285	1,587709334	1,12352E-01	3,11401E-01	0	15,62961946	1,348352778
0,438010256	2,197395075	2,79922E-02	NA	0	10,44988472	-1,528612862
0,589948183	-1,772962575	7,62349E-02	NA	0	7,559149298	1,900346452
0,31692482	2,644096921	8,19092E-03	6,14524E-02	0	33,11895781	-1,025800366

0,225516254	0,832812762	4,04950E-01	6,36847E-01	0	1902,182124	0,812188429
0,286939191	0,392523376	6,94672E-01	8,49355E-01	0	12,54051956	1,389323444
0,170568561	3,371705877	7,47042E-04	1,21916E-02	0	90,60510675	0,569888324
0,325157282	2,930172191	3,38774E-03	3,43632E-02	0	342,9370357	-1,047640883
0,330801821	2,089776368	3,66379E-02	1,57842E-01	0	25,25673427	0,969753701
0,425585671	2,398380905	1,64677E-02	9,62886E-02	0	124,3916977	-1,425736463
0,389604992	1,782704823	7,46344E-02	2,44257E-01	0	37,22780124	-1,391598132
0,371643601	0,950751262	3,41731E-01	5,78965E-01	0	20,25592515	-1,153228987
0,323845543	-0,482599225	6,29380E-01	8,06003E-01	0	17,26889215	1,124302354
0,158329907	4,129031667	3,64294E-05	1,23553E-03	0	65,1240426	0,598212534
0,289511288	2,506963284	1,21773E-02	7,95210E-02	0	25,20515167	-1,073486169
0,176878375	3,556632493	3,75639E-04	7,37509E-03	0	110,1997526	0,559871805
0,55010963	2,680802848	7,34458E-03	5,71536E-02	0	17,14090023	-1,958568951
0,276082156	0,509724112	6,10245E-01	7,92895E-01	0	16,28965093	1,282265362
0,372390531	0,245044149	8,06422E-01	9,14123E-01	0	18,87003374	-1,085698499
0,398925425	-1,706163273	8,79777E-02	NA	0	7,696580583	1,633430836
0,320631782	3,304864073	9,50225E-04	1,43957E-02	0	20,43300591	-1,049930102
0,366307966	-2,872932982	4,06680E-03	3,87251E-02	0	13,93106471	1,167778699
0,350350347	-0,686117396	4,92639E-01	7,07135E-01	0	15,22938035	1,433078893
0,564547992	1,418058489	1,56174E-01	3,75359E-01	0	36,22368383	-1,311268862
0,243445019	1,333749131	1,82286E-01	4,06946E-01	0	936,5161159	-1,218553462
0,75581351	-1,299149249	1,93893E-01	4,21683E-01	0	62,66326251	2,172412648
0,414336128	-0,752786063	4,51578E-01	NA	0	8,397225595	1,798533073
0,29102381	0,334401363	7,38077E-01	8,75357E-01	0	15,85395313	1,246920035
0,256167926	-0,960416911	3,36845E-01	5,74645E-01	0	33,54999452	1,054321504
0,16303649	3,394368842	6,87870E-04	1,14527E-02	0	122,8797709	0,59222195
0,444438413	-1,937930933	5,26316E-02	NA	0	7,807520851	1,944123674
0,273048362	-1,304269705	1,92142E-01	4,19728E-01	0	23,88294376	1,154551917
0,321160598	-1,674781419	9,39771E-02	2,80341E-01	0	12,73264849	1,313825247
0,586269127	-2,966700664	3,01014E-03	NA	0	6,480971204	1,860995295
0,234956846	1,227766864	2,19534E-01	4,52380E-01	0	704,226019	-1,006091301
0,37439842	-0,766423148	4,43425E-01	6,68646E-01	0	10,75730185	1,612075573
0,372265316	-2,61545039	8,91099E-03	6,45058E-02	0	109,0101341	1,195035818
0,30157231	-1,337931925	1,80919E-01	4,05450E-01	0	20,80679498	1,160884555
0,448930136	1,734505119	8,28285E-02	2,60397E-01	0	356,9322208	-1,433176731
0,366035639	-1,20012943	2,30089E-01	NA	0	9,260340982	1,486267016
0,446515318	-1,823851006	6,81746E-02	NA	0	9,185179549	1,555632701
0,380553295	-1,694507787	9,01688E-02	NA	0	8,652925223	1,496996962
0,461917503	2,787002923	5,31980E-03	4,62236E-02	0	28,83122537	-1,992782565
0,248801901	4,377795857	1,19886E-05	5,32634E-04	1	86,88705544	-0,937348054
0,332939247	2,748636514	5,98437E-03	4,97896E-02	0	692,8545611	-1,093484178
0,266535285	0,344642847	7,30363E-01	8,70846E-01	0	15,49722897	1,065742597
0,358318447	0,571847444	5,67425E-01	7,62140E-01	0	10,32883593	1,355247464
0,305436978	-3,459260349	5,41661E-04	9,54888E-03	1	22,41421905	0,949233344
0,277468091	1,129246087	2,58794E-01	4,95059E-01	0	13,5450483	1,119212435
0,091165102	8,560659968	1,12223E-17	1,84978E-14	0	616,7145109	0,282122238
0,162384474	3,746261082	1,79490E-04	4,31902E-03	0	79,74460007	0,544753281
0,1466976	4,289450061	1,79116E-05	7,42165E-04	0	1291,200984	0,418283515
0,198821116	2,044484521	4,09057E-02	1,69452E-01	0	86,15640244	0,706602513
0,3267836	0,945769987	3,44266E-01	5,80897E-01	0	14,14753571	1,163974308

0,244342917	0,840077224	4,00865E-01	6,32777E-01	0	20,7046612	0,86421737
0,316292202	3,481409153	4,98783E-04	8,96558E-03	1	16,72274474	-1,011132513
0,324888536	3,481868105	4,97929E-04	8,96558E-03	1	6,980316091	1,441481327
0,215165315	1,80832283	7,05563E-02	2,35851E-01	0	96,19345715	0,618007436
0,25183108	1,614306072	1,06461E-01	3,01771E-01	0	32,90383077	0,751152556
0,367467764	3,510602329	4,47093E-04	8,38388E-03	1	22,77515171	-1,264889363
0,356584753	0,990089681	3,22130E-01	5,60074E-01	0	7,911715934	1,315244519
0,302824114	1,829058129	6,73909E-02	2,28994E-01	0	18,59453044	1,084247682
0,238473578	1,835638837	6,64111E-02	2,27012E-01	0	36,68628451	0,752893218
0,199919651	2,386514122	1,70090E-02	9,82673E-02	0	65,660462	0,668341658
0,308741458	0,836080087	4,03110E-01	6,35226E-01	0	20,55482532	0,947120822
0,237032496	1,700133836	8,91058E-02	2,71133E-01	0	23,29738703	0,764224616
0,213165831	2,671955902	7,54106E-03	5,80295E-02	0	69,70816965	0,579373531
0,211387426	4,021106069	5,79255E-05	1,81864E-03	0	25,53896462	0,62969301
0,277470458	4,901503538	9,51059E-07	6,99721E-05	1	21,48837687	-0,963626817
0,271399027	1,938204213	5,25983E-02	1,97534E-01	0	15,62828541	0,892833369
0,315035495	2,490599488	1,27528E-02	8,19509E-02	0	18,45903962	0,930940212
0,259820726	1,383578057	1,66488E-01	3,88369E-01	0	22,03794234	0,660928771
0,3481418	-3,504808631	4,56936E-04	8,50076E-03	1	14,12352815	0,782882415
0,345824837	1,600385209	1,09513E-01	3,07095E-01	0	9,140483401	1,05870987
0,304273507	2,426127786	1,52609E-02	9,20737E-02	0	12,06488253	0,825873444
0,395606966	3,145075507	1,66044E-03	NA	0	4,826059496	1,311695082
0,232130364	5,241881628	1,58947E-07	1,66874E-05	1	38,30406522	-0,456283432
0,384765869	0,595312319	5,51635E-01	7,50641E-01	0	12,43421101	0,993240283
0,229299258	5,127585938	2,93481E-07	2,76426E-05	1	26,3520195	-0,618384873
0,25921739	-3,956339015	7,61071E-05	2,25625E-03	1	28,7030246	0,476419462
0,233967562	4,435342777	9,19259E-06	4,40469E-04	1	32,20357598	-0,488176636
0,326438527	1,330713203	1,83283E-01	4,08279E-01	0	17,39884324	0,754523039
0,269024968	2,18049333	2,92209E-02	1,38033E-01	0	34,84865948	0,508779612
0,339808506	3,513695227	4,41920E-04	8,31910E-03	1	12,58832538	-0,802975452
0,109488678	9,018625363	1,90464E-19	5,23237E-16	0	210,9360107	0,309705685
0,192737748	6,602743056	4,03619E-11	1,47841E-08	1	39,4277186	-0,410890395
0,198742885	6,372416331	1,86073E-10	5,18115E-08	1	62,00220816	0,374331302
0,298071095	2,026304612	4,27336E-02	1,74178E-01	0	10,99875491	0,733281725
0,289500164	2,069462782	3,85027E-02	1,62853E-01	0	12,81498639	0,59569365
0,161140987	6,472215642	9,65762E-11	2,94790E-08	1	94,20681012	0,302106612
0,25820614	4,173082474	3,00506E-05	1,07679E-03	1	25,06390119	-0,493670505
0,356365204	1,965540576	4,93517E-02	1,90596E-01	0	7,417317334	0,842093916
0,350382594	5,631730537	1,78410E-08	2,45061E-06	1	5,788224278	0,877763921
0,130419365	7,297140051	2,93949E-13	1,56295E-10	0	183,4564814	0,200079495
0,258483529	2,429182166	1,51329E-02	9,16370E-02	0	16,8797021	0,521407634
0,372076729	2,108367954	3,49992E-02	1,53797E-01	0	9,013897121	0,701993562
0,425694389	1,746779425	8,06756E-02	NA	0	6,420336584	0,801971332
0,395826403	1,875063729	6,07840E-02	2,15509E-01	0	12,4117214	0,681392327
0,202711519	5,193017917	2,06912E-07	2,10527E-05	1	46,35750896	-0,300256677
0,15239516	7,452692148	9,14545E-14	5,58313E-11	1	72,47015194	0,294835416
0,420794651	-1,972481738	4,85546E-02	NA	0	13,81421891	-0,471172913
0,318437027	2,181728842	2,91296E-02	1,37732E-01	0	11,34320393	0,53271172
0,40487701	1,935284802	5,29554E-02	1,98499E-01	0	8,592087382	0,78287319
0,534594791	3,484102314	4,93791E-04	8,94412E-03	1	4,639815333	0,815564513

0,319080761	-3,614903945	3,00459E-04	6,31692E-03	1	27,20633904	0,441787639
0,328643766	4,176790305	2,95651E-05	1,06688E-03	1	10,2482314	-0,494279433
0,297132313	4,100498846	4,12260E-05	1,38732E-03	1	15,33840233	-0,271778776
0,307697394	3,519900828	4,31708E-04	8,20439E-03	1	19,37863512	-0,297233887
0,237980498	5,261402059	1,42961E-07	1,53015E-05	1	20,52374574	-0,23181177
0,281648324	4,099317834	4,14370E-05	1,39105E-03	1	14,93397905	0,200132798
0,414756154	3,027261364	2,46780E-03	NA	0	6,019031532	0,301926672
0,396408524	3,86741597	1,09995E-04	2,98689E-03	1	11,44594456	0,232827057
0,216320223	5,935003154	2,93840E-09	5,26452E-07	1	28,852352	-0,133519871
0,272130343	4,500743171	6,77163E-06	3,45563E-04	1	21,34512706	-0,150499501
0,36194459	3,314976014	9,16510E-04	1,40529E-02	0	11,3185277	0,145462371
0,300128786	4,201349674	2,65328E-05	9,82788E-04	1	15,44955262	-0,094161145

ctr-p01_lfcSE	ctr-p01_stat	ctr-p01_pvalue	ctr-p01_padj	ctr-p01_twofold-padj1e-2	ctr-p31_baseMean	ctr-p31_log2FoldChange
0,116380333	16,49051717	4,29259E-61	7,82540E-57	1	7524,148096	2,519097727
0,280740987	15,50884343	3,02275E-54	2,75523E-50	1	9149,944697	3,729112638
0,203884608	15,29513973	8,23838E-53	5,00619E-49	1	113,50708	3,421926611
0,081997986	14,86536323	5,53141E-50	2,52094E-46	1	1352,838405	1,308315193
0,094471766	-14,33794679	1,26750E-46	4,62131E-43	1	1610,621127	-0,577950261
0,098726524	13,4272509	4,18667E-41	1,27205E-37	1	1084,033123	1,642324414
0,073881212	13,31375082	1,92566E-40	5,01498E-37	0	1007,368985	1,071401689
0,17148141	13,15453194	1,60273E-39	3,65222E-36	1	3056,302148	2,572047853
0,239356377	13,09969918	3,30565E-39	6,69578E-36	1	1085,689271	2,559669875
0,285178064	12,78363782	2,02378E-37	3,68934E-34	1	464,9555853	3,608302194
0,208757204	12,70898145	5,27166E-37	8,73658E-34	1	152,4665748	3,211464791
0,107535416	-12,61930384	1,65276E-36	2,51082E-33	1	1089,20247	-0,489423343
0,427106032	12,55526621	3,71928E-36	5,21558E-33	1	630,0230115	3,649985706
0,388070453	12,38749487	3,05436E-35	3,97722E-32	1	441,0293896	3,598460913
0,161260387	12,33983719	5,52675E-35	6,71685E-32	1	217,0517904	1,823531998
0,132479543	12,02439329	2,64524E-33	2,83663E-30	1	2701,558086	1,820971928
0,367575872	11,81877131	3,12217E-32	3,16207E-29	1	953,7270525	3,504521252
0,07014008	11,72694591	9,27450E-32	8,89863E-29	0	1679,618497	1,199772321
0,110322938	11,63459022	2,74907E-31	2,50578E-28	1	2628,898075	0,904868786
0,250836178	11,62545852	3,05946E-31	2,65590E-28	1	5793,553717	2,10210895
0,120052485	11,00546211	3,59667E-28	2,98033E-25	1	1118,894684	0,537519996
0,141178465	10,98721959	4,40281E-28	3,48970E-25	1	522,9156629	1,440881657
0,122738881	10,93540327	7,80581E-28	5,92917E-25	1	308,6227741	0,905715094
0,149086362	10,92877333	8,39759E-28	6,12352E-25	1	243,0790254	1,317128485
0,249764636	10,72771071	7,54420E-27	5,09373E-24	1	2682,784033	2,391361087
0,226802188	10,53520797	5,94517E-26	3,87073E-23	1	2175,169572	1,76950765
0,10543111	10,46853715	1,20491E-25	7,57428E-23	1	613,307362	0,418554979
0,303745073	10,4434979	1,56920E-25	9,53549E-23	1	738,5161954	2,215026223
0,349672051	10,36847793	3,44976E-25	2,02868E-22	1	8318,728545	3,081571148
0,092150051	10,20842989	1,81783E-24	1,00421E-21	0	2979,345153	1,371846212
0,130455709	10,09802649	5,63650E-24	3,02216E-21	1	1963,499338	0,281256504
0,124798885	9,936966781	2,87447E-23	1,41626E-20	1	2293,418076	0,614009593
0,14234019	9,906320791	3,90772E-23	1,87468E-20	1	154,2080958	0,73788809
0,169802277	9,894817812	4,38408E-23	2,04928E-20	1	267,1237916	2,565080773
0,124009219	9,867225068	5,77398E-23	2,63149E-20	1	1906,161498	0,478156034
0,292759343	9,764061017	1,60593E-22	7,14050E-20	1	437,9003853	1,895699844

0,133073831	9,694707459	3,17546E-22	1,37830E-19	1	2718,362286	1,790268352
0,110653283	9,600310189	7,97042E-22	3,37909E-19	1	3202,546504	0,623287824
0,132757648	9,545507299	1,35443E-21	5,61165E-19	1	667,8999918	0,710242649
0,203756284	9,372841495	7,06056E-21	2,86031E-18	1	108,2297191	1,001103021
0,179722647	9,062400443	1,27611E-19	4,65269E-17	1	54,96156084	0,602509579
0,131543932	-8,956159357	3,36184E-19	1,15635E-16	1	334,0659681	-0,454561578
0,137329259	8,843923769	9,24147E-19	2,95565E-16	1	1845,661031	0,559871176
0,166156122	8,729133752	2,56631E-18	7,66947E-16	1	162,1645617	1,103195473
0,131523285	8,624902284	6,41474E-18	1,85620E-15	1	9786,326578	1,147174712
0,162494585	8,394992339	4,65925E-17	1,24909E-14	1	296,7802584	0,601255556
0,153817888	8,333577156	7,84357E-17	2,04269E-14	1	568,550942	0,836362011
0,19883056	8,300506969	1,03668E-16	2,66179E-14	1	49,49201561	0,865045709
0,127966022	8,096297914	5,66570E-16	1,39575E-13	1	2838,638194	0,57359339
0,577691186	8,064084564	7,37867E-16	1,76991E-13	1	91,4728741	5,130443195
0,165325455	7,955273882	1,78736E-15	3,97360E-13	1	348,1782205	1,634168769
0,158942088	7,84561306	4,30843E-15	9,35033E-13	1	2623,319492	0,347492614
0,137290773	7,725558062	1,11364E-14	2,30701E-12	1	1849,535784	0,813134282
0,113730668	7,69911052	1,37017E-14	2,77535E-12	0	296,7445723	1,070846643
0,142808172	7,598869825	2,98728E-14	5,73243E-12	1	94,10909302	0,780727534
0,154654704	-7,546754389	4,46239E-14	8,30096E-12	1	225,2164965	-0,411851569
0,785691986	7,541293484	4,65333E-14	8,56870E-12	1	12,65004978	4,635883701
0,191310452	7,434151584	1,05241E-13	1,82719E-11	1	98,47475196	1,029578802
0,211613621	7,424131888	1,13522E-13	1,93412E-11	1	56,98882584	0,986313995
0,19726046	-7,337960017	2,16874E-13	3,59419E-11	1	74,62539357	-0,346517987
0,138153694	7,286780304	3,17450E-13	5,12134E-11	1	430,7043137	1,118588831
0,193238151	7,153654096	8,44978E-13	1,26262E-10	1	111,4850743	1,041861645
0,330844879	7,142181127	9,18614E-13	1,36149E-10	1	25,79532197	1,526020733
0,153968671	-6,905701764	4,99559E-12	6,23764E-10	1	1912,989094	-0,1572826
0,166260339	6,842484233	7,78315E-12	9,33466E-10	1	68,29261646	0,772578906
0,191696416	-6,789469413	1,12547E-11	1,29039E-09	1	573,4745886	-0,513921857
0,157206871	6,767149615	1,31344E-11	1,46896E-09	1	356,897016	0,753712544
0,164153984	6,653929867	2,85369E-11	2,89015E-09	1	90,57332816	1,460905894
0,181257896	6,62279878	3,52461E-11	3,47317E-09	1	216,8534522	1,265727882
0,217309003	6,593084944	4,30780E-11	4,19953E-09	1	91,11127988	2,051258445
0,294078741	6,566474687	5,15204E-11	4,92685E-09	1	1839,47506	1,073050373
0,262873281	6,377187212	1,80370E-10	1,57327E-08	1	23,51065842	1,063583698
0,28223408	6,303624092	2,90765E-10	2,46542E-08	1	29,7036259	1,723308611
0,213423231	6,256041732	3,94871E-10	3,20078E-08	1	43,19769579	0,140700077
0,192782513	6,204047942	5,50290E-10	4,36165E-08	1	41,45711428	0,598229988
0,238644311	6,157615631	7,38483E-10	5,65653E-08	1	68,05702613	0,483345592
0,195020516	6,147132653	7,88961E-10	5,94417E-08	1	51,21340387	0,736002494
0,228016474	6,130531833	8,75858E-10	6,57074E-08	1	58,78019383	1,526147316
0,176594855	6,085382929	1,16213E-09	8,47427E-08	1	53,66033523	0,854587338
0,199411039	6,003995186	1,92520E-09	1,33956E-07	1	269,0221266	0,703716273
0,185904635	5,911688939	3,38618E-09	2,17359E-07	1	45,94342418	0,171101815
0,157340026	5,86963144	4,36765E-09	2,71748E-07	0	374,7692828	1,085098299
0,223384522	5,863405459	4,53469E-09	2,81182E-07	1	39,94983312	0,925732001
0,179401747	5,821466686	5,83334E-09	3,47522E-07	1	193,7132453	0,324391807
0,213587301	5,79837023	6,69625E-09	3,86306E-07	1	81,91548666	0,973582855
0,183540021	-5,717288088	1,08238E-08	5,80344E-07	1	149,9595566	-0,276604646

0,219872015	5,662568944	1,49123E-08	7,72307E-07	1	43,94851809	0,914616147
0,204889984	5,645424199	1,64774E-08	8,42889E-07	1	102,8245077	0,833295455
0,225976247	-5,645122319	1,65064E-08	8,42889E-07	1	1574,520359	-0,119394937
0,272642258	-5,641911396	1,68173E-08	8,53980E-07	1	8583,669031	-0,476915501
0,197916948	5,617041068	1,94255E-08	9,70212E-07	1	94,23604401	1,543181612
0,212744536	5,597157389	2,17895E-08	1,06780E-06	1	156,5638515	0,740029862
0,19127423	5,595720681	2,19707E-08	1,07380E-06	1	45,79558841	0,704603317
0,199805526	5,582297538	2,37362E-08	1,14474E-06	1	66,32894473	0,86871226
0,381678641	5,560033392	2,69723E-08	1,27716E-06	1	76,85541552	0,907282416
0,415594377	5,396272646	6,80395E-08	2,93229E-06	1	33,47288497	3,614827441
0,242397979	5,379874909	7,45376E-08	3,17364E-06	1	36,10113489	1,490885886
0,195176321	5,330831752	9,77640E-08	4,03063E-06	1	104,1317129	0,52423916
0,598539861	5,330492493	9,79468E-08	4,03063E-06	1	178,9225996	2,284391434
0,478819316	5,230057736	1,69457E-07	6,54492E-06	1	8,644191838	2,194663135
0,225064496	-5,184694883	2,16369E-07	8,08279E-06	1	136,6629231	-0,63344939
0,387159422	5,172225879	2,31322E-07	8,55374E-06	1	16,87913619	1,722983638
0,285737242	5,164589523	2,40967E-07	8,87441E-06	1	28,83379153	0,904180872
0,201218336	-5,155731729	2,52642E-07	9,28563E-06	1	243,2602731	-0,601321105
0,369503329	-5,130757883	2,88578E-07	1,02549E-05	1	320,3201259	-0,704916259
0,289077858	5,120802796	3,04238E-07	1,07071E-05	1	16,66951774	0,721479701
0,281598592	5,07940075	3,78627E-07	1,27822E-05	1	20,60903194	-0,167669996
0,290180179	5,023048326	5,08577E-07	1,64971E-05	1	13,40876034	0,405863886
0,302880988	4,976001132	6,49113E-07	2,04729E-05	1	23,58382348	0,606828149
0,291328805	4,944852766	7,62014E-07	2,34654E-05	1	26,13482613	1,64855051
0,192826003	4,939252592	7,84226E-07	2,39873E-05	0	87,096825	1,244955606
0,220172395	4,867797959	1,12849E-06	3,26544E-05	1	99,25667974	0,589177867
0,260092792	4,860378067	1,17162E-06	3,37952E-05	1	29,34958889	0,819536895
0,221802537	-4,838483193	1,30834E-06	3,72090E-05	1	2671,731998	-0,122983081
0,371815475	-4,802401428	1,56774E-06	4,33029E-05	1	41,80611597	-2,721885176
0,270544357	-4,792762098	1,64501E-06	4,51615E-05	1	108,4070369	-0,443755071
0,335083365	-4,792091142	1,65052E-06	4,51786E-05	1	27,45075049	-0,326143543
0,263252559	4,785771165	1,70332E-06	4,63456E-05	1	29,82948102	0,874456953
0,169960227	4,776986573	1,77942E-06	4,77373E-05	0	191,6632377	1,04209487
0,285850163	-4,754204924	1,99229E-06	5,26368E-05	1	52,03984459	-0,528895356
0,247377236	-4,696001331	2,65304E-06	6,77379E-05	1	1066,8598	-0,423146269
0,481746068	4,653969518	3,25605E-06	8,04306E-05	1	19,9110454	3,345712214
0,235720761	4,610189093	4,02303E-06	9,55083E-05	1	45,60761495	0,815025707
0,253385459	4,584034647	4,56089E-06	1,06342E-04	1	36,27940873	0,645529849
0,227396675	-4,580507681	4,63849E-06	1,07650E-04	1	220,9980151	-0,079250165
0,387432105	-4,559361113	5,13095E-06	1,16384E-04	1	22,04768974	-0,182820563
0,221974851	4,547135279	5,43810E-06	1,22089E-04	1	33,91464878	0,292604962
0,33824179	4,486043628	7,25579E-06	1,58601E-04	1	14,4640577	0,905471852
0,367925645	-4,476448372	7,58950E-06	1,64391E-04	1	37,23888768	-0,61773658
0,266914325	4,444823011	8,79643E-06	1,86247E-04	1	45,31025294	1,453044249
0,267541235	-4,437114078	9,11730E-06	1,91705E-04	1	1259,853709	-0,333630643
0,30717057	4,407229722	1,04701E-05	2,13980E-04	1	4933,839162	0,443291664
0,292109779	4,388096743	1,14347E-05	2,30591E-04	1	34,07858864	1,239319044
0,374803297	4,374694303	1,21603E-05	2,43606E-04	1	15,06128239	0,621475542
0,262393966	-4,344888418	1,39346E-05	2,75221E-04	1	111,926495	0,279620548
0,232913293	4,334096479	1,46360E-05	2,85058E-04	1	43,6085982	0,721889297

0,263941955	4,243537395	2,20024E-05	4,00702E-04	1	31,21855206	0,757040656
0,170739829	-4,243038247	2,20514E-05	4,01194E-04	0	125,4461783	0,423428309
0,359745413	-4,225934808	2,37951E-05	4,27643E-04	1	54,97980219	-0,514431238
0,326221075	4,208405721	2,57179E-05	4,56956E-04	1	20,9102995	1,430782521
0,198984006	4,165851454	3,10193E-05	5,37530E-04	0	125,769918	1,008574824
0,277931674	4,137534275	3,51058E-05	5,97650E-04	1	35,84992643	1,397902387
0,26103693	-4,110734989	3,94402E-05	6,60233E-04	1	161,0414455	-0,145314547
0,285345985	-4,096091582	4,20184E-05	6,95054E-04	1	102,7456757	-0,225440863
0,213939972	4,079466585	4,51392E-05	7,33411E-04	0	124,804604	1,490226189
0,559864998	4,066816864	4,76597E-05	7,68881E-04	1	4,736628106	0,648064345
0,353439149	-4,064471859	4,81413E-05	7,75280E-04	1	19,82517334	-0,821984669
0,268995548	-4,062305032	4,85905E-05	7,81823E-04	1	2919,113563	-0,178197142
0,246324838	4,060091377	4,90535E-05	7,87882E-04	1	51,54283406	0,609028155
0,319606642	-4,040680221	5,32964E-05	8,37580E-04	1	78,64852423	-0,31503779
0,615455328	-4,007633681	6,13301E-05	9,37174E-04	1	10,8509056	-0,274302131
0,358967938	-3,996555429	6,42708E-05	9,77424E-04	1	29,14291013	0,154330217
0,590464777	3,992952585	6,52556E-05	9,90516E-04	1	4,343594796	1,479308919
0,267866728	3,945227773	7,97242E-05	1,16737E-03	1	27,91193432	0,287306937
0,296062055	3,94096301	8,11551E-05	1,18095E-03	1	28,899561	1,166185462
0,318203353	-3,94082828	8,12007E-05	1,18095E-03	1	34,65646119	-0,181287663
0,15957147	3,905213881	9,41421E-05	1,33974E-03	0	361,2639066	1,01463533
0,275824778	3,894187021	9,85286E-05	1,38677E-03	1	35,47533818	0,914373878
0,311743047	3,893332383	9,88765E-05	1,38869E-03	1	20,51683877	0,616963899
0,322229644	-3,884843885	1,02396E-04	1,42926E-03	1	22,1126928	-0,741583227
0,249555795	-3,876073123	1,06156E-04	1,47840E-03	0	575,7967396	-1,042891357
0,305480338	-3,844552382	1,20773E-04	1,64060E-03	1	44,08066365	-0,452959611
0,386929752	-3,837770519	1,24156E-04	1,66915E-03	1	40,73354549	-0,991286827
0,312309939	3,831484411	1,27372E-04	1,70235E-03	1	13,32819308	0,515491495
0,204679243	3,808883583	1,39596E-04	1,84141E-03	0	134,0553757	0,9996133
0,499085221	-3,798051097	1,45838E-04	1,90994E-03	1	20,80235195	-0,676497328
0,310569054	3,796118868	1,46979E-04	1,92211E-03	1	19,88836999	0,790056628
0,363730726	-3,777228253	1,58583E-04	2,04956E-03	1	184,7261439	-0,561540022
0,283975527	3,7752799	1,59828E-04	2,06204E-03	1	91,44928416	0,893512635
0,298200995	-3,771428047	1,62316E-04	2,08522E-03	1	27,82757993	-0,533206183
0,326897634	3,76239977	1,68291E-04	2,13794E-03	1	620,8007504	0,523094656
0,404269097	3,755498528	1,72997E-04	2,18705E-03	1	17,26125127	1,581576927
0,27031644	3,748839089	1,77655E-04	2,23825E-03	1	19,61332869	0,104821609
0,334931781	3,74710285	1,78889E-04	2,25062E-03	1	27,13181316	1,132862042
0,310742955	3,731356602	1,90451E-04	2,36830E-03	1	17,44522568	0,962499019
0,275761031	-3,717092317	2,01529E-04	2,47399E-03	1	107,9874475	-0,559872485
0,579398959	3,707246011	2,09525E-04	2,55837E-03	1	6,319611227	2,112337682
0,333827944	3,705125522	2,11286E-04	2,57642E-03	1	115,9156929	0,635412221
0,636146475	3,692318687	2,22219E-04	2,68442E-03	1	6,076494422	1,993593009
0,374885254	3,661715039	2,50532E-04	2,97926E-03	1	11,15060383	0,758330409
0,435231209	-3,659878628	2,52335E-04	2,99288E-03	1	41,20618461	-0,653923641
0,378523869	-3,635925422	2,76984E-04	3,19382E-03	1	32,000886	-0,448751631
0,371102163	3,633373536	2,79740E-04	3,21745E-03	1	21,46234997	1,839524952
0,420974383	-3,631130358	2,82183E-04	3,23464E-03	1	13,96433474	-0,567277313
0,523763222	3,628254854	2,85344E-04	3,26337E-03	1	4,95785883	0,890247321
0,282800134	-3,62729802	2,86403E-04	3,27287E-03	1	44,39311759	-0,183927415

0,224644577	3,615437507	2,99841E-04	3,39720E-03	0	2210,507402	0,999741417
0,386146773	3,597915461	3,20778E-04	3,56790E-03	1	14,42566968	1,505095443
0,158714208	3,590657269	3,29845E-04	3,64650E-03	0	124,8183092	1,139964028
0,292126451	-3,586258205	3,35457E-04	3,69509E-03	1	477,7763847	-0,094070214
0,270994512	3,578499413	3,45573E-04	3,77912E-03	0	38,10928057	1,659037535
0,399483069	-3,568953417	3,58410E-04	3,89875E-03	1	169,9787268	-0,406684805
0,390270712	-3,56572525	3,62851E-04	3,93971E-03	1	46,64919155	-0,694416793
0,323460535	-3,565284981	3,63461E-04	3,94164E-03	1	23,41547285	-0,797831359
0,31951325	3,518797277	4,33508E-04	4,57341E-03	1	17,0527135	0,970531865
0,170158854	3,515612145	4,38741E-04	4,61527E-03	0	93,50702136	1,251635107
0,305653239	-3,512104671	4,44573E-04	4,65780E-03	1	32,35394472	-0,354077767
0,160535951	3,487516659	4,87529E-04	4,98186E-03	0	155,5852178	1,191404849
0,561688637	-3,486929986	4,88599E-04	4,99001E-03	1	25,07000947	-0,484320441
0,370745874	3,458609927	5,42971E-04	5,45064E-03	1	18,68373815	1,408721364
0,314041926	-3,457176916	5,45866E-04	5,46766E-03	1	20,72635537	-0,999731832
0,474634538	3,441449586	5,78606E-04	5,69239E-03	1	5,857618111	0,948407312
0,305239437	-3,439693488	5,82373E-04	5,72019E-03	1	29,2163639	0,015040719
0,33959046	3,43878535	5,84330E-04	5,73632E-03	1	9,51023895	0,115627249
0,420860652	3,405114934	6,61362E-04	6,38931E-03	1	14,73091599	1,203809279
0,386223525	-3,395103559	6,86026E-04	6,57532E-03	1	46,89172289	-0,50600683
0,360099976	-3,383930969	7,14560E-04	6,80942E-03	1	1075,41089	-0,895955166
0,642427468	3,381568746	7,20732E-04	6,85749E-03	1	39,97756974	1,19236644
0,533355174	3,372111422	7,45943E-04	7,05318E-03	1	7,747600916	1,493913202
0,369868885	3,3712488	7,48282E-04	7,05700E-03	1	17,85209697	1,357930849
0,31329271	3,365292176	7,64626E-04	7,16297E-03	1	32,05788862	0,798697789
0,176290371	3,359355065	7,81246E-04	7,30365E-03	0	167,7475393	1,141573992
0,578777969	3,359014644	7,82209E-04	7,30891E-03	1	5,363638012	1,085057785
0,343742289	3,358771827	7,82897E-04	7,31158E-03	1	21,41079026	0,794729968
0,392155805	3,350263417	8,07347E-04	7,51377E-03	1	10,67329123	0,779486774
0,556153224	3,34619169	8,19297E-04	7,58991E-03	1	3,172955549	0,120105565
0,301735011	-3,334353867	8,54978E-04	7,85202E-03	1	807,0288885	-0,719327377
0,484099928	3,330047126	8,68313E-04	7,93849E-03	1	9,974831802	1,328339499
0,359126868	3,327614626	8,75929E-04	7,98011E-03	1	76,72256326	0,224956127
0,348934961	3,326936774	8,78063E-04	7,99156E-03	1	18,35766969	0,760379742
0,433056194	-3,309447484	9,34803E-04	8,41969E-03	1	454,8545022	-0,656674904
0,449739614	3,304727828	9,50687E-04	8,53745E-03	1	8,051655357	1,051444462
0,471672258	3,298122108	9,73338E-04	8,69375E-03	1	6,721991486	0,737017066
0,45443165	3,294218093	9,86959E-04	8,79664E-03	1	6,617910562	0,847953505
0,606592176	-3,285209804	1,01906E-03	9,04852E-03	1	39,8096442	-0,704241849
0,285767951	-3,280102096	1,03770E-03	9,19202E-03	0	128,2172083	0,148000893
0,333386922	-3,279925231	1,03835E-03	9,19332E-03	1	948,6742191	-0,180002301
0,326269885	3,266444881	1,08907E-03	9,54507E-03	1	17,63956874	1,163579672
0,418777755	3,236197357	1,21134E-03	1,03772E-02	0	11,98325699	1,562604628
0,29560595	3,21114424	1,32208E-03	1,11840E-02	0	15,57580533	-0,112527348
0,34940843	3,203163799	1,35927E-03	1,14244E-02	0	16,74557823	1,429305458
0,090368074	3,121923778	1,79673E-03	1,41794E-02	0	918,1615675	1,062527427
0,17450845	3,121644148	1,79844E-03	1,41868E-02	0	111,086633	1,15284275
0,135878442	3,078365543	2,08139E-03	1,59027E-02	0	1810,53814	1,048514472
0,234682682	3,010884767	2,60488E-03	1,88515E-02	0	109,6716394	1,106211837
0,392634231	2,964525797	3,03150E-03	2,12711E-02	0	17,58307519	1,470930738

0,292252247	2,957094014	3,10553E-03	2,16770E-02	0	24,44163438	1,073933556
0,343315043	-2,945203054	3,22743E-03	2,22490E-02	0	24,42376447	0,083462978
0,493726643	2,919593967	3,50488E-03	2,36732E-02	0	13,95217388	2,571311261
0,214186166	2,885375129	3,90948E-03	2,55264E-02	0	121,9386552	1,00722329
0,263605134	2,849536901	4,37829E-03	2,79331E-02	0	42,29386421	1,150395737
0,448014733	-2,823320906	4,75290E-03	2,96021E-02	0	34,78221654	0,023503817
0,469813451	2,799503755	5,11812E-03	3,12543E-02	0	10,30941297	1,667381963
0,391645955	2,768438354	5,63256E-03	3,36446E-02	0	25,65023315	1,636512823
0,27506781	2,7371186	6,19799E-03	3,61566E-02	0	47,83532057	1,182709756
0,244636416	2,731979435	6,29551E-03	3,66114E-02	0	86,67557633	1,142046528
0,346871155	2,730468669	6,32443E-03	3,67414E-02	0	25,22797088	1,20514544
0,280279084	2,726655893	6,39797E-03	3,70959E-02	0	30,18304928	1,168210401
0,215420925	2,689495137	7,15602E-03	4,01151E-02	0	95,66104078	1,151882789
0,245955731	2,560188405	1,04615E-02	5,25817E-02	0	40,82468075	1,480392135
0,377157684	-2,55497066	1,06197E-02	5,31421E-02	0	35,23917257	0,39375196
0,355519462	2,511348787	1,20271E-02	5,85247E-02	0	21,6391822	1,430818399
0,380333796	2,447692584	1,43774E-02	6,66075E-02	0	29,09809838	1,714412703
0,272571425	2,424791125	1,53172E-02	6,96340E-02	0	27,54590631	1,023280261
0,331214315	2,363673244	1,80948E-02	7,85960E-02	0	9,669202581	-0,436147932
0,462301015	2,290087702	2,20162E-02	9,03955E-02	0	12,78098696	1,609573979
0,361434872	2,284985506	2,23137E-02	9,13903E-02	0	18,42053772	1,563897023
0,579791152	2,262357879	2,36753E-02	NA	0	10,33097063	2,56203662
0,209153108	-2,181576145	2,91408E-02	1,10454E-01	0	63,65570916	0,764854215
0,458492429	2,16631774	3,02869E-02	1,13165E-01	0	14,50800986	1,203047296
0,293384632	-2,107761641	3,50516E-02	1,25662E-01	0	41,93408497	0,555006409
0,226701406	2,101528485	3,55946E-02	1,26984E-01	0	21,55878127	-0,546897135
0,235893547	-2,069478555	3,85012E-02	1,33767E-01	0	49,3825172	0,549909856
0,368929364	2,04516938	4,08382E-02	1,39051E-01	0	22,56469311	1,196702464
0,249251224	2,041232148	4,12278E-02	1,39881E-01	0	48,11871966	1,09820209
0,401698919	-1,998948501	4,56139E-02	1,50017E-01	0	19,5600573	0,379463027
0,163515479	1,894045059	5,82190E-02	1,77451E-01	0	347,5648098	1,295156728
0,219934196	-1,868242427	6,17283E-02	1,85266E-01	0	66,92132988	0,858635398
0,206530332	1,812476157	6,99127E-02	2,00952E-01	0	118,8922314	1,641433497
0,413937324	1,771480084	7,64809E-02	2,13472E-01	0	15,42186757	1,331281031
0,348220165	1,710681086	8,71400E-02	2,32620E-01	0	18,05033731	1,198034624
0,177468179	1,702314257	8,86965E-02	2,35465E-01	0	160,0130798	1,344306681
0,293480423	-1,682124146	9,25448E-02	2,42363E-01	0	38,94619234	0,580714084
0,506393941	1,662922573	9,63279E-02	2,49016E-01	0	10,85574128	1,525311187
0,536739861	1,635361904	1,01973E-01	NA	0	17,75970706	2,84273717
0,124482593	1,607288941	1,07991E-01	2,68431E-01	0	294,3944859	1,151354743
0,328219726	1,58859323	1,12152E-01	2,75581E-01	0	23,63524599	1,139174596
0,442902677	1,584983786	1,12970E-01	2,76993E-01	0	13,8814475	1,487189751
0,530368013	1,512103505	1,30508E-01	3,05450E-01	0	9,635972822	1,526660698
0,464590054	1,46665285	1,42471E-01	3,23678E-01	0	18,67525484	1,423314083
0,20724817	-1,448778424	1,47399E-01	3,30800E-01	0	73,84877346	0,751062416
0,208869828	1,411574945	1,58075E-01	3,46193E-01	0	128,0791256	1,427198783
0,334652646	-1,407946175	1,59147E-01	3,47781E-01	0	11,98721937	-1,300097162
0,382936324	1,391123503	1,64188E-01	3,54891E-01	0	16,53743377	1,231239294
0,568251805	1,377687116	1,68300E-01	3,60106E-01	0	12,96880001	1,538867667
0,61950153	1,316485067	1,88011E-01	NA	0	13,08275925	2,681911426

0,355380903	1,243138375	2,13817E-01	4,17914E-01	0	20,06022038	-0,704767728
0,460998912	-1,072192188	2,83634E-01	4,97799E-01	0	18,40453687	0,88256447
0,324911475	-0,836470229	4,02890E-01	6,15314E-01	0	25,72251925	0,944618683
0,357028543	-0,832521359	4,05115E-01	6,16972E-01	0	30,50509467	0,772090463
0,280761443	-0,825653861	4,09000E-01	6,19790E-01	0	35,86141343	1,023434163
0,388450755	0,515207642	6,06408E-01	7,79177E-01	0	26,3098718	1,331126249
0,595198672	0,507270406	6,11965E-01	7,82646E-01	0	11,55996162	1,572900295
0,479212748	0,48585322	6,27071E-01	7,93457E-01	0	24,75021121	1,762847449
0,278437323	-0,479532951	6,31560E-01	7,95955E-01	0	51,43577764	1,125905141
0,328357226	-0,458340761	6,46708E-01	8,05512E-01	0	36,9538981	1,053876739
0,423914519	0,34314081	7,31493E-01	8,57618E-01	0	20,4220987	1,342256043
0,372202638	-0,252983552	8,00281E-01	8,96468E-01	0	27,42047364	1,15481534

ctr-p31_lfcSE	ctr-p31_stat	ctr-p31_pvalue	ctr-p31_padj	ctr-p31_twofold-padj1e-2	Chromosome	GeneStartHg38	GeneEndHg38	Strand
0,153975496	16,36038072	3,66827E-60	1,57983E-56	1	19	10271093	10286615	+
0,382298025	9,754464825	1,76529E-22	1,08610E-19	1	4	73869393	73871308	+
0,306386079	11,16867522	5,80400E-29	5,88151E-26	1	17	34255218	34257203	+
0,099344373	13,16949475	1,31475E-39	2,05901E-36	1	6	14117256	14136918	+
0,117147733	-4,933516402	8,07623E-07	4,22885E-05	0	6	31815543	31817946	+
0,103680731	15,8402087	1,64275E-56	5,65992E-53	1	19	45001449	45038198	+
0,087609833	12,22924018	2,16959E-34	3,11462E-31	1	6	44258166	44265788	-
0,251455036	10,22865915	1,47548E-24	1,10514E-21	1	4	73836640	73849064	+
0,225551856	11,34847624	7,54664E-30	8,66706E-27	1	1	37474580	37484377	+
0,17849381	20,2152792	7,18377E-91	1,23755E-86	1	5	160438594	160487426	+
0,345634706	9,291499767	1,52129E-20	8,45398E-18	1	6	31580525	31582522	-
0,121147513	-4,039895918	5,34749E-05	1,44257E-03	0	6	31827738	31830254	+
0,314603385	11,60186405	4,03199E-31	4,96136E-28	1	4	74097040	74099196	-
0,419046717	8,587254758	8,90720E-18	3,74254E-15	1	5	132073789	132076170	+
0,225333043	8,092608047	5,84006E-16	1,82921E-13	1	1	186671791	186680423	-
0,334758477	5,439658902	5,33827E-08	3,86396E-06	1	2	112829751	112836816	-
0,299487919	11,70171159	1,24908E-31	1,65523E-28	1	4	74036589	74038807	-
0,060689003	19,76918831	5,48513E-87	4,72462E-83	1	3	10164919	10243745	+
0,122856414	7,365254722	1,76809E-13	3,76035E-11	0	19	12791486	12793315	+
0,147639347	14,23813499	5,31260E-46	1,30743E-42	1	14	35401511	35404749	-
0,098985557	5,430287126	5,62635E-08	4,02179E-06	0	1	151540305	151583583	+
0,128026267	11,25457838	2,19875E-29	2,36737E-26	1	1	109910242	109930992	+
0,141367499	6,406812731	1,48593E-10	1,86848E-08	0	21	36460621	36576569	-
0,132713704	9,924585364	3,25453E-23	2,15637E-20	1	10	30434021	30461833	+
0,12735034	18,77781471	1,14705E-78	6,58673E-75	1	11	102317450	102339403	+
0,125607888	14,08755201	4,52994E-45	9,75466E-42	1	5	132481609	132490777	-
0,111097895	3,767442928	1,64928E-04	3,49473E-03	0	19	57819721	57846238	+
0,244709487	9,051656507	1,40816E-19	7,13480E-17	1	6	137867214	137883312	+
0,307378778	10,02532176	1,17975E-23	8,12940E-21	1	4	73740541	73743716	+
0,098386083	13,94349855	3,44624E-44	6,59649E-41	1	10	102394110	102402524	+
0,214013647	1,31419892	1,88779E-01	4,67995E-01	0	6	131948176	131951372	-
0,125985487	4,873653353	1,09553E-06	5,47777E-05	0	5	140332843	140346603	-
0,172710221	4,272405459	1,93376E-05	6,35741E-04	0	19	35887653	35902303	-
0,335754286	7,63975585	2,17634E-14	5,43360E-12	1	17	40015361	40017813	+
0,112231506	4,260443881	2,04021E-05	6,66921E-04	0	1	67685201	67688334	+
0,33030756	5,739196051	9,51270E-09	7,91668E-07	1	1	205302063	205321760	-

0,165273612	10,83214875	2,42399E-27	2,19780E-24	1	14	103123442	103137439	+
0,112384905	5,546010136	2,92262E-08	2,23769E-06	0	21	38805183	38824955	+
0,116942434	6,073438206	1,25200E-09	1,29151E-07	0	1	119619377	119648266	-
0,245386201	4,079703824	4,50931E-05	1,26107E-03	1	2	172099438	172102900	-
0,217588494	2,769032345	5,62231E-03	5,00977E-02	0	2	144364364	144521057	-
0,118816238	-3,825752986	1,30373E-04	2,92439E-03	0	5	140125937	140129392	+
0,245318289	2,282223548	2,24761E-02	1,27661E-01	0	3	134355874	134375479	-
0,130706422	8,440254568	3,16647E-17	1,26858E-14	1	2	60881521	60931610	+
0,139733876	8,209710781	2,21722E-16	7,52972E-14	1	22	30240453	30246759	-
0,13451636	4,469757847	7,83082E-06	3,03150E-04	0	4	139015781	139045939	+
0,135576206	6,168943922	6,87476E-10	7,35599E-08	0	3	112086335	112131004	+
0,296736477	2,915198419	3,55462E-03	3,57684E-02	0	3	159988835	159996019	+
0,170659069	3,361048396	7,76472E-04	1,15015E-02	0	17	45263119	45317029	-
0,478460645	10,72281126	7,95481E-27	6,52559E-24	1	2	227805739	227817564	+
0,315576507	5,178360019	2,23845E-07	1,38214E-05	1	12	56334174	56340410	+
0,225149997	1,543382713	1,22738E-01	3,69200E-01	0	5	58453982	58460139	-
0,162245363	5,011756676	5,39354E-07	2,99724E-05	0	5	10564070	10657816	+
0,148635476	7,204515875	5,82504E-13	1,14032E-10	1	19	29665459	29675477	+
0,180142017	4,333955777	1,46454E-05	5,06618E-04	0	1	203305491	203309602	+
0,155108591	-2,655246665	7,92504E-03	6,35294E-02	0	1	222872271	223005995	+
0,733377136	6,321282015	2,59402E-10	2,99914E-08	1	6	31575565	31578336	+
0,17830006	5,774416476	7,72202E-09	6,52094E-07	1	1	1169357	1170343	+
0,194679282	5,066353149	4,05509E-07	2,36804E-05	0	10	73715843	73730469	-
0,188112401	-1,842079442	6,54635E-02	2,52573E-01	0	6	31809619	31815283	-
0,118278986	9,457206783	3,16279E-21	1,81618E-18	1	19	58305319	58315663	+
0,157651419	6,608641078	3,87864E-11	5,47683E-09	1	19	40798996	40808434	+
0,312600904	4,88169009	1,05180E-06	5,31362E-05	1	14	96256210	96268967	+
0,138684849	-1,134100819	2,56752E-01	5,48490E-01	0	11	95976598	96343195	-
0,202610709	3,813119801	1,37224E-04	3,03310E-03	0	7	116952446	116954334	-
0,285903666	-1,797535036	7,22507E-02	2,68710E-01	0	9	12775020	12823060	+
0,168786537	4,465477865	7,98902E-06	3,06615E-04	0	X	45745211	45770274	-
0,169992623	8,593937023	8,40391E-18	3,61935E-15	1	5	55995167	56003649	+
0,191486706	6,610003932	3,84310E-11	5,47149E-09	1	8	47736913	47738164	-
0,223367357	9,18334029	4,17922E-20	2,18168E-17	1	19	49889654	49929539	-
0,148074757	7,246679938	4,27112E-13	8,68805E-11	1	3	101827991	101861022	+
0,275717165	3,857517176	1,14545E-04	2,62053E-03	1	6	150018334	150025532	-
0,270379468	6,373666702	1,84561E-10	2,25492E-08	1	15	73567012	73569294	-
0,283778033	0,495810319	6,20028E-01	8,32260E-01	0	12	65830750	65831050	+
0,210014865	2,84851259	4,39241E-03	4,17825E-02	0	15	77067654	77068325	-
0,25781277	1,874793062	6,08212E-02	2,41811E-01	0	13	91347820	91354579	+
0,176354669	4,173422228	3,00058E-05	9,16507E-04	0	6	152983331	152991322	+
0,211383443	7,219805375	5,20620E-13	1,03089E-10	1	12	48857145	48865870	-
0,180395177	4,737307021	2,16577E-06	1,00837E-04	0	1	94318479	94324569	-
0,28588918	2,461500196	1,38357E-02	9,28147E-02	0	9	5450503	5470566	+
0,20654196	0,828411888	4,07437E-01	6,93176E-01	0	2	73456764	73459482	+
0,12042198	9,010799341	2,04560E-19	1,00684E-16	1	16	31700590	31711986	+
0,214760993	4,310522081	1,62870E-05	5,53403E-04	0	21	6484623	6499261	-
0,220383986	1,471939105	1,41037E-01	3,98776E-01	0	8	13083361	13604610	-
0,201189722	4,839128185	1,30410E-06	6,40049E-05	0	6	31670167	31673776	+
0,141890695	-1,949420609	5,12452E-02	2,16851E-01	0	17	48724408	48724475	-

0,254069887	3,599860487	3,18388E-04	5,73731E-03	0	17	81388126	81390319	-
0,207137634	4,02290709	5,74842E-05	1,53213E-03	0	17	7572706	7579006	+
0,135928677	-0,878364593	3,79746E-01	6,68911E-01	0	2	165469647	165689407	+
0,252868317	-1,886023153	5,92918E-02	2,38594E-01	0	17	72121020	72126416	+
0,20774763	7,428155087	1,10123E-13	2,46375E-11	1	9	120902393	120929173	-
0,167160931	4,427050386	9,55304E-06	3,54677E-04	0	20	63659300	63698684	+
0,193893488	3,633971023	2,79092E-04	5,22600E-03	0	14	51649516	51651744	-
0,226493212	3,835489162	1,25315E-04	2,82565E-03	0	6	17706257	17707344	+
0,286469328	3,167118878	1,53957E-03	1,92329E-02	0	6	12290361	12297194	+
0,404499677	8,936539742	4,01547E-19	1,92151E-16	1	8	78835307	78840525	+
0,275946773	5,402802395	6,56077E-08	4,63207E-06	1	5	178113532	178126081	+
0,169254889	3,097335401	1,95269E-03	2,30562E-02	0	X	101390824	101396154	+
0,591537554	3,861785983	1,12561E-04	2,58237E-03	1	7	22725884	22732002	+
0,499551307	4,393268723	1,11659E-05	NA	0	1	158025550	158031166	+
0,213444862	-2,967742507	2,99996E-03	3,16280E-02	0	9	110190048	110208189	-
0,4697503	3,667871285	2,44578E-04	4,76085E-03	1	2	112773925	112784493	-
0,303896086	2,97529621	2,92706E-03	3,10932E-02	0	2	100822661	100847220	+
0,197571626	-3,043560031	2,33797E-03	2,63760E-02	0	X	37571569	37684463	+
0,425900123	-1,65512105	9,78999E-02	3,21733E-01	0	1	161524540	161526894	+
0,315802909	2,284588521	2,23370E-02	1,26970E-01	0	12	12813316	12829981	+
0,294558662	-0,56922446	5,69204E-01	8,05460E-01	0	2	85751344	85791383	+
0,355271468	1,142404958	2,53286E-01	5,45105E-01	0	X	45746157	45746266	-
0,343324014	1,767508607	7,71431E-02	2,79336E-01	0	10	62811996	62919900	-
0,271076359	6,08149864	1,19064E-09	1,23562E-07	1	16	2516658	2517999	+
0,155500987	8,006094546	1,18409E-15	3,51694E-13	1	17	82249067	82251844	+
0,222067821	2,653143817	7,97459E-03	6,37190E-02	0	3	86876388	86991149	-
0,261893825	3,129271552	1,75240E-03	2,12315E-02	0	9	32566148	32567126	-
0,237455093	-0,517921427	6,04513E-01	8,23660E-01	0	3	184561785	184582408	+
0,369402087	-7,368353539	1,72748E-13	3,71992E-11	1	MT	15956	16023	-
0,378778624	-1,171542012	2,41381E-01	5,30866E-01	0	19	16719975	16817963	+
0,266793336	-1,222457605	2,21535E-01	5,06958E-01	0	5	178895898	178933212	+
0,255396644	3,423917157	6,17254E-04	9,66676E-03	0	1	9148011	9198906	-
0,138449141	7,526914669	5,19533E-14	1,22603E-11	1	3	129382922	129399655	-
0,315577228	-1,675961729	9,37457E-02	3,13706E-01	0	3	194496317	194501503	-
0,303784398	-1,392916399	1,63645E-01	4,32911E-01	0	4	77157207	77433388	+
0,432002891	7,744652376	9,58437E-15	2,46433E-12	1	1	202122917	202133592	+
0,242640043	3,358990948	7,82276E-04	1,15506E-02	0	6	71343427	71420745	-
0,224057926	2,881084641	3,96309E-03	3,90127E-02	0	18	63871692	63903888	+
0,31536462	-0,251296943	8,01585E-01	9,20908E-01	0	8	19404161	19758029	-
0,329204649	-0,555340162	5,78662E-01	8,09995E-01	0	4	40191053	40246967	+
0,271024652	1,079624897	2,80309E-01	5,72894E-01	0	12	104303739	104305205	+
0,375384294	2,412119706	1,58601E-02	1,01292E-01	0	8	119838736	119840385	-
0,349128711	-1,769366313	7,68328E-02	2,78690E-01	0	2	42048021	42058517	+
0,222092639	6,54251423	6,04931E-11	8,20562E-09	1	12	126729787	126772519	-
0,244436422	-1,364897428	1,72285E-01	4,45070E-01	0	10	4747846	4785100	-
0,351326772	1,261764546	2,07034E-01	4,90635E-01	0	1	85580761	85583950	+
0,298539195	4,151277499	3,30625E-05	9,88832E-04	1	6	30914205	30926459	+
0,415890356	1,494325446	1,35091E-01	3,89990E-01	0	7	131493964	131497694	-
0,185572379	1,506800468	1,31862E-01	3,85052E-01	0	15	40929340	40939073	+
0,190882031	3,781860943	1,55660E-04	3,35195E-03	0	21	43092956	43107587	-

0,290005239	2,610437864	9,04264E-03	6,90635E-02	0	1	77881348	77889539	-
0,129332695	3,273946388	1,06057E-03	1,45577E-02	0	9	124517275	124771311	-
0,47988178	-1,071995769	2,83722E-01	5,77603E-01	0	7	11370365	11832198	-
0,353977333	4,042017353	5,29933E-05	1,43540E-03	1	10	73796514	73811651	-
0,154751367	6,51738878	7,15418E-11	9,62852E-09	1	14	24305734	24312053	+
0,26768006	5,22228808	1,76726E-07	1,13177E-05	1	20	63744689	63745958	+
0,407981078	-0,356179625	7,21706E-01	8,87172E-01	0	6	135181308	135219173	+
0,253269222	-0,89012341	3,73400E-01	6,63505E-01	0	4	92303966	93810157	+
0,26764729	5,56787325	2,57867E-08	1,99205E-06	1	19	2249309	2252073	+
0,738095893	0,878021882	3,79932E-01	NA	0	15	41908204	41908714	-
0,336265404	-2,444452088	1,45072E-02	9,58076E-02	0	3	64067964	64103131	+
0,268655643	-0,663292013	5,07144E-01	7,68370E-01	0	1	239386565	239915452	+
0,280102984	2,174300847	2,96825E-02	1,53142E-01	0	19	5782960	5784746	-
0,44629247	-0,705899856	4,80250E-01	7,48306E-01	0	1	107571161	107965180	-
0,451833941	-0,607086157	5,43794E-01	7,91334E-01	0	2	57289648	57380132	-
0,281643555	0,547962892	5,83717E-01	8,12617E-01	0	17	39566915	39567559	+
0,657337243	2,250456571	2,44200E-02	NA	0	13	106506046	106506713	-
0,303175911	0,947657538	3,43304E-01	6,35106E-01	0	7	100093560	100093643	-
0,297469065	3,920358787	8,84172E-05	2,12732E-03	1	7	43866558	43869893	-
0,291383753	-0,62216119	5,33836E-01	7,85272E-01	0	6	1312098	1314758	+
0,122226081	8,301299716	1,02979E-16	3,77449E-14	1	3	15254184	15264515	+
0,215497898	4,243075617	2,20477E-05	7,08517E-04	0	16	28974221	28984548	+
0,299675032	2,058776451	3,95157E-02	1,83888E-01	0	X	153447666	153495516	-
0,274447163	-2,702098358	6,89034E-03	5,81862E-02	0	22	30653877	30654814	-
0,287696621	-3,62496908	2,88996E-04	5,35640E-03	1	2	178829757	179050086	-
0,241526639	-1,875402289	6,07374E-02	2,41645E-01	0	7	76521611	76522074	+
0,412070914	-2,405621928	1,61450E-02	1,02555E-01	0	1	48552991	48558106	+
0,35796722	1,440052234	1,49853E-01	4,11856E-01	0	12	62601751	62603690	-
0,142038277	7,037633269	1,95532E-12	3,62198E-10	0	1	207801518	207879115	-
0,489967444	-1,380698527	1,67372E-01	4,38395E-01	0	4	87303789	87322886	-
0,313267974	2,521983391	1,16695E-02	8,30007E-02	0	3	159839861	159897360	+
0,355456913	-1,579769591	1,14160E-01	3,53029E-01	0	6	133987581	134052624	-
0,268328067	3,329926107	8,68690E-04	1,25125E-02	0	16	14911551	14935708	+
0,243952865	-2,185693467	2,88380E-02	1,50589E-01	0	5	34019448	34043832	-
0,311598964	1,678743247	9,32021E-02	3,12433E-01	0	12	52249300	52309163	+
0,399355194	3,960326421	7,48474E-05	1,87140E-03	1	1	1169005	1169087	+
0,300512384	0,348809616	7,27232E-01	8,89691E-01	0	3	101521891	101522979	+
0,279726411	4,049893027	5,12411E-05	1,39894E-03	1	3	73061659	73063337	+
0,360238753	2,671836413	7,54374E-03	6,17075E-02	0	20	38425083	38425354	-
0,238427998	-2,348182633	1,88653E-02	1,13846E-01	0	7	76524515	76532692	+
0,601174126	3,513686952	4,41933E-04	NA	0	1	89258950	89272804	-
0,387889662	1,638126208	1,01395E-01	3,29139E-01	0	5	65148738	65481920	-
0,592084874	3,367073027	7,59706E-04	NA	0	1	1167863	1167952	+
0,489386184	1,549554185	1,21249E-01	3,66898E-01	0	11	78423982	78429836	-
0,558371286	-1,171126915	2,41548E-01	5,31097E-01	0	6	63719980	65707226	-
0,414325345	-1,083089985	2,78768E-01	5,71708E-01	0	13	71437966	71867204	-
0,371450441	4,952275593	7,33506E-07	3,92426E-05	1	3	64004022	64012148	+
0,339294387	-1,6719325	9,45376E-02	3,15231E-01	0	4	183516894	183517527	+
0,784799798	1,134362322	2,56643E-01	NA	0	5	95768999	95770700	+
0,331503877	-0,554827341	5,79013E-01	8,10157E-01	0	19	44259880	44275317	+

0,128177488	7,799664602	6,20719E-15	1,62017E-12	0	1	6205475	6221299	+
0,359895051	4,182039843	2,88905E-05	8,90335E-04	1	15	77063397	77064910	-
0,174954511	6,515773856	7,23159E-11	9,65725E-09	1	1	241532134	241595642	+
0,358067331	-0,262716551	7,92769E-01	9,17236E-01	0	17	17494437	17496395	-
0,37183711	4,46173201	8,12999E-06	3,11234E-04	1	17	49495293	49515008	+
0,498094875	-0,816480605	4,14225E-01	6,98301E-01	0	3	84958981	86074429	+
0,525689499	-1,32096379	1,86513E-01	4,64988E-01	0	15	20642799	20643448	-
0,327113439	-2,43900514	1,47278E-02	9,66902E-02	0	8	74599775	74823313	+
0,367584208	2,640298042	8,28331E-03	6,50395E-02	0	2	96497646	96508109	-
0,153597851	8,148780072	3,67614E-16	1,19488E-13	1	4	99816827	99870190	+
0,259424513	-1,364858562	1,72298E-01	4,45070E-01	0	15	99423769	99435160	-
0,155842348	7,644936475	2,09049E-14	5,29600E-12	1	1	89052319	89065230	-
0,668285358	-0,724721012	4,68623E-01	7,38472E-01	0	2	154697855	154858354	+
0,3154741	4,46541052	7,99154E-06	3,06615E-04	1	3	98804978	98805084	-
0,316266065	-3,161046794	1,57203E-03	1,95393E-02	0	2	168915498	169031324	-
0,519866978	1,824326897	6,81027E-02	NA	0	5	177260340	177263909	+
0,259836756	0,057885265	9,53840E-01	9,82574E-01	0	9	131258076	131276510	-
0,432998055	0,267038726	7,89439E-01	NA	0	17	41026026	41027208	-
0,385998077	3,118692424	1,81655E-03	2,18532E-02	0	17	68267026	68291267	-
0,510154511	-0,991869755	3,21261E-01	6,15468E-01	0	X	124227868	124373197	+
0,301167981	-2,974934996	2,93051E-03	3,10932E-02	0	2	178525989	178830802	-
0,415136571	2,872226936	4,07590E-03	3,97147E-02	0	12	52314301	52321398	-
0,543847174	2,74693567	6,01549E-03	NA	0	5	179595904	179603741	-
0,315856783	4,299198001	1,71417E-05	5,74515E-04	1	12	128813186	128814750	-
0,240665607	3,318703484	9,04364E-04	1,28904E-02	0	X	47204921	47205865	+
0,139182219	8,202010303	2,36400E-16	7,83166E-14	1	9	128108581	128118693	-
0,580754756	1,868357984	6,17122E-02	NA	0	10	68230595	68232113	-
0,314198391	2,529389048	1,14261E-02	8,19134E-02	0	X	103687284	103691772	+
0,426115797	1,829283915	6,73571E-02	2,57286E-01	0	2	201410544	201413308	-
0,770723059	0,155834918	8,76163E-01	NA	0	5	170896929	170904461	+
0,269851283	-2,665643718	7,68411E-03	6,25291E-02	0	3	171600404	171810950	-
0,493550724	2,691394083	7,11541E-03	5,93594E-02	0	7	74191198	74191294	+
0,298162026	0,754476117	4,50563E-01	7,25814E-01	0	1	101236865	101243713	+
0,305233332	2,491142557	1,27333E-02	8,78346E-02	0	17	75145261	75146546	-
0,534083158	-1,229536814	2,18871E-01	5,04345E-01	0	1	117606048	117628389	+
0,512650318	2,050997384	4,02672E-02	NA	0	16	29613104	29613640	-
0,559602819	1,317036013	1,87827E-01	NA	0	1	162593103	162593754	+
0,48806127	1,737391504	8,23181E-02	NA	0	9	117704175	117724735	+
0,581845689	-1,210358455	2,26141E-01	5,13475E-01	0	1	161606291	161608217	+
0,343235757	0,43119311	6,66328E-01	8,58423E-01	0	4	105552620	105708093	+
0,335823286	-0,536003038	5,91956E-01	8,18442E-01	0	2	167868948	167874041	+
0,302447171	3,84721625	1,19468E-04	2,71871E-03	1	15	45361124	45402327	-
0,439777805	3,553168461	3,80621E-04	6,58328E-03	1	16	66921679	66925536	-
0,363839479	-0,309277455	7,57110E-01	9,02507E-01	0	17	62003700	62007518	-
0,327483521	4,364511091	1,27407E-05	4,53481E-04	1	2	43227210	43228855	+
0,078100638	13,60459348	3,76054E-42	6,47827E-39	1	11	34150987	34358010	-
0,179761904	6,413164981	1,42529E-10	1,80540E-08	1	6	132680849	132714055	-
0,125623514	8,346482612	7,03260E-17	2,63371E-14	1	1	211571568	211579161	-
0,168953434	6,547436241	5,85332E-11	8,00279E-09	1	8	144495458	144505444	-
0,376250766	3,909442506	9,25094E-05	2,20806E-03	1	16	30984630	30988270	-

0,295753688	3,631175536	2,82133E-04	5,26577E-03	1		18	9102630	9134345	+
0,275552099	0,302893639	7,61971E-01	9,04715E-01	0		3	111292719	111665750	+
0,419681209	6,126820082	8,96528E-10	9,41737E-08	1		19	10286955	10288522	+
0,224876276	4,479010886	7,49897E-06	2,93578E-04	1		17	7921859	7929803	-
0,287142558	4,006357483	6,16623E-05	1,59498E-03	1		15	45430529	45448761	+
0,344207492	0,068283864	9,45560E-01	9,79976E-01	0		11	67612651	67616257	-
0,424791339	3,925178816	8,66653E-05	2,09101E-03	1		16	31118078	31118747	+
0,279351629	5,858254089	4,67759E-09	4,21889E-07	1		20	58651434	58715410	+
0,224948021	5,257702419	1,45866E-07	9,55452E-06	1		16	29913144	29915337	-
0,179887134	6,348683785	2,17165E-10	2,56240E-08	1		15	43796142	43803043	+
0,332564482	3,623794795	2,90312E-04	5,37186E-03	1		15	78290527	78291221	-
0,261189025	4,47266267	7,72516E-06	3,00470E-04	1		16	67929614	67936017	-
0,227620591	5,060538601	4,18074E-07	2,42497E-05	1		16	675666	678268	+
0,225216744	6,573188611	4,92490E-11	6,81171E-09	1		17	82244770	82245591	+
0,305960044	1,286939151	1,98115E-01	4,79968E-01	0		2	196804415	196810276	-
0,283688866	5,04361845	4,56810E-07	2,58864E-05	1		14	55394940	55395233	-
0,31133254	5,506692953	3,65637E-08	2,72677E-06	1		12	54019910	54022589	+
0,274819354	3,723465056	1,96507E-04	4,00643E-03	1		11	65027439	65040572	+
0,39039699	-1,117190817	2,63913E-01	5,55502E-01	0		7	5495819	5495917	-
0,388671209	4,14122256	3,45460E-05	1,02785E-03	1		8	144353228	144355609	-
0,331299351	4,720495273	2,35271E-06	1,07507E-04	1		16	31259967	31332892	+
0,507369444	5,04964706	4,42627E-07	2,52046E-05	1		7	134549110	134579875	+
0,219409344	3,485969191	4,90357E-04	8,03748E-03	0		19	42152569	42157523	+
0,345458285	3,482467629	4,96815E-04	8,11503E-03	1	X		103910305	103911352	-
0,252165614	2,200959917	2,77389E-02	1,46582E-01	0		3	49140086	49160851	-
0,270600388	-2,021050814	4,32745E-02	1,94696E-01	0		6	19837370	19842197	+
0,21355336	2,575046609	1,00227E-02	7,42625E-02	0		2	240605430	240631259	+
0,318106624	3,761953934	1,68591E-04	3,55687E-03	1		1	150730188	150765792	-
0,258037937	4,255971445	2,08143E-05	6,76544E-04	1		3	51927071	51932483	-
0,328703738	1,15442261	2,48327E-01	5,39734E-01	0		14	101634454	101731108	-
0,157328804	8,23216532	1,83859E-16	6,59863E-14	1		21	44217014	44240966	-
0,168440988	5,097544308	3,44088E-07	2,03000E-05	0		22	36140330	36166177	-
0,193288794	8,492129649	2,02884E-17	8,32165E-15	1		8	90791741	90959393	+
0,367198651	3,625506322	2,88396E-04	5,35366E-03	1		6	33800142	33802960	+
0,315429998	3,798099839	1,45810E-04	3,18764E-03	1		6	31164337	31180731	-
0,166314564	8,082916194	6,32361E-16	1,94530E-13	1		21	5022493	5040666	+
0,274513874	2,115427086	3,43936E-02	1,67799E-01	0		4	185585444	185956652	-
0,421050859	3,622629324	2,91624E-04	5,39034E-03	1		1	44808482	44815585	+
0,422311231	6,731379512	1,68062E-11	2,60829E-09	1		8	78805293	78956082	+
0,140193817	8,212592875	2,16463E-16	7,52972E-14	1		1	7915894	7943165	-
0,268419306	4,244011402	2,19559E-05	7,08305E-04	1		1	32204769	32206814	-
0,394307496	3,771649703	1,62172E-04	3,44480E-03	1		11	33698261	33700801	-
0,436404395	3,498270679	4,68286E-04	7,75688E-03	1		1	150560202	150574552	-
0,35120052	4,052710636	5,06276E-05	1,38879E-03	1		17	28204616	28223735	+
0,179537103	4,183327042	2,87274E-05	8,86893E-04	0		6	37212178	37258155	-
0,212221476	6,725044104	1,75539E-11	2,70001E-09	1		1	89181144	89198942	-
0,392748294	-3,3102554	9,32109E-04	1,31511E-02	0		11	122115340	122116215	-
0,334256696	3,68351423	2,30040E-04	4,53941E-03	1		17	43640389	43661922	-
0,398489457	3,861752524	1,12577E-04	2,58237E-03	1		2	219075329	219170827	-
0,62362377	4,300527909	1,70392E-05	5,72877E-04	1		16	30222937	30254510	-

0,429825214	-1,639661205	1,01076E-01	3,28658E-01	0	3	48561718	48563781	-
0,369737731	2,387001366	1,69864E-02	1,05909E-01	0	3	57293083	57300187	+
0,25997749	3,633463355	2,79642E-04	5,22984E-03	0	11	65261928	65326543	+
0,257123703	3,002797692	2,67510E-03	2,90934E-02	0	19	51685363	51693456	-
0,22523409	4,543868845	5,52310E-06	2,23349E-04	1	17	61452404	61485110	+
0,273141974	4,873385912	1,09702E-06	5,47777E-05	1	2	226804036	226805061	+
0,448039987	3,510624811	4,47055E-04	7,45539E-03	1	19	17601328	17688365	-
0,413047732	4,267902502	1,97320E-05	6,47471E-04	1	6	30102897	30113090	-
0,201233347	5,595022678	2,20593E-08	1,73523E-06	1	8	22984596	23019335	-
0,24624838	4,279730654	1,87120E-05	6,16350E-04	1	5	140157319	140173051	+
0,325665054	4,12158451	3,76275E-05	1,09814E-03	1	20	63953384	63956985	+
0,32069631	3,600962358	3,17041E-04	5,71903E-03	1	21	44200602	44207399	-